Understanding optically stimulated charge movement in quartz and feldspar using time-resolved measurements

Christina Ankjærgaard
Ph.D. Thesis
February 2010
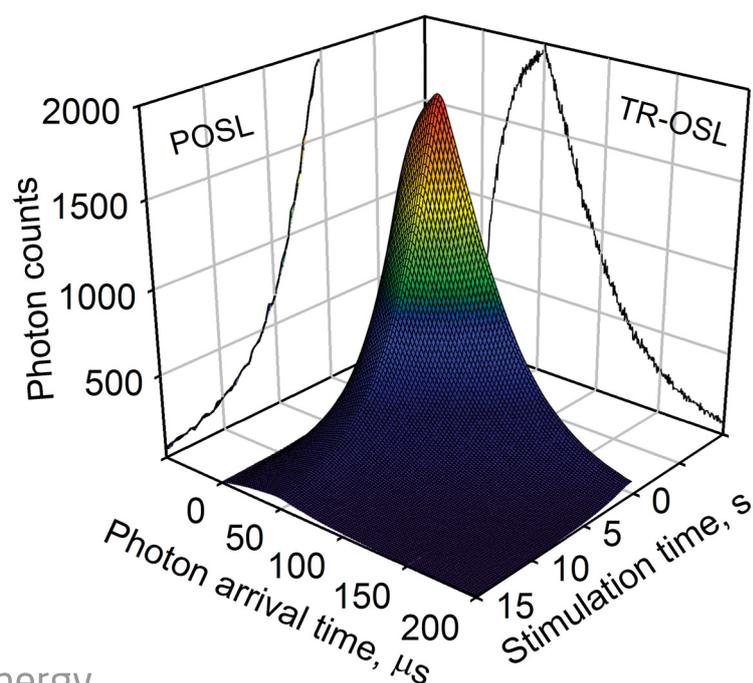
Ph.D. thesis

Christina Ankjærgaard

Understanding optically stimulated charge movement in quartz and feldspar using time-resolved measurements

Submitted: February 9th, 2010

Author: Christina Ankjærgaard

Title: Understanding optically stimulated charge movement in quartz and feldspar using time-resolved measurements

Division: Radiation Research

Academic advisors:

Lektor Ph.D. Stig Steenstrup
Niels Bohr Institute
University of Copenhagen

Scenior Scientist Ph.D. Mayank Jain
Radiation Research Division
Risø National Laboratory
Technical University of Denmark

Contents

Preface

The present thesis describes the scientific research carried out in the period November 1st 2006 − January 30th 2010 and is submitted as a partial fulfilment of the requirements for the Ph.D. degree in Physics at the University of Copenhagen, Denmark. The work has been funded by and took place at Risø National Laboratory (now a part of the Technical University of Denmark as Risø National Laboratory for Sustainable Energy).

Acknowledgements

To thank and acknowledge everybody who helped and supported me during these past three years would result in a thesis twice as long and I therefore apologise for my briefness and the inevitable omissions. You know who you are, thank you so much!

That said, there are a few people I would like to thank explicitly, starting with my external supervisor, Mayank Jain, Risø, who has always been very supportive and encouraging but at the same time pushed me to my limits and on a single occasion beyond them. It has been a great journey and I am proud to be your first Ph.D. student of many to come. I hope we will keep collaborating in the future.

Secondly, I would like to thank my internal supervisor, Stig Steenstrup (University of Copenhagen), for his invaluable help not only during these three years, but also during my M.Sc. Thesis and my B.Sc. project. Stig is a magician when it comes to administrative problems and paperwork, a task that has not lessened with the years.

Special thanks to Torben Lapp and Lars Pirzel for always stepping in and helping me whenever something was wrong with the pulsing unit, the photon timer or the photon timer software, you are a great team and I am happy you always had my back. Also thanks to Henrik E. Christiansen, Jørgen Jakobsen, Finn Jørgensen and Finn Willumsen for help with problems of all sizes.

Furthermore, I would like to thank Andrew Murray (Aarhus University) for great ideas and the many hours of reading through my papers correcting the English, Kristina Thomsen for encouragement and long discussions, several which were not work related, Jan-Pieter Buylaert for generous help in the lab and for always willingly starting measurements for me in the weekends, Paul Morthekai for sharing his feldspar samples and knowledge on these with me, and Reza Sohbati for always looking at the bright side of things. All of you I also thank for the many discussions during the often prolonged Wednesday science meetings. Two other very important persons from Risø are Sidsel Skov

Abstract

Thermoluminescence (TL) and optically stimulated luminescence (OSL) from quartz and feldspar are widely used in accident dosimetry and luminescence dating. In order to improve already existing methods or to develop new methods towards extending the current limits of the technique, it is important to understand the charge movement within these materials. Earlier studies have primarily focussed on examination of the trap behaviour; however, this only tells half of the story as OSL is a combination of charge stimulation and recombination. By using time-resolved OSL (TR-OSL), one can directly examine the recombination route(s), and thus obtain insight into the other half of the process involved in luminescence emission.

This thesis studies the TR-OSL and optically stimulated phosphorescence signals from quartz and feldspars spanning several orders of magnitude in time (few ns to the seconds time scale) in order to identify various charge transport mechanisms in the different time regimes.

The techniques employed are time-resolved OSL, continuous-wave OSL, TL, optically stimulated exo-electron (OSE) emission, and time-resolved OSE. These different techniques are used in combination with variable thermal or optical stimulation energy.

The thesis first delves into three main methodological developments, namely, (i) research and development of the equipment for TR-OSL measurements, (ii) finding the best method for multiple-exponential analysis of a TR-OSL curve, and (iii) optimisation of the pulsing configuration for the best separation of quartz OSL from a mixed quartz-feldspar sample. It then proceeds to study the different charge transport mechanisms subsequent to an optical stimulation pulse in quartz and feldspars.

The results obtained for quartz conclude that the main lifetime component in quartz represents an excited state lifetime of the recombination centre, and the more slowly decaying components on the millisecond to seconds time scale arise from charge recycling through the shallow traps.

The results from feldspars show the relative roles of an IR excited state (IR resonance), band tails and the conduction band in determining charge transport. It is suggested that unlike quartz, the excited state lifetime does not play an important role in our measurements. Finally, it is shown that one of these routes favors production of a least fading signal (due to quantum mechanical tunnelling) in feldspars. Although, results are only presented for some quartz and feldspar samples, they were found to be very similar within the each group during the course of this work.

Dansk resume

Termisk luminescens (TL) og optisk stimuleret luminescens (OSL) fra kvarts og feldspat er ofte anvendt i ulykkesdosimetri og luminescensdatering. Det er vigtigt at forstå ladningers bevægelse i disse materialer for at kunne forbedre allerede eksisterende metoder samt at udvikle nye metoder til at overvinde de nuværende begrænsninger i de allerede eksisterende teknikker.

Tidligere studier har hovedsageligt fokuseret på at undersøge defekters opførsel, men dette udgør dog kun halvdelen af fænomenet idet OSL er en kombination af både ladningsstimulering og rekombinering. Ved brug af tidsopløst OSL (TR-OSL) er det muligt at undersøge rekombineringsvejen(e) direkte og dermed opnå indsigt i den anden halvdel af processen i luminescensemission.

Denne afhandling studerer TR-OSL samt optisk stimuleret fosforescens fra kvarts og feldspat over flere størrelsesordener i tid (fra et par nanosekunder op til et par sekunder) for at identificere de forskellige mekanismer der spiller en rolle i ladningstransporten i disse forskellige tidsregimer. De anvendte målemetoder er OSL, tidsopløst OSL, TL, optisk stimuleret exo-elektron (OSE) emission samt tidsopløst OSE og disse bliver brugt i forbindelse med variabel termisk og optisk stimuleringsenergi.

Først fordyber afhandlingen sig i tre metodeudviklinger, disse er: (i) forskning i og udvikling af udstyr til TR-OSL målinger, (ii) undersøgelse af den bedste metode til multi-eksponentiel analyse af TR-OSL kurver samt (iii) optimering af pulsbredde og frekvens med henblik på at opnå den bedst mulige separation af kvarts-OSL signalet fra en blandet kvarts-feldspat prøve.

Det kan konkluderes for kvarts at den dominerende livstidskomponent i TR-OSL repræsenterer livstiden for rekombinationscentrets excitered tilstand. Den langsommere aftagende komponent i kvarts (som henfalder i løbet af et par millisekunder og helt op til flere sekunder) er forårsaget af elektroner som bliver fanget i fælder lige under ledningsbåndets kant hvorfra de efterfølgende kan undslippe ved hjælp af den omgivende termiske energi.

Feldspat resultaterne afdækker de relative betydninger af IR-fældens exciterede tilstand (IR resonansen), ledningsbånds "band tails" samt selve ledningsbåndet, for ladningstransporten i feldspat. Desuden antydes det at livstiden for rekombinationscentrets exciterede tilstand i feldspat (meget ulig kvarts) ikke spiller nogen stor rolle i vores målinger. Til slut er det vist at en af de ovenstående ruter i feldspat producerer et signal som udviser reduceret fading forårsaget af kvantemekanisk tunnelering.

Selvom de ovenstående resultater kun bliver vist for enkelte kvarts og feldspat-prøver har det under dette projekt vist sig at opførslen af forskellige kvarts og feldspat mineraler er meget ensartet indenfor hver gruppe. Resultaterne kan derfor antages at gælde mere generelt end blot for de enkelte prøver præsenteret

her.

List of publications

The following papers have been either published or submitted during the Ph.D. project (November 1st 2006 – January 30th 2010):

- **Ankjærgaard, C.**, Jain, M., Kalchgruber, R., Lapp, T., Klein, D., Mc-Keever, S.W.S., Murray, A.S., Morthekai, P., 2009. Further investigations into pulsed optically stimulated luminescence from feldspars using blue and green light. Radiation Measurements 44, 576–581.

- Lapp, T., Jain, M., **Ankjærgaard, C.**, Pirzel, L., 2009. Development of pulsed stimulation and Photon Timer attachments to the Risø TL/OSL reader. Radiation Measurements 44, 571–575.

- **Ankjærgaard, C.**, Jain, M., Thomsen, K.J., Murray, A.S., 2010. Optimising the separation of quartz and feldspar optically stimulated luminescence using pulsed excitation. Radiation Measurements 45, 778–785.

- Hansen, P.C., Nielsen, H.B., **Ankjærgaard, C.**, Jain, M., 2010. Two exponential models for optically stimulated luminescence, Chapter in *Exponential Data Fitting and its Applications*, edited by Pereyra, V. and Scherer, G., Bentham e-books.

- **Ankjærgaard, C.**, Jain, M., Hansen, P.C., Nielsen, H.B., 2010. Towards multi-exponential analysis in optically stimulated luminescence. Journal of Physics D: Applied Physics 43, 195501 (14pp).

- **Ankjærgaard, C.**, Jain, M., 2010. Optically stimulated phosphorescence in quartz over the millisecond to second time scale: insights into the role of shallow traps in delaying luminescent recombination. Journal of Physics D: Applied Physics 43, 255502 (12pp).

- **Ankjærgaard, C.**, Jain, M., 2010. Optically stimulated phosphorescence in orthoclase feldspar over the millisecond to second time scale. Journal of Luminescence 130, 2346–2355.

- Tsukamoto, S., Murray, A.S., **Ankjærgaard, C.**, Jain, M., Lapp, T., 2010. Charge recombination processes in minerals studied using optically stimulated luminescence and time-resolved exo-electrons. Journal of Physics D: Applied Physics 43, 325502 (9pp).

- Pagonis, V., **Ankjærgaard, C.**, Murray, A.S., Jain, M., Chen, R., Lawless, J., Greilich, S., 2010. Modelling the thermal quenching mechanism in quartz based on time-resolved optically stimulated luminescence. Journal of Luminescence 130, 902–909.

- Jain, M., **Ankjærgaard, C.**, 2011. Towards a non-fading signal in feldspar: insight into charge transport and tunnelling from time-resolved optically stimulated luminescence. Radiation Measurements 46, 292–309.

Presentations made at international conferences during the Ph.D. project:

- Ankjærgaard, C., Jain, M., Hansen, P.C., Nielsen, H.B., How to fit exponentials to OSL data. Presented at the *UK Luminescence and ESR Meeting*, August 26-28th 2009 at Royal Holloway University, UK. Oral presentation.

- Ankjærgaard, C., Jain, M., Kalchgruber, R., Klein, D., McKeever, S.W.S., Lapp, T., and Murray, A.S., Further Investigations into Pulsed Stimulation of Feldspars. Presented at the *12th International Conference on Luminescence and Electrons Spin Resonance Dating*, September 18-22nd 2008 held by Peking University, Beijing, China. Oral Presentation

- Ankjærgaard, C., Jain, M., Thomsen, K.J., and Murray, A.S., The time-resolved response of feldspar and quartz to pulsed optical stimulation. Presented at the *UK Luminescence and ESR Meeting*, September 12-14th 2007 at University of Sheffield, UK. Oral presentation.

- Ankjærgaard, C., Jain, M., Thomsen, K.J., and Murray, A.S., The response of feldspar and quartz to OSL to pulsed stimulation. Presented at the *15th International Conference on Solid State Dosimetry*, July 8-13th 2007 held at Delft University, the Netherlands. Poster presentation.

List of acronyms

CB   conduction band

CW-OSL   continuous wave optically stimulated luminescence

CW-IRSL   continuous wave infrared optically stimulated luminescence

DIRSL   delayed infrared stimulated luminescence

DOSL   delayed optically stimulated luminescence

IR   infrared

FIE   Fredholm integral equation

FWHM   full-width at half-maximum

H_2O_2   hydrogen peroxide

HCl   hydrochloric acid

HF   hydrofluoric acid

IRSL   infrared stimulated luminescence

IRSP   infrared stimulated phosphorescence

ISBR   initial-signal to background ratio

LED   light emitting diode

LM-OSL   linearly modulated optically stimulated luminescence

NaCl   sodium chloride

NLS   nonlinear least squares

OSA   optically stimulated afterglow

OSE   optically stimulated exo-electron emission

OSL   optically stimulated luminescence

OSP   optically stimulated phosphorescence

PMT   photomultiplier tube

POSL   pulsed optically stimulated luminescence

PIRSL   pulsed infrared optically stimulated luminescence

PTTL   photo-transferred thermoluminescence

RC   recombination centre

TL   thermoluminescence

TR-BLSL   time-resolved blue light optically stimulated luminescence

TR-GLSL   time-resolved green light optically stimulated luminescence

TR-IRSL   time-resolved infra red optically stimulated luminescence

TR-OSE   time-resolved optically stimulated exo-electron emission

TR-OSL   time-resolved optically stimulated luminescence

TR-POSL   time-resolved pulsed optically stimulated luminescence

TSE   thermally stimulated exo-electron emission

UV   ultraviolet

Chapter 1

Introduction

Thermally stimulated luminescence (TL) and optically stimulated luminescence (OSL) from natural minerals such as quartz and feldspar are widely used in retrospective dosimetry for estimating absorbed dose from exposure to ionizing radiation. Retrospective dosimetry can be divided into two main application areas; (i) archaeological, geological, and planetary dating, and (ii) accident dosimetry [see Bøtter-Jensen et al. (2003)]. Because of their ability to store information on deposited energy (dose) these minerals are also called dosimeters.

In dating applications, the aim is to determine the dose deposited in the mineral during burial ('the natural dose') as a result of exposure to naturally occurring ionizing radiation in the environment. The natural dose is found by estimating the dose using laboratory beta or gamma irradiation that would have been needed to produce the same luminescence intensity as the natural signal; this is called the equivalent dose, D_e. With a knowledge of the rate of energy absorption during the burial time, the dose rate, an estimate of the age (or burial time) of the mineral can then be determined (Aitken, 1998):

$$\text{Age [ka]} = \text{Equivalent dose, } D_e[\text{Gy}]/\text{Dose rate [Gy/ka]}. \qquad (1.1)$$

The unit of dose is Gray (Gy = J/kg), and ka denotes 1000 years. The dose rate is derived from the decay of radioactive nuclides mainly from the Thorium and Uranium decay series and from Potassium-40 contained within the mineral and in the surrounding sediment/soil matrix. There is also a usually small additional contribution from cosmic rays.

In accident dosimetry, the aim is to estimate the amount of dose absorbed in the mineral as a result of a radiation accident. The techniques used to estimate the absorbed dose is identical to those in dating, but the dose rates are usually much higher and the exposure much shorter.

Exposure to ionising radiation results in the storage of charge in the crystal lattice. The amount of trapped charge is related to the dose, and so a measurement of the trapped charge population will provide an estimate of the burial dose. One way to measure this population is using the luminescence emitted from a crystal when charge recombines. Luminescence originates in a two step process: (i) irradiation with ionising radiation and (ii) stimulation with heat or light. When crystalline materials such as quartz and feldspar are exposed to ionizing radiation, free electrons and holes are created within
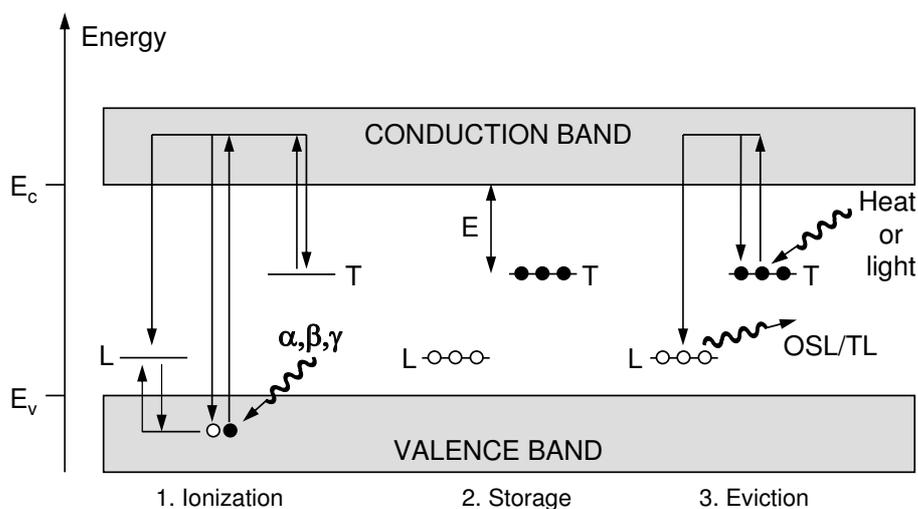
Figure 1.1: Band diagram showing 1) the ionisation process, 2) storage and, 3) trapped charge eviction followed by recombination. T is a trap at depth E below the conduction band and L is a luminescence recombination centre. E_c and E_v are the conduction band and valence band edges, respectively.

the crystal causing charge redistribution; a large proportion of these electrons and holes recombine instantaneously, but a small fraction is trapped at defects in the crystal structure. They then remain in these metastable energy states for a finite period (e.g.~ms to Ma) depending on the thermodynamic stability of the trapped charge and the ambient (storage) temperature. For stable electrons (lifetime $\gg$ burial time) the amount of accumulated trapped charge is uniquely related to the duration of the irradiation. In the laboratory these trapped electrons/holes are exposed to either heat or light, a process that results in eviction, transport and eventual recombination.

Only a fraction of the stimulated electrons recombine radiatively and emit luminescence. Moreover, luminescence detection is usually wavelength specific; one only examines a small proportion of all the recombinations going on in a crystal. As a result there is not always a simple relationship between the amount of trapped charge and the observed luminescence. Before this is discussed in detail, we first need to examine the current view of charge transfer processes in insulators. The concept of luminescence generation can be understood more clearly with the help of a band model described below.

1.1 Band model

When atoms are placed in close proximity of each other in a lattice structure, the individual energy levels of the atoms separate and form two wide bands of allowed energy states, the ground state (the valence band) and the excited states (the conduction band). These bands are separated by an energy band forbidden to the atomic electrons; this is termed 'the forbidden band gap'. The width E_g of the band gap is defined as the difference in energy between the highest ground state, E_v and the lowest excited state, E_c (Elliott, 2000,

p. 314–317); $E_g = E_c - E_v$, see Fig. 1.1. Solids with wide band gaps ($\sim$3–10 eV) are called insulators because ambient temperature cannot easily excite electrons from the ground states into the excited states; if this process were to take place, the material would be a conductor at ambient temperature. Quartz and feldspar minerals are insulators and their lattice structures are in general imperfect, because of either empty lattice sites or occupied sites that should be empty or the random placement of foreign atoms in the crystal. Such defects create allowed energy states within the otherwise forbidden band gap and are defined as 'trap centres' if they can trap electrons and 'recombination centres' if they can trap holes (i.e. emit electrons into the valence band) (Elliott, 2000, p. 497).

An energy diagram is shown in Fig. 1.1 for a simple one trap (T) and one luminescence recombination centre (L) configuration. During irradiation by either high energy particles or photons, electrons from the valence band receive enough energy to overcome the band gap, E_g: $\sim$9 eV indirect band gap for quartz (Itoh et al., 1989) and $\sim$7.7 eV direct band gap for feldspars (Malins et al., 2004), and are ionized into the conduction band leaving behind empty spaces or 'holes' in the valence band. Most of the electrons in the conduction band will, after some time, relax back into the valence band or to a hole trap (recombination centre) and thus recombine, thereby giving up the excess energy either thermally or optically. However a small fraction of the electrons will be trapped in forbidden states in the band gap (T). Depending on the trap depth E below the conduction band, an electron has a certain probability of escape which determines its mean life. For instance, the main trap in quartz used for OSL dating is geologically stable over $\sim 10^8$ years (Murray and Wintle, 1999). The holes corresponding to the trapped electrons will be trapped at recombination centres (L) by an electron leaving the recombination centre and filling the hole in the valence band, thus putting the crystal in a lower energy configuration. In dating applications, the ionization usually takes place over periods from a few years to several hundred thousands of years, while in accident dosimetry it is much shorter, usually on the timescale of hours to days.

To release the stored electrons, energy greater than the trap depth, E, must be applied to the crystal either in form of heat or light. The electrons escape into the conduction band from where a fraction is re-trapped back into the trap, while the remaining recombine with trapped holes at the recombination centres (L); if the recombination centre is radiative, light may be emitted. If the stimulating energy is in the form of photons, the emitted light is called optically stimulated luminescence (OSL), and if instead heat is applied, the emitted light is called thermoluminescence (TL). The latter is not further discussed here, but more information can be obtained from Chen and McKeever (1997).

1.2 Different OSL stimulation methods

During an OSL measurement, the sample is stimulated with light of a specific wavelength, and the luminescence emission is detected at a shorter wavelength. There are several different modes of stimulation available during optical stimulation: (i) continuous-wave OSL (CW-OSL), (ii) linearly modulated OSL (LM-OSL) and (iii) pulsed OSL (POSL) (Bøtter-Jensen et al., 2003).

1.2.1 Continuous wave OSL (CW-OSL)

During a continuous wave OSL measurement, the incident photon flux Φ is held constant with time. For a simple one-trap one recombination centre model (Fig. 1.1) and assuming negligible re-trapping of electrons into the trap T during stimulation, the CW-OSL intensity as a function of stimulation time can be described with a single decaying exponential:

$$I_{\mathrm{CW-OSL}}(t) = n_0 \sigma \Phi \exp(-\sigma \Phi t), \qquad (1.2)$$

where $I_{\mathrm{CW-OSL}}$ is the CW-OSL intensity at time t [s], n_0 is the number of trapped electrons at time $t = 0$, σ [cm^2] is the photoionisation cross-section of the electron trap, and Φ is the incident photon flux [cm^{-2}s^{-1}] (Bøtter-Jensen et al., 2003). For prolonged stimulation the OSL intensity tends to zero as the traps are progressively depleted. In the case of multiple traps with different cross-sections the observed OSL decay will consist of contributions from each trap. In this case, the luminescence emitted will consist of a sum of exponential terms, each with a characteristic decay constant describing the rate of emptying of the corresponding trap during optical stimulation (Bøtter-Jensen et al., 2003).

1.2.2 Linearly modulated OSL (LM-OSL)

During a linearly modulated OSL measurement, the intensity of the stimulation light is not kept constant as in CW-OSL, but is increased (or ramped) linearly from zero to some maximum intensity with time according to $\Phi(t) = \gamma t$, where γ is the ramp rate. By using the model from Fig. 1.1, the LM-OSL intensity with time is described by (Bøtter-Jensen et al., 2003):

$$I_{\mathrm{LM-OSL}}(t) = n_0 \sigma \gamma t \exp\left[-(\sigma \gamma / 2)t^2\right]. \qquad (1.3)$$

By linearly ramping the stimulation intensity from zero, the rate of released trapped charge is initially small; the signal increases with increased stimulation intensity until a maximum is reached and then decreases as a result of trapped charge depletion, thereby creating a peak shaped signal. If stimulating a system with multiple traps with different trap depths, various peaks will appear at different stimulation times, each corresponding to a different trap, and the curve can be described as a sum of first-, second- or general-order LM-OSL curves (Bøtter-Jensen et al., 2003).

1.2.3 Pulsed OSL (POSL)

Pulsed stimulation is a fundamentally different approach from continuous stimulation. Here the incident photon flux is delivered in pulses with a certain fixed pulse width, T, such that ΦT for each pulse is kept constant throughout a measurement. The stimulation pulses are separated by an 'off-time' during which it is possible to measure the decay of the luminescence signal generated from the preceding pulse. POSL offers an alternative method to discriminating stimulation light from luminescence; this separation is normally obtained by wavelength resolution using optical filters, but in POSL this can be by time resolution (Bøtter-Jensen et al., 2003).
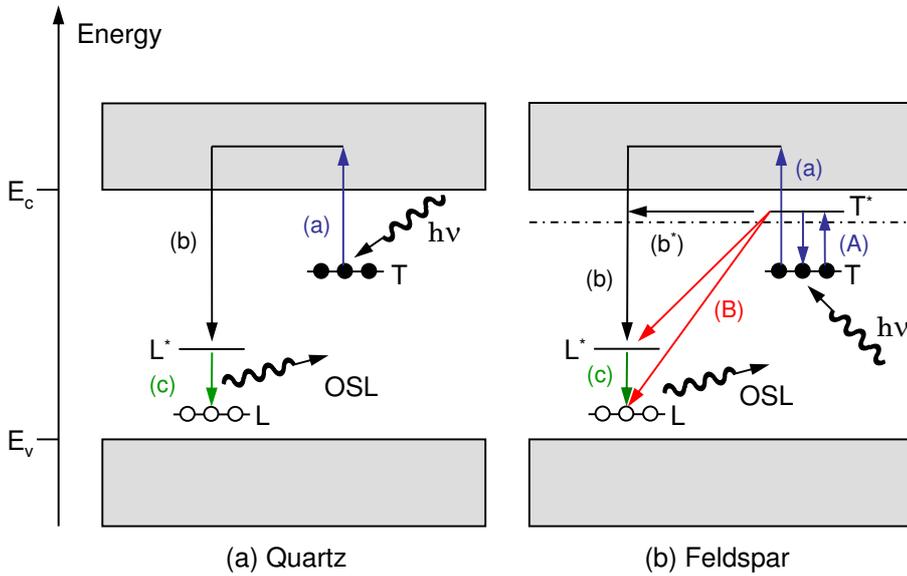
Figure 1.2: Band diagrams showing the different steps involved in producing luminescence during optical stimulation in (a) quartz and (b) feldspar. The notation is the same as that of Fig. 1.1. Furthermore, T^* is the excited state of the trap, T, and L^* is the excited state of the luminescence recombination centre, L. The dashed-dotted line indicates the band-tails as shown by Poolton et al. (2002b).

In Section 1.1 it was stated that each electron recombining with a hole at a radiative (luminescence) centre will emit a photon. However, there will, in general, be a delay between stimulation and light emission. POSL allows the study of the mechanisms causing this delay; the luminescence photons arriving after a stimulation pulse are measured as a function of time and this signal is known as time-resolved OSL (TR-OSL) (Bøtter-Jensen et al., 2003). TR-OSL measurements are usually resolved on the nanosecond to millisecond time scale depending on the material [e.g. Tsukamoto et al. (2006); Chithambo (2007b) and references therein].

In the following sections some fundamental aspects of TR-OSL as applied to quartz and feldspars are described.

1.3 Time-resolved OSL (TR-OSL): Theoretical considerations

This section has been split into two parts, Section 1.3.1 dealing with quartz and Section 1.3.2 with feldspar, as the dynamics governing the processes in the two minerals are very different.

1.3.1 Quartz

During a TR-OSL measurement using quartz, usually with blue or green light stimulation, a very small fraction of the trapped charge is raised to the con-

duction band during the stimulation pulse, and before commencement of the next pulse, some or all of the charge recombines and the resulting excited state then relaxes to emit light. There are different steps involved in this process between photon absorption (from stimulation light) and emission, see Fig. 1.2a (Bøtter-Jensen et al., 2003):

(a) Charge eviction from the trap by photon absorption: The photoionisation cross-section, σ_T, of the electron trap governs the charge de-trapping probability during stimulation.

(b) Transition from conduction band to a recombination centre L: The probability of this is proportional to the number of trapped holes m at L, and the proportionality constant is A_L. A_L is the probability that an electron will recombine with a hole at L and is a characteristic of L.

(c) Relaxation from the excited state to the ground state of the recombination centre: This is a characteristic time of the recombination centre and is determined by whether the transition from the excited state to the ground state is forbidden (long lifetime) or allowed (short lifetime).

In pulsed stimulation where the luminescence signal is measured after the pulse, i.e. in the off-time, process (a) can be eliminated. Moreover, it can be assumed that there is negligible change in the concentration of recombination centres as the energy delivered to the sample during a pulse is small. The occurrence or non-occurrence of process (c) depends upon the atomic nature of the recomination centre. In the absence of process (c), process (b) would determine the lifetime of the TR-OSL signal (denoted the 'recombination lifetime', the inverse of the recombination probability defined above). However, for a system with many different recombination centres and re-trapping phenomena, the lifetime of the TR-OSL signal will be determined by the lifetime of an electron in the conduction band, and not the recombination lifetime of any one centre. When process (c) is active, depending on the nature of the recombination centre, the recombination will result in an excited state of the centre. If the subsequent relaxation to the ground state is radiative, then process (c) will result in luminescence emission with a characteristic lifetime denoted as the 'excited state lifetime'.

If the conduction band lifetime and the excited state lifetime are orders of magnitude different from each other, then the resulting TR-OSL decay can be approximated by an exponential decrease with a lifetime dictated by that of the slowest process. However, if the two lifetimes are comparable, the TR-OSL form will be the sum of increasing and decreasing exponential components. Similarly, if there is more than one radiative recombination centre involved in the luminescence emission and the process (c) governs the lifetimes, then the resulting TR-OSL decay can be approximated by the sum of exponential components, the number of which corresponds to the number of radiative centres.

For a single one-trap one luminescence recombination centre model [Fig. 1.2a] with negligible or very slow re-trapping, if it assumed that one of the processes, either process (b) or (c), is essentially instantaneous, the quartz TR-OSL curve will build-up during the excitation pulse and decay after the pulse according to (Chithambo and Galloway, 2000b; Chithambo, 2007a):

$$\text{During pulse:} \quad I_{\text{TR}-\text{OSL}}(t) \;=\; n_0 p\,[1 - \exp(-t/\tau_{\text{TR}-\text{OSL}})] \qquad (1.4)$$

$$\text{After pulse:} \quad I_{\text{TR-OSL}}(t) \quad = \quad n_{\text{T}} p \cdot \exp\left[-(t-T)/\tau_{\text{TR-OSL}}\right] \quad (1.5)$$

where $p = \sigma\Phi$ is the rate of stimulation $[\text{s}^{-1}]$, T is the stimulation pulse width, t is the time since the start of the stimulation pulse, n_{T} is the number of trapped electrons at $t = T$, and $\tau_{\text{TR-OSL}}$ is the lifetime of the TR-OSL curve.

If the pulse width is much bigger than the TR-OSL lifetime ($T \gg \tau_{\text{TR-OSL}}$), most of the light is emitted during the stimulation pulse and it approximates the CW-OSL decay. However, if the pulse width is smaller than the relaxation time ($T < \tau_{\text{TR-OSL}}$), some of the light is emitted during the stimulation pulses, but the main part is emitted between the stimulation pulses (Bøtter-Jensen et al., 2003). From Eqns. (1.4) and (1.5), the light emitted after the end of the pulse as a fraction of the total integrated luminescence both during and after the pulse is given as:

$$f = \frac{\tau_{\text{TR-OSL}}}{T} \cdot \left[1 - \exp(-T/\tau_{\text{TR-OSL}})\right]. \quad (1.6)$$

There have been extensive studies reported in the literature which were intended to investigate mainly the role of traps in charge movement leading to the emission of luminescence using CW-OSL or LM-OSL [e.g. Jain et al. (2003); Singarayer and Bailey (2003)]. However, investigating trap behaviour tells only half of the story. Using TR-OSL, one can directly examine the recombination process on its own, and thus obtain insight into the other half of the process involved in luminescence emission.

1.3.2   Feldspar

The properties of feldspar minerals differ from those of quartz in two main areas, (i) feldspars are sensitive to IR stimulation (Hütt et al., 1988) as well as visible light, and (ii) the feldspar signal suffers from a anomalous loss of charge during storage (Wintle, 1973). It is now widely accepted that this loss occurs due to quantum mechanical tunnelling from the ground state of the electron in a trap.

The IRSL trap in alkali-feldspar is believed to lie approximately 2–2.5 eV below the conduction band (Poolton et al., 2002a; Baril and Huntley, 2003) and therefore, electrons in the IR trap do not receive enough energy during IR stimulation to be excited into the conduction band even with thermal assistance (Bailiff and Barnett, 1994). It was therefore suggested by (Poolton et al., 2002a,b) that the IRSL from feldspar is the product of two processes, (i) electronic transfer from the excited state through band tail states below the conduction band to the recombination centre and (ii) tunnelling from the excited state to the recombination centre. The different steps involved in either visible or IR stimulation of feldspar to produce luminescence in process (i) can be described as (see Fig. 1.2b):

(a) Charge eviction from the trap by photon absorption.

(b) Transition from the conduction band and/or the band tail states to the recombination centre. Unlike quartz, where the residence time in the conduction band entirely depends on the probability of recombining/re-trapping, charge in feldspar can migrate through the band tails which may take significant time. This route is indicated by (b*) in the figure.

   (c) Relaxation from the excited state to the ground state of the recombination centre.

The alternative tunnelling mechanism, process (ii), is:

   (A) Excitation of charge into the excited state of the trap by photon absorption.

   (B) Tunnelling from the excited state of the trap, either into the ground state of the recombination centre (giving a photon emission directly), or into an excited state.

   (c) Relaxation from the excited state to the ground state of the recombination centre, giving somewhat delayed photon emission.

Transitions (a) and (A) are not relevant when studying the TR-OSL signal after the pulse as this step only occurs during light stimulation [although re-trapping cannot be ignored in process (ii)]. (b) and (b*) can be described by a 'recombination lifetime' and is discussed in Section 1.3.1. The residence time in the band tail states (b*) is a strongly temperature dependent process; as more recombination sites become available with increased band tail hopping at higher temperatures, the probability of recombination will increase (Poolton et al., 2002a,b)). Transition (c) is exponential and is described by the 'excited state lifetime' as discussed in Section 1.3.1. In process (ii) tunnelling (B) does not necessarily require any thermal assistance. The probability of tunnelling recombination depends on overlap of the electron and hole wave functions. In general, the shorter distance between the trap and the recombination centre, the higher the probability of recombination. This process cannot be described in terms of a single lifetime, but is instead expected to follow a power law (Huntley, 2006). If this transition delivers charge directly to the ground state of the recombination centre and emits a photon, then the power law is likely to govern the shape of the TR-OSL decay. If, however, the charge is delivered to the excited state, the TR-OSL signal may have a significant component of exponential form.

1.4 Time-resolved OSL (TR-OSL): previous work

Some of the first time-resolved OSL measurements feldspars were carried out using an array of 880 nm LEDs to identify possible food irradiation, and later by using a nitrogen dye laser to stimulate feldspars at 470 nm (Sanderson and Clark, 1994, and references therein). Bailiff (2000) used a pulsed, tuneable laser to stimulate quartz with light between 600 and 450 nm, and Chithambo and Galloway (2000a,b,c) stimulated samples of quartz with a pulsed LED array emitting at 525 nm. In this section, relevant studies on quartz (Subsection 1.4.1) and feldspar (Subsection 1.4.2) using time-resolved OSL will be discussed to highlight the progress within this field prior to and during this Ph.D. thesis.

1.4.1 Quartz

TR-OSL lifetimes

By using pulsed 525 nm LEDs, Chithambo and Galloway (2000b) measured time-resolved OSL at room temperature from quartz; prior to measurement

this had been annealed to 500°C for 2 min, irradiated to 150 Gy and pre-heated to 220°C. By fitting the TR-OSL decay after the light pulse with Eqn. (1.5), they found lifetimes in the range of 30–40 µs. Bailiff (2000) found similar lifetimes (33 ± 0.3 µs) from seven granular quartz samples extracted from ceramics and sedimentary deposits using a pulsed 470 nm laser, and a lifetime of 40 ± 0.6 µs for synthetic quartz. Chithambo and Galloway (2001) state that in most materials (including quartz), the luminescence lifetime is dominated by the intra-luminescence centre relaxation time and not the trap eviction time or the conduction band transit time and recombination time (see Fig. 1.2a). Furthermore, Bailiff (2000) found that lifetimes from synthetic quartz were within experimental error when the stimulation wavelength was varied in the range 450–650 nm, suggesting that a very similar recombination process occurs when the emission is detected at $\sim$280–380 nm, this is supported by Chithambo (2002) using both 525 nm and 470 nm pulsed LED stimulation on annealed quartz. It is likely that $[AlO_4/h]$ acts as the recombination centre responsible for the OSL emission band centred at 380 nm in quartz, and a common recombination site might thus be expected to yield comparable values of lifetimes (Chithambo, 2003).

In general all work done on natural quartz measured at room temperature suggests that there is one dominant lifetime with a value approximately between 30 and 40 µs depending on pre-treatment, annealing history, and irradiation (Chithambo et al., 2007). Furthermore, it has been shown (Chithambo and Ogundare, 2007; Chithambo et al., 2008a) that for certain high annealing temperatures a second shorter lifetime is present, but in a study of eight low sensitive quartz from crystalline rocks, Chithambo et al. (2007) found lifetimes at room temperature to lie in a much wider range from 4.0 ± 0.5 µs to 100 ± 23 µs.

Stretched exponentials

Time-resolved OSL decay curves following the stimulation pulse are generally fitted with Eqn. (1.5) to evaluate the lifetime, but Chen and Leung (2003) show by numerical simulations of TR-OSL curves from a one-trap, one luminescence recombination centre model (Fig. 1.1), that these could also be fitted well with a stretched exponential law:

$$I_{\mathrm{TR-OSL}}(t) = n_{\mathrm{T}}p \cdot \exp\left\{[-(t-T)/\tau_{\mathrm{TR-OSL}}]^{\beta}\right\}, \quad \text{with } 0 < \beta < 1. \quad (1.7)$$

Although, more often than not, the decay curve was found to be nearly simple exponential. This approach was tested in Chithambo (2005), where a measured TR-OSL decay was fitted with both Eqns. (1.5) and (1.7), yielding almost identical results of 40.3 ± 0.5 µs and 40.3 ± 3.2 µs respectively.

Studies on the effect of stimulation temperature

The main lifetime in quartz was shown by both Bailiff (2000) and Chithambo and Galloway (2000c) to decrease with increasing stimulation temperatures in the range 20°C to 200°C, and Bailiff (2000) noted that the TR-OSL signal intensity also decreased with temperature. By comparing these findings with Radioluminescence (RL) spectra measured from the same sample, Bailiff
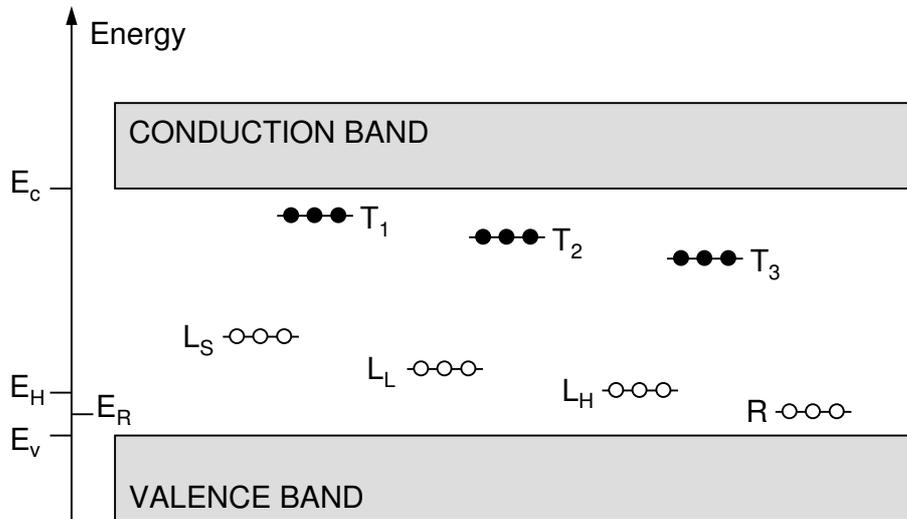
Figure 1.3: Band diagram redrawn from Galloway (2002) containing three traps, T_1, T_2, T_3, three luminescence recombination centres, L_S, L_L, L_H, and a non-radiative recombination centre, R.

(2000) concluded that the observed temperature effects were due to thermal quenching, where a change in competition between radiative and non-radiative transitions within the luminescence centre caused a decrease in luminescence lifetime and intensity. This is supported by Chithambo and Galloway (2001) for the slow OSL component region in quartz and by Chithambo (2002) for the fast OSL component region. Both studies fitted their data to estimate the thermal assistance energy at lower temperatures and the activation energy for thermal quenching at higher stimulation temperatures.

Studies on the effect of thermal annealing

Galloway (2002) did a further study on the same quartz used in Chithambo and Galloway (2000a,b,c) to examine the effect of high temperature annealing on luminescence lifetime measured at 20°C using green 525 nm LED stimulation. The samples were annealed at each temperature for 7 min prior to beta irradiation, and for no pre-heat applied, the lifetime was constant at 41.5 μs for annealing temperatures up to 500°C, after which they decreased steadily to 31.5 μs as the annealing temperatures were increased in steps of 100°C to a maximum of 1000°C.The extent of decrease in lifetime could be reduced to 34 μs or 36 μs by pre-heating to 220°C for either 60 s or 300 s respectively prior to measurement; lifetimes below 500°C were not affected by the pre-heat. The decrease in lifetime with anneal temperature could be reversed by either prolonged beta irradiation or preheating. Galloway (2002) also found a second shorter lifetime component for certain annealing temperatures, which was also seen to decrease with increased stimulation temperature.

Galloway (2002) interprets the change in lifetime in terms of a band model with three luminescence centres and a non-radiative centre, R, see Fig. 1.3, where L_S is associated with the second shorter lifetime component, L_L with

the 31.5 µs lifetime, and L_H with the 41.5 µs lifetime. The decrease in lifetime for different annealing temperatures relates to the transfer of holes from R to L_H and L_L, and from L_H to L_L. For high anneal temperatures, holes will also be transferred to L_S and the shorter lifetime component is observed. This model is further supported by Ogundare and Chithambo (2007) investigating the lifetime dependence on annealing temperature, irradiation dose and stimulation temperature using blue (470 nm) pulsed LED stimulation on a quartz sample from Nigeria. In order to explain their results, they assume that L_S has the highest hole capture probability during irradiation, followed by L_L and L_H, and that the recombination probability (via the conduction band) of holes and electrons at L_S far exceeds that of L_L and L_H.

Effect of optical bleaching prior to irradiation

Using the same quartz from Nigeria, Ogundare and Chithambo (2008) found that the duration of optical bleaching prior to irradiation caused a decrease in lifetime for samples annealed to 600°C, but did not have an effect on the lifetime for samples annealed to 500°C. A phase change occurs in quartz at 573°C, and below this temperature - and thereby at 500°C, most of the holes transferred from the L_H and R centres are moved to the L_L centre; the latter will then dominate the measured signal even for prolonged bleaching. In order to explain the decrease in lifetime with optical bleaching for the samples annealed at 600°C (where the number of holes transferred to L_S is much greater than to L_L), Ogundare and Chithambo (2008) make the assumption that during the bleaching the recombination probability of electrons with holes through the valence band is greater at L_L than at L_S; this results in an overall decrease in lifetime as L_S is associated with the fastest lifetime.

The role of re-trapping in thermal quenching

In Galloway (2002) and Ogundare and Chithambo (2007), the temperature dependence of the lifetime could be well explained by thermal quenching, but in Chithambo (2006) for natural quartz annealed 600°C for 30 min and in Chithambo et al. (2008b,c) for natural sediments with no prior annealing, the lifetimes only fit the thermal quenching relationship for stimulation temperatures > 120°C. To explain these results in terms of the model in Fig. 1.3, Chithambo (2006) argues that the lifetimes of the centres L_L and L_H probably have different temperature characteristics such that they can not simply be described by the simple thermal quenching relationship, and Chithambo et al. (2008c) suggests that it may not be completely correct to neglect re-trapping at low stimulation temperatures, and that this could cause the deviations below 120°C. Furthermore, Chithambo et al. (2008c) demonstrated that the dependence of lifetime on dose in samples without prior annealing can both be increasing, decreasing or unchanged. These results are explained in terms of preferential capture of holes produced during the irradiation by a primary radiative recombination centre.

Synthetic quartz

In a recent study (Pagonis et al., 2009) using annealed (900°C for 1 hour) high purity synthetic quartz, an unusual TR-OSL signal showing non-monotonic

behaviour was presented. These authors modelled this behaviour using the three-centre model of Galloway (2002), see Fig. 1.3. Three very different TR-OSL curve shapes were simulated using the same model and the differences in the curve shapes were explained by the relative prevalence of holes in different recombination centres (L_S, L_L, and L_H) for each curve.

Summary

The main objective of the studies into time-resolved OSL of quartz so far have been to examine the luminescence lifetimes as a means to understand the OSL characteristics in this widely used dosimetric material.

The main lifetime in quartz measured at room temperature has been found to lie between 30 and 40 μs depending on the sample, and this lifetime decreases steadily with increasing stimulation temperature due to thermal quenching. A study on the effect of annealing temperature prior to dosing showed a steady decrease in the lifetime measured at room temperature for annealing temperatures between 500°C and 1000°C. It was further shown that prolonged optical bleaching prior to irradiation of quartz annealed to 600°C showed a decrease in lifetime, whereas quartz annealed to 500°C did not show a decrease. A kinetic model consisting of three luminescence centres and a non-radiative centre was developed to explain the observed behaviour in the quartz lifetime. This model is recently used to successfully model non-monotonic behaviour from synthetic quartz.

1.4.2 Feldspar

Compared to quartz, much less work has been done in the field of pulsed OSL from feldspars. The first time-resolved OSL curves measured from feldspar (IAEA, type F1 feldspar) was carried out by Sanderson and Clark (1994) using blue (470 nm) laser stimulation. They reported that feldspar decay curve following the excitation pulse contains at least two fast continua and a pronounced series of lines which they call 'fine structure'. They observed this fine structure in both natural and regenerated signals. They suggest that this shape indicates a complex recombination mechanism involving structured coordination between traps and centres. This series of lines described by Sanderson and Clark (1994) was not observed by Clark et al. (1997) using pulsed IR (850 nm) and they suggest them to be an artifact of the measurement equipment. No such fine structure has been reported since.

TR-IRSL lifetimes

Clark et al. (1997) used pulsed IR (850 nm) stimulation on six museum feldspar samples to obtain time-resolved measurements at temperatures ranging from 50°C to 100°C in three different emission windows (280–380 nm, 350–575 nm, and 460–625 nm). Although the authors argue that the feldspar time-resolved IRSL decay is complex, they fit the curves adequately with a sum of up to five exponentially decaying components with different lifetimes, falling into well-defined groups: 30–50 ns, 300–500 ns, 1–2 μs, ∼5 μs, and > 10 μs. The absolute values and relative contributions of these components varied between the samples, and there seemed to be little correlation between the lifetimes

and the K, Na, and Ca composition. The study was further extended by Clark and Bailiff (1998) using a set of bandpass interference filters to measure time-resolved IRSL at 300, 350, 400, 450, 500, and 550 nm for the same six samples, and lifetimes of up to 11 ± 0.1 ms was observed for Amelia albite at 550 nm. Several curves in both Clark et al. (1997) and Clark and Bailiff (1998) show an initial rising component (indicated with a negative pre-exponential factor) and it is suggested this is due to self-absorption of rapidly produced UV luminescence in the 420–460 nm emission region. The lifetimes found by Clark et al. (1997) and Clark and Bailiff (1998) were largely supported by Chithambo and Galloway (2000b) using green (525 nm) LED stimulation of two feldspar samples in the detection band 330–380 nm.

Application to Anomalous fading

Sanderson and Clark (1994) also measured TR-OSL from a volcanic lava sample, to try and identify a non-fading component in the signal. The same volcanic lava had in TL measurements shown a 50 % loss of signal after 4 days of storage due to anomalous fading [see e.g. Wintle (1977) on anomalous fading using the same sample]. By stimulation with blue light, the aim was to identify a luminescence component not affected by fading, as it would be associated with long-range charge transport; they concluded that components occurring on the $40 \text{ ns} - 8 \text{ }\mu\text{s}$ timescale show major signal loss due to fading, but that both the faster and slower components did not appear to show signs of fading. The fine structure showing less fading described by Sanderson and Clark (1994) could not be supported by Clark et al. (1997) using pulsed IR (850 nm) stimulation on six museum feldspar samples; they suggest the possibility that the fine structure is an artefact from the experimental setup.

The work originally initiated by Sanderson and Clark (1994) of identifying a non-fading component in feldspar was continued by Tsukamoto et al. (2006) using pulsed IR (875 ± 40 nm) LED stimulation on Na- and K-feldspars and detecting in the bands 280–380 nm, 320–460 nm, and 665–735 nm. Tsukamoto et al. (2006) identified three components in regions < 1 μs, 3–4 μs, and $\sim$20 μs, broadly consistent with those from Clark et al. (1997) and Clark and Bailiff (1998), but could not resolve the short 30–50 ns component previously identified, as the LED switch-off time was approximately 400 ns. Furthermore they observed that the relative contribution from the $\sim$20 μs component is greater in K-feldspars than in Na-feldspars, and that this component seems to be more stable than the short lived components for a storage time of 30 days.

By comparing D_e values found using pulsed IR-OSL and CW IR-OSL from four different samples in the three detection windows, Tsukamoto et al. (2006) found that all D_e values calculated using POSL (data collection only in the off-time with a dead time of 10 μs following the end of the on-time) were larger than those obtained using CW-OSL. Some of the POSL De values were consistent with the expected D_e, but the data is scattered and several values were within error both larger and smaller than the expected D_e. This work was continued by Huot (2007) but he concluded that it was unclear whether pulsed stimulation gave any additional benefit with respect to the anomalous fading problem, as previously examined by Tsukamoto et al. (2006). This is an important issue and requires further investigation.

Applications of POSL to mixed quartz-feldspar samples

An instrumental signal separation method, based on the difference in the TR-OSL decay shapes of quartz and feldspar was developed by Denby et al. (2006). With this approach, Denby et al. (2006) and Thomsen et al. (2006) demonstrated that by using pulsed blue stimulation (with a prior IR stimulation) on an artificial mixed sample consisting of dosed quartz (23 Gy) and undosed feldspar (0 Gy), the measured dose was indistinguishable from the known quartz dose of 23 Gy. This result applied to mixed samples with feldspar contamination of up to 40% by mass. This work was continued in Thomsen et al. (2008), where post-IR pulsed blue light stimulation of eleven natural samples show that the dose in quartz can be measured accurately without any prior chemical separation.

Summary

The time-resolved OSL off-time decay from different feldspars has generally been explained using a multi-exponential model with up to five components. Measurements using both IR stimulation (emission at 300, 350, 400, 450, 500, and 550 nm) and green stimulation (emission at 330–380 nm) broadly show that the lifetimes fall within the groups: 30–50 ns, 300–500 ns, 1–2 µs, ∼5 µs, and > 10 µs.

Previous work gives a suggestion that the longer component of ∼20 µs undergoes lesser anomalous fading than the faster decaying components. This suggestion has, however, not been thoroughly tested. Finally, using POSL, an instrumental method for separating the quartz signal from a mixed quartz-feldspar sample gives a better method for estimating quartz doses in the presence of feldspar contamination.

1.5 Thesis objectives

During this Ph.D. project, the purpose was to obtain further understanding of the optically stimulated charge movement within the quartz and feldspar minerals by use of time-resolved measurements. With the background of the previous work on these minerals described above, this section outlines the key questions that are examined in this thesis:

1. Extraction of physical information from time-resolved luminescence signals from both quartz and feldspar has to a large extent been based on data fitting with multiple exponential curves. The problem of exponential fitting is highly 'ill-posed' and it is therefore important to investigate which is the most robust method for parameter estimation, and furthermore, to understand the impact of subjectivity (user input) in the curve fitting analysis.

2. In quartz, although, the previous work has mainly focussed on the study of the dominant component on the microseconds time scale (∼40 µs lifetime), it remains unclear whether this component arises from recombination lifetime or the excited state lifetime. One of the main objectives in this thesis is to understand the origin of this main component in quartz

and to estimate the time-scales on which the conduction band empty-ing occurs. Furthermore, the slowly decaying components have not been studied in the past; these could potentially give insights into the shallow traps and their interactions following an optical pulse. Thus, it was considered important to extend the time scale of the measurement by many orders of magnitude in order to examine transport processes and dynamic interactions on these time scales.

3. In feldspar there are several areas of interest. The limited previous work has mainly restricted to the fitting of feldspar time-resolved decay curves with a sum of decaying exponentials. It is important to investigate whether it is a valid assumption that these signals can be mathematically described as such. Similarly, feldspars have been accepted to consist of complex energy levels, in particular an IR excited state, and also perhaps the band tails based on spectroscopic measurements; however, the occurrence and role of these states have not been tested by direct observation of the electronic transport rates during optical stimulation. TR-OSL in combination with different thermal and optical stimulation energies offers a unique tool for such investigations.

4. From the application point of view the work initiated on identifying a part of the feldspar TR-OSL signal less prone to fading is of great importance and, therefore, requires further detailed investigations and understanding of the underlying causes; this objective strongly overlaps with objective 3. Similarly, the question of separation of signals from mixed samples based on pulsed stimulation is also very relevant both for laboratory and for development of procedures for future *in-situ* dating and dosimetry. Earlier work has shown application to quartz-feldspar mixture based on arbitrarily chosen on-time and off-time. It is important to find out optimum pulsing configuration that gives the best signal separation of quartz signal from a mixed sample.

1.6 Thesis outline

This thesis is a collection of papers published or submitted during my Ph.D. project, and this section outlines the overall thesis structure and describes the motivation for each of the following chapters.

Chapter 2 is the paper: *Development of pulsed stimulation and Photon Timer attachments to the Risø TL/OSL reader*, published in Radiation Measurements. It describes the new instrumental developments which are used to make time-resolved OSL measurements during the course of this thesis.

Chapter 3 is the paper: *Towards multi-exponential analysis in optically stimulated luminescence*, submitted to Journal of Physics D: Applied Physics (provisionally accepted). This paper examines the best method of fitting TR-OSL using a multi-exponential model. It investigates on two different methods: a nonlinear least squares method and a first-kind Fredholm integral equation, to test if the subjectivity (user's definition of the number of parameters) plays and important role in fitting. It also investigates whether data in the 'decay form' or the 'peak form' is better suited mathematically for fitting.

Chapter 4 is the paper: *Modelling the thermal quenching mechanism in quartz based on time-resolved optically stimulated luminescence*, in press in Journal of Luminescence. This paper explores the possibility that the lifetime of the main ∼40 µs component in quartz reflects the excited state lifetime using experimental TR-OSL data together with a new kinetic model based on Mott-Seitz thermal quenching mechanism. This work also examines the validity of the relevant parameter values in the commonly used, well established kinetic model for quartz OSL with respect to its success in predicting quartz TR-OSL decay form.

Chapter 5 is the paper: *Charge movement in minerals studied by optically stimulated time-resolved exo-electron emission*, submitted to Journal of Physics D: Applied physics. This paper presents an experimental determination of the rate of emptying of the conduction band in quartz, K-feldspar and common salt (NaCl) using time-resolved exo-electron emission (TR-OSE). Together with chapter 4 and chapter 6, this chapter contributes to the understanding of the TR-OSL components in quartz.

Chapter 6 is the paper: *Optically stimulated phosphorescence in quartz over the millisecond to second time scale: insights into the role of shallow traps in delaying luminescent recombination*, submitted to Journal of Physics D: Applied Physics. This paper investigates on the TR-OSL and optically stimulated phosphorescence (OSP) decay in quartz continuing over eight decades on the time scale (50 ns to ∼8 s). The objective here is to understand the underlying mechanisms behind the slowly decaying components (components that appear after the main component discussed above) from the millisecond to second time scales.

Chapter 7 is the paper: *Further investigations into pulsed optically stimulated luminescence from feldspars using blue and green light*, published in Radiation Measurements. This paper is the first of a series of papers focusing on feldspars and it investigates the properties of the TR-OSL decay from 14 feldspar mineral specimens on the nanosecond and microsecond time scales. This paper discusses which process governs the luminescence production in feldspars and furthermore questions the validity of using a multiple-exponential model for describing feldspar TR-OSL.

Chapter 8 is the paper: *Optically stimulated phosphorescence in orthoclase feldspar over the millisecond to second time scale*, submitted to Journal of Luminescence. This paper characterises time-resolved and phosphorescence decay curves obtained from IR stimulation, elevated temperature post-IR IR stimulation of feldspar. This article is complementary to the similar work on quartz presented in Chapter 6. The aim of this investigation is to understand the origins of the signals on the millisecond to second time scales, and their role in optical stimulation.

Chapter 9 is the paper: *Further insight into charge recombination and tunnelling in feldspars from time-resolved optically stimulated luminescence*, manuscript near submission. This paper presents time-resolved IR, elevated temperature post-IR, IR and green stimulated luminescence measurements from a set of feldspar samples. The measurements focus on TR-OSL decay from ∼500 ns to 500 µs. The article discusses the origins of these signals in terms of charge transport through various energy states in feldspar: the IR excited state, the band tails and the conduction band. The investigations are carried out based on the dependence of TR-OSL decay shapes on thermal

energy, optical energy, and storage time (anomalous fading). The work has implications for developing protocols to cope with anomalous fading.

Chapter 10 is the paper: *Optimising the separation of quartz and feldspar optically stimulated luminescence using pulsed excitation*, accepted for publication in Radiation Measurements. The final paper is a more application oriented paper and investigates on an optimum pulsing configuration for separating the quartz signal from that of feldspar's in a mixed quartz-feldspar sample using blue light stimulation.

Chapter 11 provides a summary of the main results and future directions.

References

Aitken, M. J. (1998). *An Introduction to Optical Dating - The Dating of Quaternary Sediments by the Use of Photon-stimulated Luminescence.* Oxford University Press, Great Clarendon Street, Oxford, UK. ISBN: 0–1–854092–2.

Bailiff, I. K. (2000). Characteristics of time-resolved luminescence in quartz. *Radiation Measurements*, 32:401–405.

Bailiff, I. K. and Barnett, S. M. (1994). Characteristics of infrared-stimulated luminescence from a feldspar at low temperature. *Radiation Measurements*, 23:541–545.

Baril, M. R. and Huntley, D. J. (2003). Optical excitation spectra of trapped electrons in irradiated feldspars. *Journal of Physics: Condensed Matter*, 15:8011–8027.

Bøtter-Jensen, L., McKeever, S. W. S., and Wintle, A. G. (2003). *Optically Stimulated Luminescence Dosimetry.* Elsevier, Amsterdam, The Netherlands. ISBN: 0–444–50684–5.

Chen, R. and Leung, P. L. (2003). The decay of OSL signals as stretched-exponential functions. *Radiation Measurements*, 37:519–526.

Chen, R. and McKeever, S. W. S. (1997). *Theory of Thermoluminescence and Related Materials.* World Scientific.

Chithambo, M. L. (2002). Time-resolved luminescence from annealed quartz. *Radiation Protection Dosimetry*, 100:273–276.

Chithambo, M. L. (2003). Dependence of the thermal influence on luminescence lifetimes from quartz on the duration of optical stimulation. *Radiation Measurements*, 37:167–175.

Chithambo, M. L. (2005). Towards models for analysis of time-resolved luminescence spectra from quartz. *Applied Radiation and Isotopes*, 62(6):941–942.

Chithambo, M. L. (2006). On the correlation between annealing and variabilities in pulsed-luminescence from quartz. *Radiation Measurements*, 41:862–865.

Chithambo, M. L. (2007a). The analysis of time-resolved optically stimulated luminescence: I. Theoretical considerations. *J. Phys. D: Appl. Phys.*, 40:1874–1879.

Chithambo, M. L. (2007b). The analysis of time-resolved optically stimulated luminescence: II. Computer simulations and experimental results. *J. Phys. D: Appl. Phys.*, 40:1880–1889.

Chithambo, M. L. and Galloway, R. B. (2000a). On luminescence lifetimes in quartz. *Radiation Measurements*, 32:621–626.

Chithambo, M. L. and Galloway, R. B. (2000b). A pulsed light-emitting-diode system for stimulation of luminescence. *Meas. Sci. Technol.*, 11:418–424.

Chithambo, M. L. and Galloway, R. B. (2000c). Temperature dependence of luminescence time-resolved spectra from quartz. *Radiation Measurements*, 32:627–632.

Chithambo, M. L. and Galloway, R. B. (2001). On the slow component of luminescene stimulated from quartz by pulse blue light emitting diodes. *Nuclear Instruments and Methods B*, 183:358–368.

Chithambo, M. L. and Ogundare, F. O. (2007). Relative features of the principal and secondary luminescence lifetimes in quartz. *Physica Status Solidi (C)*, 4(3):914–917.

Chithambo, M. L., Ogundare, F. O., and Feathers, J. (2008a). Principal and secondary luminescence lifetime components in annealed natural quartz. *Radiation Measurements*, 43:1–4.

Chithambo, M. L., Ogundare, F. O., Feathers, J., and Hong, D. G. (2008b). The dependence of luminescence lifetimes on additive irradiation in natural sedimentary quartz: sands from Santa Elina, Brazil. *Physica Status Solidi C*, 5(2):630–633.

Chithambo, M. L., Ogundare, F. O., Feathers, J., and Hong, D. G. (2008c). On the dose-dependence of luminescence lifetimes in natural quartz. *Radiation Effects and Defects in Solids*, 163:945–953.

Chithambo, M. L., Preusser, F., Ramseyer, K., and Ogundare, F. O. (2007). Time-resolved luminescence of low sensitivity quartz from crystalline rocks. *Radiation Measurements*, 42:205–212.

Clark, R. J. and Bailiff, I. K. (1998). Fast time-resolved luminescence emission spectroscopy in some feldspars. *Radiation Measurements*, 29:553–560.

Clark, R. J., Bailiff, I. K., and Tooley, M. J. (1997). A preliminary study of time-resolved luminescence in some feldspars. *Radiation Measurements*, 27:211–220.

Denby, P. M., Bøtter-Jensen, L., Murray, A. S., Thomsen, K. J., and Moska, P. (2006). Application of pulsed osl to the separation of the luminescence components from a mixed quartz/feldspar sample. *Radiation Measurements*, 41:774–779.

Elliott, S. R. (2000). *The Physics and Chemistry of Solids*. John Wiley & Sons Ltd, England. ISBN: 0471 98195 8 (pbk.).

Galloway, R. B. (2002). Luminescence lifetimes in quartz: dependence on annealing temperature prior to beta irradiation. *Radiation Measurements*, 35:67–77.

Huntley, D. J. (2006). An explanation of the power-law decay of luminescence. *J. Phys.: Condens. Matter*, 18:1359–1365.

Huot, S. (2007). *Investigations of alternative and innovative ways of performing luminescence dating in an attempt to extend the age range.* Unpublished Ph.D. thesis, Aarhus University, Denmark.

Hütt, G., Jaek, I., and Tchonka, J. (1988). Optical dating: K-feldspars optical response stimulation spectra. *Quaternary Science Reviews*, 7:381–385.

Itoh, C., Tanimura, K., Itoh, N., and Itoh, M. (1989). Threshold energy for photogeneration of self-trapped excitons in SiO_2. *Physical Review B*, 39:11183–11186.

Jain, M., Murray, A. S., and Bøtter-Jensen, L. (2003). Characterisation of blue-light stimulated luminescence components in different quartz samples: implications for dose measurement. *Radiation Measurements*, 37:441–449.

Malins, A. E. R., Poolton, N. R. J., Quinn, F. M., Johnsen, O., and Denby, P. M. (2004). Luminescence excitation characteristics of Ca, Na and K aluminosilicates (feldspars) in the stimulation range 5–40 eV: determination of the band-gap energies. *Journal of Physics D: Applied Physics*, 37:1439–1450.

Murray, A. S. and Wintle, A. G. (1999). Isothermal decay of optically stimulated luminescence in quartz. *Radiation Measurements*, 30:119–125.

Ogundare, F. O. and Chithambo, M. L. (2007). Time resolved luminescence of quartz from Nigeria. *Optical Materials*, 29:1844–1851.

Ogundare, F. O. and Chithambo, M. L. (2008). The influence of optical bleaching on lifetimes and luminescence intensity in the slow component of optically stimulated luminescence of natural quartz from Nigeria. *Journal of Luminescence*, 128:1561–1569.

Pagonis, V., M., M. S., Chithambo, M. L., Christensen, E., and Barnold, C. (2009). Experimental and modelling study of pulsed optically stimulated luminescence in quartz, marble and beta irradiated salt. *Journal of Physics D: Applied Physics*, 42:1–12.

Poolton, N. R. J., Wallinga, J., and Murray, A. S. (2002a). Electrons in feldspar I: on the wavefunction of electrons trapped at simple lattice defects. *Phys. Chem. Minerals*, 29:210–216.

Poolton, N. R. J., Ozanyan, K. B., and Wallinga, J. (2002b). Electrons in feldspar II: a consideration of the influence of conduction band-tail states on luminescence process. *Phys. Chem. Minerals*, 29:217–225.

Sanderson, D. C. W. and Clark, R. J. (1994). Pulsed photostimulated luminescence of alkali feldspars. *Radiation Measurements*, 23:633–639.

Singarayer, J. S. and Bailey, R. M. (2003). Further investigations of the quartz optically stimulated luminescence components using linear modulation. *Radiation Measurements*, 37:451–458.

Thomsen, K. J., Bøtter-Jensen, L., Denby, P. M., Moska, P., and Murray, A. S. (2006). Developments in luminescence measurement techniques. *Radiation Measurements*, 41:768–773.

Thomsen, K. J., Jain, M., Murray, A. S., Denby, P. M., Roy, N., and Bøtter-Jensen, L. (2008). Minimizing feldspar OSL contamination in quartz UV-OSL using pulsed blue stimulation. *Radiation Measurements*, 43:752–757.

Tsukamoto, S., Denby, P. M., Murray, A. S., and Bøtter-Jensen, L. (2006). Time-resolved luminescence from feldspars: New insight into fading. *Radiation Measurements*, 41:790–795.

Wintle, A. G. (1973). Anomalous fading of thermoluminescence in mineral samples. *Nature*, 245:143–144.

Wintle, A. G. (1977). Detailed study of a thermoluminescent mineral exhibiting anomalous fading. *Journal of Luminescence*, 15:385–393.

Chapter 2

Development of pulsed stimulation and Photon Timer attachments to the Risø TL/OSL reader

T. Lapp, M. Jain, C. Ankjærgaard, L. Pirtzel

Radiation Research Department, Risø National Laboratory for Sustainable Energy — Technical University of Denmark, NUK-201, P.O. Box 49, DK-4000 Roskilde, Denmark

Abstract

Pulsed stimulation has earlier been proven useful for several applications in dosimetry and luminescence research. Pulsed stimulation has been integrated in the Risø TL/OSL reader along with a software control built into the Sequence Editor. To facilitate research of the lifetime or delay involved in the OSL/IRSL process, a Photon Timer attachment to the Risø reader has been developed which measures data at 100 ps resolution. Furthermore a post-processing program has been developed to present the data in a compressed 3D form that gives a useful overview of the data before further analysis of relevant data. An example of how the Photon Timer has been used to characterise the performance of the pulsed stimulation unit is presented.

Keywords: Pulsed OSL, time-resolved OSL, Photon Timer, photon arrival time distribution, quartz, feldspar.

2.1 Introduction

Pulsed optical stimulation has been shown to be a powerful method in optically stimulated luminescence (OSL) based dosimetry both for increasing the signal-to-background ratio and for studying characteristics of charge recombination in the dosimeter of interest (Sanderson and Clark, 1994). OSL involves several

steps which may all give rise to a delay between the stimulation and the emission of luminescence light. When using continuous stimulation and concurrent detection of luminescence signal (CW-OSL or Continuous-Wave OSL) one cannot identify the rate governing steps involved from electron detrapping to the eventual production of luminescence. Stimulating the sample with a series of optical pulses and measurement of the luminescence signal during and/or after each pulse provides one way to examine these intermediate processes.

Pulsed stimulation together with time-resolved data acquisition has been widely used to study luminescence lifetimes of quartz and feldspars (Clark et al., 1997; Sanderson and Clark, 1994; Bailiff, 2000; Chithambo and Galloway, 2000). These studies describe in details the many possibilities of pulsed stimulation. Pulsed LED stimulation has also been used to study the effect of thermal annealing on the luminescence lifetimes and thus in turn obtain information on the redistribution of charge in the crystal (Chithambo and Galloway, 2000; Chithambo, 2007, and references therein).

As far as routine dosimetry is concerned, there have been two main applications of pulsed stimulation. Firstly, if the stimulation and detection wavelengths are closely located, e.g. green–blue or blue–UV, a significant reduction in background could be achieved by using pulsed stimulation and gating the detection between the stimulation pulses (e.g. McKeever et al., 1996; Sanderson and Clark, 1994). Secondly, pulsed stimulation could be used for isolating mineral specific luminescence from a mixed sample if the lifetimes of the signals from the two phases are widely separated. An example of the latter is a successful separation of quartz signal from a feldspar contaminated quartz sample by using blue LED pulse stimulation (Denby et al., 2006; Thomsen et al., 2008). These authors showed that the pulsed stimulation approach can tolerate very high level of feldspar contamination almost rendering any need for chemical pre-treatment unnecessary (Thomsen et al., 2008). There is also some evidence that pulsed stimulation can isolate a more stable (less fading) signal in feldspars (Tsukamoto et al., 2006; Sanderson and Clark, 1994). Because of these important advantages of pulsed stimulation in OSL dosimetry using natural sediments, it is desirable to have a system that can be easily used for routine measurements. The first prototype attachment capable of pulsing IR and blue LEDs in the Risø TL/OSL reader together with a gated detection was presented by Denby et al. (2006). These authors also presented time-resolved data acquisition with a prototype of a so-called fast counter. Since then the two attachments have been further improved and integrated into the Risø TL/OSL reader system. In the current paper we further describe these improvements in pulsing and data acquisition and the new software for visualisation and data analysis.

2.2   Semantics and methods

The following terminology has been used throughout the paper.

- *On-time* is the duration of each stimulation pulse.

- *Off-time* is the duration of the pause before the next stimulation pulse.

- *Pulse period* is the inverse of *pulse frequency* and refers to combined *on-time* + *off-time*.
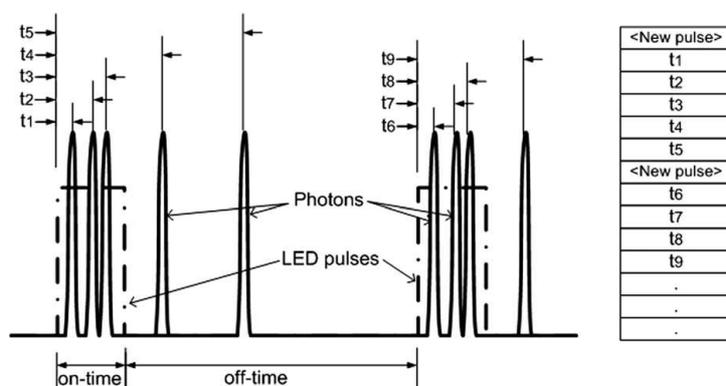
Figure 2.1: Diagram showing the principle of Photon Timer data recording. The list to the right illustrates the sequential listing of events.

- *Stimulation time* is the time elapsed since the start of the OSL stimulation.

- *Photon arrival time* is the time elapsed since the start of the preceding stimulation pulse to the emission of a luminescence photon.

Time-resolved data acquisition may be done in several ways. The method previously used by Sanderson and Clark (1994), Clark et al. (1997) and Chithambo (2002) has been based on the use of a multichannel scaler. A multichannel scaler records the distribution of *photon arrival times*. One may record several distributions during the total *stimulation time* and in this way have the possibility of studying the development of the *photon arrival time distribution*.

Alternatively, one may time stamp arrival of every photon with respect to the preceding pulse. The principle of *Photon Timer* recording of data is illustrated in Fig. 2.1.

A *Photon Timer* records all events sequentially in a list file. For each stimulation pulse a marker is inserted in the list file, and each photon detected during the subsequent *pulse period* is recorded as the *photon arrival time*. Luminescence is however a rather inefficient process and therefore individual stimulation pulses with peak intensity of for example 40 mW/cm^2 generate only a few detectable photons from the sample per pulse period. Adding up the luminescence response of several thousands of pulses gives a *Photon Arrival Time Distribution* which could then be used to determine the characteristic lifetimes of the luminescence (phosphorescence) decay. This data collection method generates a large amount of raw data, but gives a full flexibility in post-processing of the data e.g. changing the binning of time-resolved data, summing of pulses, and the channel numbers corresponding to the total *stimulation time*. This method has been used widely in nuclear science for many years and Denby et al. (2006) applied this method to OSL with their own dedicated electronic design termed a fast counter. Because of its increased capabilities we have now used a commercially available board for what we now refer to as a *Photon Timer*.
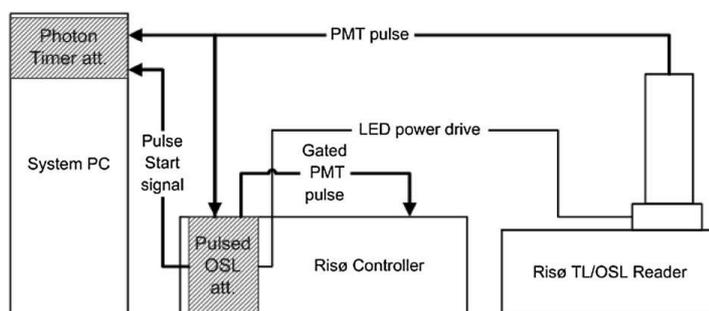
Figure 2.2: Block diagram of Risø TL/OSL reader system with pulsed OSL and Photon Timer attachments.

In the following sections we describe the two new hardware features now available for the Risø reader viz. pulse stimulation attachment and Photon Timer, and the software designed for measurement, visualisation and data analysis. Some measurement examples are shown to demonstrate the hardware and software capabilities.

2.3   Pulsed stimulation attachment

A block diagram of the Risø TL/OSL reader DA-20 system with a *Pulsed Stimulation attachment* and a *Photon Timer* is shown in Fig. 2.2.

In contrast to the prototype, which consisted of a separate box attachment with manual parameter settings, the *Pulsed OSL attachment* is now installed in the Risø controller. It is performing the following tasks:

- Receiving the set-up of pulse parameters from the controller via an SPI bus interface.

- Regulating the power of the stimulation LEDs to the prescribed level.

- Turning on the periodic pulsing when ordered by the controller.

- Implementing linearization of the power output.

This integration of the pulsed attachment into the controller makes it possible to use software settings for adjusting on-time, off-time and peak power. Pulse power can be adjusted from 1% to 99%. 100% power corresponds to approx. 145 mW/cm^2 for IR LED and 50 mW/cm^2 for blue LEDs at sample position. The power regulation is based on feedback from a photodiode in the OSL stimulation head. The processor samples the LED power during the stimulation pulses, and a moving average of the LED power is used for regulating the power to the prescribed level. The attachment may do an auto-linearization that assures that the output power is correct in the entire power range. The *Sequence Editor*, which is the program executed on the System PC (cf. Fig. 2.2) that controls the data acquisition, has been modified to include a POSL command that makes it possible to set up the pulse parameters. The

Table 2.1: Relevant specifications for ORTEC 9353 Time Digitizer board.

Time resolution	100 ps
Dead time:	1 ns
Buffer sizes:	
Fast FIFO	256 words (count rate < 1 Gs^{-1})
Slow FIFO	8 Mwords (count rate < 33 Ms^{-1})
Acquisition memory	PC RAM and hard disk size (count rate $<$ approx. 10 Ms^{-1})

on-time can be adjusted from 0.2 μs to 9.9 s, and the *off-time* from 0.6 μs to 9.9 s.

The *Pulsed Stimulation attachment* has the ability to gate the photon pulses such that only photon pulses detected in the *off-time* will be passed on to the photon counter in the controller. Parameters controlling the detailed position of the *gating period* within the *off-time* may be specified from the POSL command in the *Sequence Editor*. The gating makes it possible to minimize the contribution of feldspar contamination to the OSL signal as described by Thomsen et al. (2008), and also gives an additional possibility to move the detection filter closer to the stimulation wavelength. The latter feature could be useful to optimise detection of the 380 nm emission in quartz which is not otherwise possible with blue LED based stimulation in a continuous-wave mode.

2.4 Photon Timer attachment

The *Photon Timer* is based on an *ORTEC 9353 100 ps Time Digitizer board*. This board is operated in list mode, which gives *Photon Timer* data files as described for Fig. 2.1. The important specifications for this application are listed in Table 2.1.

The photon count signal is shaped by the controller electronics to be a 12 ns long pulse. Therefore the dead time of 1 ns (minimum distance between photons registered by the *Photon Timer*) means that no photon events are missed due to the *Photon Timer*. The time resolution of the time digitizer is 0.1 ns. The precise accuracy of the rising edge of the 12 ns PMT pulses relative to the emission of the photons is not known, so the overall accuracy of the time stamping may be > 0.1 ns. The buffer system of the board and PC ensures that generally an average count rate of 10 ms^{-1}, and in burst up to 1 Gs^{-1}, may be achieved, which will be sufficient as the PMT starts saturating at about 5 Ms^{-1}. However, as the PCI bus of the system PC may be serving other units at the same time, buffer overflow may occur in theory. However, buffer overflow will be signalled by the data acquisition software and written to the data file, such that the post-processing program may issue a warning about buffer overflow, when the data is used. The *Photon Timer* data acquisition is controlled from *Sequence Editor*.

2.5   Data visualisation and analysis

The gated pulsed OSL data is recorded as an OSL decay curve with integrated gated counts as a function of the *stimulation time*. The data is recorded in a bin file which can then be read and analysed using the Analyst software.

For the Photon Timer data a post-processing program *PTanalyse* has been developed to give different ways of presenting, analysing and exporting data. An overview of the data is presented as a 3D *TR-POSL surface plot* which plots time-resolved photon count rate during a *pulse period* as a function of *stimulation time*. The *pulse period* is divided into a number of *bins*. The lowest possible bin size is the resolution of the *Photon Timer* i.e. 100 ps. The bin size is specified as $2^n \times 100$ ps as this gives a very fast calculation time. The total *stimulation time* is divided into a number of *channels*. The channel width is specified as a number of *pulse periods*.

Examples of such surface plots for typical quartz and a feldspar samples are shown in Fig. 2.3a and b. The 3D surface shows the number of counts within each bin and channel. The bin and channel widths may be changed to give the desired resolution on both *photon arrival time* axis and *stimulation time* axis. When making the *bin* and/or *channel* width smaller you may have such a small number of counts within a *bin-channel* cell that the Poisson noise of the counts will blur the overview. The viewing angle of the 3D surface plot may easily be controlled with a mouse in order to get the best view of the data.

The two most important ways of further processing the data are to integrate cross-sections in either *X-Z* or *Y-Z* plane. Summing of time-resolved data in several *X-Z* planes in a given stimulation time interval produces a *photon arrival time distribution* for that interval. Likewise the integration of counts for a specified range of *photon arrival times* produces a *POSL curve* for that *photon arrival time interval*. This presentation is similar to what could also be obtained using a gated counting system. However, the advantage of acquiring the 3D data is that one can produce an apparent *POSL curve* or gated POSL decay curve for any gating period from a single data set measured only once. In order to obtain the same results with gated OSL one would require re-measuring the data for all those intervals; this may not always be possible if the signal is destroyed after the first measurement, for example, as in case of the natural OSL.

2.6   Application example — characterisation of LED light pulse

The *Photon Timer* attachment has been used to measure the shape of the stimulation LED output. For measuring the pulse shape, the standard detection filter has been removed and instead an attenuator (greyscale filter combined with a pin-hole) has been inserted to avoid saturation of the PM tube.

The shape of the blue LED stimulation pulses is shown in Fig. 2.4a and b. The distributions are shown with a resolution of 25.6 ns, as a further increase of resolution does not reveal any more details. It is noted that the rise time of the blue LED stimulation pulses is in the order of 200 ns and the fall time is in the order of 100 ns. It is worth noting that such a resolution was not possible with the earlier system described by Denby et al. (2006).
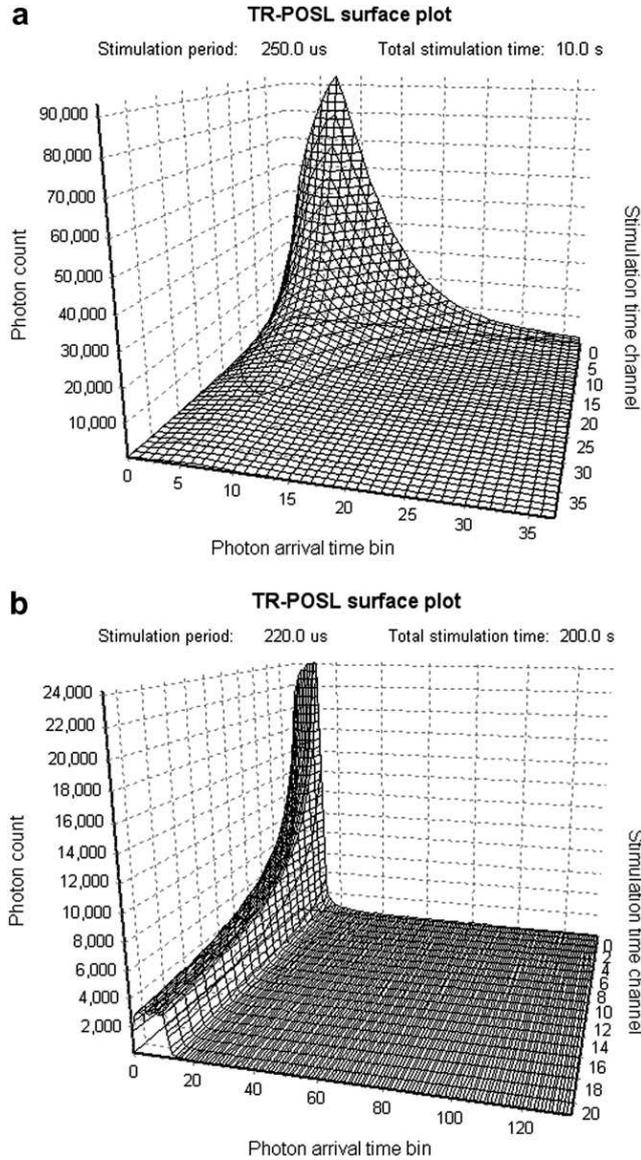
Figure 2.3: (a) PTanalyse TR-POSL surface plot of a quartz sample with on-/off-time of 50/200 μs. Bin width: 0.1 ns $\times 2^{16} = 6.55$ μs, channel width: 1000 pulse periods = 250 ms, irradiation: 10 Gy, preheat at 260°C, blue LED stimulation at 125 °C. (b) PTanalyse TR-POSL surface plot of an orthoclase feldspar sample with on-/off-time of 20/200 μs. Bin width: 0.1 ns $\times 2^{14} = 1.64$ μs, channel width: 40,000 pulse periods = 8.80 s, irradiation: 500 Gy, preheat at 250°C, blue LED stimulation at 50°C.
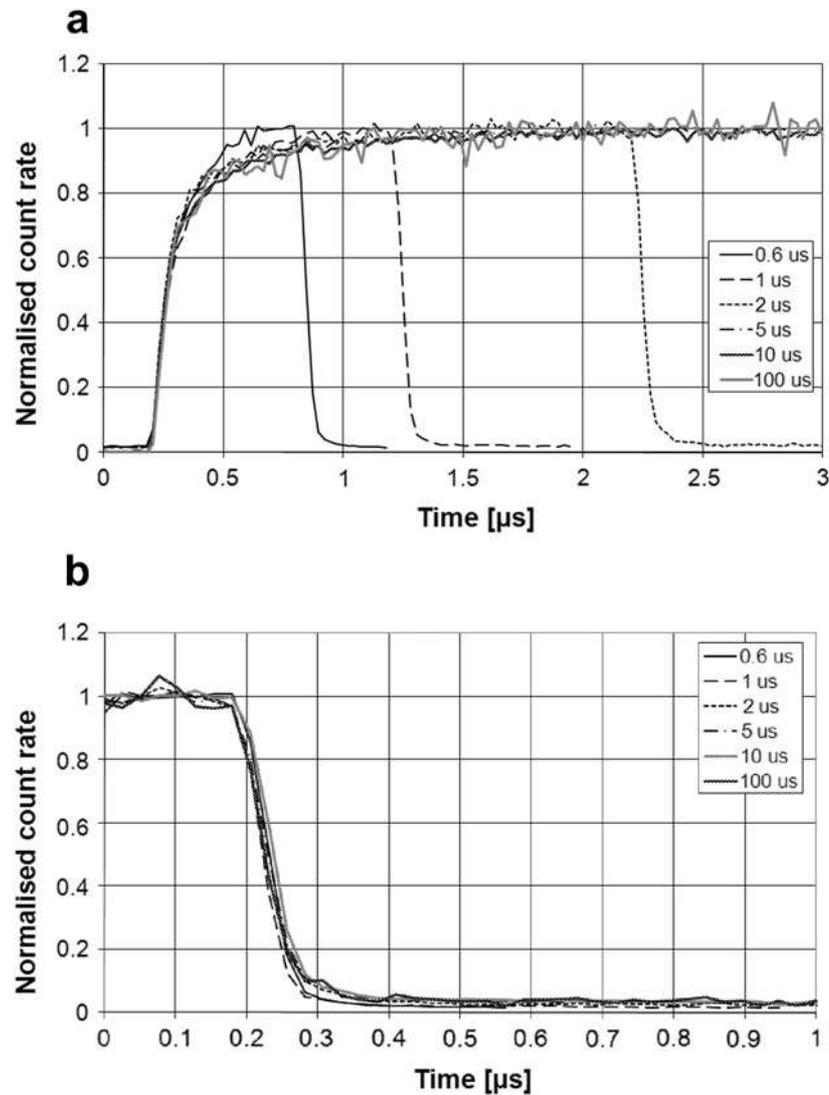
Figure 2.4: (a) The shape of the turn on part of the blue LED stimulation pulses for different pulse widths. Time resolution on plot: 25.6 ns. (b) The shape of the turn off part of the blue LED stimulation pulses for different pulse widths. Time resolution on plot: 25.6 ns.

The shape of the IR LED stimulation pulses is shown in Fig. 2.5. It should be noted that the rise time is significantly slower than for the blue LEDs and in the order of 1-2 μs. The fall time is like for the blue LEDs in the order of 100 ns. This means that the power regulation does not work properly for short pulses and this should be taken into consideration if IR stimulation pulses shorter than approx. 5 μs are used.

In Ankjærgaard et al. (2009, Chapter 7 of this thesis) it is shown that the fall time of the blue LEDs of approx. 100 ns is too slow to enable study of the
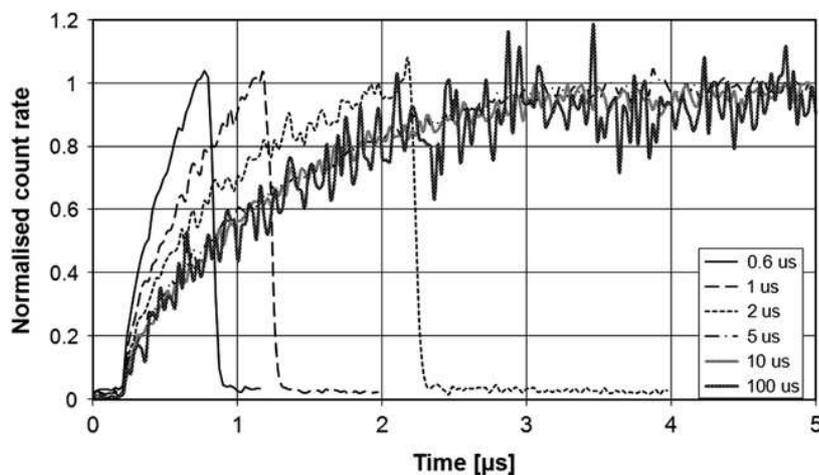
Figure 2.5: The shape of the turn on part of the IR LED stimulation pulses for different pulse widths. Time resolution on plot: 25.6 ns.

fastest lifetimes in the feldspar OSL process.

2.7 Conclusion

Gated pulsed OSL (*POSL*) and Time-resolved pulsed OSL (*TR-POSL*) can now be used within a routine measurement sequence in the Risø reader. Time-resolved data is acquired using a *Photon Timer* which works on the principle of photon time stamping at 100 ps resolution. This data can be visualised and exported by a versatile post-processing program in the most appropriate way for the purpose. The software uses a *3D TR-POSL surface plot* as a standard way of presenting the time-resolved data; different section of this plot can be derived depending on the application.

A high-resolution (100 ps) measurement of blue and IR LED pulses in the Risø reader has been possible for the first time. It is observed that IR pulses have a much longer rise time than the blue pulses, however, both these fall at approximately the same rate at the end of the pulse. These rise and fall times are not significant for quartz since the luminescence decay occurs at 10s of microseconds. However, the *photon arrival time distribution* of a feldspar sample generally follows the fall time of the stimulation light followed by some slower decay. This implies that the currently used pulsed stimulation LED unit is inappropriate for studying the characteristics of the fast decaying phosphorescence signal in feldspars. The *Photon Timer* used with the Risø system is however capable of measuring nanosecond scale decay rates from feldspar luminescence if the data is produced using a stimulation light source that switches off faster than the current pulsed stimulation unit.

Acknowledgments

We thank A.S. Murray for many fruitful discussions.

References

Ankjærgaard, C., Jain, M., Kalchgruber, R., Lapp, T., Klein, D., McKeever, S. W. S., Murray, A. S., and Morthekai, P. (2009). Further investigations into pulsed optically stimulated luminescence from feldspars using blue and green light. *Radiation Measurements*, 44:576–581.

Bailiff, I. K. (2000). Characteristics of time-resolved luminescence in quartz. *Radiation Measurements*, 32:401–405.

Chithambo, M. L. (2002). Time-resolved luminescence from annealed quartz. *Radiation Protection Dosimetry*, 100:273–276.

Chithambo, M. L. (2007). The analysis of time-resolved optically stimulated luminescence: II. Computer simulations and experimental results. *J. Phys. D: Appl. Phys.*, 40:1880–1889.

Chithambo, M. L. and Galloway, R. B. (2000). A pulsed light-emitting-diode system for stimulation of luminescence. *Meas. Sci. Technol.*, 11:418–424.

Clark, R. J., Bailiff, I. K., and Tooley, M. J. (1997). A preliminary study of time-resolved luminescence in some feldspars. *Radiation Measurements*, 27:211–220.

Denby, P. M., Bøtter-Jensen, L., Murray, A. S., Thomsen, K. J., and Moska, P. (2006). Application of pulsed osl to the separation of the luminescence components from a mixed quartz/feldspar sample. *Radiation Measurements*, 41:774–779.

McKeever, S. W. S., Markey, B. G., and Akselrod, M. S. (1996). Pulsed optically stimulated luminescence dosimetry using α-Al_2O_3:C. *Radiation Protection Dosimetry*, 65:267–272.

Sanderson, D. C. W. and Clark, R. J. (1994). Pulsed photostimulated luminescence of alkali feldspars. *Radiation Measurements*, 23:633–639.

Thomsen, K. J., Jain, M., Murray, A. S., Denby, P. M., Roy, N., and Bøtter-Jensen, L. (2008). Minimizing feldspar OSL contamination in quartz UV-OSL using pulsed blue stimulation. *Radiation Measurements*, 43:752–757.

Tsukamoto, S., Denby, P. M., Murray, A. S., and Bøtter-Jensen, L. (2006). Time-resolved luminescence from feldspars: New insight into fading. *Radiation Measurements*, 41:790–795.

Chapter 3

Towards multi-exponential analysis in optically stimulated luminescence

C. Ankjærgaard[1], M. Jain[1], P. C. Hansen[2], H. B. Nielsen[2]

[1] *Radiation Research Division, Risø National Laboratory for Sustainable Energy, Technical University of Denmark, DK-4000 Roskilde, Denmark.*
[2] *Department of Informatics and Mathematical Modelling, Technical University of Denmark, DK-2800 Kgs. Lyngby, Denmark.*

Abstract
Optically Stimulated Luminescence (OSL) data from quartz can follow different mathematical forms depending on the stimulation mode. These data can be described in terms of different multi-exponential models and can be numerically fitted using several well-known methods. Here we make a comparative analysis of the performance and stability of two models, the decay and peak form, and we consider different transformation methods for obtaining the peak form. For the numerical computations we use a nonlinear least squares (NLS) method and a method based on a first-kind Fredholm integral equation (FIE). Our analysis uses artificial data with three components (seven parameters including the background), and ten different levels of background, both the signal and the background contain Poisson distributed noise. Parameters derived using both models are acceptable (statistically consistent and on an average within $\sim 1\%$ of the expected value) and no obvious preference is observed for any particular model, although there may be a suggestion that peak form data shows a smaller mean bias. This conclusion seems to be independent of the type of peak transformations investigated here. Furthermore, it is found that transformation of OSL decay data to a peak form gives better results than direct measurement of peak form data by, for example, varying the stimulation light intensity. The comparison of the two numerical methods suggests that the NLS method performs somewhat better than the FIE method; however, the latter has the advantage that it does not require the user's judgement on the number of components in the data. Testing of the NLS procedure on a measured quartz time-resolved OSL signal (TR-OSL) transformed

into peak form yielded reliable parameter estimates even when the signal intensity was deliberately reduced by a factor of sixteen.

3.1   Introduction

Luminescence is extensively used to determine absorbed dose (J/kg) in wide band gap insulators due to exposure to ionizing radiation. The dosimeters used are usually natural crystals, e.g., quartz and feldspars, or impurity doped artificially grown crystals such as lithium fluoride, aluminium oxide, etc. The irradiation of these crystals results in creation of free electrons and holes which are subsequently trapped in localised states (lattice defects) known as traps and recombination centres within a crystal, respectively. These trapping states thus store information about the absorbed dose, and the information can be read out in the form of luminescence by exposing the crystal to visible or near IR photons having sufficient energy to cause photoionisation of the occupied defects. Electron-hole recombination following photoionisation is the critical light generating step, and the resulting signal carrying dosimetric information is known as optically stimulated luminescence (OSL). Traditionally, OSL measurements use a constant, continuous flux of incident photons (CW-OSL); this results in a signal that usually shows monotonic decay with time. The OSL technique is widely used for estimation of absorbed dose from ionising radiation in wide ranging applications related to nuclear accidents, cosmic radiation in space, radiation facilities in health and power sectors, and in geochronology, i.e., dating sediments during the last 0.5 million years or so [see Bøtter-Jensen et al. (2003) for an overview].

In addition to being of use for dosimetry, the OSL signal contains information about the distribution of traps and recombination centres in the crystal, and together with other techniques OSL signals can provide insights into the charge excitation, movement, and recombination in crystals. Such insights are vital to our understanding of the luminescence mechanism.

There are at least two instances where the OSL signal has a multi-exponential decay form:

1. CW-OSL of quartz: In case of natural quartz (the most commonly used material in accident dosimetry and sediment dating), for example, it is generally argued that the monotonic decaying CW-OSL emitted during exposure to blue light of constant intensity consists of several transients having an exponential form (Smith and Rhodes, 1994). The lifetimes of these transients are related to the photo-ionisation cross-sections (proportional to the decay constant) of the electron traps that participate in the luminescence process (Bailey et al., 1997). In natural quartz from around the world, up to seven electron trapping states have been identified to participate in the OSL process (Jain et al., 2003; Singarayer and Bailey, 2003).

2. Pulsed OSL: An alternative method to stimulate a crystal is by pulsing the light intensity to obtain pulsed OSL. The signal measured during and between the light pulses is known as time-resolved OSL (TR-OSL). The processes that govern these signals are generally exponential in nature; in case of quartz the TR-OSL measured between the pulses is a decaying signal and consists of a dominant exponential transient having a lifetime between 30 and 45 μs and two relatively minor transients having relatively shorter and longer lifetimes than the main transient when using standard quartz dating procedure (preheating to 260°C for 10 s and stimulating at 125°C) (Chithambo et al., 2007; Pagonis et al., 2009; Ankjærgaard et al., 2010, Chapter 10 of this thesis). These lifetimes reflect the relaxation of the excited state following electron hole-recombination (Chithambo, 2007; Pagonis et al., 2010, Chapter 4 of this thesis).

Thus, the experimental data acquired during either continuous stimulation (CW-OSL) or between the pulses in pulsed stimulation (TR-OSL) of quartz, and perhaps also other dosimeters, can be described by the model:

$$I_{\text{decay}}(t) = \sum_{i=1}^{n} N_i \lambda_i \exp\left(-\lambda_i t\right) + b + \xi(t), \qquad 0 \leq t \leq T, \qquad (3.1)$$

where t is the time, N_i is proportional to the initial population undergoing decay, and λ_i is the decay constant for each of the n components in the signal. The constant $b \geq 0$ accounts for any background light and dark counts of the detector, and $\xi(t)$ represents the noise in the data. The purpose of such multi-component analysis is to determine the constants n, N_i and λ_i from the measured data, as these quantities give information on the relative number density and a physical characteristic of the trap or centre such as photoionisation cross-section or recombination/relaxation lifetime, respectively.

In case of CW-OSL, the model [Eqn. (3.1)] applies only in the case of negligible retrapping (first order kinetics); this is applicable, e.g., to the fast, medium and some of the slow components in quartz [see Jain and Lindvold (2007a)], but may not be applicable to all dosimeters. In TR-OSL the two dominant processes, i.e., the electronic transition from the conduction band to the recombination centre, and the relaxation of the excited state of the recombination centre, both follow first order kinetics. However, there are some materials that have non-first order processes, e.g., tunnelling, which will follow a different mathematical form. As discussed later a more general case can be defined using a spectral function for a continuous trap distribution; this can be reduced to a sum of n delta functions for discrete traps (Istratov and Vyvenko, 1999).

In addition to better the understanding of the OSL processes, it is also highly desirable that we can estimate the individual transients in the OSL for higher accuracy in retrospective dosimetry [see, e.g., Jain et al. (2005)]. This objective can be achieved by fitting some form of Eqn. (3.1) to the CW-OSL or the TR-OSL data. Unfortunately, fitting multiple exponential functions is an ill-posed problem (e.g., see an excellent review by Istratov and Vyvenko (1999)). Bulur (1996) suggested that fitting of multi-exponential OSL data could be made more robust if the data had a peak form rather than a monotonic decay form. An OSL peak form could be obtained experimentally by linearly

increasing the stimulation light intensity during the OSL measurement; this technique was named as linearly modulated OSL (LM-OSL) (Bulur, 1996). LM-OSL results in a signal that can be described by the following model:

$$I_{\mathrm{peak}}(t) = \sum_{i=1}^{n} \frac{N_i \lambda_i}{T} t \cdot \exp\left(-\frac{\lambda_i t^2}{2T}\right) + b + \xi(t), \qquad 0 \le t \le T, \qquad (3.2)$$

where T is the total measurement time, and N_i, λ_i, b, and $\xi(t)$ are as described above. Bulur (2000) and Poolton et al. (2003) have further shown that the same peak shaped signal could be achieved by transformation of the monotonically decaying multi-exponential data (assuming first order kinetics). However, note that the transformation approach (to be discussed below) produces a linearly increasing background as a function of stimulation time t.

Although the shape of the LM-OSL curve is fundamentally different from the CW-OSL curve, the physical process causing them and the information contained in the two types of data are identical; the apparent differences arise because we view data in the time domain rather than in the event domain (Jain and Lindvold, 2007a). If one considers the probability of luminescence light produced per incident stimulation photon, and if there are two components X and Y ($n = 2$) then

$$\frac{a_{\mathrm{X}}}{a_{\mathrm{Y}}} = \frac{a_{\mathrm{X}_0}}{a_{\mathrm{Y}_0}} \exp\left[(\sigma_{\mathrm{Y}} - \sigma_{\mathrm{X}})\Phi\right] \qquad (3.3)$$

where a_{X} and a_{Y} are the number density of the trapped electrons (cm^{-3}) for the two different traps X and Y, a_{X_0} and a_{Y_0} are the initial concentrations, Φ defines the time integrated number of excitation photons per unit area (fluence in cm^{-2}), and σ_{X} and σ_{Y} (cm^2) are the photoionisation cross-sections. For a given OSL measurement, $a_{\mathrm{X}_0}/a_{\mathrm{Y}_0}$ and $\sigma_{\mathrm{Y}} - \sigma_{\mathrm{X}}$ are constant; therefore, for a given photon fluence, the ratio of the light output from any two components will be constant, no matter how that fluence was achieved in time. In the time domain, however, different shapes of luminescence intensity can be achieved by varying the fluence-rate or flux during the measurement, i.e., $\mathrm{d}\Phi/\mathrm{d}t = I(t)$, but the actual overlap of the signals will not differ for a given fluence (Jain and Lindvold, 2007a). This problem has also been investigated by Wallinga et al. (2008) and Bos and Wallinga (2009b) in which several interesting examples of the data forms obtained by changing incident photon flux were studied. Nonetheless, it was concluded that the separation of the components at any given time was the same for all the different stimulation modes. One method of increasing the physical separation of the transients is differentiation of the OSL signal (Bos and Wallinga, 2009a); however, this approach is not suited to low amplitude, slowly decaying components because of low signal-to-noise ratio. Since the nature of multi-exponential decay and multi exponential peak data (in other than differentiation based methods) are fundamentally identical, it has been discussed in the literature whether peak-form data has in fact any advantage over the decay-form data for exponential analysis (Huntley, 2006, 2007; Jain and Lindvold, 2007a,b; Wallinga et al., 2008; Bos and Wallinga, 2009a,b). However, this question has not been thoroughly investigated to date.

The aim of this work is to carry out a comparative analysis of the performances of the two above-mentioned data collection systems, decay and peak form, in predicting the 'true' trap parameters. This analysis is based on artificially generated multi-exponential TR-OSL data with seven parameters.

We use two fundamentally different numerical approaches which have previously been used for fitting luminescence signals by different workers viz. a) multi-exponential analysis using a nonlinear least squares (NLS) formulation solved by a Levenberg-Marquardt approach [see, e.g., Jain et al. (2003)], and b) the spectroscopic analysis using a first-kind Fredholm integral equation (FIE) (Agersnap, 1997; Whitley and McKeever, 2001); also see the review by Istratov and Vyvenko (1999) with a view to derive a general protocol for multiexponential analysis of three discrete OSL components. The NLS method is a standard method for fitting data and is implemented in most mathematical and statistical software packages. This method requires that the number of exponential components is specified beforehand by the user. The FIE method is a radically different approach compared to NLS as this method automatically determines the number (or spectrum) of components without prior user input. These approaches are briefly described in Section 3.5. We emphasize that our goal is (primarily via simulation studies) to compare the above-mentioned methods for analysing OSL and TR-OSL data, with a focus on the robustness of the estimation of the parameters N_i and λ_i in the underlying OSL models. We note that related work in Hansen et al. (2010) focused on the fitting (or prediction) abilities of the two methods based on the properties of the residuals; we note that this is an altogether different mathematical problem and leads to a different conclusion than in the present study where the focus is on the precision and accuracy of the derived parameters.

3.2 Instrumentation and methods

Much of this paper uses artificial data. However, laboratory measurements on a quartz sample are used to test the methods and to generate realistic artificial data for exponential analysis. These measurements were undertaken using a colluvium quartz sample from Tanzania, sample: 963602 consisting of 150–300 μm grains. The grains were extracted from the bulk sample by sieving, heavy liquid separation, and HF treatment as described in Wintle (1997). Sample measurements were carried out on a Risø TL/OSL-20 reader with an integrated pulsing option to control the stimulation LEDs, and with a photon timer attachment with detection resolution of 100 ps to record the TR-OSL data (Lapp et al., 2009, Chapter 2 of this thesis). The apparent bin-resolution can be redisplayed after data collection, as it is specified as $2^n \times 100$ ps. Blue light stimulation was performed with a 470 ± 30 nm LED array delivering 50 mW/cm^2 at the sample, and a 7.5 mm thick Hoya U340 filter detecting between 340–350 nm was inserted beneath the photomultiplier tube (PMT).

The TR-OSL data are recorded by time-stamping photons emitted from beta irradiated and preheated (260°C for 10 s) samples between the stimulation light pulses at 125°C. The net signal is then derived by summing several hundred thousands of these light pulses emitted from the sample. The duty cycle consisted of a 50 μs on-time and a 500 μs off-time. The data are then summed up to be presented at the resolution of 0.4 μs.

In addition to the OSL counts, the PMT will register counts that constitute a background to the OSL signal. Background counts are generated by thermal excitation of electrons in the photocathode, system electronics, and interac-

tion of the detector with cosmic radiation, which together constitute the 'dark counts' of the PMT, and any scattered or stray light from the stimulation source. As it is important to include these in the artificial data model, the background counts were also measured in the same way as above but using an annealed quartz sample (700°C for 5 min to remove nearly all trapped charge) instead of a beta irradiated sample. Note that in pulsed OSL measurements, the stimulation light is switched off, therefore for the annealed sample, the background would be equivalent to the 'dark counts' of the detector.

3.3   Data simulation for decay-form data

Artificial TR-OSL data was created in order to compare the performance of different methods, and the data comprises two contributions - the light from the sample and the background counts.

In order to generate artificial data it is first important to understand the PMT counting statistics for these two processes; this involves measurement of a constant count rate by the detector and determination of the mean and spread in the distribution of the counts. Since the TR-OSL is a decaying signal it cannot as such be used for this type of analysis. Therefore, we used a constant light source; blue LEDs operated with attenuated detection (a neutral density filter inserted underneath the PMT instead of the U340 filter) is used to do the statistical analysis applicable to signal counts. We generated a similar count rate as the sample, and this was used to mimic the distribution of luminescence counts. Data was collected during a 500 µs on-time. The background was measured in the same way as TR-OSL but on an annealed sample. Figure 3.1a shows the distribution of the background noise for a data resolution set to ~ 0.4 µs, and a Poisson distribution function with a mean of 5.7 cts/(0.4 µs) (derived from integration of 40,000 pulse stimulations) has been fitted to the data (black line). A Matlab Chi-square goodness-of-fit test could not reject the hypothesis that the data is Poisson distributed with the probability of observing the given result: $p = 0.9957$. Therefore, in our artificial data model, we can assume that our instrumental background noise is Poisson distributed.

The distribution of counts from the LEDs is shown in Fig. 3.1b, with the same resolution as in Fig. 3.1a, where it has been fitted to a Poisson distribution with a mean value of 14.8 cts/(0.4 µs) shown as the black line. The Chi-square goodness-of-fit test rejected the hypothesis that the diode noise data is Poisson distributed with a probability of $p = 2.21 \cdot 10^{-9}$. It is very likely that this distribution is not perfectly Poisson distributed as the dark count noise is also contained in this data, and so the condition to test whether the distribution is a single Poisson distribution is in fact false. For practical purposes, as can be seen in the figure, the data approximates a Poisson distribution, and so we will assume that the noise in the TR-OSL signal follows a Poisson distribution.

The values of the decay constants and amplitudes for generating the artificial data analogous to the TR-OSL of quartz in the 380 nm emission is based on experimental values found by Chithambo et al. (2007). The artificial data is chosen to contain three exponential transients following Eqn. 3.1 with amplitudes $A_i = N_i \cdot \lambda_i$ [cts/(0.408 µs)] and decay constants λ_i (µs^{-1}) of $A_1 = 7000$, $\lambda_1 = 0.500$, $A_2 = 20000$, $\lambda_2 = 0.0300$, $A_3 = 3000$, and $\lambda_3 = 0.0125$ (the decay constants correspond to lifetimes, τ of 2, 33 and 80 µs). For the analysis, the
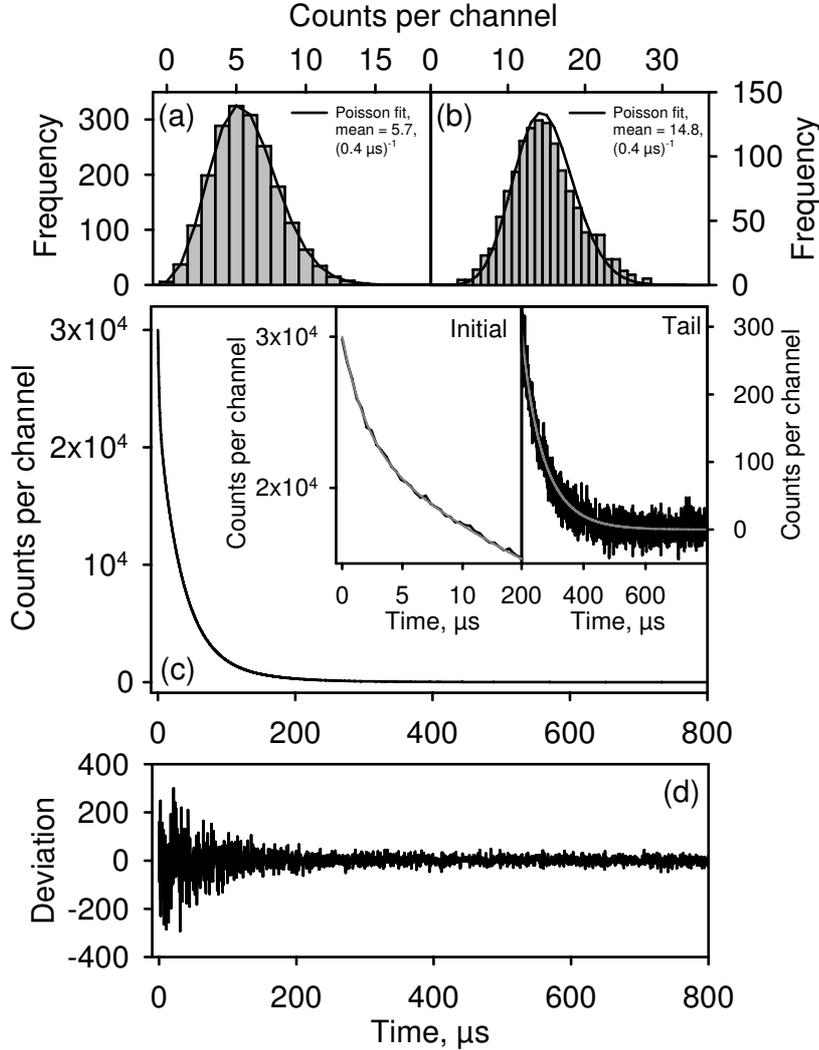
Figure 3.1: (a) Distribution of dark counts measured during the off-time in 0.4 µs bins. The data was measured for 22 s with an on-time of 50 µs and an off-time of 500 µs. The noise distribution has been fitted to a Poisson distribution with a mean value of 5.7 cts/(0.4 µs) shown as the black line. (b) The distribution of photon counts from the blue LEDs. A Neutral Density filter was inserted underneath the diodes to reduce the light level significantly and data was collected for 22 s during an on-time of 500 µs. The diode noise distribution has been fitted to a Poisson distribution with a mean value of 14.8 cts/(0.4 µs) shown as the black line. (c) Time-resolved OSL curve calculated from the expression: $4500 \exp(-t/2) + 22500 \exp(-t/33) + 3000 \exp(-t/80)$, with t from 0 to 816 in steps of 0.4 µs (grey line) and the artificial data produced from the same curve including Poisson noise (both for the signal and the background dark counts) for an initial-signal to background ratio (ISBR) of 600 (black line). Note that the average background level $\bar{b}$ (the average of the last 10 points) has been subtracted. Left inset: A close view of the initial 20 µs, right inset: A close view of the last 600 µs. (d) The difference between the exact curve (grey line in (a)) and the curve resulting after the addition of noise (black line in (a)).

lifetimes are converted into their reciprocal values, i.e., the decay constants used in Eqn. (3.1). The artificial data sets are generated to contain $m = 2000$ points with a bin width of 0.408 μs giving a decay length between the light pulses of 816 μs. From Eqn. (3.1) we can express the exact data through the model:

$$I(t) = \sum_{i=1}^{3} A_i \exp(-\lambda_i t) \tag{3.4}$$

The individual points Y_j in the artificial data, with background, can therefore be written as:

$$Y_j = I_j + b_j, \quad j = 1, \ldots, m \tag{3.5}$$

where $I_j \sim P(I(t_j))$ and $b_j \sim P(b)$ are numbers randomly selected from Poisson distributions with mean values $I(t_j)$ and b, respectively (recall that b is the background).

The relative level of background in an artificial TR-OSL curve is estimated by the initial-signal to background ratio (ISBR) defined as the ratio between the maximum signal amplitude at $t = 0$ and the constant background b, i.e., $I(0)/b$. For this study, ten different ISBR in the range 6–6000 were used to cover for the variations in the OSL sensitivities of different quartz samples. For each ISBR ratio we generated five instances of the same decaying TR-OSL signal but with different noise realisations. Thereby for each ISBR level, more realistic error estimates of the parameters were obtained than those estimated by the fitting algorithm. In total, 50 different instances of artificial decay data were produced. Before fitting the artificial data, an average background value $\bar{b}$ found from the average over the last 10 data points is subtracted in order to remove the constant background component, such that the final artificial data is:

$$y_j = Y_j - \bar{b} \tag{3.6}$$

This is standard procedure for analysis of measured TR-OSL data. As long as the background is truly constant (for times t greater than six times the lifetime of the slowest component), the number of data points used in the average background estimation is not critical. We used 10 points for reasonable statistics.

Figure 3.1c shows an artificial TR-OSL curve from Eqn. (3.6) with an ISBR of 600 (black line) together with the 'exact' curve from the model in Eqn. (3.4) (grey line). The curves were calculated using the parameters defined above. The insets to Fig. 3.1c zoom in on the early and later parts of these curves. In Fig. 3.1d the deviation between the 'exact' curve $I(t)$ and the noisy and background-corrected data y_j (both from Fig. 3.1c) are shown. As expected from the Poisson statistics the random deviation increases with the magnitude of the data. More importantly, the errors do not show any structure and our model fitting should at best be able to mimic this.

3.4   Data simulation for peak-form data

Since TR-OSL is always a decaying signal, irrespective of the manner in which the sample was excited during a pulse, it is not possible to directly obtain a peak form signal such as in the LM-OSL. However the decaying TR-OSL can be converted into a peak form such as LM-OSL either by varying the integration

intervals [e.g. Poolton et al. (2003)] or by variable rescaling of the intensity and time axis [e.g. Bulur (2000)].

In this work we transform the decay-form data y_j, generated as described above, into two different types of peak forms: (i) a simple variable rescaling of the intensity (simple transformation) and (ii) a variable rescaling of the intensity and time space [pseudo LM-OSL of Bulur (2000)]. Note, however, that in the context of the TR-OSL off-time signal, the term LM-OSL does not have any physical connotation; it merely serves as a different mathematical transformation. The two transformations correspond to the two models:

$$\text{Simple transformation:} \quad I(t) \;=\; (2tT)^{1/2} \cdot \sum_{i=1}^{3} A_i \exp(-\lambda_i t) + b \quad (3.7)$$

$$\text{Pseudo LM-OSL:} \quad I(u) \;=\; \sum_{i=1}^{3} \frac{A_i}{T} u \cdot \exp\left(-\frac{\lambda_i u^2}{2T}\right) + b \quad (3.8)$$

Here we define $T = 2t_{\text{TR}-\text{OSL,max}}$, twice the length of the TR-OSL decay length (1632 μs), and we introduce a new independent variable $u = (2tT)^{1/2}$. Moreover, $A_i = N_i \cdot \lambda_i$, where N_i is proportional to the initial population undergoing decay, λ_i is the decay constant for each of the n components in the signal, and $b \geq 0$ is a term to account for any background light and dark counts of the detector. The two types of peak data thus correspond to the transformations:

$$y_j \to (2t_j T)^{1/2} y_j, \qquad t_j \text{ unchanged,} \tag{3.9}$$

and

$$y_j \to (2t_j/T)^{1/2} y_j, \qquad t_j \to u_j \qquad (\text{by } u_j = (2t_j/T)^{1/2}), \tag{3.10}$$

respectively, of the artificial decay data after correction for background. The artificial decay data and the simple transformed peak data share the same linear time domain t, in contrast to the pseudo LM-OSL peak data which is a function of a 'nonlinear' time domain u.

In Fig. 3.2, the artificial TR-OSL data from Eqn. (3.6) with an ISBR ratio of 15 is shown together with the same curve after the simple peak transformation in Eqn. (3.9), and after the peak transformation in Eqn. (3.10) to obtain pseudo LM-OSL. The pseudo LM-OSL curve is 'stretched' compared to the simple peak transformation due to the time domain transformation and is plotted on the top axis as a function of u. The TR-OSL and the simple peak transformation is plotted on the bottom axis, t.

3.5 Numerical methods

Two different numerical methods are used for parameter estimation. Both methods are least squares methods in the sense that they minimize the sum of squared residuals between the data and the model. One method is a standard nonlinear least squares (NLS) method, which is perhaps the most used method for exponential fitting. As an alternative, we also consider a method based on a Fredholm integral equation (FIE) approach, which has the advantage that it
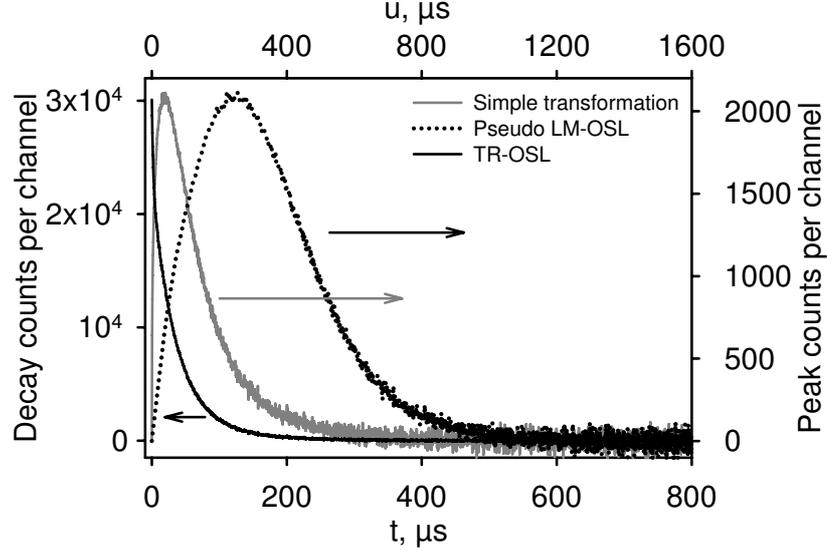
Figure 3.2: Artificial decay data from Eqn. (3.6) with an ISBR of 15 (black line), together with the same data transformed into peak form by using the simple transformation in Eqn. (3.9) (grey line) and transformed into pseudo LM-OSL using Eqn. (3.10) (dotted black line). Note that the decay data and the peak data belong to different abscissa axes, and that the decay data and the simple transformed data share the same linear time domain t, while the pseudo LM-OSL data has a nonlinear time domain u.

does not require the user to select the number of components in the model. To make a fair comparison between the two methods, we do not use any weighting in the least squares problems.

For the decay form in Eqn. (3.1), the nonlinear least squares (NLS) method fits the model $I(t) = \sum_{i=1}^{n} A_i \exp(-\lambda_i t)$ to the m data points y_j after the background has been subtracted:

$$\min_{A_i, \lambda_i} \sum_{j=1}^{m} \left(y_j - \sum_{i=1}^{n} A_i \exp(-\lambda_i t_j) \right)^2 \tag{3.11}$$

Here we have introduced the amplitudes $A_i = N_i \cdot \lambda_i$, and $t_1, \ldots, t_m$ denote the measurement times. A similar expression can be written for the simple peak transformation in Eqn. (3.7). For the peak form in Eqn. (3.2), the model $I(u) = \sum_{i=1}^{n} \frac{A_i}{T} u \cdot \exp\left(-\frac{\lambda_i u^2}{2T}\right)$ is fitted to the data points:

$$\min_{A_i, \lambda_i} \sum_{j=1}^{m} \left[y_j - \sum_{i=1}^{n} \frac{A_i}{T} u_j \cdot \exp\left(-\frac{\lambda_i u_j^2}{2T}\right) \right]^2 \tag{3.12}$$

where u_j is the transformed time from Eqn. (3.10). The underlying numerical method is known as the variable projection method, which is a Levenberg-Marquardt algorithm tailored to the specific problem; see Golub and Pereyra (2003) and Pereyra and Scherer (2009) for details. This algorithm is built into

the software package SigmaPlot, which was used in this study. Since the data is fitted to a specific model, the user must specify the number of components n in this model prior to fitting the data. We impose the positivity constraints $\lambda_i > 0$ on the decay constants, but did not enforce positive amplitudes as negative values never were encountered.

In the second method, a spectroscopic analysis approach is used [see, e.g., Agersnap (1997); Istratov and Vyvenko (1999); Whitley and McKeever (2001)], in which λ is considered as a continuous variable and $a(\lambda) \geq 0$ is an unknown 'amplitude density function' which identifies the decay constants (and thereby the components) present in the data $y(t)$:

$$\int_{\lambda_{\min}}^{\lambda_{\max}} \exp(-\lambda t) a(\lambda) \mathrm{d}\lambda = y(t) \tag{3.13}$$

This is illustrated in Fig. 3.3 for a set of artificial data $y(t)$, shown inset, containing three components. The areas under the peaks of $a(\lambda)$ are related to the amplitudes of the decay constants. The similar equation for the peak form is:

$$\int_{\lambda_{\min}}^{\lambda_{\max}} \exp\left(-\frac{\lambda u^2}{2T}\right) \frac{u}{T} a(\lambda) \mathrm{d}\lambda = y(u) \tag{3.14}$$

Equations (3.13) and (3.14) have the form of a Fredholm integral equation (FIE) of the first kind [see Hansen (1998)]. Unlike in the NLS method, the user does not have to specify the number of components; the amplitude density function $a(\lambda)$ determines this number (see below).

To solve the FIE in Eqn. (3.13) numerically, it is discretized by means of a quadrature method (Hansen (1998)) which leads to the linear least squares problem:

$$\sum_{j=1}^{m} \left(y_j - \sum_{k=1}^{p} \Delta\lambda_k \exp\left(-\lambda_k t_j\right) a_k \right)^2 \tag{3.15}$$

where λ_k are the quadrature points, $\Delta\lambda_k$ denotes the width of the interval that contains the k-th quadrature point, and a_k are the approximations to $a(\lambda)$ at the quadrature points, i.e., $a(\lambda_k) \approx a_k$. We use $p = 500$ quadrature points, and due to the large range of λ-values needed in OSL problems, the quadrature points are distributed logarithmically between $\lambda_{\min} = 0.001$ and $\lambda_{\max} = 100$. The same technique is used to discretize Eqn. (3.14). No weighting of the data is used and non-negativity constraints are enforced on the solution which has the side effect of causing the spikes in the solution to be narrower than without constraints. The constrained problem is solved by means of the NLS algorithm (Lawson and Hanson, 1995, Chapter 23) implemented in Matlab. It is beyond the scope of this paper to go into further details of the computational algorithms, and we refer to the above-mentioned books for details.

When the data adheres to the model in either Eqn. (3.13) or (3.14), it is expected that the nonnegative function $a(\lambda)$ has narrow spikes for $\lambda \approx \lambda_i$, see Fig. 3.3. Moreover, if this is the case then it is also expected that the amplitudes are approximately equal to the area under each of the spikes, i.e., $A_i \approx \int_{\Omega_i} a(\lambda) \mathrm{d}\lambda$ where Ω_i denotes a small interval around λ_i. For each spike we therefore compute the corresponding amplitude by means of

$$A_i = \sum_{k \in \mathrm{spike}_i} \Delta\lambda_k a_k. \tag{3.16}$$
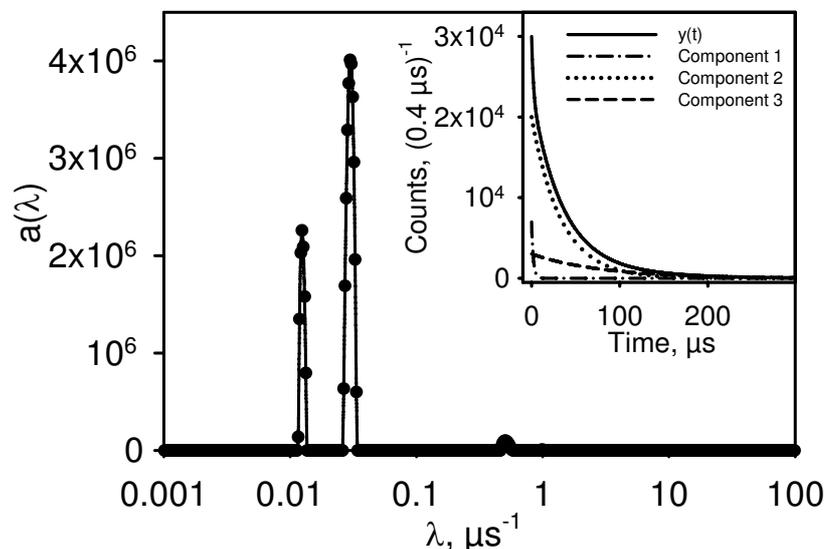
Figure 3.3: A plot of the amplitude density function $a(\lambda)$ given in Eqn. (3.13) vs. the parameter variable, λ, for a set of artificial data $y(t)$ with three components. The artificial data y_j and its three components $A_i \exp\left(-\lambda_i t_j\right)$ are shown inset, see Eqn. (3.6).

More than n spikes were occasionally encountered (although a situation with less than n spikes never occurred), and thus a 'rejection criterion' was needed to remove spurious spikes. It is noted that the contribution to the total signal from the i-th component can be measured by the integral:

$$\int_0^T a_i \exp(-\lambda_i t)\mathrm{d}t = \frac{a_i}{\lambda_i}\left[1 - \exp\left(-\lambda_i T\right)\right] \approx \frac{a_i}{\lambda_i}. \qquad (3.17)$$

Spikes with ratios a_i/λ smaller than a fixed threshold value determined by the area under the data and the noise level in the data are therefore rejected. In this paper, a threshold of 0.01 was used, i.e., components whose contribution is less than 1% of the total signal are rejected.

3.6   Artificial data results

In this section the two fitting methods are used for analysing the artificial data sets for both decay and peak forms.

3.6.1   Nonlinear least squares method: decay vs. peak form

As described in Section 3.5, the nonlinear least squares algorithm, as implemented in SigmaPlot, is not able to identify the number of components present in the data, and therefore a model with a specific set of components must be chosen by the user prior to fitting the data under examination. To eliminate the advantage that the number of components is known in the artificial data
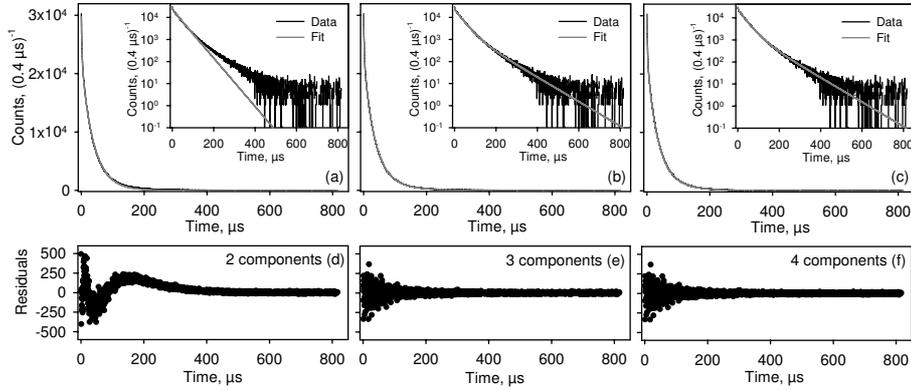
Figure 3.4: Artificial decay data with an ISBR of 600 are shown together with (a) two, (b) three, and (c) four component fits to the data. The insets show the same on the log intensity scale. (d)-(f) show the corresponding residuals from the fits.

sets, a systematic approach was used for each set of data to identify the number of components as if it was unknown. Each data set was fitted with first two, then three, and finally with four (and so on) components to identify the correct number of components present in the data set. This is illustrated in Fig. 3.4a–c for an artificial data set with an ISBR of 600 and fitting using a model with 2, 3, and 4 components, respectively, with corresponding parameter values listed in Table 3.1. Fitting with too few components caused a systematic behaviour in the residuals (Fig. 3.4d) which is undesirable, while the residuals from the three-component fit (Fig 3.4e) are evenly spread around zero and they do not visibly behave systematically, which according to Fig. 3.1d is the desired result. When fitting with four components, and thereby forcing the algorithm to find more components than what is truly present in the data, either of two situations occur: (i) two components have identical decay constants or (ii) the algorithm creates a fourth component with a decay constant very similar to an already existing decay constant and changes the remaining three decay constants slightly. Both of these possibilities resulted in no further visible improvement of the residuals, see Fig. 3.4f. The redundancy in the four-component fit becomes clear by looking at the second (3 component fit parameters) and third column (4 component fit parameters) in Table 3.1. The fourth fitted component merely splits the third component into two parts and, as a result, the residuals are identical in the 3 and 4 component fits. This was tested for several curves and it is concluded that the condition for the best fit is the minimum number of components for fits with identical residuals.

In Table 3.1, the A_i and λ_i parameters in the first three columns are listed with internal uncertainties estimated by SigmaPlot. To test whether these uncertainties are large enough to contain the variations in parameter values caused by the noise, five datasets with an ISBR of 600 were fitted to calculate the mean and standard error on the parameters. These values are presented in the last column of Table 3.1. The calculated standard errors based on five different realisations of the noisy curve are systematically bigger than those estimated by SigmaPlot for any individual curve. We therefore fit five datasets

Table 3.1: Amplitude and decay constant parameters obtained from fitting an artificial data set with an ISBR of 600 with 2, 3, and 4 components (columns 1-3) using the nonlinear least squares algorithm in SigmaPlot. The uncertainties in the parameter values quoted in these columns are internal error estimates calculated by SigmaPlot. In column 4, the average parameters are calculated from fittings of five different realisations of TR-OSL curves for the identical parameters, noise distribution, and an ISBR of 600. The quoted uncertainties are one σ (standard deviation).

# components in LM fit	2	3	4	3 (average)
$A_1 = 7,000$ cts$/(0.4$ μs$)$	7439 ±61	6750 ±29	6750 ±29	7046 ±150
$A_2 = 20,000$ cts$/(0.4$ μs$)$	$21,950$ ±31	$20,100$ ±112	$20,100$ ±118	$19,997$ ±189
$A_3 = 3,000$ cts$/(0.4$ μs$)$	-	2899 ±122	1449 ±502	2994 ±255
A_4 cts$/(0.4$ μs$)$	-	-	1450 ±502	-
$\lambda_1 = 0.5000$ μs^{-1}	0.3554 ±0.0056	0.4871 ±0.0041	0.4871 ±0.0041	0.5003 ±0.0266
$\lambda_2 = 0.0300$ μs^{-1}	0.0252 ±0.0001	0.0298 ±0.0001	0.0298 ±0.0001	0.0300 ±0.0003
$\lambda_3 = 0.0125$ μs^{-1}	- -	0.0124 ±0.0002	0.0124 ±0.0059	0.0125 ±0.0003
λ_4 μs^{-1}	-	-	0.0124 ±0.0061	-

for each of the different ISBR values as presented in Section 3.3 to get more realistic estimates of uncertainties on the parameters from the fits.

Using the built-in nonlinear least squares algorithm in SigmaPlot, we fitted the 50 decay formed curves, the 50 simple peak transformation data sets, and the 50 pseudo LM-OSL peak data sets. The results are shown in Fig. 3.5. The computed amplitudes A_1, A_2, and A_3 are compared in a–c, for the 10 different ISBR. Likewise, the decay constants λ_1, λ_2, and λ_3 are compared in Fig. 3.5d–f. The dashed lines in each plot represent the 'true' values used in creating the artificial data. It is first observed that all amplitudes and decay constants using the two peak forms are identical; the NLS method does not seem to be able to distinguish the two types of data from each other. Secondly, the results from decay and peak form data are consistent with each other and within the 'true' value. The uncertainties on the parameters derived for fitting peak data are generally smaller than those for the decay form data. For very high ISBR there is a slight tendency for underestimation of the parameters from the peak-form data fits, see Fig. 3.5c, e, and f.

3.6.2 Spectroscopic method: decay vs. peak form

The Fredholm integral equation model was used to fit the same data sets from the previous section. It was observed that the number of components ($n = 3$) present in a data set is often overestimated by one, two, or three components;
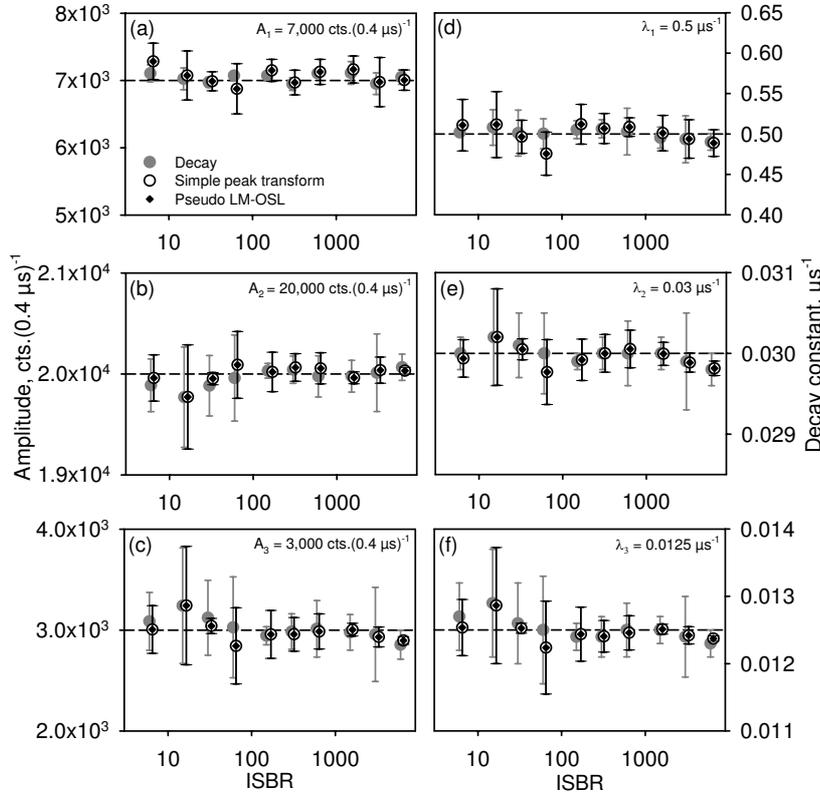
Figure 3.5: Results from fitting decay-form data (grey filled circles), simple transformed peak data (open black circles), and pseudo LM-OSL data (black diamonds) using the NLS method. In each plot the dashed line indicates the known parameter value, and each point is the average over five parameter values for the same ISBR. The left column shows the results for the amplitudes (a) $A_1 = 7000$ cts/(0.4 μs), (b) $A_2 = 20000$ cts/(0.4 μs), and (c) $A_3 = 3000$ cts/(0.4 μs). The right column shows the results for the decay constants (d) $\lambda_1 = 0.5$ μs^{-1}, (e) $\lambda_2 = 0.03$ μs^{-1}, and (f) $\lambda_3 = 0.0125$ μs^{-1}.

but with the rejection criterion from Section 3.5 almost all of these extra components are rejected by our method. This is shown in Table 3.2, which lists the number of extra components found in the 50 data sets before and after the rejection criterion (RC) has been used. The two peak forms had identical numbers of components present before and after use of the rejection criteria, and are therefore only described in one column. Out of the 50 decay-form data sets, 38 had too many components and this number got reduced to 5 after using the rejection criterion. Similarly, from the 50 peak-form data sets, 42 had too many components and this number was reduced to 3.

Figure 3.6 shows the results from fitting with the Fredholm integral equation model, and again the amplitudes are compared in a–c while the decay constants are compared in d–f. Similar to Fig. 3.5, the points in Fig. 3.6 are averages over the parameters from five data sets with the same ISBR. As described above, the results from five decay-form data sets and three peak-form data sets

Table 3.2: Number of OSL curves with over-fitting by either one, two, or three exponential components, when using the Fredholm integral equation model (Section 3.5). The numbers are given before and after the use of the rejection criterion (RC).

	Before RC		After RC	
No. extra components	Decay	Peak	Decay	Peak
1	24	24	5	3
2	11	17	0	0
3	3	1	0	0

were rejected due to the overestimation of the number of components (see Table 3.2). Again we note that the parameters from the two peak forms are identical. The parameter estimates generally have larger uncertainties using this fitting method compared to those using NLS. Furthermore, there is a tendency to underestimate the parameters in Fig. 3.6c, e, and f, and to overestimate the parameters in Fig. 3.6b for high ISBR levels for both decay and peak shaped data. For all three data forms, several of the parameters are not consistent with the 'true' parameter values at high ISBR levels.

3.7   Comparison of the methods

To make an overall assessment of the performance of the two fitting methods and the two types of data, the parameters from the fitted decay- and peak-form data were analyzed by calculating the mean and the standard deviation of every parameter divided by its expected value. The optimum mean value should therefore be 1. The values are given in Table 3.3; columns 2 and 3 list the parameters found using the FIE method for decay- and peak-form data respectively, whereas columns 4 and 5 list the parameters found using the NLS method for decay- and peak-form. Note that the values given in rows 3 and 5 are valid for both the simple peak transformation and for the pseudo LM-OSL transformation, as these parameter values were identical (see Figs. 3.5 and 3.6). The number of data sets included in the calculation of the mean and standard deviations is given in row 2; for the FIE method this number is not 50 due to a few instances where the rejection criteria did not remove all over fitted components (see Table 3.2 and Section 3.6.2).

If the decay and peak parameter results from the FIE method (columns 2 and 3) are compared, four peak parameters (A_1, A_3, λ_2, and λ_3) are slightly better estimated, i.e., have a smaller mean bias than the decay parameters, but the overall spread in the individual parameter estimates (standard deviation) is larger for peak fitting compared to the decay curve fitting. If the decay and peak parameters from the NLS method (columns 4 and 5) are compared instead, then the three peak parameters (A_2, A_3, and λ_3) have smaller mean bias compared to the decay parameters, and the value of λ_1 is identical for the two data types. Similarly the standard deviations are smallest for the four peak parameters (A_2, A_3, λ_2, and λ_3) compared to the decay parameters. There is an overall greater concordance in the mean values from the two models for the NLS method compared to the FIE method. In general both the models perform very well and the mean values are statistically indistinguishable from the expected

Table 3.3: Summary of the mean (% mean bias) and standard deviations for the parameters presented in Figs. 3.5, 3.6, and 3.8 based on data for all the ISBR values for the FIE method using decay (column 2) and peak (column 3) data, and for the NLS method using decay (column 4) and peak (column 5) data. The % mean bias has been defined as [(expected value − measured value)/expected value] × 100. Columns 6 lists the values for the 'true' LM-OSL parameters, and these are to be compared to the values pseudo-LM-OSL in column 5. For each of the six parameters, the mean and standard deviation were calculated using the number of data sets given in row 1, for the FIE method, this number is less than 50 due to imperfect removal of components by the rejection criteria (see Table 3.2). Note that the values in columns 3 and 5 represent both the simple peak transformation parameters as well as the pseudo LM-OSL parameters as these are identical.

Fitting approach	FIE, decay Mean (% bias) ± Rel. St. Dev.	FIE, peak Mean (% bias) ± Rel. St. Dev.	NLS, decay Mean (% bias) ± Rel. St. Dev.	NLS, peak Mean (% bias) ± Rel. St. Dev.	NLS, 'true' peak Mean (% bias) ± Rel. St. Dev.
# data sets used for mean and std	45	47	50	50	50
$A_1 = 7000$ cts/(0.4 μs)	0.978 (+2.2) ±5.2%	0.995 (+0.5) ±7.8%	1.006 (-0.6) ±1.7%	1.008 (-0.8) ±3.7%	0.997 (+0.3) ±4.8%
$A_2 = 20{,}000$ cts/(0.4 μs)	1.003 (-0.3) ±1.2%	1.005 (-0.5) ±1.5%	0.998 (+0.2) ±1.4%	1.000 (0) ±1.1%	0.999 (+0.1) ±2.3%
$A_3 = 3000$ cts/(0.4 μs)	0.945 (+5.5) ±7.8%	0.967 (+3.3) ±10.8%	1.007 (-0.7) ±10.9%	0.995 (+0.5) ±8.6%	1.003 (-0.3) ±15.3%
$\lambda_1 = 0.5000$ μs^{-1}	0.994 (+0.6) ±6.2%	1.043 (-4.3) ±8.2%	1.001 (-0.1) ±3.7%	1.001 (-0.1) ±5.0%	0.994 (+0.6) ±7.4%
$\lambda_2 = 0.0300$ μs^{-1}	0.991 (+0.9) ±1.0%	0.995 (+0.5) ±1.2%	1.000 (0) ±1.2%	0.999 (+0.1) ±0.9%	1.000 (0) ±1.5%
$\lambda_3 = 0.0125$ μs^{-1}	0.986 (+1.4) ±2.9%	0.997 (+0.3) ±3.6%	1.003 (-0.3) ±3.9%	0.998 (+0.2) ±3.2%	1.000 (0) ±6.0%
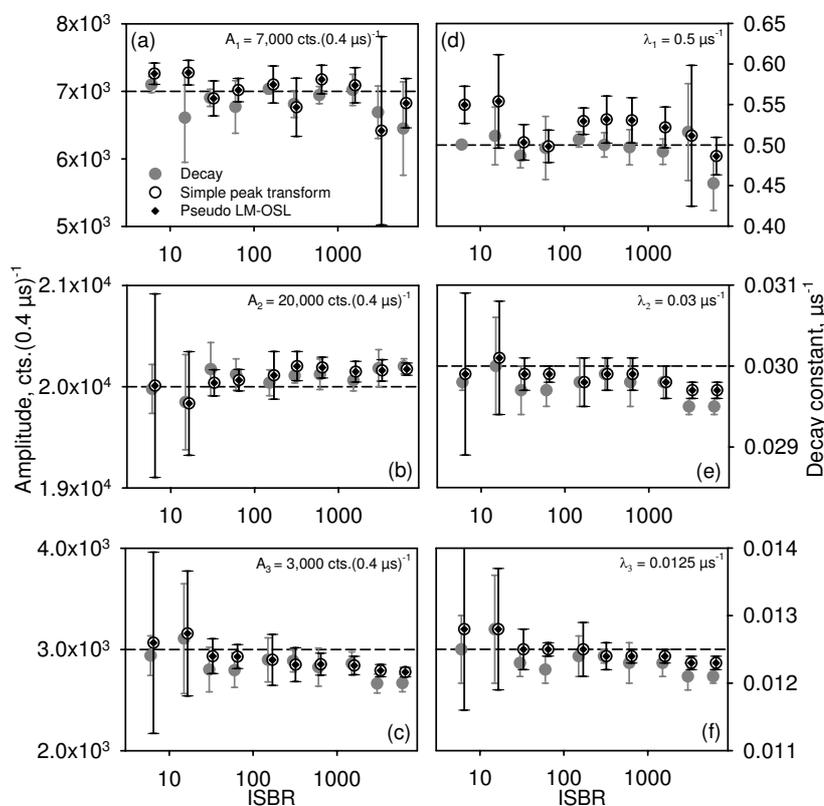
Figure 3.6: Results from fitting decay-form data (grey filled circles), simple transformed peak data (open black circles), and pseudo LM-OSL data (black diamonds) using the FIE model. See Fig. 3.5 for figure description. The results from eight data sets were discarded (five for decay-form and three for peak-form) as a result of inadequate removal of false components by the rejection criterion (see Section 3.5).

values if one considers the measured spread in parameter estimates. However, even though there is no clear preference between the two models, our data may hint in favour of the peak model if one only considers the mean bias.

When comparing the two fitting methods, FIE and NLS, on the basis of the six parameters each estimated for each of the two models (decay and peak), the NLS fitted 10 out of 12 parameters more accurately, and 8 out of 12 standard deviations were the smallest compared to the FIE values. Although the FIE method is more objective, the numbers in Table 3.3 suggests that the NLS method estimates the parameters more accurately and with smaller error.

3.8 'True' LM-OSL vs. pseudo LM-OSL

We now investigate the relative performance of the peak model for two cases 1) pseudo LM-OSL data derived from transformation of decay form (CW-OSL or TR-OSL) data, and 2) 'true' LM-OSL. There could be differences in the performance of the two data sets as the signals are measured with different

signal to background ratios, and moreover, the transformation step in case 1) also involves transformation of the noise. Thus, it is not apparent whether a true peak measurement such as LM-OSL is preferable compared to a pseudo-LM-OSL or otherwise. Note that a true peak measurement is only possible in the conventional OSL where varying the stimulation light intensity gives rise to a peak shaped signal (see Equation 3.2). This is not an option in TR-OSL measurements where the signal always decays with time between pulses. In this section we will compare the results from artificial 'true' LM-OSL with the previous results obtained using pseudo LM-OSL.

We create artificial 'true,' i.e., experimentally obtained LM-OSL containing three components with the same parameter values as in Section 3.4 and including a background $b \geq 0$ arising from any dark counts of the detector (possible minor time dependent background from stray stimulation light is neglected in order to simplify the analysis), and a noise component $\xi(u)$ that reflects the Poisson noise in the data:

$$I(u) = \sum_{i=1}^{3} \frac{A_i}{T} u \cdot \exp\left(-\frac{\lambda_i u^2}{2T}\right) + b + \xi(u) \qquad (3.18)$$

where T is twice the length of the OSL decay length of 1632 μs (Bulur, 1996). Prior to fitting, an average background $\bar{b}$ estimated from the last 10 data points is removed. As in the previous sections 50 'true' LM-OSL curves are produced, 5 curves for each of the 10 ISBR levels. Figure 3.7a shows the true LM-OSL (grey curve) and the pseudo LM-OSL (black curve) for the highest ISBR level, 6000 and in Fig. 3.7b the same curves but for the lowest ISBR of 6. In both figures, the 'true' LM-OSL curves appear much noisier than the pseudo LM-OSL and therefore one might presume that the pseudo LM-OSL would be a better choice for fitting.

Using the NLS method the 50 new curves are fitted, and the parameters are shown in Fig. 3.8 (black circles) together with the values found from fitting the pseudo LM-OSL in Section 3.6.1 (grey circles). The computed amplitudes A_1, A_2, and A_3 are compared in a–c, for the 10 different ISBR. Likewise, the decay constants λ_1, λ_2, and λ_3 are compared in Fig. 3.8d–f. For the low background levels (ISBR< 100), the true LM-OSL generally have very large error bars reflecting bad fits and large scatter in the parameter values within each level, and several parameter values are inconsistent with the known true parameter values. It is clear that the noise in the data for ISBR< 100 results in very poor fits and for noise levels of this magnitude, pseudo LM-OSL is clearly preferable. To make an overall assessment of the accuracy of the parameters compared to those of the pseudo LM-OSL data (column 5, Table 3.3), the mean and standard deviation was calculated for each of the six parameters and listed in column 6 in Table 3.3. Although the mean values of the 'true' LM-OSL parameters are either very similar or better than the pseudo LM-OSL estimated parameters, the standard deviation is bigger for all the parameters, reflecting the much larger scatter found in the parameter estimates.

It is therefore concluded, that using pseudo LM-OSL data results in better fits irrespectively of the noise level in the data compared to 'true' LM-OSL data. This conclusion assumes that the conditions of measuring the OSL decay curve or the LM-OSL data are the same i.e. the same instrument is used and thereby the same light stimulation source. That pseudo LM-OSL is better
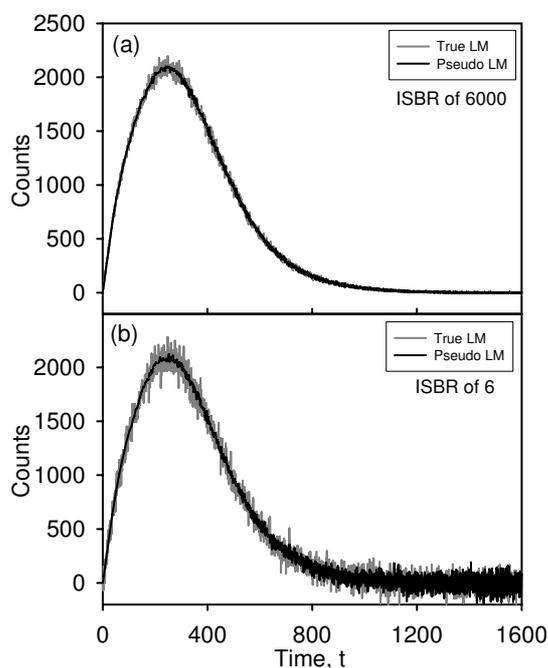
Figure 3.7: Pseudo LM-OSL (black curve) and 'true' LM-OSL (grey curve) as calculated from Eqns. (3.8) and (3.18) respectively, for (a) the lowest noise-level with an ISBR of 6000 and (b) and the highest noise-level with an ISBR of 6. The parameters are the same as given in the caption of Fig. 3.1.

than 'true' LM-OSL is probably because the signal-to-noise ratio for the decay curve measurement (CW-OSL) is always much higher than that for the corresponding true LM-OSL measurement. Therefore, the pseudo LM-OSL derived by transforming CW-OSL data is less noisy than the 'true' peak measurement. Moreover, there may be a problem of time varying background arising form the stimulation light in the true LM-OSL measurement. This problem can further complicate the exponential analysis of the true LM-OSL data.

3.9 Performance of the NLS method on measured quartz TR-OSL data

TR-OSL data was measured from the Tanzanian quartz sample for a regenerative irradiation dose of 30 Gy. Furthermore, this dose was repeated but now measured with a neutral density filter inserted beneath the PMT to attenuate the light from the sample by approximately a factor of 16 and thereby obtaining a smaller ISBR. Both curves were transformed into peak-shape according to the model in Eqn. (3.8) and are shown in Fig. 3.9a. The curves are shown on a log intensity scale in the inset.

    The data was initially fitted in SigmaPlot with one component, and the corresponding residuals are shown as the grey curve (30 Gy) and black curve (30 Gy, attenuated) in Fig. 3.9b, upper and lower graph respectively; the grey residuals shows a strong trend indicating that the data is not fitted adequately,
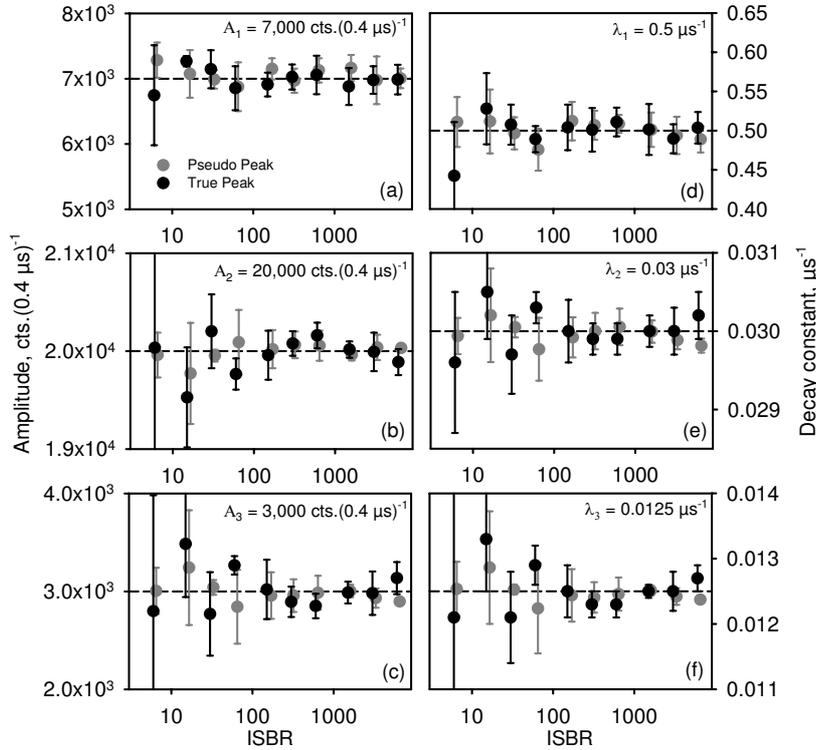
Figure 3.8: Results from fitting pseudo LM-OSL data (grey filled circles) and 'true' LM-OSL data (filled black circles) using the NLS method. In each plot the dashed line indicates the known parameter value, and each point is the average over five parameter values for the same ISBR. The left column shows the results for the amplitudes (a) $A_1 = 7000$ cts/(0.4 μs), (b) $A_2 = 20000$ cts/(0.4 μs), and (c) $A_3 = 3000$ cts/(0.4 μs). The right column shows the results for the decay parameters (d) $\lambda_1 = 0.5$ μs^{-1}, (e) $\lambda_2 = 0.03$ μs^{-1}, and (f) $\lambda_3 = 0.0125$ μs^{-1}.

whereas the black curve show a much less visible trend. As the two curves are from the same sample, they must contain the same number of components, and so one component is not sufficient to fit the data. The residuals from a two-component fit is shown in Fig. 3.9c, the upper grey curve being the 30 Gy residuals and the lower curve the attenuated 30 Gy residuals. The trend in the grey residuals has been reduced significantly and the black residuals have been improved slightly indicating that only two components are present in the measured TR-OSL data. Finally the curves were fitted with three components and the residuals from these two fits are shown in Fig. 3.9d; the residuals have not improved to the eye, and the third component is clearly in excess as the decay constants are identical in both cases to an already identified component and the amplitudes have been halved (not shown). It is therefore clear that only two components are present in the data. The decay constants and amplitudes found from the two-component fits are given in Table 3.4. The 30 Gy curve fit resulted in two components with lifetimes of 39 μs and 103 μs for amplitudes of 36,959 cts/(0.4 μs) and 685 cts/(0.4 μs). The attenuated 30 Gy curve fit gave the lifetimes 38 μs and 107 μs for amplitudes 2,219 cts/(0.4 μs) and 65
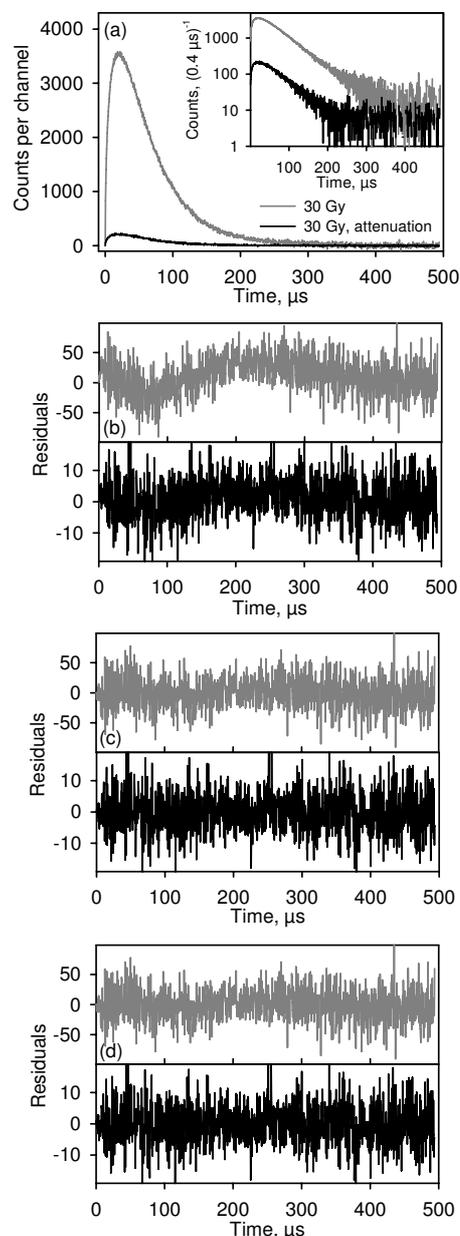
Figure 3.9: TR-OSL data measured from a colluvium quartz sample from Tanzania. The sample was given a dose of 30 Gy and was heated to 260°C for 10 s prior to blue LED stimulation at 125°C for 22 s. The on-time was 50 μs and the off-time was 500 μs. Prior to fitting, the data was transformed into a peak shape using Eqn. (3.7) (grey curve). The experiment was then repeated, but with a neutral density filter inserted beneath the PMT to attenuate the incoming light from the sample (black curve) by a factor of 16. The inset shows the curves on log-scale. (b) Residual curves for a one-component fit of the 30 Gy data (grey curve) and the attenuated 30 Gy data (black curve) using the NLS method, (c) residual curves for a two-component fit of the two data sets, and (d) residual curves for a three-component fit of the curves for the same notation as in (b).

Table 3.4: Amplitude and decay constant parameters from fitting quartz TR-OSL from a 30 Gy dose (columns 1-2) and TR-OSL from a 30 Gy dose and attenuating the signal by a factor of 16 (columns 3-4).

30 Gy		30 Gy, attenuated	
Amplitude, A_i cts/(0.4 μs)	Decay constant, λ_i, μs^{-1}	Amplitude, A_i cts/(0.4 μs)	Decay constant, λ_i, μs^{-1}
36,959	0.0259	2,219	0.0267
685	0.0097	65	0.0093

cts/(0.4 μs).

In Ankjærgaard et al. (2010, Chapter 10 of this thesis), it was shown that for a wide selection of quartz samples, the main dominant commonly observed component has a lifetime of 37 ± 5 μs found from the mean and standard deviation from the 30 samples investigated. Furthermore they found that in some samples, a longer or a shorter lifetime component was present with lifetimes of 100 ± 40 μs and 6 ± 1 μs. The lifetimes found here are in good agreement with each other despite different noise levels, and are in very good agreement with published values in Ankjærgaard et al. (2010), Chithambo and Galloway (2000), Chithambo (2007). Given the above amplitudes, the ISBR ratios for the individual component for the attenuated curve were calculated to be 44 and 1.3. Thus it is possible to estimate the parameters A_2, λ_2 for a second component even though the initial intensity of this component has a comparable size to the background.

3.10 Conclusions

A thorough study of two different models for multi-exponential OSL data, the decay form and the peak form, has been undertaken to investigate which data form is better suited for fitting noisy data. Each of these data types were analysed using two fundamentally different numerical methods, one based on solving the nonlinear least squares (NLS) data fitting problem by a Levenberg-Marquardt algorithm, and the other based on solving a linear first-kind Fredholm integral equation (FIE) by means of a non-negativity constrained linear least squares problem. We conclude the following:

1. Parameters derived using both models are statistically consistent with the expected value, given the spread in the data. The mean values themselves are on an average within $\sim 1\%$ of the expected values for both the models. Of the two data types, the decay form and the peak form, neither is clearly superior over the other in estimating parameters when fitting with the FIE or the NLS method, although there seems to be a slight tendency for the peak form to show smaller mean bias in our limited dataset. Furthermore, the two numerical methods are insensitive to whether the peak shape is obtained by only variable scaling of the intensity, or by variable scaling of both intensity and the time space (e.g., pseudo LM-OSL).

2. Although both numerical methods tested here perform well, there is a suggestion that the NLS method is marginally better and relatively less

sensitive to the noise in the data. However, as demonstrated here, if an appropriate rejection criterion is incorporated into the routine, then the FIE method has an advantage that it does not require user to define the number of components. The computation time was similar for the two methods.

3. For the continuous-wave OSL (CW-OSL) measurements we conclude that the fitting of peak transformed data (i.e., pseudo LM-OSL) is more robust than the fitting of 'true' LM-OSL data. This is probably because, for the same parameters, the CW-OSL can be measured with a higher signal-to-noise ratio than in the corresponding LM-OSL. It should, however, be noted that CW-OSL data should be collected with high enough frequency so as to be able to resolve the fastest decaying component in the signal to obtain the best fit of multi-exponential OSL data.

Based on the above observations, a possible recommendation for analysing multiexponential data could be fitting peak-transformed decaying OSL signal using the NLS approach. This algorithm is already implemented in many commercial types of software such as SigmaPlot (used here).

Acknowledgements

References

Agersnap, N. (1997). *Dosimetry based on thermally and optically stimulated luminescence.* Unpublished Ph.D. thesis, Niels Bohr Institute, University of Copenhagen.

Ankjærgaard, C., Jain, M., Thomsen, K. J., and Murray, A. S. (2010). Optimising the separation of quartz and feldspar optically stimulated luminescence using pulsed excitation. *Radiation Measurements*, 45:778–785.

Bailey, R. M., Smith, B. W., and Rhodes, E. J. (1997). Partial bleaching and the decay form characteristics of quartz OSL. *Radiation Measurements*, 27:123–136.

Bos, A. J. J. and Wallinga, J. (2009a). Analysis of the quartz OSL decay curve by differentiation. *Radiation Measurements*, 44:588–593.

Bos, A. J. J. and Wallinga, J. (2009b). Optically stimulated luminescence signals under various stimulation modes assuming first-order kinetics. *Physical Review B*, 79:195118 (12pp).

Bøtter-Jensen, L., McKeever, S. W. S., and Wintle, A. G. (2003). *Optically Stimulated Luminescence Dosimetry.* Elsevier, Amsterdam, The Netherlands. ISBN: 0–444–50684–5.

Bulur, E. (1996). An alternative technique for optically stimulated luminescence (OSL) experiment. *Radiation Measurements*, 26:701–709.

Bulur, E. (2000). A simple transformation for converting CW-OSL curves to LM-OSL curves. *Radiation Measurements*, 32:141–145.

Chithambo, M. L. (2007). The analysis of time-resolved optically stimulated luminescence: I. Theoretical considerations. *J. Phys. D: Appl. Phys.*, 40:1874–1879.

Chithambo, M. L. and Galloway, R. B. (2000). A pulsed light-emitting-diode system for stimulation of luminescence. *Meas. Sci. Technol.*, 11:418–424.

Chithambo, M. L., Preusser, F., Ramseyer, K., and Ogundare, F. O. (2007). Time-resolved luminescence of low sensitivity quartz from crystalline rocks. *Radiation Measurements*, 42:205–212.

Golub, G. H. and Pereyra, V. (2003). Separable nonlinear least squares: the variable projection method and its applications. *Inverse Problems*, 19(2):R1–R26.

Hansen, P. C. (1998). *Rank-Deficient and Discrete Ill-Posed Problems: Numerical Aspects of Linear Inversion*. SIAM, Philadelphia.

Hansen, P. C., Nielsen, H. B., Ankjærgaard, C., and Jain, M. (2010). Two exponential models for optically stimulated luminescence. In Pereyra, V. and Scherer, G., editors, *Exponential Data Fitting and its Applications*. Bentham eBooks.

Huntley, D. (2006). Thoughts arising from "Choi, Duller and Wintle: Analysis of quartz LM-OSL curves. Ancient TL 24, 9-20 (2006)". *Ancient TL*, 24:69–70.

Huntley, D. (2007). Response to Jain and Lindvold. *Ancient TL*, 25:76–80.

Istratov, A. A. and Vyvenko, O. F. (1999). Exponential analysis in physical phenomena. *Review of Scientific Instruments*, 70(2):1233–1257.

Jain, M. and Lindvold, L. R. (2007a). Blue light stimulation and linearly modulated optically stimulated luminescence. *Ancient TL*, 25:69–75.

Jain, M. and Lindvold, L. R. (2007b). Response to Huntley. *Ancient TL*, 25:80.

Jain, M., Murray, A. S., and Bøtter-Jensen, L. (2003). Characterisation of blue-light stimulated luminescence components in different quartz samples: implications for dose measurement. *Radiation Measurements*, 37:441–449.

Jain, M., Murray, A. S., Bøtter-Jensen, L., and Wintle, A. G. (2005). A single-aliquot regenerative-dose method based on IR (1.49 eV) bleaching of the fast OSL component in quartz. *Radiation Measurements*, 39:309–318.

Lapp, T., Jain, M., Ankjærgaard, C., and Pirzel, L. (2009). Development of pulsed stimulation and photon timer attachments to the Risø TL/OSL reader. *Radiation Measurements*, 44:571–575.

Lawson, C. L. and Hanson, R. J. (1995). *Solving Least Squares Problems*, volume 15 of *Classics in Applied Mathematics*. SIAM, Philadelphia.

Pagonis, V., Ankjærgaard, C., Murray, A. S., Jain, M., Chen, R., Lawless, J., and Greilich, S. (2010). Modelling the thermal quenching mechanism in quartz based on time-resolved optically stimulated luminescence. *Journal of Luminescence*, 130:902–909.

Pagonis, V., M., M. S., Chithambo, M. L., Christensen, E., and Barnold, C. (2009). Experimental and modelling study of pulsed optically stimulated luminescence in quartz, marble and beta irradiated salt. *Journal of Physics D: Applied Physics*, 42:1–12.

Pereyra, V. and Scherer, G., editors (2009). *Exponential Data Fitting and its Applications*. Bentham eBooks.

Poolton, N. R. J., Bøtter-Jensen, L., Andersen, C. E., Jain, M., Murray, A. S., Malins, A. E. R., and Quinn, F. M. (2003). Measuring modulated luminescence using non-modulated stimulation: ramping the sample period. *Radiation Measurements*, 37:639–645.

Singarayer, J. S. and Bailey, R. M. (2003). Further investigations of the quartz optically stimulated luminescence components using linear modulation. *Radiation Measurements*, 37:451–458.

Smith, B. W. and Rhodes, E. J. (1994). Charge movement in quartz and their relevance to optical dating. *Radiation Measurements*, 23:329–333.

Wallinga, J., Bos, A. J. J., and Duller, G. A. T. (2008). On the separation of quartz OSL signal components using different stimulation modes. *Radiation Measurements*, 43:742–747.

Whitley, V. H. and McKeever, S. W. S. (2001). Linearly modulated photoconductivity and linearly modulated optically stimulated luminescence measurements on Al_2O_3:C. *Journal of Applied Physics*, 90(12):6073–6083.

Wintle, A. G. (1997). Luminescence dating: laboratory procedures and protocols. *Radiation Measurements*, 27:769–817.

Chapter 4

Modelling the thermal quenching mechanism in quartz based on time-resolved optically stimulated luminescence

V. Pagonis[1], C. Ankjærgaard[2], A. S. Murray[3], M. Jain[2], R. Chen[4], J. Lawless[5], and S. Greilich[2]

[1] *McDaniel College, Physics Department, Westminster, MD 21157, USA*
[2] *Radiation Research Division, Risø National Laboratory for Sustainable Energy, Technical University of Denmark, DK-4000 Roskilde, Denmark*
[3] *Nordic Laboratory for Luminescence Dating, Department of Earth Science, Aarhus University, Risø DTU, DK-4000 Roskilde, Denmark.* [4] *Raymond and Beverly Sackler School of Physics and Astronomy, Tel-Aviv University, Tel-Aviv 69978, Israel*
[5] *Redwood Scientific Inc., Pacifica CA 94044, USA*

Abstract

This paper presents a new numerical model for thermal quenching in quartz, based on the previously suggested Mott-Seitz mechanism. In the model electrons from a dosimetric trap are raised by optical or thermal stimulation into the conduction band, followed by an electronic transition from the conduction band into an excited state of the recombination centre. Subsequently electrons in this excited state undergo either a direct radiative transition into a recombination centre, or a competing thermally assisted non-radiative process into the ground state of the recombination centre. As the temperature of the sample is increased, more electrons are removed from the excited state via the non-radiative pathway. This reduction in the number of available electrons leads to both a decrease of the intensity of the luminescence signal and to a simultaneous decrease of the luminescence lifetime. Several simulations are carried out of time-resolved optically stimulated luminescence (TR-OSL) experiments, in which the temperature dependence of luminescence lifetimes in quartz is studied as

a function of the stimulation temperature. Good quantitative agreement is found between the simulation results and new experimental data obtained using a single-aliquot procedure on a sedimentary quartz sample.

Keywords: Time resolved luminescence, optically stimulated luminescence, pulsed OSL, thermoluminescence, quartz, luminescence lifetimes, kinetic rate equations, kinetic model.

4.1   Introduction

The phenomenon of thermal quenching of the stimulated luminescence in quartz has been well known for several decades [see for example, Bøtter-Jensen et al. (2003, p. 44, and references therein)]. Thermal quenching manifests itself as a reduction of the measured luminescence intensity from quartz as the sample temperature is raised, and has been observed in both thermoluminescence (TL) and optically stimulated luminescence (OSL) experiments on quartz (Wintle, 1975; Smith et al., 1990; Spooner, 1994). A model has been suggested previously for explaining thermal quenching in quartz, known as the Mott-Seitz mechanism [see for example Bøtter-Jensen et al. (2003); Chen and McKeever (1997); Bailey (2001); and references therein]. Although the Mott-Seitz mechanism has been discussed extensively in the TL/OSL literature for quartz, to the best of our knowledge there has been no numerical modeling of the kinetic processes involved.

In addition to the well-known effects on the TL and OSL intensities, thermal quenching also affects the apparent luminescence lifetimes in quartz [and other dosimetric materials, see for example Kitis (2002)]. Over the past decade, extensive time-resolved OSL (TR-OSL) measurements have been carried out using samples of both quartz and feldspars, reflecting the importance of these materials in dating and retrospective dosimetry (Sanderson and Clark, 1994; Bailiff, 2000; Tsukamoto et al., 2006; Denby et al., 2006; Chithambo et al., 2008; Pagonis et al., 2009; Ankjærgaard et al., 2009, Chapter 7 of this thesis). During TR-OSL measurements, the stimulation is carried out with a brief light pulse and photons are recorded based on their arrival at the luminescence detector with respect to the light pulse. Summing signals from several pulses gives rise to the typical TR-OSL curve that shows the build up of luminescence during the pulse and the subsequent decrease after the pulse on ns to ms time scales, depending on the processes involved. The decaying signal immediately following any light pulse can be analyzed using the linear sum of exponential decays, and can therefore be characterized using decay constant(s) or lifetime(s). The main advantage of TR-OSL over CW-OSL is that it allows study of such recombination and/or relaxation pathways.

Several researchers have studied the temperature dependence of luminescence lifetimes and luminescence intensity from time-resolved luminescence spectra in quartz [see for example, Galloway (2002); Chithambo (2003, 2006, 2007a,b) and references therein]. The luminescence lifetimes for unannealed sedimentary quartz typically are found to remain constant at ∼42 μs for stimulation temperatures between 20°C and 100°C, and then to decrease continuously to ∼8 μs at 200°C.

The purpose of this paper is to present a new kinetic model for thermal quenching in quartz based on the Mott-Seitz mechanism. In this model all recombination transitions are localized within the recombination centre [in contrast to a delocalized model, where all charge transitions take place to or from the conduction and valence bands — e.g. Bailey (2001)].

Several simulations of typical TR-OSL experiments are carried out using the model, and the results are compared to new measurements of the luminescence lifetimes and luminescence intensity of a sedimentary quartz sample as a function of the stimulation temperature.

4.2   Experimental

In the experimental work presented here, sedimentary quartz [sample WIDG8; Wintle and Murray (1997)] with grain size 90–125 μm has been used. The quartz were extracted from the sample by sieving, heavy liquid separation and HF treatment; the absence of significant feldspar contamination was confirmed by tests using IR stimulation. Sample measurements were carried out on a Risø TL/OSL-20 reader with an integrated pulsing option to control the stimulation LEDs, and with a photon timer attachment with a channel width of 100 ps to record the TR-OSL data (Lapp et al., 2009, Chapter 2 of this thesis). Blue light stimulation was performed with an LED array emitting at 470 ± 30 nm, and delivering 50 mW/cm^2 CW stimulation at the sample position; a 7.5 mm thick Hoya U340 filter was used. The duration of both the on- and off- pulse widths can be set independently to between 0.2 μs and 9.9 s (on-time) and between 0.6 μs and 9.9 s (off-time), although the pulse shape deteriorates for pulse widths <6 μs. During a pulsed measurement, the photon timer records the time of arrival of photons detected during and after the pulse (relative to the beginning of the pulse).

In the measurements, a single aliquot of the quartz sample WIDG8 was optically bleached with blue light for 100 s at 260°C in order to empty all optically active traps, and was subsequently given a beta dose of 5 Gy. It was then preheated for 10 s at 260°C and the TR-OSL was measured by repeatedly turning the optical stimulation ON for 50 μs and OFF for 500 μs. This was followed by an optical bleach for 100 s at 260°C. The whole process was repeated for higher stimulation temperatures, from 20°C to 320°C in steps of 20°C. Recycling measurements were done for the stimulation temperatures 40°C, 100°C, 200°C, and 300°C.

4.3   The Mott-Seitz mechanism of thermal quenching in quartz

The principles behind the Mott and Seitz mechanism of thermal quenching in quartz have been summarized previously, for example in Bøtter-Jensen et al. (2003, p. 44). The Mott-Seitz mechanism is usually shown schematically using a configurational diagram as in Fig. 4.1a, and consists of an excited state of the recombination centre and the corresponding ground state. In this mechanism, electrons are captured into an excited state of the recombination centre, from which they can undergo either one of two competing transitions. The first transition is a direct radiative recombination route resulting in the emis-

CONFIGURATIONAL DIAGRAM

(a)

(b)
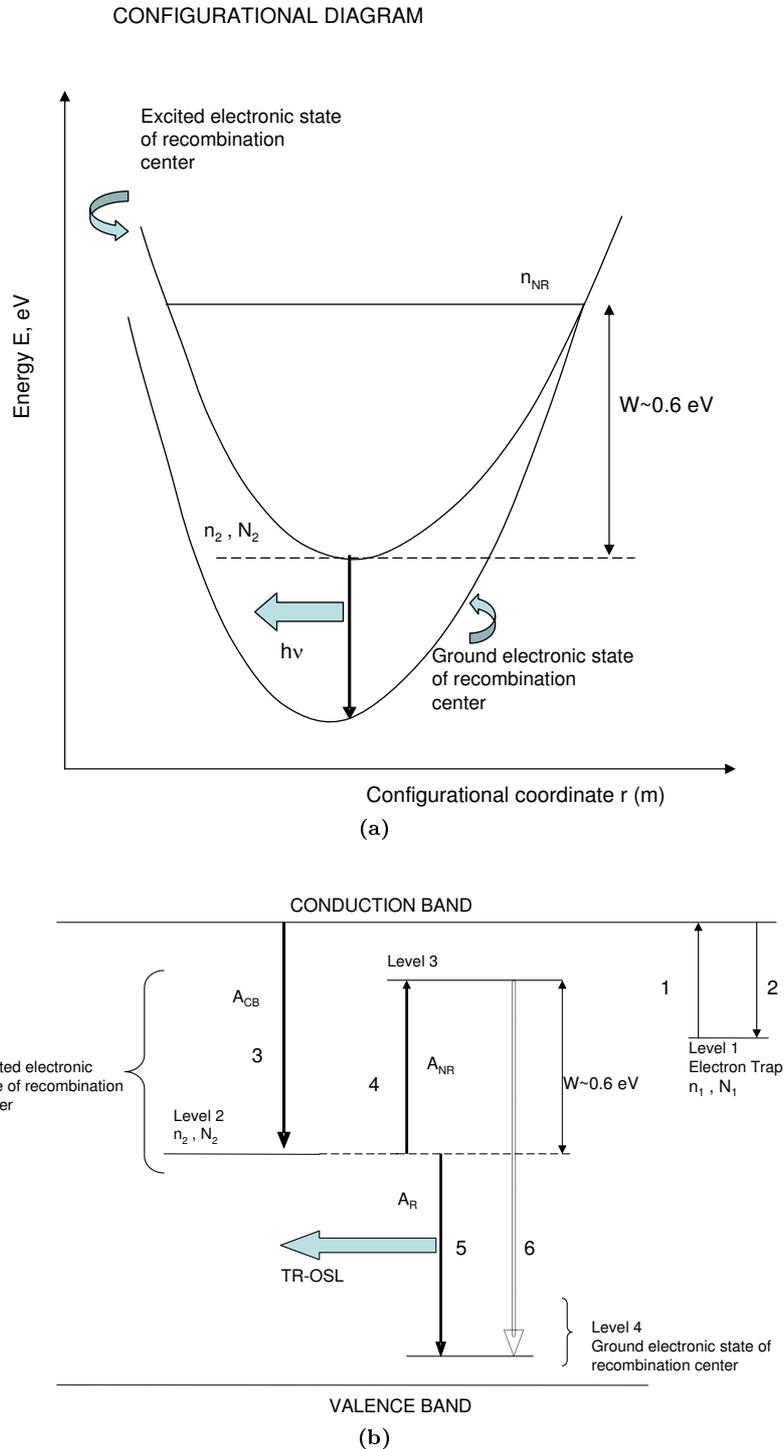
Figure 4.1: (a) The configurational diagram outlining the Mott-Seitz mechanism in quartz. (b) Schematic diagram of the thermal quenching model for quartz, which contains a dosimetric trap (level 1), two excited states within the radiative recombination centre (levels 2 and 3), and the corresponding ground state (level 4). The various transitions shown and the parameters used in the model are described in the text.

sion of light and is shown as a vertical arrow in Fig. 4.1a. The second route
is an indirect thermally assisted non-radiative transition into the ground state
of the recombination centre; the activation energy W for this non-radiative
process is also shown in Fig. 4.1a. The energy given up in the non-radiative
recombination is absorbed by the crystal as heat, rather than being emitted
as photons. One of the main assumptions of the Mott-Seitz mechanism is that
the radiative and non-radiative processes compete within the confines of the
recombination centre, hence they are referred to as localized transitions. Dur-
ing TR-OSL experiments a brief exposure to stimulating light (a light pulse)
raises a small number of electrons from the electron trap into the conduction
band (CB); some of these electrons are then trapped by the excited state of the
recombination centre (RC). Electrons trapped in this excited state may then
relax to the ground state of the RC through a direct radiative transition (re-
sulting in emission of a photon) or through a non radiative transition (in which
the relaxation energy increases the thermally induced vibrations of the lattice,
Fig. 4.1a). In the approach first described by Mott (Mott and Gurney, 1948;
Curie, 1963), the probability of the non-radiative process, A_{NR}, is assumed to
have a temperature dependent scaling described by a Boltzmann factor of the
form $\exp(-W/k_BT)$, where W is the activation energy, T is temperature and
k_B is Boltzmann's constant, while the radiative probability A_{R} is assumed to
be a constant independent of temperature. The constants A_{R} and A_{NR} have
dimensions of s^{-1}. Thus, the experimentally observed luminescence will be
proportional to the luminescence efficiency ratio $\eta(T)$ defined by the relative
probabilities of radiative and nonradiative transitions:

$$\eta(T) = \frac{A_{\mathrm{R}}}{A_{\mathrm{R}} + A_{\mathrm{NR}}\exp(-W/k_BT)} = \frac{1}{1 + \frac{A_{\mathrm{R}}}{A_{\mathrm{NR}}}\exp(-W/k_BT)}. \tag{4.1}$$

Experimentally it has been found that the CW-OSL or the 325°C TL peak
intensity from quartz samples follow a very similar expression to Eqn. (4.1)
with the empirical form:

$$I(T) = \frac{I_0}{1 + C\exp(-W/k_BT)}, \tag{4.2}$$

where I_0 is the luminescence intensity at low temperatures and C is a dimen-
sionless constant [Chithambo (2007b), Eqn. (7); Wintle and Murray (1997);
Wintle (1975)]. As the temperature of the quartz sample is increased dur-
ing stimulation, the experimentally measured luminescence intensity $I(T)$ de-
creases with temperature according to Eqn. (4.2). This empirically observed
form is similar to the expression derived on the basis of Mott-Seitz mechanism
ie. Eqn. (4.1). By comparison of the empirical expression (4.2) with the lu-
minescence efficiency expression (4.1), the dimensionless empirical constant C
appearing in Eqn. (4.2) can be interpreted as the ratio of the non-radiative and
radiative probabilities $A_{\mathrm{NR}}/A_{\mathrm{R}}$.

However, in order to test whether the Mott-Seitz mechanism could be re-
sponsible for thermal quenching in quartz, one should be able to make esti-
mates of transition probabilities as a function of temperature; these estimates
are unfortunately not possible in CW-OSL or TL measurements. However,
the analysis of time-resolved OSL signals offers such a possibility. Recently
Chithambo (2007b, Eqn. (5)) has shown that the luminescence lifetime (τ)

derived from the TR-OSL signals of quartz samples also shows a similar temperature dependence:

$$\tau = \frac{\tau_0}{1 + C \exp(-W/k_B T)},$$ (4.3)

where $\tau_0 = 42$ µs is the experimentally-observed lifetime for the radiative process in unannealed quartz at low temperatures. As the temperature T of the sample is increased during the optical stimulation the lifetime $\tau(T)$ of the electrons in the excited state decreases according to Eqn. (4.3). A good agreement between Eqn. (4.2) [or (4.3)] and the TR-OSL data thus lends support to the Mott-Seitz model as possible explanation for thermal quenching in quartz. To our knowledge a mathematical implementation of this model has not been undertaken before; the schematic approach in Fig. 4.1a is not based on a detailed numerical model involving electronic transitions between energy states within the recombination centre. The purpose of this paper is to develop and test such a kinetic model.

4.4   A kinetic model for thermal quenching in quartz

Figure 4.1b shows the energy level diagram in a simple new model based on the Mott-Seitz mechanism, with the corresponding electronic transitions taking place during a typical TR-OSL experiment. The model consists of a dosimetric trap shown as level 1, and three levels labeled 2-4 representing energy states within the recombination centre. During the transition labeled 1 in Fig. 4.1b, electrons from a dosimetric trap are raised by optical stimulation into the CB, with some of these electrons being retrapped as shown in transition 2 with a probability A_n. Transition 3 corresponds to an electronic transition from the CB into the excited state located below the conduction band with probability A_{CB}. Transition 5 indicates the direct radiative transition from the excited level into the ground electronic state with probability A_R, and transition 4 indicates the competing thermally assisted route. The probability for this competing thermally assisted process is given by a Boltzmann factor of the form $A_{NR} \exp(-W/k_B T)$ where W represents the activation energy for this process and A_{NR} is a constant representing the non-radiative transition probability (i.e. the probability of non radiative transition at infinite temperature). Transition 6 denotes the non-radiative process into the ground state, the dashed arrow in the Fig. 4.1b indicating that it is not a discrete energy loss but rather a continuous energy loss resulting in heat. The details of the non-radiative process of releasing energy in the model are not important; what is important in determining the thermal quenching effects is the ratio of the non-radiative and radiative probabilities A_{NR}/A_R, or the constant C defined from empirical observations, and the value of the thermal activation energy W.

The competing transitions 4 and 5 in Fig. 4.1b form the basis of our description of the thermal quenching process in quartz and are the causes of two simultaneous effects. As the temperature of the sample is increased, electrons are removed from the excited state according to the Boltzmann factor described above. This reduction leads to both a decrease of the intensity of the luminescence signal and to a simultaneous apparent decrease of the luminescence lifetime.

Several experiments (Wintle, 1975; Smith et al., 1990; Spooner, 1994; Chithambo, 2003) have reported a range of values of the constants C, W appearing in Eqns. (4.1) through (4.3). Typical ranges for the numerical values for these constants in quartz are $W = 0.5$–0.8 eV and $C = 10^6$–10^8 [see for example, Chithambo (2003, Table 1) for a tabulation of several results]. The parameters used in the model are defined as follows; N_1 is the concentration of electrons in the dosimetric traps (m^{-3}), n_1 is the corresponding concentration of trapped electrons (m^{-3}), N_2 and n_2 are the concentrations of electron traps and filled traps correspondingly in the excited level 2 of the recombination centre (m^{-3}), $W = 0.64$ eV is the activation energy for the thermally assisted process (eV), A_n is the conduction band to electron trap transition probability coefficient (m^{3}s^{-1}), A_R and A_{NR} are the radiative and non-radiative transition probability coefficients (s^{-1}), and A_{CB} is the transition probability coefficient (m^{3}s^{-1}) for the conduction band to excited state transition. The parameter n_c represents the instantaneous concentration of electrons in the conduction band (m^{-3}) and P denotes the probability of optical excitation of electrons from the dosimetric trap (s^{-1}).

The equations used in the model are as follows:

$$\frac{dn_1}{dt} = n_c(N_1 - n_1)A_n - n_1 P, \tag{4.4}$$

$$\frac{dn_c}{dt} = -n_c(N_1 - n_1)A_n + n_1 P - A_{CB}n_c(N_2 - n_2), \tag{4.5}$$

$$\frac{dn_2}{dt} = A_{CB}n_c(N_2 - n_2) - A_R n_2 - n_2 A_{NR}\exp(-W/k_B T), \tag{4.6}$$

The instantaneous luminescence $I(t)$ resulting from the radiative transition is defined as

$$I(t) = A_R n_2. \tag{4.7}$$

It is noted that transitions 4, 5 and 6 in Fig. 4.1a are of a localized nature, while transition 3 involves electrons in the CB and hence is delocalized. The difference in the nature of these transitions can also be seen in their mathematical forms in Eqns. (4.4–4.7). The term $A_{CB}n_c(N_2 - n_2)$ in Eqns. (4.5) and (4.6) expresses the fact that there are $N_2 - n_2$ empty electronic states available for electrons in the CB; these states are excited states of the recombination centre, in agreement with the general assumptions of the Mott-Seitz mechanism of thermal quenching.

The values of the parameters used in the model are as follows: $A_n = 5 \cdot 10^{-14}$ cm^3/s, $A_R = \frac{1}{42\mu s} = 2.38 \cdot 10^4$ s^{-1}, $A_{CB} = 10^{-8}$ cm^3/s, $P = 0.2$ s^{-1}, $N_1 = 10^{14}$ cm^{-3}, $N_2 = 10^{14}$ cm^{-3}. In the absence of any experimental evidence to the contrary, we will make the assumption that the conduction band empties much faster than the luminescence process in the recombination centre which is assumed to take place with the experimentally observed luminescence lifetime of $\sim$42 μs. We therefore choose the values of the delocalized transition probability A_{CB} and of the concentration N_2 such that the conduction band empties very quickly when the stimulating light is switched off, on a time scale of $\sim$1 μs. Note that the chosen values of A_{CB} and N_2 are about 1 and 3 orders of magnitude higher than those used by Bailey (2001), respectively. Without such an increase in either the transition probability and/or the value of N_2, it is not possible to empty the conduction band sufficiently quickly to explain
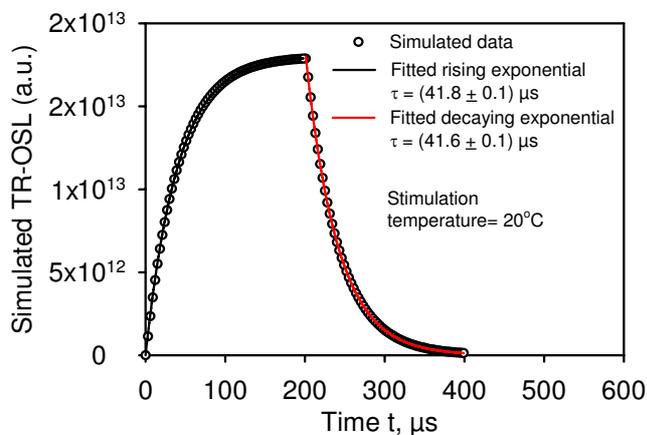
Figure 4.2: Simulated time resolved spectrum for quartz using the model shown in Fig. 4.1. The LED stimulation is ON for 200 µs and OFF for the same amount of time. The rising and decaying parts of the signal are fitted with a rising exponential and a decaying exponential correspondingly.

the experimental TR-OSL results using a model in which the recombination centre is thermally quenched. The value of the radiative transition probability $A_{\mathrm{R}} = \frac{1}{42\mu\mathrm{s}} = 2.38 \cdot 10^4\,\mathrm{s}^{-1}$ is taken from experimentally measured luminescence lifetime of $\tau = 42$ µs at room temperature (Chithambo, 2007b; Ankjærgaard et al., 2009, Chapter 7 of this thesis). The value of the non-radiative probability A_{NR} was treated as an adjustable parameter within the model, and is adjusted to obtain the best possible fits to the experimental data. The initial conditions for the different concentrations are taken as: $n_1(0) = 9 \cdot 10^{13}\,\mathrm{cm}^{-3}$, $n_2(0) = 0$, $n_{\mathrm{c}}(0) = 0$.

The results of the simulation were tested by varying the parameters in the model within a physically reasonable range of values. Not surprisingly given the choice of a conduction band lifetime very much less than the lifetime of the excited state of the recombination centre, it was found that the results remained unchanged when the parameters were varied within the following ranges of values: $A_{\mathrm{n}} = 5 \cdot 10^{-12}$–$5 \cdot 10^{-16}\,\mathrm{cm}^3/\mathrm{s}$, $A_{\mathrm{CB}} = 10^{-5}$–$10^{-8}\,\mathrm{cm}^3/\mathrm{s}$, $N_1 = 10^{10}$–$10^{17}\,\mathrm{cm}^{-3}$, $N_2 = 10^{13}$–$10^{16}\,\mathrm{cm}^{-3}$, $n_1(0) = 9 \cdot 10^{10}$–$9 \cdot 10^{13}\,\mathrm{cm}^{-3}$. The results of the simulation only depended significantly on the values of the radiative and non-radiative probabilities A_{R} and A_{NR} used in the model. These dependencies of the results on the parameters make physical sense, since the Mott-Seitz mechanism is primarily an internal competition mechanism within the recombination centre, and should not depend critically on the values of the external parameters in the model. Thus, TR-OSL gives us a very useful insight into the lower limits of these parameter values.

4.5 Simulation of a typical TR-OSL experiment using the new model

We have simulated a typical TR-OSL experiment in which the optical stimulation is initially ON for 200 µs and is subsequently turned OFF for the
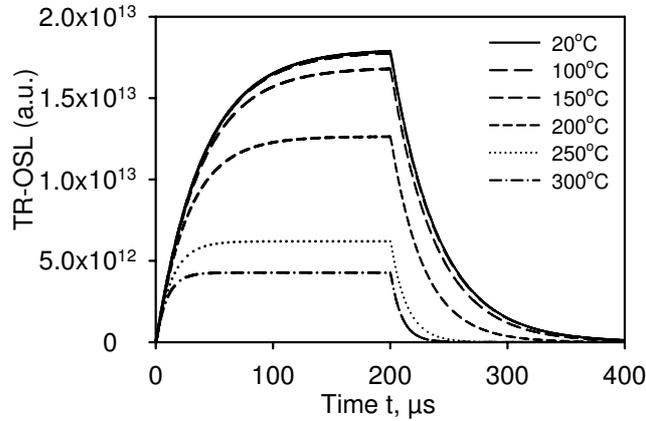
Figure 4.3: Simulated time resolved spectra for quartz at various stimulation temperatures between 20 and 300°C. As the stimulation temperature increases the corresponding luminescence lifetime decreases for both parts of the signal.

same amount of time. Figure 4.2 shows the results of this simulation using the model in Fig. 4.1b, and with the parameters listed in the previous section. The decaying part of the signal in Fig. 4.2 has been fitted to a decaying exponential, while the rising part of the signal in the same figure is fitted to a saturating exponential function. The fits are shown as solid lines through the simulated data, and they yield almost identical luminescence lifetimes with values $\tau_{\text{rise}} = (41.8 \pm 0.1)$ μs and $\tau_{\text{decay}} = (41.6 \pm 0.1)$ μs.

We have repeated this simulation by varying the stimulation temperature in the range 20-300°C, with the results shown in Figs. 4.3 and 4.4. It is noted that the preheat and irradiation parts of the experimental procedure are not part of the simulation, but we assume instead a non-zero initial concentration of electrons in the dosimetric trap, as was explained in the previous section. Figure 4.3 shows clearly that as the stimulation temperature increases, the luminescence lifetime for both the rising and falling part of the signal decrease continuously because of thermal quenching. The luminescence lifetimes τ, obtained by fitting single exponentials to the simulated TR-OSL curves in Fig. 4.3, are shown in Fig. 4.4. The simulation results in Fig. 4.4a show that as the stimulation temperature increases, the luminescence lifetimes obtained from the exponential fits decrease smoothly from $\sim$42 μs to $\sim$2 μs in the temperature range 20-300°C. It is noted that the rising and decaying parts of all simulated TR-OSL signals in Fig. 4.3 yield indistinguishable luminescence lifetimes, in agreement with the results of several previous experimental studies (Chithambo, 2007b). Because we have chosen parameter values such that the conduction band empties much faster than the excited state of the recombination centre, we see no evidence for the presence of multiple exponential components in these simulations.

Superimposed on the simulated data of Fig. 4.4a we show the experimental data on the luminescence lifetime for sample WIDG8 (open triangles), including recycling points at 40, 100, 200 and 300°C (filled triangles). The solid line in Fig. 4.4a indicates the best fit to the simulation data using the thermal quenching Eqn. (4.3) with an activation energy $W = 0.64$ eV and a value of
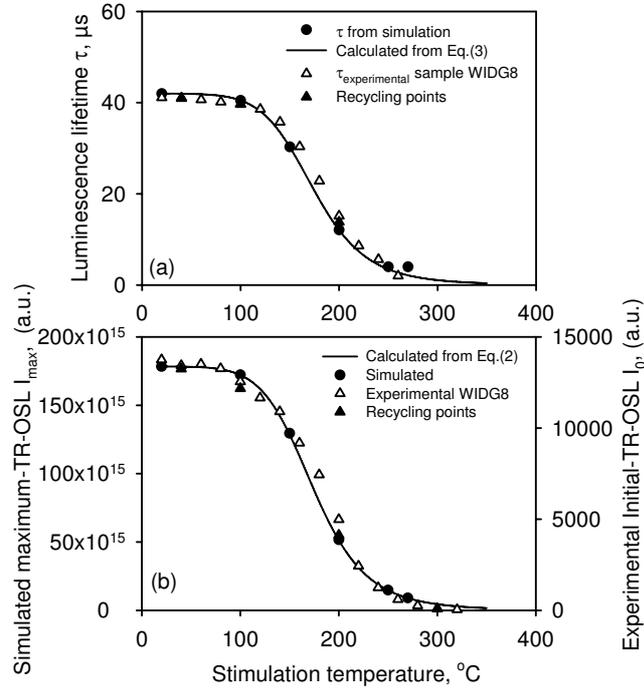
Figure 4.4: (a) Experimental dependence of the luminescence lifetime τ on the stimulation temperature for sample WIDG8 is shown as the open triangles and filled triangles denote recycling points. The solid line indicates the best fits to the simulated data using the thermal quenching Eqn. (4.4) with an activation energy $W = 0.64$ eV and the dimensionless constant $C = 1.64 \cdot 10^7$. The solid circles show the simulated luminescence lifetimes obtained from Fig. 4.3. (b) The experimental dependence of the maximum luminescence intensity on the stimulation temperature for sample WIDG8 is shown by the open triangles and recycling points as filled triangles. The solid line is calculated using the thermal quenching Eqn. (4.3). The solid circles show the maximum luminescence intensity obtained from the simulated TR-OSL spectra in Fig. 4.3.

the non-radiative probability $A_{NR} = 3.9 \cdot 10^{11}$ s^{-1}, corresponding to a value of the dimensionless constant $C = A_{NR}/A_R = 1.64 \cdot 10^7$.

Figure 4.4b shows the maximum TR-OSL intensity of the simulated signals shown in Fig. 4.3, as a function of the stimulating temperature. Superimposed on the simulated data we show the corresponding experimental data for sample WIDG8, as well as the calculated maximum intensity using Eqn. (4.2). The solid line in Figure Fig. 4.4b indicates the best fit to the simulated data using the thermal quenching Eqn. (4.3), and with the same parameters C, W used in Fig. 4.4a.

The simulation data in Fig. 4.5 show typical examples of the time variation of the concentrations of electrons in the CB and in the excited state (n_2) during the decaying signal of the TR-OSL experiment at room temperature. As expected from our choice of parameters, the lifetimes of electrons in the CB are extremely short as compared with the lifetime in the excited state. With the choice of parameters in the model the CB empties very quickly within a few
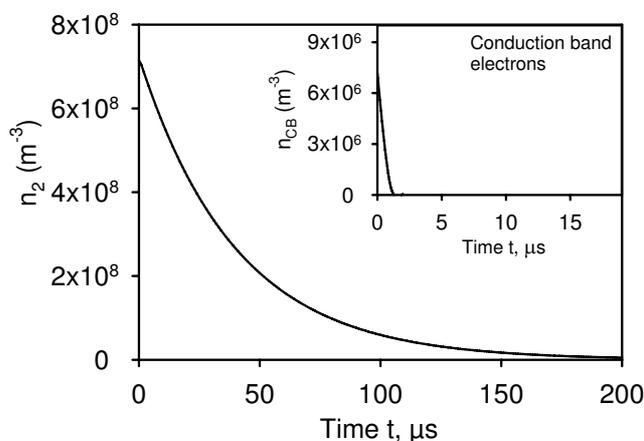
Figure 4.5: (a) The variation of the electron concentration n_2 in the excited state of the recombination centre (level 2 in Fig. 4.1b), as a function of time during the decaying OFF-time period of the TR-OSL signal at room temperature. The luminescence lifetime of electrons in the CB is very short as seen in the inset, while the lifetime of the excited state (n_2) is much longer. (b) The observed TR-OSL signal decays at exactly the same rate as the concentration of electrons in the excited state, as shown in (a).

μs as shown in the inset of Fig. 4.5, while the excited state decays radiatively much slower in agreement with the experimentally observed lifetime of ∼40 μs at room temperature. The corresponding TR-OSL signal decays at the exact same rate as the excited state (n_2), in agreement with Eqn. (4.7).

4.6 Further results of the model

During a typical TR-OSL experiment, the signals from several thousands of pulses are added digitally to yield the measured total luminescence signal. An important consideration during such experiments is whether the shape of the individual TR-OSL spectra stays the same between pulses, and therefore whether one can justifiably add many individual pulses. We have simulated such a sequence of 100,000 pulses using the model of Fig. 4.1, with the concentrations at the end of each pulse being used as the initial concentrations of the next pulse. The resulting TR-OSL signals in this simulation are shown in Fig. 4.6, where it is seen that even after 100,000 pulses the TR-OSL signal maintains its shape and yields the same luminescence lifetime. The results of the simulation show that after 100,000 pulses the concentration of holes in the recombination centre decreases by only 3.5% of its initial value.

An important result from the model is that it produces reasonable results for very long illumination times of the order of seconds. In such a case one expects that the results of the simulation would resemble what is seen experimentally during a continuous-wave (CW-OSL) experiment. In this simulation of long illumination times, the optical stimulation is left ON for a time period of several seconds, while the OFF part of the simulation is not important in this type of simulation. As seen in Fig. 4.7a, the resulting signal is very similar to
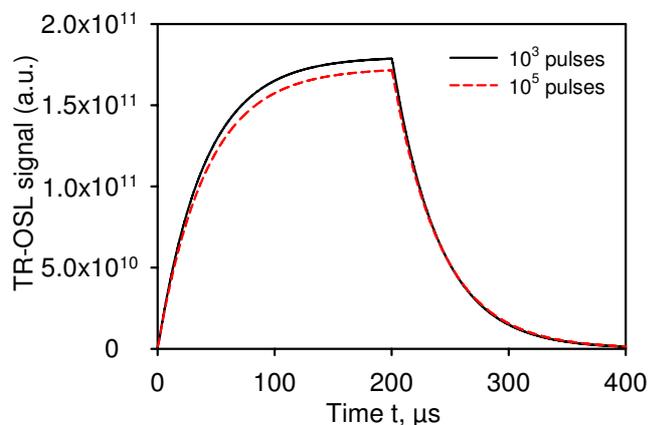
Figure 4.6: Simulation of the TR-OSL signals after summation of 1,000 pulses and after summation of 100,000 pulses.

an OSL decay curve measured during a CW-OSL experiment. The simulation was repeated for different simulation temperatures and the results are shown in Fig. 4.7a. Figure 4.7b shows the area under the stimulation curves in Fig. 4.7a as a function of the stimulation temperature, together with the results from Eqn. (4.3), showing good agreement between the results of the simulation and the thermal quenching factor.

A third important result of the model is that it reproduces the well-known decrease in the thermoluminescence (TL) signal due to thermal quenching. Specifically when TL glow curves are measured using a variable heating rate, the TL intensity is found to decrease as the heating rate increases. The result of simulating the TL glow curves using different heating rates is shown in Fig. 4.8, using typical kinetic parameters for the 325°C TL peak of quartz (activation energy $E = 1.65$ eV and frequency factor $s = 10^{12}$ s^{-1}). As the heating rate increases, the TL glow peaks become wider and shift towards higher temperatures, while their intensity decreases significantly. The inset to Fig. 4.8 shows the decrease of the total area under the TL glow curves with the heating rate, a well-known experimental effect due to thermal quenching.

4.7   Discussion

Several experimental studies of quartz samples have elucidated the nature of the recombination centres in quartz. It is believed that the main quartz emission band at 380 nm is due to recombination processes taking place at $(H_3O_4)^0$ hole centres (Yang and McKeever, 1990). Furthermore, it is thought that the 110°C TL signal and at least part of the main OSL signal from quartz are also associated with this hole centre. Additional quartz emission bands have been identified at 420 nm (Bailiff, 1994) and at 460 nm, with the latter emission believed to be due to $(AlO_4)^0$ centres (Yang and McKeever, 1990). Later experimental studies have provided important links between specific impurities in quartz and ionic movements in the crystal, as well as additional information on the nature of the ionic complexes involved in the luminescence process in
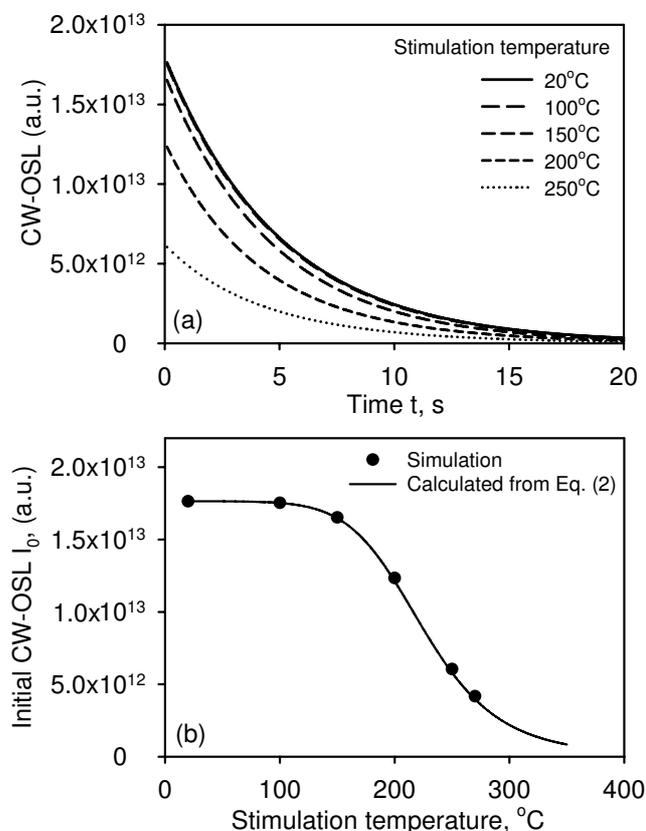
Figure 4.7: (a) Simulation of the TR-OSL signal when the optical stimulation is ON for very long times, while the OFF period is not important in this type of simulation. The resulting curves are similar to "shine down" curves obtained experimentally during a continuous-wave CW-OSL experiment. (b) Variation of the area under the shine down curves in (a), with the stimulation temperature (solid circles). The solid line is calculated using Eqn. (4.3) for thermal quenching.

quartz (Itoh et al., 2001; Schilles et al., 2001; Poolton et al., 2000; Vartanian et al., 2000).

In the rest of this section we discuss the relationship between the quartz model presented in this paper and the more comprehensive quartz models found in the literature (Bailey, 2001; Adamiec, 2005; Pagonis et al., 2008). For comparison purposes we choose the model of Bailey (2001) as a representative example of commonly used phenomenological quartz models. The purpose of this discussion is to emphasize the differences between localized and delocalized transitions contained in the models. The Bailey model contains a total of 5 electronic levels and 4 hole centres, and has been used successfully to simulate a wide variety of TL and OSL experiments in quartz. In this model the luminescence intensity from quartz is written as [Bailey (2001), p. 22, Eqn. (6)]:

$$I(t) = A_{\mathrm{CB}} m n_{\mathrm{c}} \eta(T), \tag{4.8}$$

where A_{CB} represents the probability of electronic transitions from the con-
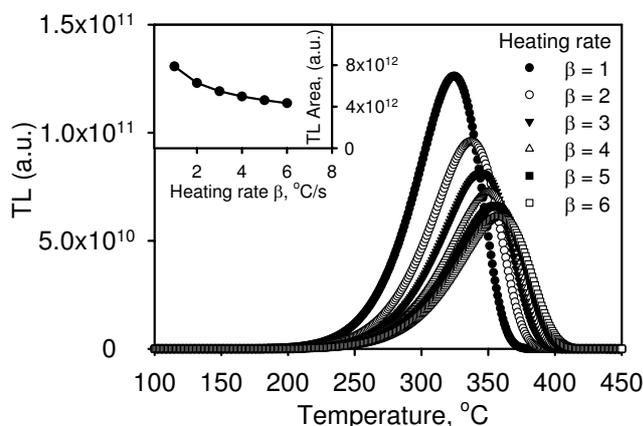
Figure 4.8: Simulation of the thermoluminescence (TL) signal measured with different heating rates, by using the model in Fig. 4.1. The inset shows the variation of the area under the TL glow curves as function of the heating rate. The simulated decrease of the TL area with the heating rate is due to the presence of thermal quenching.

duction band into the recombination centre, m represents the instantaneous concentration of holes in the recombination centre, n_c is the concentration of electrons in the CB, and $\eta(T)$ is the "luminescence efficiency factor" given by a Mott-Seitz type of expression:

$$\eta(T) = \frac{1}{1 + C \exp(-W/k_B T)}. \tag{4.9}$$

Within the Bailey model, Eqn. (4.8) above clearly represents mathematically a *delocalized* transition involving electrons in the conduction band. Furthermore, Eqn. (4.9) above in the Bailey model expresses mathematically the thermal quenching process by using a phenomenological efficiency factor $\eta(T)$.

By contrast, in the model presented in this paper the luminescence intensity is expressed by the expression:

$$I(t) = A_R n_2, \tag{4.10}$$

which represents mathematically a *localized* transition from the excited level of the recombination centre into the ground state of the same centre. In the model of Fig. 4.1b, all transitions are of a localized nature, except for transition 3 which involves electrons in the CB and hence is delocalized. Mathematically this delocalized transition is expressed by the term $A_{CB} n_c (N_2 - n_2)$ in Eqns. (4.5) and (4.6). The present model is therefore a mathematical description of a completely internal mechanism within the recombination centre, and is based on electronic transitions of a localized nature. Furthermore, the present model is developed in terms of electrons occupying multiple energy states within the recombination centre, while in the Bailey delocalized model one considers a single radiative transition from the CB into the recombination centre.

We have attempted to simulate the TR-OSL experiment described in this paper using the Bailey (2001) model, and found that the relaxation time within

the model is $\tau \sim 0.1$ s, three orders of magnitude larger than the experimentally found value of $\tau = 42$ μs. It is possible to select parameter values within the Bailey model that will give a lifetime consistent with experiment, and also with the experimentally observed decrease in luminescence intensity with stimulation temperature. However, in the Bailey and other similar models there is no process by which this lifetime is temperature dependent, in contrast to experimental observation and the predictions of our model.

The ultimate goal of a comprehensive thermal quenching model for quartz should be a more inclusive model, namely a model which would combine the delocalized processes in the Bailey model with an appropriate modification of the parameter values to explain observed emptying of the conduction band from the TR-OSL experiments, and the localized processes described in this paper. Such a comprehensive model would be able to describe a wider variety of luminescence phenomena in quartz, from a time scale of microseconds to tens of seconds. Such an encompassing effort is currently in progress.

4.8 Conclusions

The Mott-Seitz mechanism for thermal quenching in quartz was first suggested several decades ago, and provides a physical explanation based on localized transitions for several thermal quenching phenomena in quartz. In this paper we presented a simple kinetic model for the Mott-Seitz mechanism. The model provides a satisfactory mathematical description of the internal thermal quenching mechanism of luminescence in quartz. The results of the model compare quantitatively with new experimental results obtained using a single aliquot procedure on a sedimentary quartz sample.

The model can be applied to several types of luminescence experiments involving very different time scales. In the case of TR-OSL experiments the model can describe thermal quenching phenomena within a time scale of microseconds, while in the case of CW-OSL and TL experiments the model provides a satisfactory description of the thermal quenching kinetics within a time scale of tens of seconds.

One important conclusion from the model presented here, is that the existing model parameters for quartz do not allow quick enough emptying of the CB, and therefore can not explain the TR-OSL data. Specifically, all available experimental evidence points that no matter what the quartz type, the TR-OSL lifetime at room temperature should be of the order of tens of μs. However, as pointed out above, the relaxation time within the Bailey model is $\tau \sim 0.1$ s, three orders of magnitude larger than the experimental value. This is of course not a fundamental failure in the current models, but rather it calls for a re-evaluation of the available model parameters for quartz.

Acknowledgement

References

Adamiec, G. (2005). Investigation of a numerical model of the pre-dose mechanism in quartz. *Radiation Measurements*, 39:175–189.

Ankjærgaard, C., Jain, M., Kalchgruber, R., Lapp, T., Klein, D., McKeever, S. W. S., Murray, A. S., and Morthekai, P. (2009). Further investigations into pulsed optically stimulated luminescence from feldspars using blue and green light. *Radiation Measurements*, 44:576–581.

Bailey, R. M. (2001). Towards a general kinetic model for optically and thermally stimulated luminescence of quartz. *Radiation Measurements*, 33:17–45.

Bailiff, I. K. (1994). The pre-dose technique. *Radiation Measurements*, 23:471–479.

Bailiff, I. K. (2000). Characteristics of time-resolved luminescence in quartz. *Radiation Measurements*, 32:401–405.

Bøtter-Jensen, L., McKeever, S. W. S., and Wintle, A. G. (2003). *Optically Stimulated Luminescence Dosimetry*. Elsevier, Amsterdam, The Netherlands. ISBN: 0–444–50684–5.

Chen, R. and McKeever, S. (1997). *Theory of thermoluminescence and related phenomena*. World Scientific Publishing, P O Box 128, Farrer Road, Singapore 912805.

Chithambo, M. L. (2003). Dependence of the thermal influence on luminescence lifetimes from quartz on the duration of optical stimulation. *Radiation Measurements*, 37:167–175.

Chithambo, M. L. (2006). On the correlation between annealing and variabilities in pulsed-luminescence from quartz. *Radiation Measurements*, 41:862–865.

Chithambo, M. L. (2007a). The analysis of time-resolved optically stimulated luminescence: I. Theoretical considerations. *J. Phys. D: Appl. Phys.*, 40:1874–1879.

Chithambo, M. L. (2007b). The analysis of time-resolved optically stimulated luminescence: II. Computer simulations and experimental results. *J. Phys. D: Appl. Phys.*, 40:1880–1889.

Chithambo, M. L., Ogundare, F. O., and Feathers, J. (2008). Principal and secondary luminescence lifetime components in annealed natural quartz. *Radiation Measurements*, 43:1–4.

Curie, D. (1963). *Luminescence in Crystals*. Wiley, New York.

Denby, P. M., Bøtter-Jensen, L., Murray, A. S., Thomsen, K. J., and Moska, P. (2006). Application of pulsed osl to the separation of the luminescence components from a mixed quartz/feldspar sample. *Radiation Measurements*, 41:774–779.

Galloway, R. B. (2002). Luminescence lifetimes in quartz: dependence on annealing temperature prior to beta irradiation. *Radiation Measurements*, 35:67–77.

Itoh, N., Stoneham, D., and Stoneham, A. M. (2001). The predose effect in thermoluminscent dosimetry. *Journal of Physics: Condensed Matter*, 13:2201–2209.

Kitis, G. (2002). Confirmation of the influence of thermal quenching on the initial rise method in α-Al$_2$O$_3$:C. *Physica Status Solidi (A), Applied Research*, 191:621–627.

Lapp, T., Jain, M., Ankjærgaard, C., and Pirzel, L. (2009). Development of pulsed stimulation and photon timer attachments to the Risø TL/OSL reader. *Radiation Measurements*, 44:571–575.

Mott, N. F. and Gurney, R. W. (1948). *Electronic Processes in Ionic Crystals*. Oxford University Press, London, 2$^{\text{nd}}$ edition.

Pagonis, V., M., M. S., Chithambo, M. L., Christensen, E., and Barnold, C. (2009). Experimental and modelling study of pulsed optically stimulated luminescence in quartz, marble and beta irradiated salt. *Journal of Physics D: Applied Physics*, 42:1–12.

Pagonis, V., Wintle, A. G., Chen, R., and Wang, X. L. (2008). A theoretical model for a new dating protocol for quartz based on thermally transferred OSL (TT-OSL). *Radiation Measurements*, 43:704–708.

Poolton, N. R. J., Smith, G. M., Riedi, P. C., Bulur, E., Bø tter Jensen, L., Murray, A. S., and Adrian, M. J. (2000). Luminescence sensitivity changes in natural quartz induced by high temperature annealing: a high frequency EPR and OSL study. *Journal of Physics D: Applied Physics*, 33:1007–1017.

Sanderson, D. C. W. and Clark, R. J. (1994). Pulsed photostimulated luminescence of alkali feldspars. *Radiation Measurements*, 23:633–639.

Schilles, T., J., P. N. R., E., B., tter Jensen L., B., S., M. A., M., S. G., Riedi, P. C., and J., W. G. A. (2001). A multi-spectroscopic study of luminescence sensitivity changes in natural quartz induced by high-temperature annealing. *Journal of Physics D: Applied Physics*, 34:722–731.

Smith, B. W., Rhodes, E. J., Stokes, S., and Spooner, N. A. (1990). The optical dating of sediments using quartz. *Radiation Protection Dosimetry*, 34:75–78.

Spooner, N. A. (1994). On the optical dating signal from quartz. *Radiation Measurements*, 23(2–3):593–600.

Tsukamoto, S., Denby, P. M., Murray, A. S., and Bøtter-Jensen, L. (2006). Time-resolved luminescence from feldspars: New insight into fading. *Radiation Measurements*, 41:790–795.

Vartanian, E., Guibert, P., Roque, C., Bechtel, F., and Schvoerer, M. (2000). Changes in OSL properties of quartz by preheating: an interpretation. *Radiation Measurements*, 32:647–652.

Wintle, A. G. (1975). Thermal quenching of thermoluminescence in quartz. *Geophysical Journal of the Royal Astronomical Society*, 41:107–113.

Wintle, A. G. and Murray, A. S. (1997). The relationship between quartz thermoluminescence, photo-transferred thermoluminescence, and optically stimulated luminescence. *Radiation Measurements*, 27(4):611–624.

Yang, X. H. and McKeever, S. W. S. (1990). The pre-dose effect in crystalline quartz. *Journal of Physics D: Applied Physics*, 23:237–244.

Chapter 5

Charge recombination processes in minerals studied using optically stimulated luminescence and time-resolved exo-electrons

S. Tsukamoto[1,2], A. S. Murray[2], C. Ankjærgaard[3], M. Jain[3] and T. Lapp[3]

[1] *Leibniz Institute for Applied Geophysics, Geochronology and Isotope Hydrology, Stilleweg 2, D-30655 Hannover, Germany*
[2] *Nordic Laboratory for Luminescence Dating, Department of Earth Sciences, Aarhus University, Risø DTU, DK-4000 Roskilde, Denmark*
[3] *Radiation Research Division, Risø National Laboratory for Sustainable Energy, Technical University of Denmark, DK-4000 Roskilde, Denmark*

Abstract

A time-resolved optically stimulated exo-electron (TR-OSE) measurement system has been developed using a Photon Timer attached to a gas-flow semi-proportional pancake electron detector within a Risø TL/OSL reader. The decay rate of the exo-electron emission after the stimulation pulse depends on the probability of (1) escape of electrons into the detector gas from the conduction band by overcoming the work function of the material, and (2) thermalisation of electrons in the conduction band, and subsequent re-trapping/recombination. Thus we expect the exo-electron signal to reflect the instantaneous electron concentration in the conduction band. In this study, TR-OSE and TR-OSL were measured for the first time using quartz, K-feldspar and NaCl by stimulating the samples using pulsed blue LEDs at different temperatures between 50 and 250°C after beta irradiation and preheating to 280°C. The majority of TR-OSE signals from all the samples decayed much faster than TR-OSL signals irrespective of the stimulation temperatures. This suggests that the lifetime of OSL in these dosimeters arises mainly from the relaxation of an excited state of the recombination centre, rather than from residence time of an electron in

the conduction band.

5.1   Introduction

The luminescence lifetime of minerals has been investigated using time-resolved optically stimulated luminescence (TR-OSL) to understand the recombination process of luminescence [e.g. Clark et al. (1997); Chithambo and Galloway (2001); Ankjærgaard et al. (2009a, Chapter 7 of this thesis)]. TR-OSL has been measured using pulsed laser e.g. Sanderson and Clark (1994); Ankjærgaard et al. (2009a, Chapter 7 of this thesis) or LEDs and summing signals from many pulses (Chithambo and Galloway, 2000b; Denby et al., 2006). The time delay between stimulation and luminescence emission can be considered to result from 3 processes, see Fig. 5.1: (i) eviction of charge from the trap to the conduction band, (ii) the recombination lifetime (a function of the electron concentration in the conduction band and hole concentration) and (iii) the de-excitation time (lifetime) of the excited state of the recombination centre. As the signals here are examined after light stimulation has ceased, the first process can be neglected; the luminescence lifetime is then presumably dominated by a combination of the two latter processes, but it is difficult to determine which, if either, dominates.

One method which can be used directly to probe electron concentrations in the conduction band is the emission of optically stimulated exo-electrons (OSE). Exo-electron emission can occur when electrons in a trap absorb enough energy to overcome the work function of the crystal surface, χ, and escape from the surface, or when electrons already in the conduction band acquire sufficient thermal energy to overcome the work function. By pulsing the stimulation light source and detecting both the time-resolved OSL and OSE signals between the pulses, it is possible to compare whether the lifetime of the emitted luminescence (the TR-OSL signal) is similar or not to the mean life of the electron concentration in the conduction band (TR-OSE signal).

Here we compare the lifetimes of these signals from quartz, K-feldspar and NaCl to experimentally determine, for the first time, whether the TR-OSL lifetime is dominated by the rate at which the conduction band empties, or by the rate of relaxation of the excited state(s) of the recombination centre(s).

5.2   A model for exo-electron emission

Here we outline the model used in this paper to describe exo-electron emission, defined as the emission of low-energy electrons from the surface of a solid following excitation by ionizing radiation. The different mechanisms of exo-electron emission from a solid have been classified according to the stimulation method by Oster et al. (1999) and a mathematical model was later developed by Oster and Haddad (2003) to describe photo-stimulated exo-electron mechanisms. An overview of the different exo-mechanisms relevant to our natural dosimeters is presented in Fig. 5.1 (solid arrows denote optical stimulation and dashed
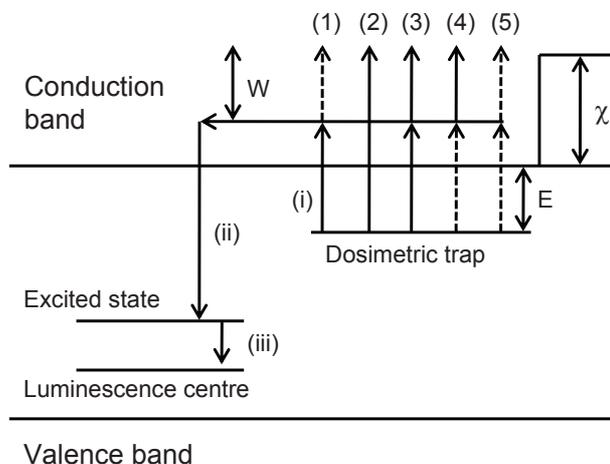
Figure 5.1: A band model describing the generation of exo-electrons and luminescence in wide band gap materials. Photon (full arrows) or phonon (dashed arrows) absorption gives rise to electron escape from the dosimetric trap of depth E, to the conduction band, process (i). From here the electron either undergoes recombination at the luminescence centre (process (ii)) or receives further optical or thermal energy (W) to overcome the work function, of the surface and escape the crystal. If the luminescence centre has an excited state, then luminescence light is emitted following de-excitation of this state to the ground state (process (iii)). Oster and Haddad (2003) suggest the following mechanisms for exo-electron escape from the trap: (1) photo-thermostimulated emission, (2) non-stationary photoemission, (3) photo-photostimulated emission, (4) thermo-photostimulated emission, and (5) thermo-thermostimulated emission. These mechanisms are discussed in the main text.

arrows denote thermal stimulation). Assuming the main dosimetric trap of the material is stable at ambient temperatures and positioned at energy E below the conduction band, and that the work function of the crystal is given by χ, then five possible mechanisms for exo-electron emission can be postulated: in transition (1) the electron is released from the trap by photon absorption, but subsequent emission from the surface results from additional thermal excitation; this process is called photo-thermostimulated emission, and is discussed further in Pagonis et al. (2009a). In transition (2), called non-stationary photoemission, both the trap release and emission occurs in a single step induced by absorption of one photon. This mechanism is unlikely in quartz and feldspar because the blue stimulation light energy ($\sim$2.6 eV) is only just sufficient to evict the electron. In feldspar the dosimetry trap is believed to be between 2 and 2.5 eV (Huntley et al., 1996; Poolton et al., 2009) and for quartz $\sim$3.0 eV (Huntley et al., 1996). Pagonis et al. (2009a) derived the work function, χ, for their natural quartz sample to be $\sim$1.2 eV, and the thermal assistance required to release stimulated electrons from the conduction band, W, to be 0.29 ± 0.02 eV, using the model of Oster and Haddad (2003). Other sources state the electron affinity of pure SiO_2 to be between 0.9 and 1.0 eV (Goodman and O'Neill, 1966; Schreiber and Fitting, 2002). Transition (3) represents photo-photostimulated emission in which electron release and emission results

from absorption of photons, but in a two-step process. This mechanism will be further discussed in Section 5.7. In transition (4) the electrons are evicted by thermal energy and the subsequent exo-electron emission requires photon absorption; this is termed thermo-photostimulated emission. As with transition (2), this mechanism is very unlikely in our work. If samples are first preheated to empty shallow traps, then at moderate temperatures the concentrations of thermally stimulated electrons in the conduction band should be very small. In addition, after the light pulse is switched off, there are no photons available to complete the stimulation process. The final transition (5) represents the thermo-thermostimulated emission process; this is observed during TSE measurements in which there is sufficient thermal energy available at higher temperatures to first evict electrons from traps, and then to overcome the work function. We conclude that only transitions (1) and (3) are likely to occur during time-resolved optically stimulated exo-electron emission at temperatures significantly below any prior thermal pre-treatment (preheating).

5.3   Previous exo-electron studies using natural dosiemeters

Ankjærgaard et al. (2006) developed an exo-electron measurement system attached to a Risø TL/OSL reader and were the first to measure OSL and OSE, and TL and TSE simultaneously. They began by comparing the dosimetric properties of surface and bulk quartz, feldspar and NaCl, using blue light stimulation, and concluded they were indistinguishable; TL and OSL originate from whole volume of the dosimeter, whereas TSE and OSE derive from only ~ 1 μm below the surface. They also observed that sensitivity change (emission intensity after giving a same repeated dose and preheat) occurred only in OSL (not OSE) and as a result suggested that this sensitivity change is primarily related to changes in recombination probability. They were unable to observe IR stimulated exo-electrons from feldspar, and concluded that the electrons giving rise to the infrared stimulated luminescence signal commonly observed from feldspar do not go through the conduction band. Ankjærgaard et al. (2008) studied the dependence on stimulation temperature of OSL and OSE from quartz. The OSL signal monotonically decreased with increasing stimulation temperature, due to thermal quenching, but OSE increased up to $\sim 280°$C and only then decreased. They also investigated the thermal stability of OSL and OSE of quartz. The OSL signal first increased with the preheat temperatures up to 260°C and rapidly decreased above 300°C whereas OSE steadily decreased from 130°C. They explained this gradual decrease of OSE with stimulation temperature by a change in competition between luminescence recombination and electron ejection from the surface. Ankjærgaard et al. (2009b) measured natural doses using OSE from 10 quartz samples and compared these equivalent doses with those obtained using OSL.

5.4   Instrumentation, samples and measurements

A time-resolved exo-electron measurement system has been developed using a windowless flow-through semi-proportional pancake detector (pulse width 5-10 μs after amplification and shaping) inserted into the LED unit of a Risø

TL/OSL reader (Ankjærgaard et al., 2006, 2008). Pulses from the detctor are time stamped with reference to the beginning of the stimulation light pulse, using a pulse timer [Lapp et al. (2009, Chapter 2 of this thesis)]. The duration of the stimulation light pulse is referred to here as the 'on-time' and the time before commencement of the next light pulse as the 'off-time'. Electrons are emitted into a counting gas (99% argon, 1% isobutane), multiplied and collected by the anode wire within the pancake detector. A more detailed description of the exo-electron system is given by (Ankjærgaard et al., 2006). The stimulation light from clusters of blue (470 nm) or infrared (870 nm) LEDs penetrates the transparent plastic walls of the gas detector, and any resulting OSL is detected through a total of 7.5 mm Hoya U-340 glass filters by a photomultiplier tube (PMT) placed directly above the cathode grid of the gas detector. The system allows the simultaneous measurement of OSE and OSL, and can also be used to simultaneously measure thermally stimulated exo-electrons (TSE) and thermoluminescence (TL). We only have one pulse timer; this can be used to analyse the signals from either the gas detector or the PMT.

The OSL and OSE signals from 180 to 250 μm grains of quartz [WIDG8; Wintle and Murray (2006)] and 75 to 125 μm grains of K-feldspar [981119KF; Tsukamoto et al. (2002)] samples were measured by pressing the grains lightly into the surface of 8 mm diameter (1 mm thick) lead discs placed in 9 mm stainless steel cups (Ankjærgaard et al. (2009b) found that a lead substrate increases the intensity of the OSE signal). The OSL and OSE signals from NaCl were measured with grains directly placed in stainless steel cups. Eight mm diameter silver discs were used instead of lead to measure TL and TSE, because of the low melting point of lead. The samples were given a beta dose, preheated to 280°C, cooled immediately and then the time-resolved OSL and OSE (TR-OSL and TR-OSE) signals were measured for either 200 s (with an on-time of 50 μs and an off-time of 100 μs) or for 2000 s (with an on-time of 200 μs and an off-time of 1.8 ms) at temperatures of 50, 100, 150, 200 and 250°C. The preheat temperature of 280°C was chosen to investigate the dependence of OSE and OSL on a wide range of stimulation temperatures (from 50 to 250°C). Different blue LED powers of 1.5, 10 and 25 mW/cm^2 were used for NaCl, quartz and K-feldspar, respectively. TL and TSE curves for NaCl and quartz were measured by heating to 400°C at 2°C/s and for K-feldspar to 350°C at 5°C/s. An optical attenuator made of thin card punctured with many small pinholes was inserted within the glass filter layers to reduce the signal intensity when the OSL signal approached PMT saturation ($>10^6$ counts/s). A similar attenuator was used to monitor the rise- and fall-times of the LED pulses.

5.5 TL and TSE

TL and TSE signals from NaCl, quartz and K-feldspar were measured following beta doses of 100, 1000 and 1000 Gy, respectively (Fig. 5.2). Similar TL and TSE curves up to 250°C were reported by Ankjærgaard et al. (2006). Peaks in the TL and TSE curves from NaCl and quartz appear in similar positions, although the relative intensities of the peaks are very different. This suggests that the main mechanism for TL production in these peaks is electron eviction during thermal stimulation. The TL signal of K-feldspar has a single broad peak at ∼200°C but the TSE was better resolved and has peaks at 100, 150,
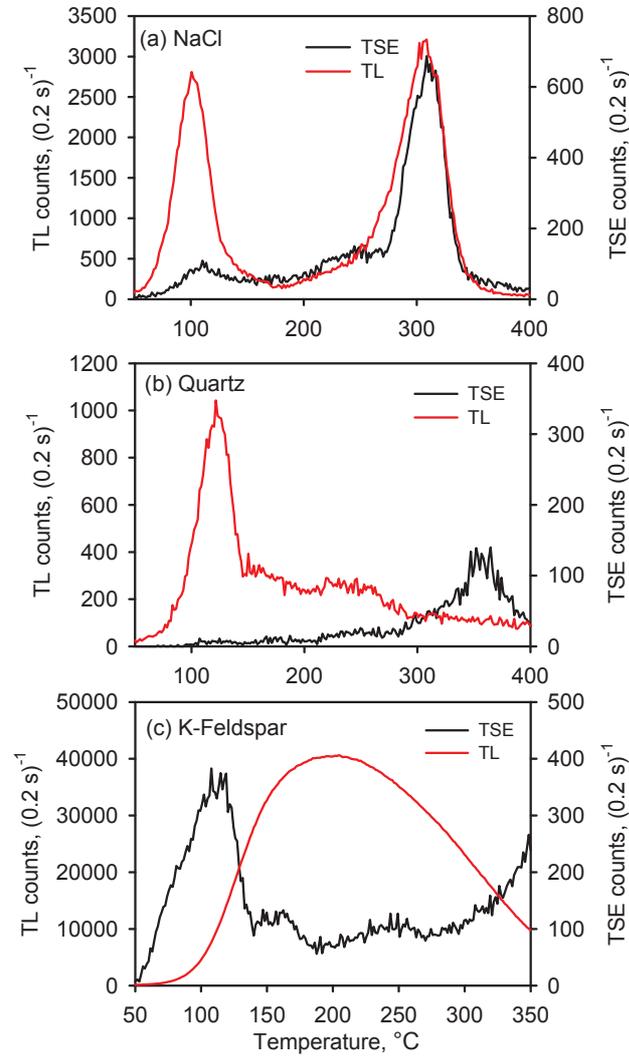
Figure 5.2: TL and TSE curves from (a) NaCl, (b) quartz and (c) K-feldspar, using doses of 100, 1000, and 1000 Gy respectively.

250 and higher than 350°C. Clearly the relationship between TL and TSE is not simple, and it can be deduced that recombination phenomena probably play a very large role in the shape of the TL curves in feldspars. This would arise, for instance, if the luminescence efficiency of electrons derived from a single trap varied with temperature, or if the available hole population changed significantly during the emptying of a trap.

5.6 Pulsed OSL and OSE decay curves

Pulsed OSL and OSE (POSL and POSE) stimulation curves were measured by pulsing the LEDs (using an on-time of 50 μs and an off-time of 100 μs) for 180 s
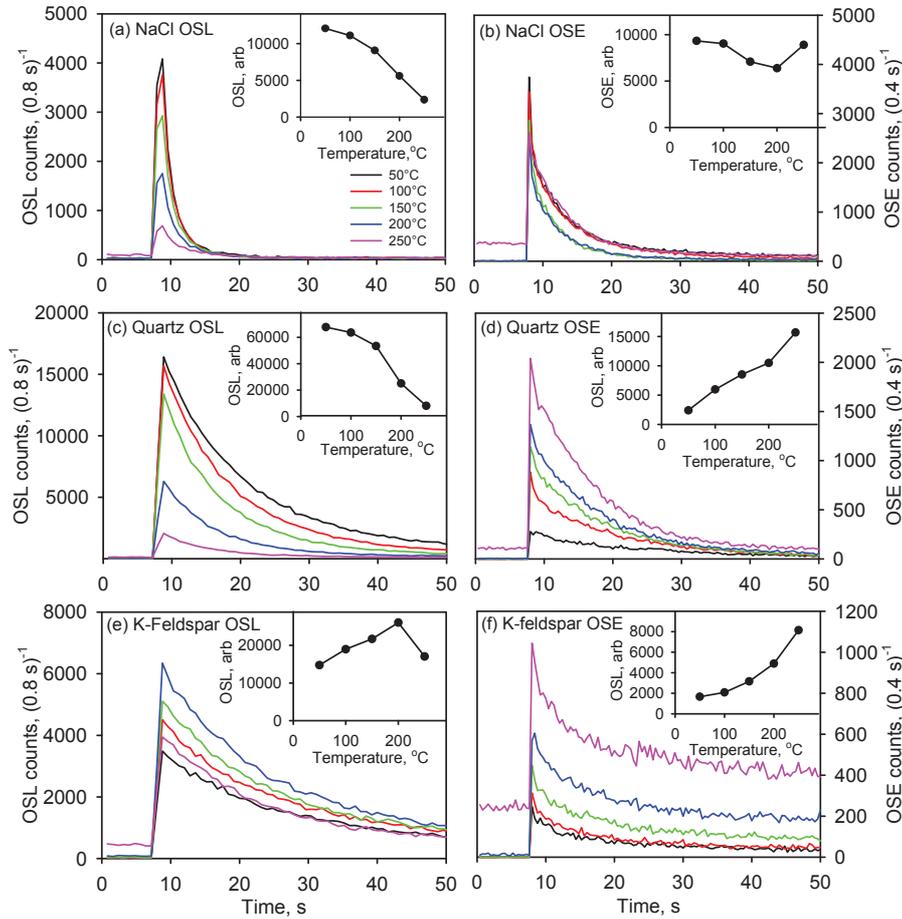
Figure 5.3: POSL and POSE decay curves from (a, b) NaCl, (c, d) quartz and (e, f) K-feldspar for stimulation temperatures of 50, 100, 150, 200 and 250°C following doses of 200, 200, and 500 Gy respectively, and a preheat to 280°C.

after giving the NaCl, quartz and K-feldspar samples doses of 200, 200 and 500 Gy respectively, preheating to 280°C and cooling immediately. The samples were then measured at temperatures of 50, 100, 150, 200 and 250°C. In order to determine the intensity of any thermally stimulated signal, the recording of the signals started 8 s before the LEDs were switched on. Figure 5.3a and b show, for NaCl, the POSL and POSE decay curves of all detected photons and electrons (i.e. for each curve, all the signal detected during both the on- and off-time of the pulsed stimulation is summed). The insets show the POSL and POSE intensities during the first 4 s as a function of stimulation temperature. The POSL from NaCl decreases towards higher temperature, whereas there was no significant temperature dependence in the POSE signal. The POSL from quartz (Fig. 5.3c) also decreases with temperature, especially above 150°C (because of thermal quenching; Wintle (1975); Murray and Wintle (1998)). However, the POSE from quartz increases as the temperature is increased (Fig. 5.3d). Thermal quenching is a recombination phenomenon, and should
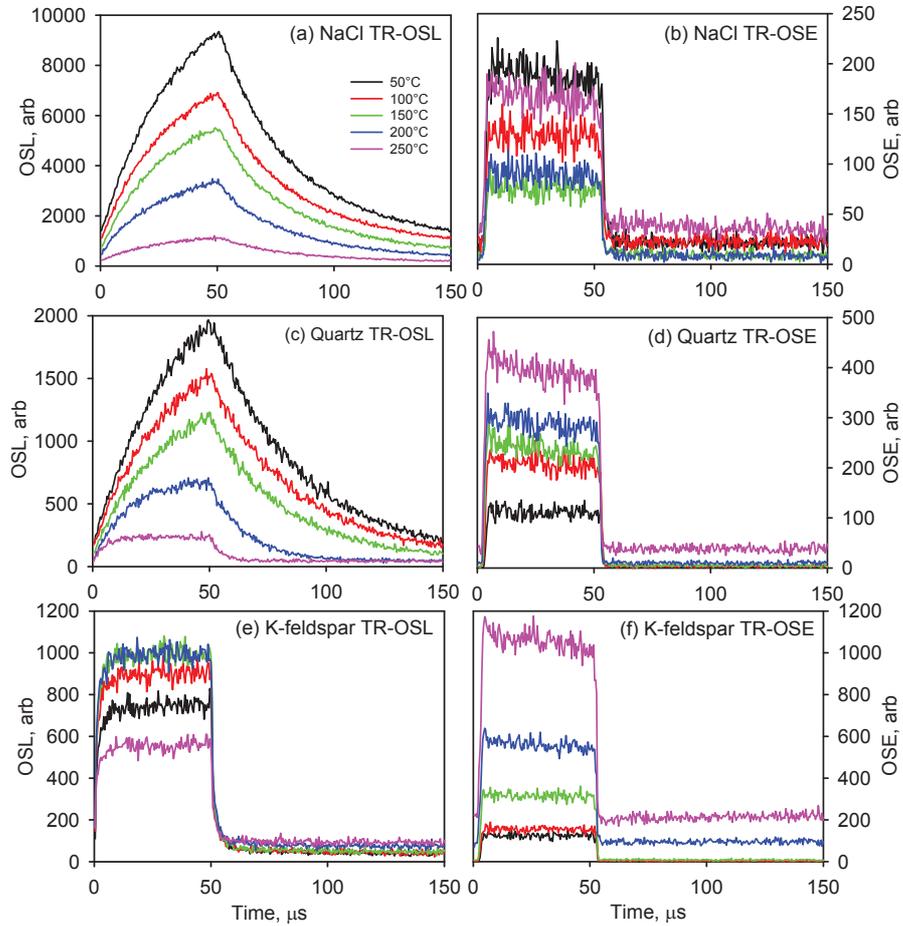
Figure 5.4: Time-resolved OSL and OSE from NaCl (a, b), quartz (c, d), and K-feldspar (e,f) for stimulation temperatures of 50, 100, 150, 200 and 250°C following doses of 200, 200, and 500 Gy respectively and a preheat to 280°C using pulsed LED stimulation (on-time: 50 μs, off-time: 100 μs). Doses and preheat similar to those of Fig. 5.3.

therefore not affect the POSE signal; the increase with temperature implies that thermal assistance plays a role at some point in the eviction process (either from the trap, or from electrons already in the conduction band). Both the POSL and POSE from K-feldspar increase with temperatures, although the POSL signal at 250°C then decreases (Fig. 5.3e, f). A strong thermally stimulated signal was observed at 250°C for all the POSE and POSL signals (the signal recorded before the stimulation begins), suggesting that this thermal signal underlies the POSE and POSL at 250°C.

5.7   Time-resolved OSL and OSE signals

Figure 5.4 shows the time-resolved OSL and OSE (TR-OSL and TR-OSE) curves from NaCl, quartz, and K-feldspars measured at different temperatures

(the curves shown in Fig. 5.3 were derived from these data by integrating the signals for all the pulses during the stimulation time, for an on-time of 50 μs and an off-time of 100 μs). The TR-OSL and TR-OSE off-time signals have been fitted with an equation of the form:

$$I(t) = \sum a_i \exp(-t/\tau_i) + k \text{ for } i = 1, ..., n \tag{5.1}$$

where I is the intensity at time t, a_i is the intensity at $t = 0$ for the 'i'th component, τ_i is the lifetime, n is the number of components, and k is a constant. This fitting does not have any physical implication and should only be seen as parameterisation of the TR-OSL and TR-OSE off-time decay shapes for intercomparison of the time scales involved. It has already been argued that the behavior of TR-OSL signals from feldspar cannot be adequately explained by an exponential model (Ankjærgaard et al., 2009a; Ankjærgaard and Jain, 2010a, Chapter 8 of this thesis) although both feldspar and quartz curves have been fitted to such models in the literature (Clark et al., 1997; Clark and Bailiff, 1998; Bailiff, 2000; Chithambo and Galloway, 2000a,b, 2001; Pagonis et al., 2009b, 2010).

The TR-OSL signal from NaCl has a constant lifetime of ∼30 μs, regardless of the temperature (Fig. 5.4a). The majority of the NaCl TR-OSE signal decays much faster than the TR-OSL but there is also a signal with a very long time constant which cannot be fitted on this measurement timescale of 100 μs off-time (Fig. 5.4b). An average lifetime of 0.7 ± 0.06 μs was obtained from fitting the 5 TR-OSE measurements at different stimulation temperatures (there is no detectable trend in the decay rate with stimulation temperature). The lifetime of the TR-OSL signal of quartz decreases from 37 to 5 μs with increasing temperature (Fig. 5.4c), as previously reported by Bailiff (2000), Chithambo and Galloway (2000c) and Pagonis et al. (2010, Chapter 4 of this thesis); this is usually attributed to thermal quenching of the luminescence centre, leading to a more rapid emptying of the excited state by a non-radiative de-excitation route. The majority of the TR-OSE signal decays much faster than the TR-OSL signal ($\tau =$∼0.6 μs; Fig. 5.4d, no trend observed with temperature). The TR-OSL signal from K-feldspar decays with apparent lifetimes of 2-3 and 20-30 μs and the intensities decrease with increasing temperature [Fig. 5.4e; the nanosecond time-scale lifetimes reported by Clark et al. (1997); Clark and Bailiff (1998); Ankjærgaard et al. (2009a, Chapter 7 of this thesis) cannot be resolved with our pulsed LEDs]. The TR-OSE signal from K-feldspar also decays much faster than the TR-OSL signal ($\tau =$∼0.4 μs; Fig. 5.4f, no trend observed with temperature). The normalised TR-OSE signals from NaCl, quartz and K-feldspar during the first 11 μs of the off-time are shown in Figs. 5.5a–c. The lifetimes found from fitting are 0.76 ± 0.07, 0.61 ± 0.05 and 0.38 ± 0.03 μs, respectively. The decay of the light signal from the blue LEDs is shown in Fig. 5.5d (measured directly through a pinhole attenuator by the photomultiplier tube). More than 60% of the LED pulse switches off with a lifetime of ∼70 ns, and almost all of the remaining light with a lifetime of ∼1.8 μs. It appears that the majority of the TR-OSE signals from all 3 minerals decay by about an order of magnitude more slowly than the dominant LED switching off time.

Time-resolved OSL and OSE signals were also recorded for 2000 s using longer on- (200 μs) and off- (1.8 ms) times. The off-time signals are shown in
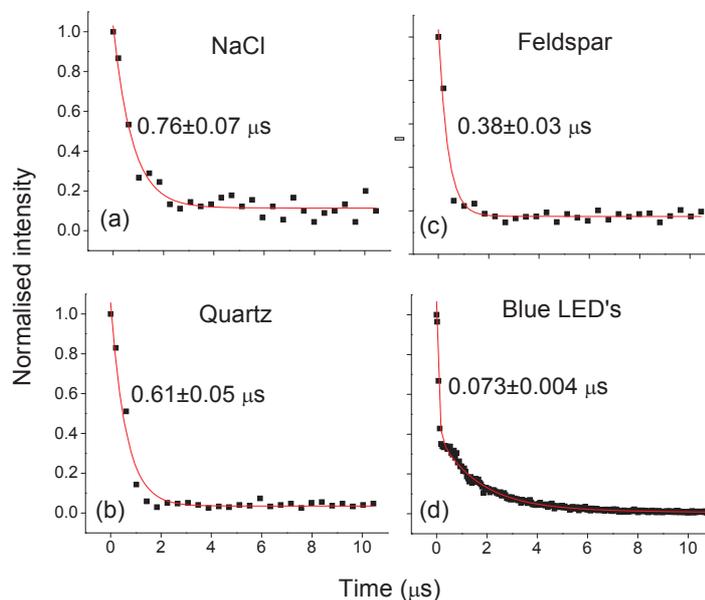
Figure 5.5: Time-resolved OSE off-time decay at 200°C from NaCl (a), quartz (b), and K-feldspar (c) fitted by a single exponential and a constant. (d) The off-time decay of the blue LED pulse fitted with three exponential components and a constant. The lifetimes for each fit are given in each figure (only the fastest lifetime for the LED pulse).

Fig. 5.6. Both the TR-OSL and TR-OSE signals from NaCl have a weak slowly-decaying signal above 100°C; this signal appears to decay more rapidly at 100°C and 250°C (Fig. 5.6a, b). There is a similar slowly-decaying quartz TR-OSE signal but the decay is much less pronounced than that from NaCl (Fig. 5.6d). A much stronger signal was observed in the TR-OSE from K-feldspar on these timescales (Fig. 5.6f). This signal does not show any detectable decay (except possibly at 100°C); there is, however, a strong systematic dependence of the signal intensity on the stimulation temperature. This signal cannot arise from the isothermal decay of shallow TL traps at ambient temperature because any thermally induced signals detected in the period before the simulation light was first turned on are negligible for temperatures below 250°C (Fig. 5.3f). Thus it is deduced that these OSE off-time signals from K-feldspar result from optical stimulation. It is considered most likely that this signal is related to photo-transferred TSE, i.e. thermal release of charges from shallow traps populated during optical stimulation (Ankjærgaard and Jain, 2010a, Chapter 8 of this thesis). Figure 5.7 presents a summary of the TR-OSL and TR-OSE lifetimes for NaCl and quartz, derived from fitting the data in Figs. 5.4 and 5.6 using a linear sum of exponential decays and a constant (5 parameters) model for TR-OSL and a single exponential for TR-OSE. For NaCl, the ~30 μs component in the TR-OSL does not show temperature dependence (Fig. 5.7a, OSL1). The decay rates of the second (slower) TR-OSL component and the slow TR-OSE component are similar and have a similar thermal dependence (Fig. 5.7a, OSL2 and OSE2). For quartz the lifetime of the first TR-OSL component varies with
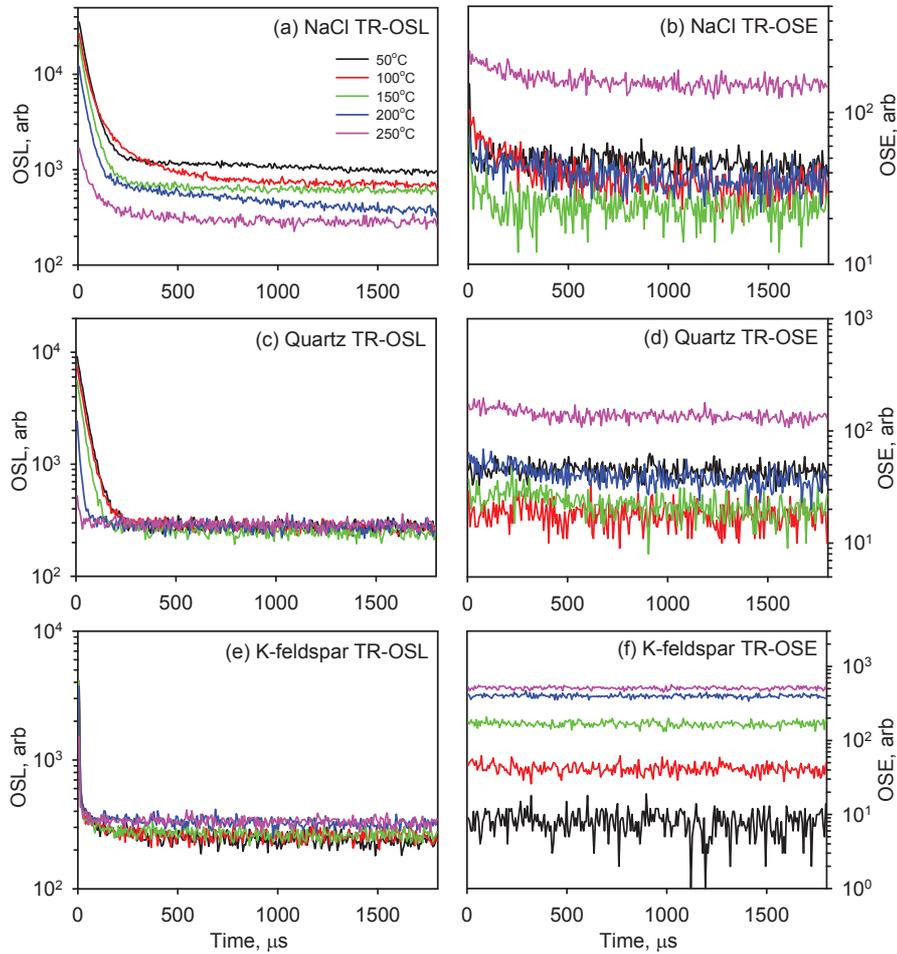
Figure 5.6: Time-resolved OSL and OSE measured for 2000 s: NaCl (a, b), quartz (c, d), and K-feldspar (e,f) for stimulation temperatures of 50, 100, 150, 200 and 250°C using on- and off-times of 200 μs and 1.8 ms. Doses and preheat similar to those of Fig. 5.3.

temperature as described earlier, between ∼37 and 5 μs (Fig. 5.7b, OSL1). The slow TR-OSE lifetime is similar to that of the slow TR-OSL lifetime (0.1–1 ms; Fig. 5.6b, OSL2 and OSE2). Ankjærgaard and Jain (2010a,b, Chapters 6 and 8 of this thesis) have observed optically stimulated phosphorescence signals lasting up to ∼8 s in quartz and feldspar. They conclude that re-trapping and subsequent thermal eviction from shallow traps is most likely to give rise to such long term phosphorescence decay. In the case of quartz a phosphorescence component with a lifetime varying from 1.4 s at 100°C to 4 ms at 200°C was attributed to trapping (during optical stimulation) and subsequent thermal detrapping of the 110°C TL peak. It is likely that our slowly decaying TR-OSE signals arise because of a gradual emptying of charge into the conduction band from such shallow traps.

We suggest that the fast decay in our TR-OSE signal is related to conduc-
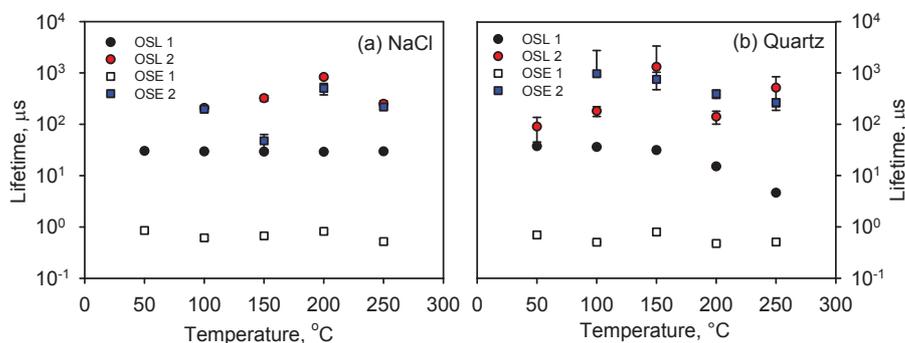
Figure 5.7: Summary of the TR-OSL and TR-OSE lifetimes for NaCl (a) and quartz (b) found by fitting the curves in Figs. 5.4 and 5.6.

tion band emptying after optical stimulation, whereas the more slowly decaying TR-OSE components are probably related to the thermal emptying of shallow traps. However, there are two possible alternative explanations for our data: it is possible that electron stimulation is a two stage process (Transition 3 in Fig. 5.1) with a photon absorption stimulating an electron into the conduction band, and a subsequent absorption causing escape of this conduction band electron from the crystal. In this case the probability of electron ejection, and thereby the intensity should be proportional to the square of the stimulation power (Oster and Haddad, 2003). We have tested whether this model applies by repeated measurement of the OSE signal as a function of stimulation power, for a single aliquot of quartz (following a dose of ∼400 Gy and a preheat to 280°C for 10 s). The data are shown in Fig. 5.8; there is no suggestion of a non-linear relationship, and so we conclude there is no evidence for a two step process in the electron eviction from quartz. Similar observations were made using an aliquot of NaCl, but signals from feldspar were too weak to measure at lower stimulation powers.

It is also possible that electrons in the conduction band thermalise very quickly (transition 1 in Fig. 5.1). This could lead to a rapid drop in the TR-OSE signal immediately following the stimulation pulse, followed by a slower recombination from the bottom of the conduction band without a corresponding TR-OSE signal. However, for both quartz and feldspars blue light stimulation is only just sufficient to cause detrapping; the stimulation energy (2.6 eV) is similar or less than the main OSL trap depth, i.e. 2–2.5 eV (Huntley et al., 1996; Poolton et al., 2009) or ∼3 eV (Huntley et al., 1996). It thus seems likely that most optically evicted electrons are put into the conduction band at or close to the conduction band edge; electrons must then escape the crystal surface because of thermal effects, to give rise to an OSE signal. In this picture, electrons do not require to lose much, if any, energy to thermalise after first entering the conduction band. It therefore seems more likely that the fast drop in the TR-OSE signals of quartz and feldspar reflects a significant drop in the conduction band population. A lack of any systematic change in the rate of decrease of fast TR-OSE signals with stimulation temperature (Fig. 5.7) further supports this interpretation.

The fastest TR-OSL lifetimes are of the order of tens of microseconds in
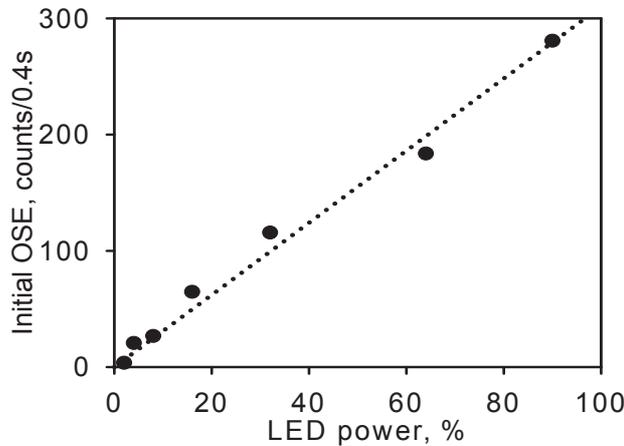
Figure 5.8: The initial intensity of continuous wave OSE from quartz as a function of stimulation power (a background signal derived from the end of the stimulation period has been subtracted from all observations).

both quartz and NaCl. This suggests that conduction band emptying must occur at either the same or faster timescales. Our TR-OSE data suggests that conduction band emptying gives rise to the initial fast drop in the TR-OSE signals. Thus, the initial (but much slower) TR-OSL decay must reflect relaxation of the recombination center in quartz and NaCl. This conclusion has important implications for the choice of parameters in the kinetic model (Bailey, 2001) currently used to describe charge movement in quartz; published model parameters (Bailey, 2001) predict several orders of magnitude slower conduction band emptying than observed here.

5.8 Conclusion

For the first time, we report on time-resolved exo-electron measurements during pulsed optical stimulation of luminescent phosphors. We observe very slowly- or non-decaying TR-OSE and TR-OSL signals from quartz, K-feldspar and NaCl; these signals probably arise from retrapping and subsequent decay from shallow traps. However, the majority of the TR-OSE signal intensity decays on timescales <1 μs; for NaCl and quartz, this is much faster than that of the corresponding TR-OSL signals ($\sim$40 μs). Thus, our data strongly suggest that the observed fast TR-OSL lifetimes in quartz and NaCl arise mainly from the decay of excited states of recombination centres, rather than from conduction band emptying. These observations provide clear time constraints on the rates of charge movement in these natural dosimeters and have significant implications for kinetic luminescence models.

References

Ankjærgaard, C., Denby, P. M., Murray, A. S., and Jain, M. (2008). Charge movement in grains of quartz studied using exo-electron emission. *Radiation*

Measurements, 43:273–277.

Ankjærgaard, C. and Jain, M. (2010a). Optically stimulated phosphorescence in orthoclase feldspar over the millisecond to second time scale. *Journal of Luminescence*, 130:2346–2355.

Ankjærgaard, C. and Jain, M. (2010b). Optically stimulated phosphorescence in quartz over the millisecond to second time scale: insights into the role of shallow traps in delaying luminescent recombination. *Journal of Physics D: Applied Physics*, 43:255502 (12pp).

Ankjærgaard, C., Jain, M., Kalchgruber, R., Lapp, T., Klein, D., McKeever, S. W. S., Murray, A. S., and Morthekai, P. (2009a). Further investigations into pulsed optically stimulated luminescence from feldspars using blue and green light. *Radiation Measurements*, 44:576–581.

Ankjærgaard, C., Murray, A., Denby, P., and Jain, M. (2009b). Using optically stimulated electrons from quartz for the estimation of natural doses. *Radiation Measurements*, 44:232–238.

Ankjærgaard, C., Murray, A. S., Denby, P. M., and Bøtter-Jensen, L. (2006). Measurement of optically and thermally stimulated electron emission from natural minerals. *Radiation Measurements*, 41:780–786.

Bailey, R. M. (2001). Towards a general kinetic model for optically and thermally stimulated luminescence of quartz. *Radiation Measurements*, 33:17–45.

Bailiff, I. K. (2000). Characteristics of time-resolved luminescence in quartz. *Radiation Measurements*, 32:401–405.

Chithambo, M. L. and Galloway, R. B. (2000a). On luminescence lifetimes in quartz. *Radiation Measurements*, 32:621–626.

Chithambo, M. L. and Galloway, R. B. (2000b). A pulsed light-emitting-diode system for stimulation of luminescence. *Meas. Sci. Technol.*, 11:418–424.

Chithambo, M. L. and Galloway, R. B. (2000c). Temperature dependence of luminescence time-resolved spectra from quartz. *Radiation Measurements*, 32:627–632.

Chithambo, M. L. and Galloway, R. B. (2001). On the slow component of luminescene stimulated from quartz by pulse blue light emitting diodes. *Nuclear Instruments and Methods B*, 183:358–368.

Clark, R. J. and Bailiff, I. K. (1998). Fast time-resolved luminescence emission spectroscopy in some feldspars. *Radiation Measurements*, 29:553–560.

Clark, R. J., Bailiff, I. K., and Tooley, M. J. (1997). A preliminary study of time-resolved luminescence in some feldspars. *Radiation Measurements*, 27:211–220.

Denby, P. M., Bøtter-Jensen, L., Murray, A. S., Thomsen, K. J., and Moska, P. (2006). Application of pulsed osl to the separation of the luminescence components from a mixed quartz/feldspar sample. *Radiation Measurements*, 41:774–779.

Goodman, A. M. and O'Neill, J. J. J. (1966). Photoemission of electrons from metals into thermally grown silicon dioxide. *Journal of Applied Physics*, 37:3580–3583.

Huntley, D. J., Short, M. A., and Dunphy, K. (1996). Deep traps in quartz and their use for optical dating. *Canadian Journal of Physics*, 74:81–91.

Lapp, T., Jain, M., Ankjærgaard, C., and Pirzel, L. (2009). Development of pulsed stimulation and photon timer attachments to the Risø TL/OSL reader. *Radiation Measurements*, 44:571–575.

Murray, A. S. and Wintle, A. G. (1998). Factors controlling the shape of the OSL decay curve in quartz. *Radiation Measurements*, 29:65–79.

Oster, L. and Haddad, J. (2003). Kinetic modeling of the photo-stimulated exoelectron emission. *Phys. Stat. Sol. A*, 196:471–476.

Oster, L., Yaskolko, V., and Haddad, J. (1999). Classification of exoelectron emission mechanisms. *Phys. Stat. Sol. A*, 174:431–439.

Pagonis, V., Ankjærgaard, C., Murray, A. S., and Chen, R. (2009a). Optically stimulated exoelectron emission processes in quartz: comparison of experiment and theory. *Journal of Luminescence*, 129:1003–1009.

Pagonis, V., Ankjærgaard, C., Murray, A. S., Jain, M., Chen, R., Lawless, J., and Greilich, S. (2010). Modelling the thermal quenching mechanism in quartz based on time-resolved optically stimulated luminescence. *Journal of Luminescence*, 130:902–909.

Pagonis, V., M., M. S., Chithambo, M. L., Christensen, E., and Barnold, C. (2009b). Experimental and modelling study of pulsed optically stimulated luminescence in quartz, marble and beta irradiated salt. *Journal of Physics D: Applied Physics*, 42:1–12.

Poolton, N. R. J., Kars, R. H., Wallinga, J., and Bos, A. J. J. (2009). Direct evidence for the participation of band-tails and excited-state tunnelling in the luminescence of irradiated feldspars. *Journal of Physics: Condensed Matter*, 21:485505 (10pp).

Sanderson, D. C. W. and Clark, R. J. (1994). Pulsed photostimulated luminescence of alkali feldspars. *Radiation Measurements*, 23:633–639.

Schreiber, E. and Fitting, H.-J. (2002). Monte carlo simulation of secondary electron emission from the insulator SiO$_2$. *Electron Spectrosc. Relat. Phenomen.*, 124:25–37.

Tsukamoto, S., Asahi, K., Watanabe, T., and Rink, W. J. (2002). Timing of past glaciations in Kanchenjunga Himal, Nepal by optically stimulated luminescence dating of tills. *Quaternary International*, 97/98:57–67.

Wintle, A. G. (1975). Thermal quenching of thermoluminescence in quartz. *Geophysical Journal of the Royal Astronomical Society*, 41:107–113.

Wintle, A. G. and Murray, A. S. (2006). A review of quartz optically stimulated luminescence characteristics and their relevance in single-aliquot regeneration dating protocols. *Radiation Measurements*, 41:369–391.

Chapter 6

Optically stimulated phosphorescence in quartz over the millisecond to second time scale: insights into the role of shallow traps in delaying luminescent recombination

C. Ankjærgaard and M. Jain

Radiation Research Division, Risø National Laboratory for Sustainable Energy, Technical University of Denmark, DK-4000 Roskilde, Denmark

Abstract

Time-resolved OSL curves from quartz are usually measured over a few hundred µs because this time range best illustrates the main component in quartz which lies in the range of 30–45 µs. In this study we present the decay form of quartz time-resolved optically stimulated luminescence (TR-OSL) and optically stimulated phosphorescence (OSP) covering over 8 orders of magnitude from 50 ns to ∼8 s. A detailed characterisation of the previously unstudied slowly decaying signals (ms–s time scales) is undertaken to understand the origin of these components and the role of re-trapping following optical stimulation. We present preheat and stimulation temperature dependence for both the TR-OSL and OSP curves in these time ranges and use the latter data to determine the E and s values for the participating shallow traps. We observe an abnormal decay behaviour seen as a sudden increase in the decay rate (a 'kink') conspicuous at about 2–3 s in the OSP curves measured at 75 and 100°C. We satisfactorily reproduce this behaviour with a numerically solved kinetic model consisting of 4 energy levels. The physical interpretation of the kinetic rate equations is discussed in terms of a three trap – one centre model, or a one trap – two centres model involving localised charge transfer.

6.1   Introduction

Natural quartz is widely used in luminescence based retrospective dosimetry (Bøtter-Jensen et al., 2003). The luminescence from previously beta or gamma irradiated quartz can be obtained by thermal, or by continuous or pulsed optical stimulation. In pulsed optical stimulation mode the luminescence measured during and between the pulses is known as Time-Resolved OSL (TR-OSL) and can be used to understand the various recombination routes in a crystal. TR-OSL of quartz has been studied for almost a decade (Bailiff, 2000; Chithambo and Galloway, 2000; Chithambo et al., 2007; Pagonis et al., 2009, and references in these papers).

The main processes that govern the time scales involved in optically stimulated luminescence generation are generally exponential in nature. The most important of these processes are: (a) detrapping: eviction of a trapped electron by stimulation to the conduction band, (b) transition from the conduction band to the luminescence centre, and (c) the relaxation from the excited state to the ground state of the luminescence centre.

The rates of each of these processes are in turn determined by the lifetimes of the electrons in transition from one energy level to the other. During optical detrapping the mean life of a trapped electron is determined by the photoionisation cross-section of the trap. In pulsed stimulation where the luminescence signal is analysed after the pulse, i.e. in the off-time, process (a) can be eliminated and moreover it can be assumed that there is negligible change in the concentration of recombination centres as the energy delivered to the sample during a pulse is rather small. Thus, the relevant parameter related to process (b) is the mean life of the electrons in the conduction band. This lifetime would normally determine the lifetime of the luminescence decay. However, in cases, where, depending on the nature of the centre, the recombination leads to an excited state there is another delay in the luminescence production; a photon is only released after relaxation from the excited to the ground state of the centre, process (c). The excited state lifetime is a characteristic of the recombination centre and is determined by the excited state to ground state transition, e.g., whether it is forbidden (resulting in a long lifetime) or allowed (resulting in a short lifetime). Thus, in pulsed OSL measurements the decay form of luminescence measured in the off-time will be a combined effect of two exponential functions, namely (b) and (c) (we note that we do not discuss localised transitions or tunnelling effects here). The timescales involved can be from ns to up to several tens of ms. However, on longer timescales, re-trapping and thermal emptying of the shallow traps can become important and give rise to long lived phosphorescence.

Examination of the luminescence decay after a pulse of stimulation light helps to understand the relative role of the above processes in luminescence generation. Different terminologies have been used to name such a signal, e.g. Time-Resolved OSL (TR-OSL), Delayed OSL or optically stimulated phospho-

rescence [see Bøtter-Jensen et al. (2003, p. 59–60)]. One could argue that the term TR-OSL is generally used when a train of pulses is used as an alternative to CW-OSL, whereas the terms DOSL or optically stimulated phosphorescence (OSP) or afterglow refer to measurements in which a single or a few short stimulations (ms to s) are followed by extended examination of the subsequent luminescence signal over ms to s time scales, such that the afterglow is resolvable by the human eye.

Quartz TR-OSL measured between the stimulation pulses (after preheating to 260°C for 10 s and stimulating at 125°C) shows a monotonic decay and consists of a dominant exponential transient having a lifetime between 30 and 45 μs and two relatively minor transients having relatively shorter and longer lifetimes (after preheating to 260°C for 10 s and stimulating at 125°C) (Chithambo et al., 2007; Ankjærgaard et al., 2010, Chapter 10 of this thesis). These lifetimes most likely reflect the relaxation of the excited state following electron hole-recombination (Chithambo, 2007; Pagonis et al., 2010, Chapter 4 of this thesis). Almost all published TR-OSL off-time decay curves from quartz have been measured over a few hundred microseconds [Chithambo et al. (2008, and references therein); Ankjærgaard et al. (2010, Chapter 10 of this thesis)]. However, on longer time scales it is likely that the effect of re-trapping will also be apparent. For example, Markey et al. (1995) using Al_2O_3:C, demonstrated that the main lifetime of ∼35 ms corresponds to the decay of the excited F-centre in Al_2O_3:C, but that the much slower decay of ∼545 ms (measured at 25°C) is due to phosphorescence from transfer of charge from deep traps to shallow traps. As these shallow traps are thermally unstable at room temperature, they start to leak charge into the conduction band from where it recombines and emits light [DOSL — Bøtter-Jensen et al. (2003)].

Only few measurements have been done to study the TR-OSL decay from quartz on the ms to s timescales. Pagonis et al. (2009) show an example from high purity synthetic quartz obtained for an off-time of 1 ms. The authors identify a slow component within this sample with a lifetime of 14 ± 8 ms and surmise that it could be caused by re-trapping in a shallow trap. This effect has previously been used by Jaek et al. (1999) to investigate deep traps in quartz, although here it was called Optically Stimulated Afterglow (OSA).

In this study we first establish the decay form of optically stimulated phosphorescence in irradiated quartz using different techniques to cover time scales over >8 orders of magnitude (50 ns to ∼8 s). We then make a detailed characterisation of the hitherto unstudied slowly decaying signals (ms–s time scales) to understand the origin of these components and the role of re-trapping following the optical stimulation.

We use the terminology time-resolved OSL (TR-OSL) while referring to the ns − μs time scales and optically stimulated phosphorescence (OSP) while referring to the ms − s time scales.

6.2   Experimental details

Sample measurements were carried out on two different Risø readers to cover three different time scales. Optical stimulation was carried out using blue light and detection was through a 7.5 mm thick Hoya U340 filter. The measurement details are described below.

Nanoseconds – microseconds: A Risø TL/OSL-20 reader was used with an integrated pulsing option to control the blue LED array, delivering 80 mW/cm^2 CW stimulation at the sample position. Furthermore a Photon Timer was attached, based on an ORTEC 9353 100 ps Time Digitizer board with a detection resolution (bin-width) of 100 ps to record the TR-OSL (Lapp et al., 2009, Chapter 2 of this thesis). We define the duration of each stimulation LED pulse as the *on*-time, and the duration of the pause before the next stimulation pulse as the *off*-time [see also Lapp et al. (2009) or Chapter 2 of this thesis]. Measurements on this timescale were undertaken using an on-time of 50 μs and an off-time of 500 μs producing ∼40,000 stimulation pulses during 22 s of pulsed stimulation with an energy of 3.6 μJ/cm^2 per pulse.

Microseconds – milliseconds: The same Risø TL/OSL-20 reader as above was used but with an on-time of 1 ms and an off-time of 5 ms. The ORTEC board has a pulse period (on-time + off-time) limitation of 6 ms, which currently cannot be exceeded. Approximately 9,000 pulses with an energy of 72 μJ/cm^2 per pulse were delivered during 54 s of pulsed stimulation in this time range.

Milliseconds – seconds: A standard Risø TL/OSL-15 reader with CW stimulation system performed by a LED array delivering ∼40 mW/cm^2 CW stimulation at the sample position (Bøtter-Jensen et al., 2003) was used to produce a single light pulse of 0.2 s duration with an average energy of 6.7 mJ/cm^2. The phosphorescence was detected during the following 7.8 s.

The on- and off-times mentioned above were adhered to unless otherwise specified in the text.

The work reported here has been undertaken using 90-125 μm sedimentary quartz grains (lab code: WIDG8). The quartz grains were extracted from the sample by sieving, heavy liquid separation and HF treatment as described in Wintle and Murray (1997) and the absence of significant feldspar contamination was confirmed by tests using IR stimulation. All aliquots used consisted of grains mounted in steel cups using silicon oil.

6.3   Extended decay form of optically stimulated phosphorescence from quartz

Time-resolved OSL off-time curves from quartz are usually measured over a few hundred μs because this time range best illustrates the main component in quartz which has a lifetime in the range of 30–45 μs. In Fig. 6.1a, this is illustrated by the black curve, which has been measured at 125°C after a 25 Gy dose and a preheat to 260°C for 10 s. The same curve is shown in Fig. 6.1b on a semi-log scale, where this main component can be seen as the linear part of the curve up to ∼150 μs, after which a much slower decaying component starts to dominate.

To observe in detail the slowly decaying part of the decay, the measurement was repeated on the millisecond timescale, which is shown as the red curve in Fig. 6.1a and reproduced in Fig. 6.1c on a semi-log scale; the initial fast drop corresponds to the main component from Fig. 6.1b marked by #1, followed by
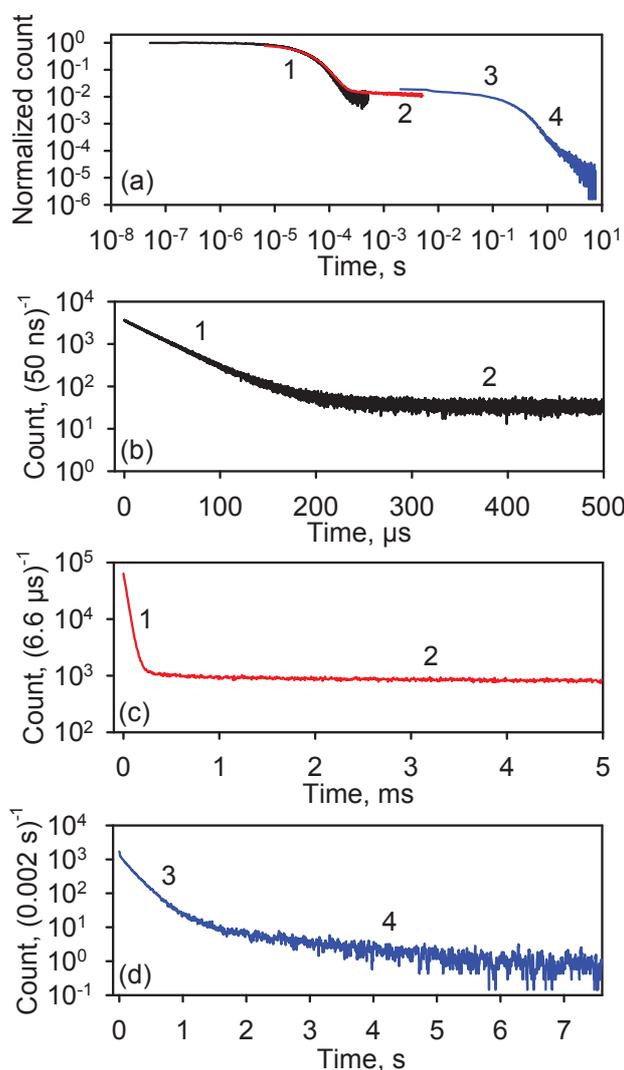
Figure 6.1: Time-resolved OSL off-time and optically stimulated phosphorescence curves from a single aliquot of quartz (WIDG8) measured on different timescales covering over eight decades. (a) The first (black) curve is measured using an on-time of 50 µs, an off-time of 500 µs (∼40,000 pulses) and has a resolution of 50 ns. The second (red) curve is measured using an on-time of 1 ms, an off-time of 5 ms (9,000 pulses) and has a resolution of 6.6 µs. The third (blue) curve is measured using an on-time of 0.2 s, an off-time of 7.8 s (a single pulse) and has a resolution of 0.002 s. In all three measurements the aliquot was dosed with 25 Gy followed by a preheat to 260°C for 10 s and blue light stimulation at 125°C. The curves have been normalized to the initial intensity, and the red curve has been reduced by a factor 0.9 and the blue curve by a factor of 0.02 for ease of illustration. Note that the scale is double-log. The curves in (b), (c), and (d) are the semi-log plots of the individual curves from (a). The numbers on the curves 1–4 represent the four major components in the signal, which has been identified by visual inspection.

the same slowly decaying component from Fig. 6.1b marked by #2, but now it is clear that the decay continues beyond several ms, as the counts have still not reached the background level of ∼4 cts. per channel (6.6 μs).

To make further extended measurements of the slowly decaying component, a measurement was carried out in the standard Risø reader with the CW-OSL attachment using a single pulse of blue stimulation. The measurement and preheat temperatures were the same as above. These data are shown as the last (blue) curve in Fig. 6.1a and on a semi-log scale in Fig. 6.1d. The initial fast drop is termed as component #3, and continues up to about 2 seconds, after which it is hidden under a new component marked as #4 which continues beyond 7 s. The dark counts in this curve will occur at ∼0.2 cts. per channel (0.002 s).

We note that the components 1, 2, 3 and 4 mentioned above are defined entirely based on visual inspection. Due to lack of data collected from 6 ms up to ∼60 ms, we cannot know whether component 2 and 3 are the same or not. The mosaic of these curves in Fig. 6.1a illustrates that the TR-OSL or OSP covers >8 orders of magnitude (50 ns to ∼8 s). The lower limit of this observation is set by the incapability of our set up to achieve pulsing with a diode fall time faster than ∼20 ns. The upper limit is set by the instrument's sensitivity; we are already quite close to the dark counts of the system by about 8 s of OSP measurement.

In the following sections we make a detailed characterisation of these components with a special focus on 2, 3, and 4.

6.4   The microsecond – millisecond time range

This section investigates the shape of the curve in Fig. 6.1c as a function of preheat and stimulation temperature. Figure 6.2 shows the normalized time-resolved OSL off-time curves measured at 125°C from a single aliquot of quartz using preheat temperatures in the range 200–300°C. It is observed that the preheat temperature does not affect the shape of the curve. The amplitude of the initial component 1 (filled circles) and the slower component 2 (estimated from the intensity at 1 ms, open circles) are shown in the figure inset as a function of preheat temperature. There is no major change in the relative importance of the two components with preheat temperature.

The normalized blue light stimulated time-resolved OSL from a single aliquot of quartz (WIDG8) measured for stimulation temperatures in the range 50–225°C are shown in Fig. 6.3a. Only the off-time decay is shown. As the stimulation temperature is increased, the area under component 2 shows an increase relative to that under component 1. For the curves with stimulation temperatures below 125°C, the initial decay has a very similar behaviour (see inset to Fig. 6.3a on log-log plot) and the relative ratios between the two components are very similar. For the curves with stimulation temperatures above 125°C, the initial decay becomes faster with increasing temperature, and the slower decay becomes relatively more dominant.

We tried to describe these data mathematically by a multi-exponential fit. However, the curves were not successfully described by either two or three or more transients, possibly because of very large difference in decay constants (microsecond and millisecond) causing an abrupt change in the decay curves
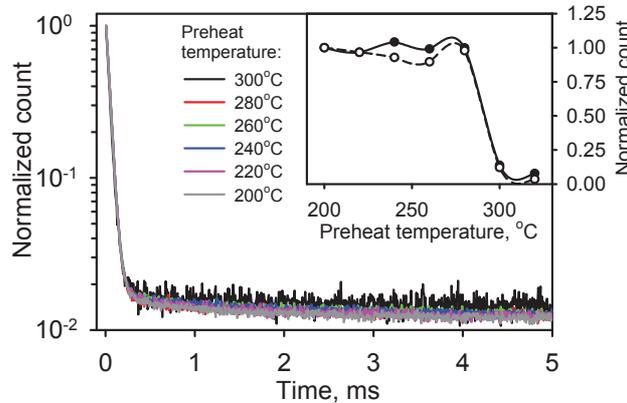
Figure 6.2: Time-resolved blue light stimulated OSL off-time curves from a single aliquot of quartz (WIDG8) for different preheats in the range: 200°C-300°C in steps of 20°C. The aliquot was dosed with 25 Gy, preheated for 10 s and stimulated at 125°C using an on-time of 1 ms and an off-time of 5 ms. The curves have been normalized to the first point in the off-time. Inset: The off-time decay counts integrated for the periods 0.0–6.6 μs (filled circles) and 1005.0-1011.6 μs (open circles) and plotted as a function of preheat temperature. For comparison, the two data sets are normalised to their value for the preheat of 200°C.

(Fig. 6.3a). Therefore in order to study the main characteristics of the curve, we used the very initial part of the curve to characterise component 1. Figure 6.3b shows the lifetime and amplitude for this component. For characterisation of component 2 we discarded the initial 400 μs of data in the off-time (to remove nearly all influence of the initial fast decay) and thereafter removed the contribution from the underlying slower components (component 3 and 4, see Fig. 6.1) by subtraction of an average over the last 50 points. The remaining data were satisfactorily approximated with a single exponential decay. The lifetime and amplitude of this component as a function of temperature is shown in Fig. 6.3c.

Component 1, the dominant component at the microseconds (and also the milliseconds) time scales in quartz (Ankjærgaard et al., 2010, Chapter 10 of this thesis), shows a decrease in both the amplitude and lifetime as a function of temperature (Fig. 6.3b). The decrease in amplitude and lifetime with stimulation temperature can be ascribed to thermal quenching (Fig. 6.3b, triangles) which arises because of an alternative non-radiative recombination and has been studied i quartz by Bailiff (2000), Chithambo and Galloway (2001) and Chithambo (2002). In Pagonis et al. (2010, Chapter 4 of this thesis) thermal quenching was measured and modelled for the same quartz sample as used here (WIDG8). A decrease in lifetime of ~45 μs to ~10 μs is observed here (Fig. 6.3b) for the temperature range 50°C to 200°C, is consistent with that the thermal quenching energy of 0.64 eV (Pagonis et al., 2010, see chapter 4 of this thesis for details).

Component 2 shows a relatively smaller decrease in intensity than component 1 with an increase in the stimulation temperature; the smaller decrease in the amplitude compared to that of component 1 causes the observed changes
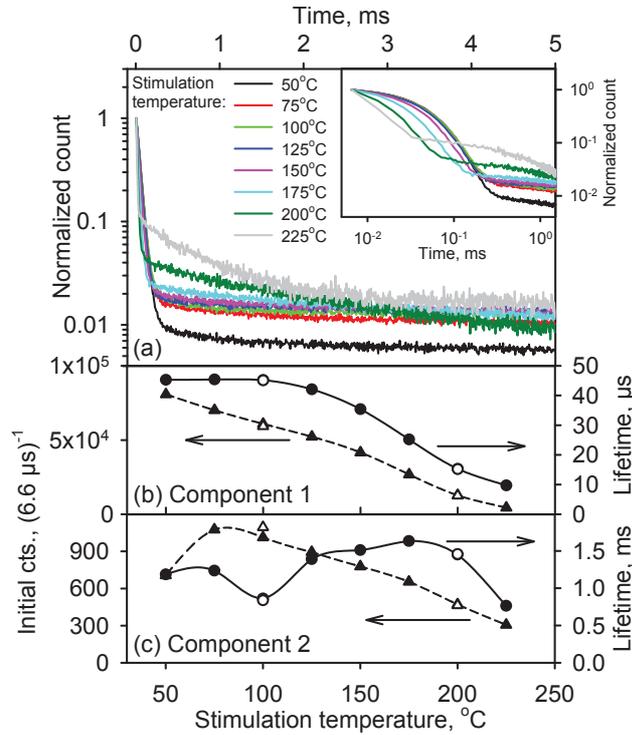
Figure 6.3: (a) Time-resolved blue light stimulated OSL off-time curves from a single aliquot of quartz (WIDG8) measured at the temperatures: 50°C–225°C. The aliquot was dosed with 25 Gy and heated to 260°C for 10 s prior to each measurement using an on-time of 1 ms and an off-time of 5 ms. The curves have been normalized to the first point in the off-time. Inset: The same curves shown on a log-log scale. (b) Intensity (triangles) and lifetime (circles) of the component shown as #1 in Fig. 6.1a plotted as a function of stimulation temperature. The intensity is calculated from integrating counts in the initial 0.0–6.6 µs of the off-time curve after a background subtraction (the average counts per channel derived from data between 5900 and 5990 µs). (c) Intensity (circles) and lifetime (triangles) of the component shown as #2 in Fig. 6.1a plotted as a function of the stimulation temperature. The lifetime in ms was determined from single exponential fitting of the curves after subtraction of an average over the last 50 points and removing the initial 400 µs of the off-time. The intensity was calculated at 400 µs into the off-time. Note that the open symbols denote recycling point measurements and that the errors on the lifetimes in (b) and (c) are not visible as they are smaller than the size of the symbols..
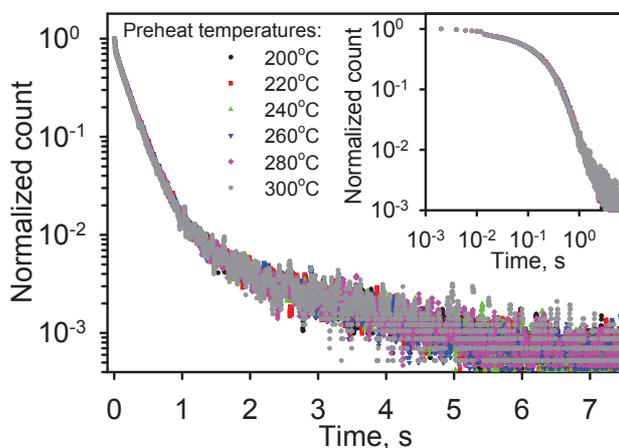
Figure 6.4: Blue light stimulated OSL off-time curves from a single aliquot of quartz (WIDG8) measured using preheats in the range: 200-300°C in steps of 20°C. The aliquot was dosed with 25 Gy and preheated for 10 s prior to each measurement and stimulated at 125°C using a pulse length of 0.2 s and detecting for 7.8 s following the stimulation pulse. The curves have been normalized to the first point in the off-time. The inset shows the curves on a log-log scale.

in the relative contributions from the two components in Fig. 6.3a. However, unlike component 1, the lifetime does not decrease concomitantly with the amplitude. In fact the lifetimes show only a slight change for the different stimulation temperatures up to 200°C; there is an overall 38% increase in lifetime with temperature up to 200°C, with a single reproducible dip at 100°C, followed by a sharp drop of about 50% between 200°C and 225°C. Thus the lifetime of component 2 does not show an undisputed constancy, or a systematic decrease expected from faster emptying of shallow traps or greater thermal quenching at a centre such as observed for component 1. One possible explanation could be that the so called component 2 in fact has different origins at different temperatures and therefore, it is not valid to intercompare the lifetimes; the apparent similarity in the lifetimes is then a mere coincidence. We later describe such an apparent behaviour in a component in the time range described in Section 6.5. On the other hand if one ignores the drop at 100°C, one could possibly assume a near constancy of the lifetimes between 50 to 200°C as a gross simplification. We discuss this again in the later sections.

6.5 The millisecond – second time range

Because of the ORTEC board pulse period limitation of 6 ms, the components in this range were investigated using a conventional reader by giving a single stimulation pulse of 0.2 s and measuring the following phosphorescence decay for 7.8 s.
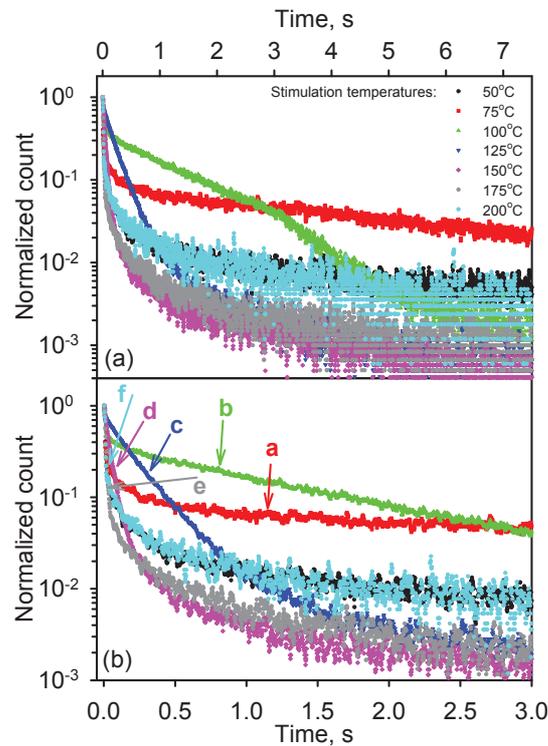
Figure 6.5: (a) Blue light stimulated OSL off-time curves from a single aliquot of quartz (WIDG8) measured in the temperature range: 50-200°C. The aliquot was dosed with 25 Gy and heated to 260°C for 10 s prior to each measurement using a stimulation pulse length of 0.2 and detecting for 7.8 s following the stimulation pulse. The curves have been normalized to the first point in the off-time. (b) The initial 3 s of the curves from (a) labelled with letters from a – f to indicate the behaviour of the OSP from the 110°C TL peak (see text for details).

6.5.1   Preheat and Stimulation temperature dependence

To investigate the off-time signal behaviour as a function of preheat, a series of curves were measured at 125°C using an aliquot of quartz following a single stimulation pulse, these are shown in Fig. 6.4, all normalized to the initial point in the off-time. All curves behave identically with a fast drop in the initial 0.01 s (see also inset on log-log scale), a slower decay up to about 1 s where the slowest decay starts to dominate and continues beyond 7 s. Based both on this and the μs to ms data presented in the previous section, we conclude that the preheat temperature range (200 to 300°C) does not affect the relative contributions of the different components.

Figure 6.5a shows the stimulation temperature dependent decay of the same aliquot of quartz used in Fig. 6.4. The aliquot was heated to 260°C for 10 s prior to blue light stimulation at temperatures in the range $50 - 200$°C. The curves show very different decay rates during the initial 3 s (see a magnification of this time range in Fig. 6.5b). However, in the data following the 3 s (Fig. 6.5a)
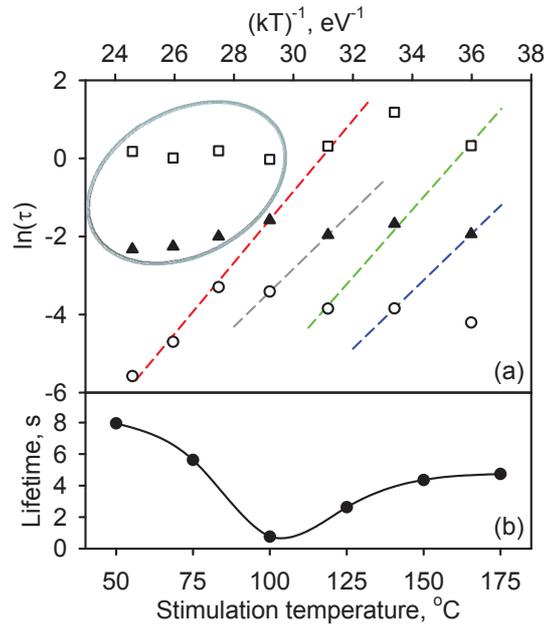
Figure 6.6: (a) Summary of lifetimes (found from fitting the initial 3 s of the curves in Fig. 6.5 with a sum of three exponentials) on an Arrhenius plot. The natural logarithm of the lifetimes for fast (circle) medium (triangle) and slow (square) components derived from fitting are plotted against the inverse of stimulation temperature (times the Boltzmann's constant). (b) Summary of lifetimes found from fitting the remaining part of the off-time decays in Fig. 6.5 after subtraction of a constant term. The curves could be adequately fitted with a single decaying exponential. Note that the errors on the lifetimes in both (a) and (b) are not visible as they are smaller than the size of the symbols.

the decay shapes are very similar for all the temperatures, with an exception of the 100°C curve (green triangles) and to some extent the 75°C curve (red squares) where a clear 'kink' is observed at ∼3 s.

A clearer picture can be obtained by separating the different components. Because of the 'kink' in two of the curves (75 and 100°C), we could not apply a simple multiexponential model to the entire curve. Therefore, to simplify the analysis we fitted only the data in the first 3 s assuming first order kinetics (see Fig. 6.5b). The data were successfully fitted with a sum of three exponentials. To determine the effect of temperature, an Arrhenius plot is used, which is shown in Fig. 6.6a. The three different components from each curve are indicated by different symbols (Fast - circles, medium - triangles, slow - squares). If one looks at the behaviour of these different components, it is apparent that the lifetime of the slow and medium component do not vary much with temperature, whereas the lifetime of the fastest component rises gradually with temperature up to 150°C ($\sim$28 eV^{-1}), and then decreases rapidly between $150 - 200$°C ($28 - 24$ eV^{-1}). The behaviour of these components is in fact very similar to that observed for component 2 on the ms time scales (see previous section, Fig. 6.3c) in that it does not show any obvious temperature dependence.

We now explore the possibility that the fast component (and similarly the medium component and slow component) actually has different origins in these different curves. If one looks closely at Fig. 6.5b, i.e. the data in the first three seconds of the curves in Fig. 6.5a, then it is apparent that a slower component increases relatively in magnitude compared to a faster decaying component from about 50 to 100°C, and the fast component is eliminated above 100°C. From 100°C to 175°C one also observes a systematic change in the decay rate of the dominant component with stimulation, which hints to a possible participation of a shallow trap(s). A common dominant component of these different curves was picked by visual inspection. This is shown by arrows and lettering from a–f for the different curves in Fig. 6.5b. It is clear that this component shows an increase in the decay rate with temperature: however, note that in some curves this is a slow component while in the others it is a fast component. The Arrhenius plot helps to test whether the change in the decay rate complies with that expected from thermodynamic considerations. Most of the data for this component does in fact fall on a straight line (first dashed red line from left in Fig. 6.6a) $\tau = E/kT - \ln(s)$, where τ [s] is the lifetime, E [eV] is the thermal activation energy of the trap giving rise to this component, and s [s^{-1}] is the frequency factor. This gives $E = 0.91$ eV and $s = 1.7 \cdot 10^{12}$ s^{-1}. Very similar values of $E = 0.89$ eV and $s = 3.8 \cdot 10^{11}$ s^{-1} were found by Spooner and Questiaux (2000) for the so called 110°C TL peak in the UV emission by varying the heating rate in a series of TL measurements. The E and s values found from our data predict a TL peak at 93°C for a heating rate of 2°C/s (confirmed later by experimental measurements).

Thus, identification of this main component helps to put the other two components derived from the multi-exponential fitting into perspective. Examination of Fig. 6.5b again for temperatures below 100°C now shows that the component derived from the 110°C peak (marked with arrows) increases relative to the faster components and almost completely replaces these between 100°C and 125°C. Thus, these faster components are completely eliminated at higher temperatures, since the data resolution is not high enough to sample them. Similarly, as the component from the 110°C peak forms the new fast component, there is appearance of new slower components in the system. Thus, we conclude that the apparent constancy of the fast and medium components is misleading since the slower components change into faster ones, the faster ones disappear (or are unresolvable at our data collection rate), and the new slower components appear at higher and higher temperatures within our data range. It is therefore misleading to intercompare the decay rates for a single component as the decay rates should in fact be compared across components to obtain a meaningful result.

To confirm the role of the 110°C peak in OSP, a TL experiment was carried out to examine possible charge recuperation during short blue light stimulations; this is called phototransferred TL (PTTL). A previously sensitised aliquot was dosed, heated to 300°C for 60 s and then stimulated with a short pulse of blue light. Figure 6.7 shows the series of 'difference' TL curves (subtraction of TL before illumination from that after illumination) measured up to 300°C following these short blue light stimulations of durations between 0.1 s and 3.2 s. The ~325°C TL peak shows an increasing depletion because of bleaching by blue light; this is observed as negative counts in the figure. All positive counts are PTTL due to photo transfer. A dominant peak is observed
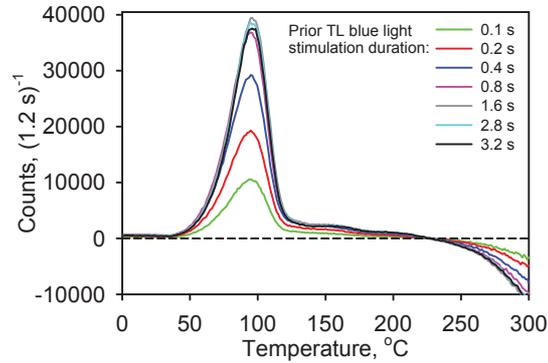
Figure 6.7: TL curves showing the effect of photo-transfer in quartz (WIDG8) due to short blue light stimulations of different length. An aliquot of quartz was dosed with 25 Gy, heated to 300°C for 10 s, blue light stimulated at 20°C, and then a TL curve to 300°C was measured using a heating rate of 2°C/s. The same cycle was repeated with 0 s of light stimulation before the TL measurement. The curves shown in the figure have all been obtained by subtraction of TL before illumination from that after illumination. Repeat measurements showed less than 2% variability.

at 97°C followed by relatively smaller peaks in the region between 125°C and 225°C. Increasing the stimulation pulse length causes an increase of charge transfer into the peak centred at 97°C, which is in reasonable agreement with our predicted TL peak at 93°C from the E and s values found from Fig. 6.6a. The charge builds up steadily, but for pulse durations longer than 1.6 s, the light stimulation starts to deplete the charge transferred into this trap. Based on these data we conclude that our multi-exponential analysis as well our approach of comparing decay constants across the fast, medium, and slow components gives physically meaningful results.

With this success we then attempted a similar E-s analysis for the components decaying faster than that from the 110°C peak for the stimulation temperatures between 50 and 100°C. These are indicated from left to right with the blue, green, and grey dashed lines in Fig. 6.6a. These yield values of $E = 0.74$ eV and $s = 1.5 \cdot 10^{12}$ s^{-1} (blue line), $E = 0.86$ eV and $s = 2.9 \cdot 10^{13}$ s^{-1} (green line), and $E = 0.56$ eV and $s = 3.6 \cdot 10^9$ s^{-1} (grey line), which correspond to TL peaks at 87°C, 63°C, and 165°C respectively. In the literature, only values for the 160°C peak are published with $E = 1.09$ eV and $s = 2.1 \cdot 10^{12}$ s^{-1} measured in the UV (Spooner and Questiaux, 2000). We recognise that our E and s values for this peak are much too small compared to their published value, and moreover the s value is smaller than the generally accepted values in the range $10^{12} - 10^{14}$ s^{-1}. Nonetheless, our PTTL results in Fig. 6.7 show the existence of the 160°C TL peak, consistent with our E-s analysis.

The slower components (slower than that for the ~110°C peak) on the other hand do not seem to be amenable to this simple E-s analysis (see the data enclosed in the ellipse in Fig. 6.6a). Fitting of these data gave absurd values of E and s. Also a closer inspection of Fig. 6.5b suggests that at the higher temperatures the curve shape encompassing the medium and slowly
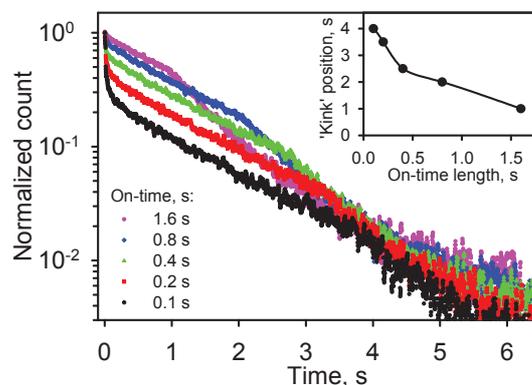
Figure 6.8: Off-time curve decay rate change ('kink') as a function of stimulation pulse duration. An aliquot of quartz (WIDG8) was dosed with 25 Gy, preheated to 260°C for 10 s and stimulated at 100°C with a single on-pulse of varying length between 0.1 s and 1.6 s. The curves have been normalized to the initial off-time point. Inset: Position of the 'kink' in the off-time curve as a function of stimulation pulse duration.

decaying parts does not change significantly. We, therefore, infer that at about 150°C there appears a new component in our data that decays slower than the component induced from the 110°C peak, and that this new component does not show a significant change in the decay rate with stimulation temperature.

The latter part of the off-time decays from 3 to 7 s in Fig. 6.5a shows a similar decay rate for the different temperatures, except the curve measured at 100°C. A summary of the lifetimes are given in Fig. 6.6b. The overall similarity in the decay rate for the different temperatures might suggest that this signal has a similar origin or is quite simply a continuation of the medium and slow components above (data shown in the ellipse, Fig. 6.6a).

The presence of the 'kink' at around 3 s (Fig. 6.5a) in the 100 and 75°C data is surprising. To our knowledge such a feature has not been reported before and suggests a rather different mechanism of luminescence generation, one that could possibly involve competition in the refuge (trap receiving charge from optical transfer) traps. This is examined in detail in the next sections.

6.5.2 'Kink' position for different stimulation pulse durations

To investigate whether the kink position is related to the amount of charge de-trapped from the OSL trap, measurements were carried out for different on-times at 100°C stimulation temperature after irradiation (25 Gy) and preheat (260°C for 10 s). Figure 6.8 shows five curves with stimulation pulse durations (on-times) between 0.1 s to 1.6 s, and it is observed that the 'kink' occurs sooner for the longer on-times. A summary of the 'kink' position is shown in the inset to the figure ranging from approximately 4 s for an on-time of 0.1 s to 1 s for an on-time of 1.6 s. We propose below a simple numerical model containing four energy levels to explain the possible origin of the kink structure in the OSP curve.
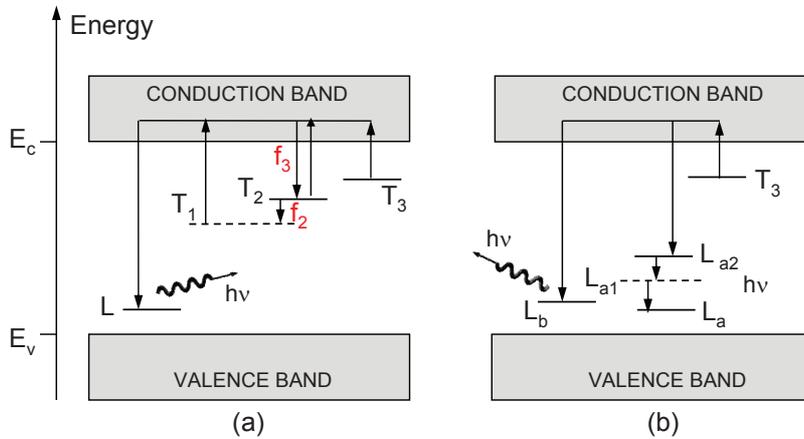
Figure 6.9: Band diagrams showing (a) A three trap (T_1, T_2, and T_3) -
one recombination centre (L) model. The traps T_1, T_2, and T_3 have initial
concentrations and decay constants n_1, λ_1, n_2, λ_2, and n_3, λ_3 respectively. f_2
represents the fraction of charge from T_2 trapped at T_1 and f_3 is the fraction of
charge from T_3 or T_1 retrapped at T_2. (b) A one trap (T_3) - two recombination
centres (L_a and L_b) model. L_a has two excited states, L_{a2} and L_{a1}. The same
subscript notation is used as in (a) for concentrations and decay constants for
the trap and the excited states.

6.5.3   A three-trap one centre phosphorescence model

Figure 6.9a shows a band model containing three traps T_1, T_2, T_3 and a
luminescence centre, L. The features of these traps are described below:

T_3: An electron trap with negligible retrapping. Thus, the charge population
decays exponentially at the ambient temperature. Non-retrapping is only
an approximation to simplify the model and it is not critical to the model
results. Majority of the charge released from T_3 undergoes recombination
at centre L, and a minor amount is trapped at T_2.

T_2: This is a deeper electron trap (smaller decay constant at the ambient
temperature than T_3). It can either lose charge to the conduction band
(and thereby cause electron-hole recombination at the centre L), or it
can lose charge by localised transition to the trap T_1. The majority of
the charge lost by T_2 is taken by T_1; this feature is the most critical
aspect of the model which helps reproduce the observed kink in the data.
For simplicity, since only a small fraction of the charge is released to the
conduction band, we assume that it all undergoes recombination at the
centre L and none of it is retrapped.

T_1: This is the third trap in the system which receives the majority of charge
released from T_2 by localised transition. The charge released from T_1
either undergoes a luminescent recombination with holes at L, or a frac-
tion is re-trapped at T_2 through the conduction band. Again it is not
critical to the model whether T_1 receives any electrons directly from the

conduction band, not as far as it is only a minor amount compared to the charge received from T_2; for convenience we have avoided this step.

The decay of electrons from these traps occurs due to the ambient temperature. The decay constants (λ) are assumed to have the following relationship: $\lambda_3 > \lambda_2 > \lambda_1$, corresponding to T_3, T_2 and T_1 respectively. At the end of the light stimulation these traps will have a certain initial concentration because of re-trapping from the conduction band, or as in the case of T_1 charge re-trapping from T_2. Because of charge decay from T_2 with $\lambda_2 > \lambda_1$, charge will initially build up at T_1 prior to recombining at L. The rate equations describing this model for the off-time are given as:

$$\frac{\mathrm{d}n_3}{\mathrm{d}t} = -n_3\lambda_3 \tag{6.1}$$

$$\frac{\mathrm{d}n_2}{\mathrm{d}t} = -n_2\lambda_2 + f_3(n_3\lambda_3 + n_1\lambda_1) \tag{6.2}$$

$$\frac{\mathrm{d}n_1}{\mathrm{d}t} = f_2 n_2\lambda_2 - n_1\lambda_1 \tag{6.3}$$

$$I \propto (1-f_3)(n_1\lambda_1 + n_3\lambda_3) + (1-f_2)n_2\lambda_2 \tag{6.4}$$

Here I is the observed luminescence intensity at time t, f_3 denotes the fraction of charge from T_3 or T_1 re-trapped at T_2, and f_2 the fraction of charge from T_2 trapped at T_1. Figure 6.10 shows the phosphorescence contribution from T_3, T_2, and T_1 together with the total phosphorescence, L, when solving the above rate-equations with the parameters: $n_{10} = 50$ cm^{-3}, $\lambda_1 = 0.04$ s^{-1}, $n_{20} = 300$ cm^{-3}, $\lambda_2 = 0.09$ s^{-1}, $n_{30} = 25$ cm^{-3}, $\lambda_3 = 0.3$ s^{-1}, $f_3 = 0.1$, and $f_2 = 0.92$. The luminescence arising from the T_3 and T_2 traps (blue curve and green curve, respectively) shows an exponential decay with time, whereas that from the T_1 trap initially builds up to a maximum before it decays (see semi-log scale in Fig. 6.10b). The total emitted luminescence from L (black curve) being the sum of the light from T_3, T_2, and T_1 therefore decrease initially, but as the light originating from T_1 starts to dominate over the light originating from T_3 and T_2, the total luminescence curve flattens out to a near constant level before the decay rate is increased again in accordance with the depletion of T_1. This simulated behaviour with three traps appears very similar to the kink observed in the 100°C measurement in Fig. 6.5a; it was furthermore observed in Fig. 6.5a that the kink disappears as the temperature is increased. From Fig. 6.5b and 6.6a we know that the lifetime of the 110°C TL trap decreases significantly (thereby an increase in the decay constant) for temperatures above 100°C. An increase in stimulation temperature would thus correspond to an increase in the decay constants λ_i in this model depending on the exact E and s values for each level. For certain combinations of these values such that the increase in λ_1 is greater than the increase in λ_2 or λ_3, it is possible to remove the kink and instead have an apparant decay in the simulation results.

In Fig. 6.8 the kink was observed to shift position as a function of the stimulation pulse duration. This can be achieved in the model by changing the initial concentration of T_1 (n_{10}) at the end of the stimulation pulse. An increase in this initial concentration, as would be expected with an increase in the length of the stimulation pulse duration, causes the kink to move towards shorter times in the off-time. This behaviour is consistent with the data presented in Fig. 6.8.
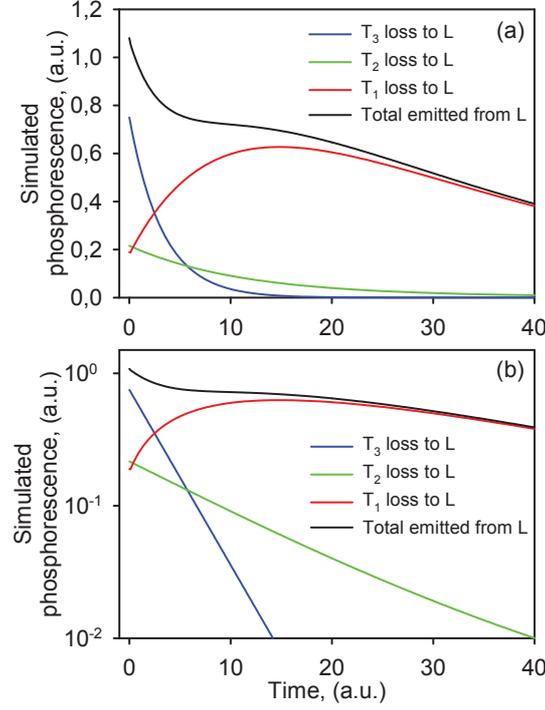
Figure 6.10: (a) Curves showing the loss from T_3, T_2, and T_1 together with the phosphorescence emitted at L when solving the rate-equations (6.1)-(6.4) using the parameters: $n_{10} = 50$ cm^{-3}, $\lambda_1 = 0.04$ s^{-1} , $n_{20} = 300$ cm^{-3}, $\lambda_2 = 0.09$ s^{-1}, $n_{30} = 25$ cm^{-3}, $\lambda_3 = 0.3$ s^{-1}, $f_3 = 0.1$, and $f_2 = 0.92$. (b) The same curves from (a) shown on a semi-log scale.

A simpler two trap model was also investigated using only T_2 and T_1 with $\lambda_2 > \lambda_1$. It is assumed that decay from both T_2 and T_1 produces light, and that a fraction of the charge from T_2 is transferred into T_1. Similar to the model above, the two traps are filled during the light stimulation to have an initial charge concentration at the end of the stimulation of $n_{20} > n_{10}$ after which they both start to decay. If f describes the fraction of charge transferred to T_1, then the rate equations describing this situation are given as:

$$\frac{\mathrm{d}n_2}{\mathrm{d}t} = -n_2\lambda_2 \tag{6.5}$$

$$\frac{\mathrm{d}n_1}{\mathrm{d}t} = fn_2\lambda_2 - n_1\lambda_1 \tag{6.6}$$

$$I \propto (1-f)n_2\lambda_2 + n_1\lambda_1 \tag{6.7}$$

Using the same values for n_{10}, λ_1, n_{20}, and λ_2 as above, the series of curves in Fig. 6.11 shows the total phosphorescence emitted at L for different fractions, f between 0.1 and 1. The inset shows the behaviour of T_1, T_2 and L for $f = 0.3$, which is the green curve in the main figure. It is seen from these curves, that it is not possible to produce a kink with this simpler model; it is crucial that there are three distinct traps and that there is a step of almost complete charge transfer from one to the other.
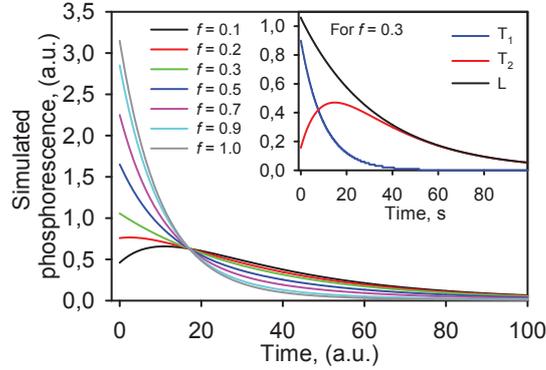
Figure 6.11: Curves showing the phosphorescence emitted at L when running the rate-equations (6.5–6.7) using the parameters: $n_{10} = 50$ cm^{-3}, $\lambda_1 = 0.04$ s^{-1}, $n_{20} = 300$ cm^{-3}, $\lambda_2 = 0.09$ s^{-1} for different values of f between 0.1 and 1. The loss from T_2 and T_1 together with the light emitted from L for $f = 0.3$ are shown inset to illustrate the dependence between the three.

6.5.4   An alternative one-trap, two-centre phosphorescence model

The mathematical equations above [Eqns. (6.1–6.4)] can equally be interpreted in terms of two different energy levels existing in a single centre. Here we propose an alternative interpretation of these equations. The model consists of a single trap, T_3 with lifetime λ_3, and two luminescence centres L_a and L_b, where L_a has two excited states, L_{a1} and L_{a2}, (Fig. 6.9b). It is assumed that the relaxation from L_{a2} to L_{a1}, by λ_a2 is non-radiative, but that the relaxation of L_{a1} to L_a (the ground state) by λ_a1 is radiative. During a short light stimulation, charge is transferred to T_3 and L_{a2}. In the off-time, a fraction of the charge from T_3 recombines at L_b and the remaining recombines at the excited state L_{a2}. The equations describing this model are identical to Eqns. (6.1–6.4), with the slight modification that the charge loss from the L_{a1} state is entirely to the ground state (unlike in the electron trap model where there is partial loss from level T_1 to level T_2 as well), i.e. the value of $f_2 = 1$, the equations thus become:

$$\frac{\mathrm{d}n_3}{\mathrm{d}t} = -n_3\lambda_3 \tag{6.8}$$

$$\frac{\mathrm{d}n_{2a}}{\mathrm{d}t} = -n_{2a}\lambda_{2a} + f_3 n_3 \lambda_3 \tag{6.9}$$

$$\frac{\mathrm{d}n_{1a}}{\mathrm{d}t} = n_{2a}\lambda_{2a} - n_1\lambda_1 \tag{6.10}$$

$$I \propto n_1\lambda_1 + (1 - f_3)n_3\lambda_3 \tag{6.11}$$

The results of these are almost identical to those in Fig. 6.10 because the retrapping terms in the trap model were very small (results not shown here). Again the key feature of this model is a non-luminescence relaxation from the level L_{a2} to L_{a1}, which produces the desired result.

The main difference between the two models is therefore not in the modelling results, but rather that they offer different advantages in the explanation
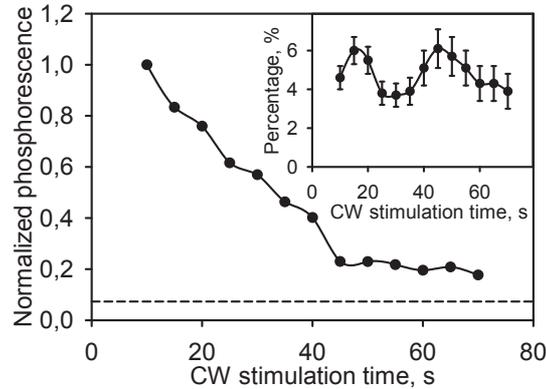
Figure 6.12: Normalized cumulative phosphorescence (integrated over 10 s) following different lengths of CW stimulations in the range of 10 s to 70 s. The sample was dosed with 25 Gy, preheated to 260°C for 10 s and stimulated at 125°C. The dashed line indicates the dark count level also integrated over 10 s. Inset: The percentage ratio between the end point of the OSL curve and the first point in the phosphorescence signal given for different CW stimulation times.

of the data in Fig. 6.5a and Fig. 6.8. By choosing the one trap − two centres model, it is relatively easier to explain the temperature independence of the latter part (after 3 s) of the curves in Fig. 6.5a, and perhaps also the component 2 in Fig. 6.3c, as the relaxation from L_a1 will dominate the curve after the kink, and this process can be temperature independent in the absence of thermal quenching. It would however require that the relaxation is strongly forbidden to cause delay on the seconds time scale; this needs to be investigated. The trap T_3 could be similar to the 110°C TL trap, which dominates the early part of the phosphorescence curves, and this process is highly temperature dependent. In this model the commonly observed 40 µs component would be derived from the centre L_b.

6.6 Phosphorescence contribution in the CW signal

It is obvious that phosphorescence is negligible compared to the fast OSL component in quartz measured at 125°C. To evaluate how large the contribution of the phosphorescence decay is in a standard CW measurement of the slow component in quartz, a series of measurements were carried out where the phosphorescence was detected for 10 s following blue CW stimulations at 125°C for durations of 10 s to 70 s. From Fig. 6.7 it was evident that light stimulation caused photo-transfer of charge into the 110°C TL trap, but that for longer stimulations >1.6 s, the light started to erode the photo-transferred charge instead. To see if this is also true for very long stimulations, or if the phosphorescence signal builds up during long stimulations, the amount of phosphorescence during the 10 s off-time was summed and is presented in Fig. 6.12, where it has been normalized to the initial 10 s stimulation point. From this curve it is clear that the phosphorescence does not increase with increased stimulation time, initially there is a faster drop in signal, but at about 40 s, the amount of phosphorescence emitted reaches a near constant level independent of the

stimulation time. The dashed line indicates the level of 'dark counts' in the PMT accumulated during 10 s after light stimulation (also normalized to the initial value as the other points) to show that the phosphorescence level is well above the dark count level. These data suggest that a fraction of the slow OSL component observed even at 125°C temperature may derive from decay of the refuge traps that initially store charge during OSL. In order to determine the percentage of the phosphorescence contained in the slow OSL signal, we calculated the ratio between the end point of the OSL signal and the first point in the phosphorescence signal (assuming that these points represent the equilibrium states at any time). This ratio is plotted for different stimulation times in the inset to Fig. 6.12. The fluctuations in the data reflect the low light levels. We note from these data that there may be a contribution from OSP of about 5% in the slow OSL signal.

6.7   Discussion

We find that the shape of the TR-OSL or OSP curves is almost independent of the preheat temperature in the range of 200 to 300°C at all time scales investigated here. This suggests that the refuge traps and centres participating in these processes must be the same irrespective of the preheat temperature. Moreover, the refuge traps must be emptied to the same relative levels for different preheats.

From our stimulation temperature data, a strong temperature dependence is seen in the initial 3 s of the phosphorescence curves in Fig. 6.5b. An E-s analysis of this changing component using an Arrhenius plot finds the trap depth $E = 0.91$ eV to be consistent with that found for the 110°C TL trap of $E = 0.89$ eV by Spooner and Questiaux (2000), and using our E and s values, a TL peak is predicted at 93°C for a heating rate of $2°Cs^{-1}$. This is further confirmed by TL measurements showing a PTTL peak at 97°C. The phosphorescence we observe during the initial 3 s of the curves is, therefore, dominated by charge recycled through the 110°C TL trap. This conclusion is consistent with the previous studies on PTTL in quartz [see Wintle and Murray (1997) and references therein]. Wintle and Murray (1997) also show for their quartz (WIDG8) the photo-transferred TL (PTTL) at room temperature illumination. In the absence of saturation effects, the ratio of 110°C PTTL to OSL is between 4 and 5% (Wintle and Murray, 1997).

In addition to the OSP component derived from the 110°C peak, we also find that there are some components both at the millisecond and second time scales that do not show an obvious dependence of their decay rates on the stimulation temperature. One possible reason for this could simply be, that we have not recorded data for sufficiently long time (e.g. in the milliseconds time scale) to track the movement of the different components. Another possible explanation could be the lack of a good mathematical model to extract individual components from the data; it is likely, as shown in the numerical modelling results, that the data do not follow a multiple-exponential form of the type used here for fitting. Thus, the apparent non-dependence on temperature could possibly be an artifact of our assumption that the OSP consists of linear superimposition of first-order processes. However, we note that the decay of the 110°C peak is conspicuous and has been picked up accurately by the

fitting analysis [as confirmed by E and s values from Spooner and Questiaux (2000)]. Similarly, the occurrence of a 160°C TL peak from the fitting analysis is supported by the PTTL data. We, therefore, consider that our analysis of the first 3 seconds of the data may be relatively error free, especially for the low temperature data (<125°C, Fig. 6.6a); the more problematic region may be the medium and slow components observed above 125°C (and the OSP data >3 s) as these could fall in the region where a peak build-up is predicted from the kinetic model (discussed below).

Two simple kinetic models are proposed to explain an abnormal change in the decay rate (the 'kink') in the OSP signals for the 75°C and 100°C stimulation temperatures (Figs. 6.5a and 6.8). The first model consists of three traps and a luminescence centre, while the second model consists of a single trap and two luminescence centres. The common trap T_3 in both these models could be similar to the 110°C TL trap. Both models share the same equations (with minor modifications) and can, therefore, both predict the behaviour observed in Fig 6.5a. The key feature of both the models that produces the desired effect is a large non-luminescent transfer and subsequent build-up from one energy level to the other. The resultant luminescence has a peak shape, and this produces a flattening followed by a steep decay in the luminescence curve. An interesting prediction of our alternative model (one trap - two recombination centres) is that there could be OSP components which do not show a change in the decay rate with the stimulation temperature, thus strengthening the possibility that the effect discussed in the previous paragraph concerning data in Figs. 6.3 and 6.5 may be real and not just an artifact of the measurement or analysis. However, this implies a relaxation time in the centre on the seconds time scale, which may or may not be realistic. The model results are encouraging, but they need to be investigated in greater detail to understand different OSP results from quartz.

Finally, we note that a similar kink was also observed in the IR stimulated phosphorescence signals from orthoclase feldspar (Ankjærgaard and Jain, 2010, Chapter 8 of this thesis). There and in the following paper (Jain and Ankjærgaard, 2011, Chapter 9 of this thesis) it is shown that the slowly decaying signals (both on the ms and s time scales) arise from the slow emptying of the band tails. As in the case of quartz, these signals show a change in the amplitude but a weak dependence of lifetime on stimulation temperature. Although band tails have not been explicitly reported in quartz, it is possible that natural quartz contains band tails because of deformational strain in the source rocks. These effects are well known in common quartz bearing rocks, e.g. quartzite and granite. If band tail states are indeed present in our quartz, they could potentially give an alternative explanation to the kink structure and temperature independence of the decay rates on the ms and s (>3 s) time scales in quartz OSP.

6.8   Summary and conclusions

1. The decay form of Time-Resolved OSL (TR-OSL) and Optically Stimulated Phosphorescence (OSP) in quartz has been observed to cover time scales of over 8 decades from 50 ns to ∼8 s.

2. The decay form of TR-OSL and OSP curves are independent of preheat

temperature, for all the examined time scales, in the range 200–300°C suggesting that the same centres and refuge traps are used for all these conditions.

3. Together the TR-OSL and OSP curves have been shown to contain at least four major components (1–4) by visual inspection. Component 1 has an average lifetime of ~40 µs at room temperature; it shows strong temperature dependent decrease as expected from an excited state life-time of a centre affected by thermal quenching. Component 2 has an average lifetime of ~1 ms and shows no real systematic behaviour with temperature in our data range. Component 3 is strongly stimulation temperature dependent and has been identified mainly to originate from the 110°C TL trap, and partly from some other TL peaks determined to lie at 87°C, 63°C, and 165°C. Component 4 with an average lifetime of ~5 s show an apparent overall temperature independence (with the exception at 100°C).

4. An abnormal decay behaviour (a 'kink') is observed conspicuously in the OSP data at 75°C and 100°C. A simple kinetic model consisting of four energy levels is proposed to explain the kink observed in the OSP data at around 3 s. This model can successfully reproduce the kink, and can be physically interpreted in terms of a 3 trap and 1 luminescence centre model, or alternatively, a 1 trap and 2 luminescence centres model with one of the centres having two excited states. The key feature of these models that produce the kink effect is a large localised, non-luminescent transfer and subsequent build-up from one energy level to the other. Although the results are encouraging, there needs to be further theoretical investigations into charge transfer and re-trapping to fully understand the optically stimulated phosphorescence results from quartz. One potential explanation for the temperature dependence of lifetimes (components 2 and 4) as well as the kink structure could be the possible presence of band tail states in natural (deformed) quartz.

5. The 110°C TL peak plays a significant role even for optical stimulation at 125°C, although, the lifetime is rather small (0.2 s). It is determined that the OSP contribution to the OSL signal in the 10 s–70 s measurement region (for blue light stimulation at ~40 mW/cm^2) is <5%. Although, this is unimportant for dosimetry, it could perhaps have a slight affect on the analysis of slow components in the slow OSL signals for derivation of physical parameters. A cleaner signal would be obtained by stimula-tions above 150°C, although at the cost of reduced sensitivity because of thermal quenching.

References

Ankjærgaard, C. and Jain, M. (2010). Optically stimulated phosphorescence in orthoclase feldspar over the millisecond to second time scale. *Journal of Luminescence*, 130:2346–2355.

Ankjærgaard, C., Jain, M., Thomsen, K. J., and Murray, A. S. (2010). Optimising the separation of quartz and feldspar optically stimulated luminescence using pulsed excitation. *Radiation Measurements*, 45:778–785.

Bailiff, I. K. (2000). Characteristics of time-resolved luminescence in quartz. *Radiation Measurements*, 32:401–405.

Bøtter-Jensen, L., McKeever, S. W. S., and Wintle, A. G. (2003). *Optically Stimulated Luminescence Dosimetry*. Elsevier, Amsterdam, The Netherlands. ISBN: 0–444–50684–5.

Chithambo, M. L. (2002). Time-resolved luminescence from annealed quartz. *Radiation Protection Dosimetry*, 100:273–276.

Chithambo, M. L. (2007). The analysis of time-resolved optically stimulated luminescence: II. Computer simulations and experimental results. *J. Phys. D: Appl. Phys.*, 40:1880–1889.

Chithambo, M. L. and Galloway, R. B. (2000). A pulsed light-emitting-diode system for stimulation of luminescence. *Meas. Sci. Technol.*, 11:418–424.

Chithambo, M. L. and Galloway, R. B. (2001). On the slow component of luminescene stimulated from quartz by pulse blue light emitting diodes. *Nuclear Instruments and Methods B*, 183:358–368.

Chithambo, M. L., Ogundare, F. O., and Feathers, J. (2008). Principal and secondary luminescence lifetime components in annealed natural quartz. *Radiation Measurements*, 43:1–4.

Chithambo, M. L., Preusser, F., Ramseyer, K., and Ogundare, F. O. (2007). Time-resolved luminescence of low sensitivity quartz from crystalline rocks. *Radiation Measurements*, 42:205–212.

Jaek, I., Hütt, G., and Streltsov, A. (1999). Study of deep traps in alkali feldspar and quartz by the optically stimulated afterglow. *Radiation protection dosimetry*, 84:467–470.

Jain, M. and Ankjærgaard, C. (2011). Towards a non-fading signal in feldspar: insight into charge transport and tunnelling from time-resolved optically stimulated luminescence. *Radiation Measurements*, 46:292–309.

Lapp, T., Jain, M., Ankjærgaard, C., and Pirzel, L. (2009). Development of pulsed stimulation and photon timer attachments to the Risø TL/OSL reader. *Radiation Measurements*, 44:571–575.

Markey, B. G., Colyott, L. E., and McKeever, S. W. S. (1995). Time-resolved optically stimulated luminescence from α-al$_2$o$_3$:c. *Radiation Measurements*, 24:457–463.

Pagonis, V., Ankjærgaard, C., Murray, A. S., Jain, M., Chen, R., Lawless, J., and Greilich, S. (2010). Modelling the thermal quenching mechanism in quartz based on time-resolved optically stimulated luminescence. *Journal of Luminescence*, 130:902–909.

Pagonis, V., M., M. S., Chithambo, M. L., Christensen, E., and Barnold, C. (2009). Experimental and modelling study of pulsed optically stimulated luminescence in quartz, marble and beta irradiated salt. *Journal of Physics D: Applied Physics*, 42:1–12.

Spooner, N. A. and Questiaux, D. G. (2000). Kinetics of red, blue and UV thermoluminescence and optically-stimulated luminescence from quartz. *Radiation Measurements*, 32:659–666.

Wintle, A. G. and Murray, A. S. (1997). The relationship between quartz thermoluminescence, photo-transferred thermoluminescence, and optically stimulated luminescence. *Radiation Measurements*, 27(4):611–624.

Chapter 7

Further investigations into pulsed optically stimulated luminescence from feldspars using blue and green light

C. Ankjærgaard[1], M. Jain[1], R. Kalchgruber[2], T. Lapp[1], D. Klein[2], S. W. S. McKeever[2], A. S. Murray[3], and P. Morthekai[1]

[1] *Radiation Research Department, Risø National Laboratory for Sustainable Energy, Danish Technical University, DK-4000 Roskilde, Denmark*
[2] *Department of Physics, Oklahoma State University, Stillwater, OK 74074, USA*
[3] *Nordic Laboratory for Luminescence Dating, Department of Earth Science, Aarhus University, Risø DTU, DK-4000 Roskilde, Denmark.*

Abstract
The purpose of this paper is to investigate characteristics of luminescence signals resulting from pulsed optical stimulation of feldspars and thereby to understand the underlying processes giving rise to the signal. Fourteen different feldspar specimens were investigated using time-resolved optically stimulated luminescence (TR-OSL), and these signals can be mathematically described as a sum of 4 exponential components (a, b, c, d). The slowest component, d, increases with the duration of the light pulse as expected from the exponential model. The stimulation temperature dependence experiment suggests that the TR-OSL signal decay is governed by the recombination process and not by the excited state lifetime. Furthermore data from the TR-OSL signal dependence on stimulation time and preheat temperature suggests that the recombination process may not be a sum of exponentials, although the model cannot be rejected definitively.

7.1   Introduction

Optically stimulated luminescence (OSL) is widely used to investigate the characteristics of traps and centres in natural dosimetric minerals. However, the resulting signals give limited information on the underlying luminescence mechanisms, as the signal is the result of complex charge detrapping and recombination processes, and so the interpretation of such curves in terms of separating and understanding the mechanisms is difficult. One way of studying the recombination process directly is by time-resolved optically stimulated luminescence (TR-OSL) measurements, which has the potential to distinguish the different recombination processes.

A few studies have examined feldspars with time-resolved luminescence using blue or green light as a stimulation source (Sanderson and Clark, 1994; Chithambo and Galloway, 2000; Tsukamoto et al., 2006). Analytical treatment of the TR-OSL data has, however, been restricted to fitting data with a multiple exponential model e.g. Clark et al. (1997); Clark and Bailiff (1998); Chithambo and Galloway (2000). This analysis is then used to derive the lifetimes of the signals, which are considered characteristic of the specimen under consideration. The assumptions or implications of multiple-exponential fitting have not been discussed in detail. One could argue that the shape of the TR-OSL signal may be influenced by both exponential and non-exponential processes:

(a) Relaxation from the excited state to the ground state of the recombination centre resulting in the release of a photon.

(b) Transition of an electron from the conduction band or band tails (Poolton et al., 2002a,b) to the recombination centre.

(c) Tunnelling recombination from the band tails or from the excited state of the trap; the latter is only likely to be significant for the TR-OSL signal during the stimulation pulse.

Process (a) is likely to be an exponential process with a characteristic 'excited-state lifetime'. Processes (b) can be exponential with a 'recombination lifetime'; this lifetime will be related to the density of available holes in the crystal. There is enough evidence in the literature to suggest that tunnelling in feldspars [process (c)] follows a power law, see a summary in Huntley (2006) which results from random spatial distribution of recombination centres; thus the concept of lifetime does not apply for this latter process.

In this article we want to test whether a model based on the linear sum of exponentially decaying signals is valid for feldspar TR-OSL, and to distinguish between the above processes. We present an analysis of the apparent lifetimes from 14 feldspar specimens using the TR-OSL signals stimulated by both a 532 nm pulsed laser and 470 nm pulsed LEDs. The dependencies of these lifetimes on stimulation time, stimulation temperature and preheat temperature are then

used to allow us to distinguish between the dominant processes that determine the shape of the signal.

7.2 Samples and instrumentation

Fourteen different feldspar specimens were used in this study: 8 mineral specimens were obtained from the Geological Museum in Copenhagen, Denmark, three were kindly supplied by Regina DeWitt, Oklahoma State University, US, and the remaining three were kindly supplied by John Bridges, University of Leicester, UK, (all samples - mineral names - are listed on the x-axis of Fig. 7.2). The minerals were chosen to represent a variety of K, Na and Ca contents. The 8 museum samples were crushed and dry-sieved to obtain a grain size fraction 90–125 µm and the other six samples were received in grain sizes between 90–250 µm. No further chemical treatment was employed.

TR-OSL measurements in the nanosecond regime were undertaken at the Radiation Dosimetry Laboratory at Oklahoma State University using a 532 nm pulsed Q-switched diode laser (Meshtel no. GSQAOM32-25) with a pulse frequency of 1 kHz and a pulse width of ∼15 ns (>25 µJ per pulse). The pulsed stimulation light passed through a laser clean-up filter and 2 mm diameter glass fibreoptic cable into the sample chamber, as described by Yukihara et al. (2007). An Electron Tubes 9235QB photomultiplier tube detected the luminescence through 7.5 mm of U-340 Hoya filter and a laser suppression filter. TR-OSL signals were recorded using a multi-channel scaler (Stanford Research Systems, model SR430) with a bin-width of 5 ns and a total number of recorded bins of 1024 (5.1 µs). Measured signals accumulated in each case for a preset number of laser pulses. Sample annealing, irradiation and preheating was carried out in a Risø TL/OSL-DA-15 reader prior to the TR-OSL measurement.

TR-OSL was also measured using a Risø TL/OSL-DA-20 reader with an integrated pulsing option to control the LEDs; Lapp et al. (2009, Chapter 2 of this thesis) give details of the photon detection and photon time-stamping. The detection resolution of this system is 100 ps. Blue light stimulation was performed with a 470 nm LED array delivering 50 mW/cm^2 at the sample position in continuous wave, and 7.5 mm of U-340 Hoya filter was used for detection.

All samples were mounted in stainless steel cups using silicone oil and, unless otherwise stated, a preheat of 250°C for 60 s was employed throughout. This was followed by either green laser stimulation at room temperature for 10 s or blue LED stimulation at 50°C for 300 s.

7.3 Time-resolved OSL from feldspars

In Fig. 7.1, the TR-OSL from Albite is plotted together with the measured light output during 50 µs stimulation pulses from the blue diodes. The feldspar signal consists of two parts; (i) a fast rise during the switch on of the pulse, and a fast decay immediately after the pulse ends; the shape of this fast rise and decay is identical to the shape of the blue LED pulse (ii), a more slowly rising component during the switch on of the pulse and a slow decay after the pulse ends. This slow component does not follow the stimulation pulse shape.
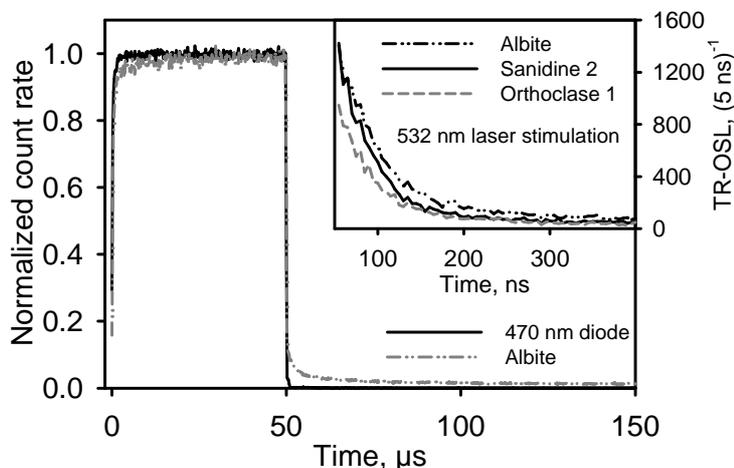
Figure 7.1: The stimulation pulse shape from the 470 nm LEDs plotted together with the OSL signal from Albite, both normalized to the 50 μs point. The Albite was given a dose of 5 Gy, preheated to 250°C for 60 s and stimulated at 50°C. Inset: Albite, Sanidine 2 and Orthoclase 1 TR-OSL signals obtained just after the 15 ns stimulation pulse width from the pulsed 532 nm laser. Note that the initial 55 ns have been removed from the data. Doses were 5, 500, and 5 Gy respectively, and the samples were preheated to 250°C for 60 s and stimulated at room temperature.

The identical shapes of the fast decaying signal and the stimulation pulse imply that the signal decay must occur at the same or shorter time scales than the switching off of the blue LEDs. In order to resolve this fast decaying signal, all samples were stimulated using a pulsed green laser (pulse width 15 ns); the resulting TR-OSL signals from Albite, Sanidine 2 and Orthoclase 1 are shown inset in Fig. 7.1. The signal seems to decay in less than 1 μs in all three cases. Because of saturation effects in the PMT during the high-peak-power stimulation pulse and to avoid any influence of the weak (known) ringing immediately after the main pulse, the initial parts of the curves were rejected. On the basis of the background signals from the laser, the first 11 channels (55 ns) following the peak of the pulse were rejected, this is only a small fraction of the 1000 channels (5000 ns) used for analysis; the data in the remaining 989 channels should be free from saturation effects and laser interference. From a consideration of both the green and blue pulsed stimulation data it appears that there is a component of the TR-OSL signal which decays in tens of nanoseconds and a component which decays in tens of microseconds.

In the following analysis of the TR-OSL decays after the stimulation light is switched off, it is assumed that the signals from both the 532 nm stimulation and the 470 nm stimulation are of the form:

$$I(t) = k + \sum a_i \cdot \exp\left(\frac{-t}{\tau_i}\right), \tag{7.1}$$

where $I(t)$ is the intensity of the signal at time t, a_i is the maximum intensity of the 'i'-th component during the pulse, τ_i is the lifetime of this component
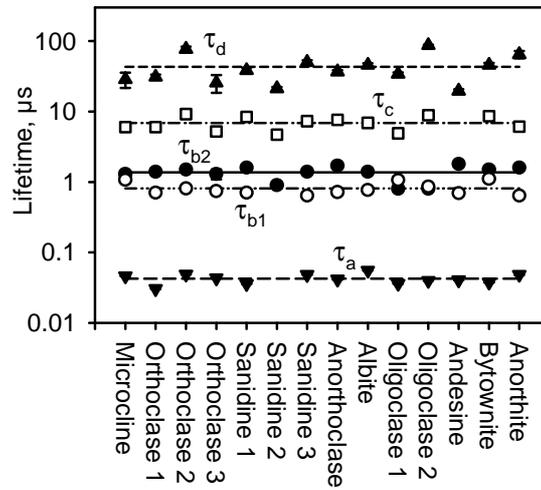
Figure 7.2: Lifetimes calculated for signals obtained with pulsed 532 nm laser stimulation (τ_a and τ_{b_1}) and pulsed (on-time 10 µs, off-time 200 µs) 470 nm LED stimulation (τ_{b_2}, τ_c, τ_d) for each of the 14 samples. The horizontal lines represent the average component lifetimes. The given doses were between 5 Gy and 1000 Gy depending on individual sample sensitivity. Heating conditions were identical to those in Fig. 7.1.

and k is a constant.

For all 14 samples, both the green- and blue-stimulated TR-OSL curves were fitted using Eqn. (7.1). For the green stimulation, two components with average lifetimes $\tau_a = 42 \pm 0.1$ ns and $\tau_{b_1} = 810 \pm 9$ ns were sufficient to describe the curves adequately, while three components were needed for the blue-stimulated curves, with average lifetimes: $\tau_{b_2} = 1.37 \pm 0.02$ µs, $\tau_c = 6.9 \pm 0.1$ µs and $\tau_d = 43 \pm 1$ µs.

These lifetimes are plotted for the 14 samples in Fig. 7.2; they all differ from each other by about a factor of 10, but the two lifetimes, τ_{b_1} and τ_{b_2} are rather similar in many samples and, given the different experimental conditions, probably represent the same component with an average lifetime $\tau_b = 1.10 \pm 0.02$ µs. Thus, the shape of the TR-OSL decay are very similar and can be adequately described by 4 exponential components in all our feldspar samples irrespective of sample chemistry or dose, which varied from 5 Gy to 1000 Gy depending on the sample sensitivity. The shortest lifetimes are similar to those found by using IR stimulation (Clark et al., 1997; Clark and Bailiff, 1998).

7.4 Testing of the first-order component analysis

To examine whether the 4 components identified above represent 'excited state lifetimes' or 'recombination lifetimes' or quite simply a parameterisation of a complex curve shape, experiments were carried out to observe the TR-OSL decay shapes as a result of changes in the stimulation temperature, stimulation pulse width, stimulation time, and preheat temperature. These observations were then compared to those expected from first-order phenomena implicated in the curve fitting. The results and analysis are described below.
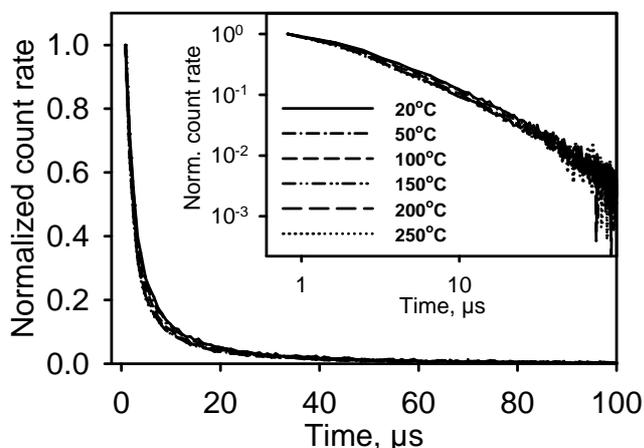
Figure 7.3: Initial-intensity-normalized TR-OSL signals measured (after stimulation) at temperatures of 20°C, and 50°C to 250°C in steps of 50°C for Sanidine 2 using on-time 20 μs and off-time 200 μs. The signal backgrounds were subtracted prior to normalization. The inset shows the curves on log-log scale. The sample was given a dose of 500 Gy prior to a preheat of 250°C for 60 s.

7.4.1 Variation of TR-OSL signal with stimulation temperature

Significant thermal quenching has been observed below 250°C in both the 440 nm and 600 nm bands of feldspars (Poolton et al., 1995), however, no results are available for the UV band measured here. An increase in stimulation temperature is expected to result in an increased importance of non-radiative recombination and thus a decrease in the apparent excited state lifetime. Thermal quenching is expected to give rise to a faster TR-OSL signal decay, thus we should see a trend with temperature. To our knowledge no measurements investigating this issue have been carried out on feldspars. Figure 7.3 shows signals from Sanidine 2 normalized to the initial intensity for stimulation temperatures between 20°C and 250°C, after removal of an initial fixed signal portion containing the unresolvable component a. The signals are scattered; there is no systematic trend with temperature (see also log-log scale of curves in the inset of Fig. 7.3), and we conclude that neither the decay times nor the relative intensities of components b, c, and d are temperature dependent; the same process(es) must govern the decay of the signal, independent of temperature. The results suggest that either (i) there is no thermal quenching in the emission band measured using a U340 filter, or (ii) the recombination process that gives rise to the slowly decaying signal in feldspars is only weakly dependent on temperature. Possibility (i) is somewhat unlikely since the 440 nm emission band that shows strong thermal quenching extends well within the transmission range of the U340 filter (Poolton et al., 1995). This result indicates that the TR-OSL decay shape is not governed by the excited state lifetime, but instead by the recombination process. In the next sections we explore the nature of the recombination process.
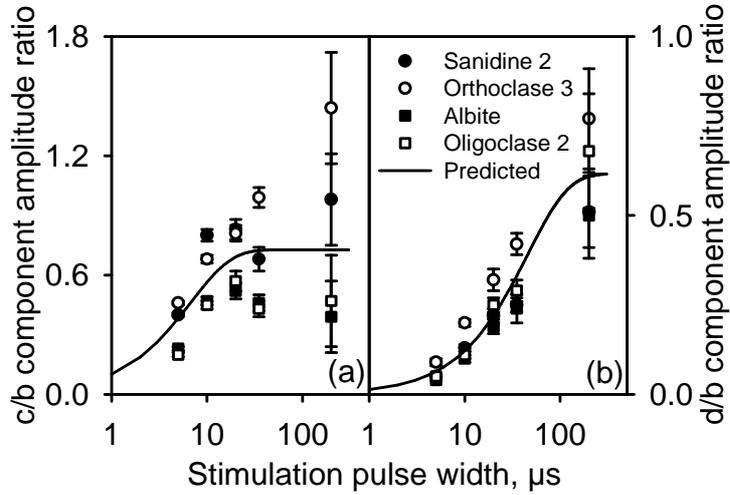
Figure 7.4: Amplitude ratios of (a) component c to component d and (b) component d to component b, as a function of the pulse width for Sanidine 2 (500 Gy), Orthoclase 3 (5 Gy), Albite (5 Gy) and Oligoclase 2 (25 Gy). The solid lines represent the predicted build-up behaviour for a single saturating exponential with (a) the mean component c lifetime (τ_c) of 6.9 μs and (b) the mean component lifetime d of (τ_d) 45 μs. The samples were heated to 250°C prior to pulsed blue LED stimulation at 50°C, the on-times varied as given on the figure and off-times kept constant at 200 μs.

7.4.2   Slow component build-up during stimulation

If the TR-OSL signal is indeed made up of 4 exponential components (a, b, c, d) then the recombination lifetimes should be independent of the stimulation pulse width. As a result, the slow components should increase in intensity with increased pulse-width, relative to the fast components, with a relative intensity ratio that should be predictable from the lifetimes. If the intensity ratio does not follow the expected trend, then it is unlikely that there are separate fast and slow processes giving rise to the signal.

To test whether our lifetimes meet these criteria, TR-OSL curves were recorded following 10 and 200 μs stimulation pulse widths using blue LEDs to allow a more detailed examination of the three slower components b, c, and d. The lifetimes obtained with 10 μs pulses ($\tau_b = 1.37 \pm 0.02$ μs, $\tau_c = 6.9 \pm 0.1$ μs, and $\tau_d = 43 \pm 1$ μs) are indistinguishable within 2 from those after 200 μs pulses ($\tau_b = 1.38 \pm 0.4$ μs, $\tau_c = 6.4 \pm 0.2$ μs and $\tau_d = 45 \pm 1$ μs) showing that the measured decay constants are independent of the stimulation pulse width. All lifetimes given here are the average of the 14 samples.

The same data were then used to test whether the slowest component, d, increases in amplitude relative to the faster component b, as the pulse width is increased from 10 μs (<25% of the decay constant for component d) to 200 μs (nearly 5 times the decay constant for d). Component b is expected to be saturated at both pulse widths because of its short lifetime of 1.4 μs, and component c will be close to saturation during the 10 μs pulse and fully in saturation during the 200 μs pulse. We have normalized the amplitude of

component d, a_d, to that of component b, a_b, such that for all 14 samples, the amplitude ratio is calculated as:

$$\frac{(a_d/a_b)_{200}}{(a_d/a_b)_{10}}, \tag{7.2}$$

where the subscripts 200 and 10 denote the pulse width. If an average is calculated for all 14 samples, the slowest component increases by a factor of 6.0 ± 0.5 as the pulse width changes from 10 to 200 μs, to be compared with a predicted increase of 5.0 ± 0.5 based on the lifetimes given above; the observed increase is consistent with that expected assuming independent behaviour.

To examine the build-up in more detail for both components c and d, the experiment was repeated for four samples (Sanidine 2, Orthoclase 3, Albite and Oligoclase 2) using pulse widths of 5, 10, 20, 35 and 200 μs, and with the off-time kept constant at 200 μs. Since, it is not possible with the current Risø TL/OSL pulsed system to use pulse widths of less than 5 μs, the components a and b could not be investigated for build-up in this range. In Fig. 7.4a, the ratios of the amplitudes of components c/b are shown for increasing pulse width and in Fig. 7.4b the ratios of the amplitudes of components d/b for increasing pulse width. In both figures the data have been plotted together with a theoretical build-up curve based on the average component lifetime derived above. The data are all consistent with the predicted curves, but for component c the scatter is too large to make useful conclusions. For component d, however, the theoretical (predicted) curve matches the data well, and we conclude that this component appears to build up relative to component b in accordance with first-order behaviour. Furthermore, in the green TR-OSL curves, no slow component is observed, presumably because it did not get time to build up during the ~15 ns pulses.

7.4.3   Variation of TR-OSL signal with stimulation time

To investigate further the relative importance of the different components, we examined whether the OSL signal, measured after the stimulation pulse, changes shape with an increase in the stimulation (measurement) time. Figure 7.5a shows the signal accumulated during various time intervals of stimulation for the green laser using Oligoclase 2 and Fig. 7.5b for blue LED stimulation using Sanidine 2. All signals were normalized to the initial count rate intensity. These two samples are representatives of the average behaviour when compared to data measured for all the samples. The green-stimulated data all lie on top of each other. In the blue-stimulated data TR-OSL curves change shape slightly but there is no systematic trend. However, if one only examines the data for the first 1000 s it appears that the decay for the 0-10 s data is slightly slower than for the 10-100 s and 100-1000 s data sets. This is unexpected if one assumes an exponential process governed by the transition from the conduction band; the lifetime should instead have increased with progressing stimulation time because of reduction in the hole population [$\tau = 1/A_m \cdot m(t)$, where m is hole concentration and A_m is a constant cross-section].

However, no change in the decay shape may be expected if (i) the number of recombining electrons is small compared to the number of hole-populated recombination centres, so that there is no significant depletion in the number of holes during the TR-OSL measurement, or (ii) if the effect of changes in hole
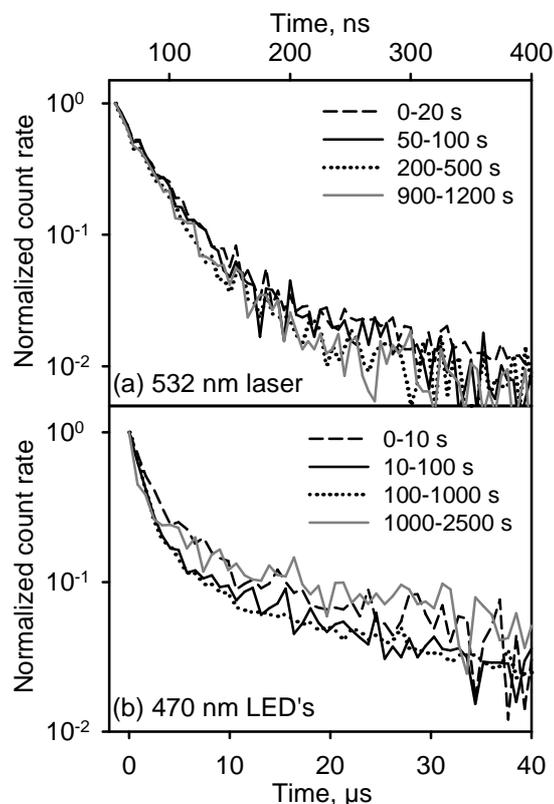
Figure 7.5: Initial-intensity-normalized TR-OSL signals (after stimulation) for different stimulation time intervals for (a) pulsed green laser stimulation of Oligoclase 2 and (b) pulsed blue LED stimulation of Sanidine 2 (on-time 20 μs, off-time 200 μs). 0–20 s denotes the signal accumulated during the first 20 s of stimulation, i.e. the signal following each of the first 20k pulses of the green laser, etc. Note that the time intervals differ. The samples were given 25 Gy and 500 Gy respectively prior to a preheat to 250°C for 60 s. Oligoclase 2 was stimulated at room temperature and Sanidine 2 at 50°C.

population is not important because of localized recombination mechanisms (e.g. in a localised transition model). Conversely, in a conduction band routed recombination process in a system with a comparable number of electrons and holes, the time resolved signal is expected to decay increasingly slowly with stimulation time; this is not apparent in our data.

7.4.4 Dependence of the TR-OSL signal on preheat temperature

Data were obtained following preheats ranging from 50°C to 300°C in steps of 50°C and multiple exponentials were fitted to post-pulse OSL signals, as described in Section 7.3, in order to derive the TR-OSL recombination lifetimes for Sanidine 2. In Fig. 7.6a the six TR-OSL decay curves have been normalized to the initial intensity and it can clearly be seen that the rate of decay increases

with increasing preheat temperature. This change in the decay rate could arise due to change in the relative proportions and/or the lifetimes of different components. The fitting analysis shows that there is a change in lifetimes for components b, c and d with preheat temperature (inset to Fig. 7.6a); the lifetime of component b decreases slightly with temperature, while those of components c and d decrease markedly. Similar results have been observed from other samples.

It is possible that the change in recombination lifetimes is simply a result of inadequate fitting, and does not have any direct physical meaning. In Fig. 7.6b data following 50°C and 300°C preheats are shown together with the best fits of Eqn. 7.1 (white lines); these curves give very different lifetimes for the three components (see Fig. 7.6a). In order to test the fitting analysis, the lifetime obtained from the fitting of 300°C data were forced to fit the 50°C data; this gave the gray line through the 50°C preheat data set. It is evident that this fit does not represent the data well (see the residuals inset to Fig. 7.6b), and it is therefore concluded that the change in apparent component lifetimes with preheat temperature is real.

Preheat is expected to decrease the hole concentration because of large electron-hole recombination evident in the TL peaks ranging from room temperature up to 300°C, see Murray et al. (2009). Thus one should in fact have expected an increase in the recombination lifetimes. Our data, on the contrary, show a systematic decrease in the three lifetimes with an increase in preheat temperature. Thus the data does not support the expectation from processes (a) and (b), see introduction, unless there is a significant redistribution of holes to the OSL centres (to be investigated for these samples).

7.5   Discussion and conclusions

The work described here represents a step towards understanding the processes governing the production of luminescence (electron recombination and de-excitation to ground state of the luminescence centre) using TR-OSL measurements in feldspars.

Assuming a multiple exponential model it is possible to express the TR-OSL decay shapes from all 14 feldspar samples in terms of four components (a, b, c, d) with well separated lifetimes that are broadly similar for all the samples, irrespective of chemical composition or dose (Fig. 7.2). This concordance suggests that the TR-OSL shapes are governed by similar processes in all the samples, although one cannot necessarily deduce from this the nature of the processes.

The stimulation temperature data help to distinguish whether the rate of the luminescence decay is governed by 'recombination lifetimes' or 'excited state lifetimes' for the slowly decaying components (b, c, d). Since the lifetime of the excited state of a centre is likely to be temperature dependent, one would expect to observe a change in OSL decay lifetimes as a function of stimulation temperature. However, Fig. 7.5 shows that the lifetimes do not change significantly between 20 and 250°C. This result suggests that the lifetimes do not represent excited-state lifetimes of the luminescence centres. The shape of the signal is then presumably related to the time required for recombination and this must be independent of stimulation temperature. The interpretation
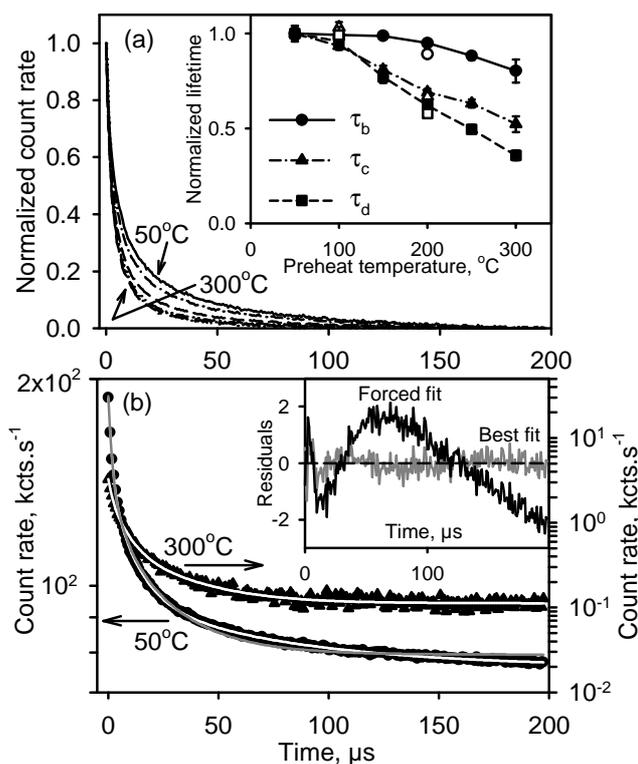
Figure 7.6: Dependence of the OSL signals measured after stimulation on preheating temperature for Sanidine 2. The sample was given a dose of 500 Gy and preheated for 60 s at temperatures varying from 50°C to 300°C in steps of 50°C prior to each measurement with pulsed (on-time 20 μs, off-time 200 μs) blue light. (a) Signals normalized to the initial intensity. The top-most curve is using 50°C stimulation from where the curves sequentially decrease to the 300°C stimulation curve. All curves had their background subtracted prior to normalization. The fitted b, c and d component lifetimes are plotted as a function of preheat temperature in the inset to (a), the open symbols are repeat points. (b) The signals from (a) following preheats of 50°C and 300°C (note these have not been normalized, nor has background been subtracted) are shown together with their best fit (white lines). The grey line represents a forced fit through the 50°C curve with the three lifetime parameters fixed to those of the 300°C best fit. The residuals for the best and forced fits for the 50°C curve data are shown inset to (b).

that the slower decay rates of the TR-OSL signal (components b, c, d) do not represent excited-state lifetimes is further confirmed by the stimulation time data (Section 7.4.3) and the preheat dependence data (Section 7.4.4).

The discussion above implies that the shape of the TR-OSL signal is governed by recombination processes. In order to check if these recombination processes are exponential in nature, analyses of component build-up with pulse width was carried out; only components c and d could be examined by this analysis due to instrument limitations. The analysis was inconclusive for component c because of large scatter in the data around the predicted build-up curve, but component d (with the longest lifetime) shows a clear build-up with increasing pulse-width as expected from the exponential model (Fig. 7.3).

A further investigation into the nature of the processes was made by observing the change in the TR-OSL decay shape down the POSL stimulation curve. The data shows no systematic dependence of the decay shape on the measurement time. If one expects the hole density to decrease with stimulation time, then an increase in recombination lifetimes would be expected as a result; this is not observed here.

Finally we looked at the variation in recombination lifetimes with changes in preheat temperatures. The recombination lifetimes of the three slow components were found to decrease with an increase in preheat temperature (Fig. 7.6). If the reduction in OSL signals with preheat is related to reduction in the hole density, then one could argue that an increase in preheat would have led to an increase in the lifetimes; the data shows an opposite trend.

We now discuss whether a 'recombination lifetime' is a useful description of the TR-OSL signal; in other words, whether the slower TR-OSL signal is actually made up of three exponential components. Note that such a recombination lifetime should be a function of the concentration of available holes in the crystal [see process (b) in Section 7.1]. One needs to take into account the following observations for this discussion:

(i) The lifetimes are very similar in the 14 samples although these were measured for very different doses (5 Gy to 1000 Gy). This suggests that the shape of the signal is similar, irrespective of sample chemistry or dose. It would be a peculiar coincidence if, despite this, the signal shape was governed only by the recombination lifetime, i.e. if it was purely determined by the density of available holes.

(ii) A slower TR-OSL decay should have been observed as a function of measurement time (assuming that the hole population would decrease with progressive stimulation). We either find no difference in the signal shapes (Section 7.4.3) or the signals become slightly faster with stimulation time.

(iii) If the hole (i.e. the recombination centre) concentration were to decrease with the preheat temperature, then one would expect a corresponding increase in the recombination lifetime. However, the opposite is observed: the decay curves become faster as a function of preheat temperature.

These three observations question the validity of the assumption that the TR-OSL signal can be defined/explained by a multiple exponential process. They do, however, not disprove the model.

In summary, we note that the slow part of the TR-OSL signal (resolvable with blue LED pulsing) represents a recombination processes and not excited-state lifetimes. There is a suggestion that this recombination process may not be the linear sum of independent exponential processes. If so, one could consider a tunnelling route [process (c) in Section 7.1] as an alternative mechanism governing the TR-OSL decay shape.

References

Chithambo, M. L. and Galloway, R. B. (2000). A pulsed light-emitting-diode system for stimulation of luminescence. *Meas. Sci. Technol.*, 11:418–424.

Clark, R. J. and Bailiff, I. K. (1998). Fast time-resolved luminescence emission spectroscopy in some feldspars. *Radiation Measurements*, 29:553–560.

Clark, R. J., Bailiff, I. K., and Tooley, M. J. (1997). A preliminary study of time-resolved luminescence in some feldspars. *Radiation Measurements*, 27:211–220.

Huntley, D. J. (2006). An explanation of the power-law decay of luminescence. *J. Phys.: Condens. Matter*, 18:1359–1365.

Lapp, T., Jain, M., Ankjærgaard, C., and Pirzel, L. (2009). Development of pulsed stimulation and photon timer attachments to the Risø TL/OSL reader. *Radiation Measurements*, 44:571–575.

Murray, A. S., Buylaert, J. P., Thomsen, K. J., and Jain, M. (2009). The effect of preheating on the IRSL signal from feldspar. *Radiation Measurements*, 44:554–559.

Poolton, N. R. J., Bøtter-Jensen, L., and Duller, G. A. T. (1995). Thermal quenching of luminescence processes in feldspars. *Radiation Measurements*, 24:57–66.

Poolton, N. R. J., Wallinga, J., and Murray, A. S. (2002a). Electrons in feldspar I: on the wavefunction of electrons trapped at simple lattice defects. *Phys. Chem. Minerals*, 29:210–216.

Poolton, N. R. J., Ozanyan, K. B., and Wallinga, J. (2002b). Electrons in feldspar II: a consideration of the influence of conduction band-tail states on luminescence process. *Phys. Chem. Minerals*, 29:217–225.

Sanderson, D. C. W. and Clark, R. J. (1994). Pulsed photostimulated luminescence of alkali feldspars. *Radiation Measurements*, 23:633–639.

Tsukamoto, S., Denby, P. M., Murray, A. S., and Bøtter-Jensen, L. (2006). Time-resolved luminescence from feldspars: New insight into fading. *Radiation Measurements*, 41:790–795.

Yukihara, E. G., Mittani, J., McKeever, S. W. S., and Simon, S. L. (2007). Optically stimulated luminescence (OSL) of dental enamel for retrospective assessment of radiation exposure. *Radiation Measurements*, 42:1256–1260.

Chapter 8

Optically stimulated phosphorescence in orthoclase feldspar over the millisecond to second time scale

C. Ankjærgaard and M. Jain

Radiation Research Division, Risø National Laboratory for Sustainable Energy, Technical University of Denmark, DK-4000 Roskilde, Denmark

Abstract

In the past, time-resolved IR stimulated luminescence (TR-IRSL) curves from feldspar have mainly been measured over a few hundred µs with the purpose of estimating the lifetimes of the components. In this study, we present the decay form of time-resolved IRSL and IR stimulated phosphorescence (IRSP) from orthoclase feldspar covering over 8 orders of magnitude (50 ns to $\sim$7 s). A detailed characterisation of the slowly decaying signals (ms to s time scales) from feldspar is undertaken to obtain further insight into the role of re-trapping in both the IR stimulated luminescence (IRSL) and the relatively more stable post-IR IRSL signals. The decay form of the different signals examined here shows a weak dependence on preheat temperature and a strong dependence on stimulation temperature. Interestingly, the IRSP curves show a conspicuous kink of which the position is linearly dependent on the on-time duration.

The data on thermal dependence of these signals might suggest that the decay behaviour of the time-resolved IRSL and phosphorescence signals mainly reflect the occupancy of electrons in the band tail states with a significant contribution from the shallow traps. This interpretation is supported by thermoluminescence (TL) curves showing the photo-transfer effect during short IR and post-IR IR stimulations.

Keywords: Infra-red stimulated luminescence, IRSL, time-resolved luminescence, infra-red stimulated phosphorescence, photo-transferred TL, PTTL, band tail states

8.1 Introduction

Natural feldspar is widely used in luminescence based retrospective dosimetry Bøtter-Jensen et al. (2003). Optically stimulated luminescence from previously beta or gamma irradiated feldspar is usually obtained by infrared stimulation (IRSL) or by green or blue light stimulation (OSL), either using continuous wave (CW) or pulsed optical stimulation modes. In pulsed optical stimulation mode the luminescence measured during and between the pulses can be termed as time-resolved OSL (TR-OSL or TR-IRSL), Delayed OSL (DOSL or DIRSL), or optically stimulated phosphorescence (OSP) [see Bøtter-Jensen et al. (2003, p. 59–60)]. We use the terms OSP and DOSL in connection with millisecond to second time scale measurements, and TR-OSL in connection with microsecond to millisecond time scale measurements.

In luminescence dosimetry of natural materials most of the earlier work using pulsed stimulation has been done with quartz where the TR-OSL decay is interpreted in terms of the residence time (lifetime) of electrons in the conduction band or the lifetime of the excited state of the luminescence recombination centre (Chithambo, 2007; Pagonis et al., 2010). The feldspar crystal, however, is much more complex than the ordered structure of the quartz crystal and moreover the range of bonding angles between atoms varies significantly (Poolton et al., 2009). It has been argued by Poolton et al. (2002) that a continuum of different bonding angles creates a continuum of 'band tail states' extending both below the conduction band edge and above the valence band edge and into the band gap. What is particularly important from the point of view of our study is that a sub-conduction band electron transport can occur in these band tail states by the hopping mechanism (Poolton et al., 2009).

Thus, for a feldspar crystal the decay form of TR-OSL measured between stimulation pulses will be a combined effect of (i) residence time of electrons in the conduction band or in the band tail states below the conduction band edge, (ii) any excited to ground state relaxation at the luminescence centre, and (iii) any transport processes involving tunnelling or localised transitions. On the other hand, the decay form of OSP will generally be a function of re-trapping and thermal eviction from the shallow traps which cause a further delay in luminescent recombination (Ankjærgaard and Jain, 2010, Chapter 6 of this thesis). Examination of the luminescence decay after a pulse of stimulation light helps to understand the relative role of these processes in luminescence generation.

TR-OSL of feldspar has been studied for more than a decade (Sanderson and Clark, 1994; Clark et al., 1997; Clark and Bailiff, 1998). Feldspar TR-IRSL measured between stimulation pulses shows a monotonic decay and has previously mainly been measured over a few hundred µs to resolve different components. The lifetimes of these components were found to lie within five groups: 30–50 ns, 300–500 ns, 1–2 µs, ∼5 µs, and >10 µs (Clark et al., 1997; Clark and Bailiff, 1998; Tsukamoto et al., 2006). Clark et al. (1997) suggest that a possible explanation for the components with lifetimes of >4 µs is temporary trapping in shallow sites with thermal lifetimes at room temperature of a few µs or less.

There exists very little information on feldspar time-resolved OSL for the millisecond to second time scales. Sanderson and Clark (1994) remark on signals observed on the ms timescale attributed to phosphorescence after optical

stimulation using LEDs. There are further references in Clark et al. (1997) to measurements on ms and longer timescales, but these refer to an unpublished Ph.D. thesis and a workshop synopsis that we have not succeeded in obtaining. Clark and Bailiff (1998) show an infrared (850 nm) stimulated TR-IRSL curve detected at 550 ± 40 nm from a cleaved chip of Amelia albite measured at room temperature. They conclude that the two slowest lifetime components in this sample (2.14 ± 0.07 ms and 11.1 ± 0.1 ms) have a minor contribution ($<5\%$) and are likely to arise from intrinsic Mn^{2+} luminescence.

This article contains characterisation of time-resolved signals from feldspars on the ms to s time scales, and complements our previous study on quartz, examining the role of shallow traps in the OSL process (Ankjærgaard and Jain, 2010, Chapter 6 of this thesis). In addition to the IR stimulated signal we also study the post-IR IR stimulated signals measured at an elevated temperature as this signal has been shown to be more stable than the IR signal (Thomsen et al., 2008; Buylaert et al., 2009).

We first present the decay form of TR-IRSL and IRSP curves covering time scales over ~ 8 orders of magnitude (50 ns to ~ 7 s). Then we make a detailed characterisation of the slowly decaying signals (ms–s time scales) to obtain further insight into the origin of these components and to understand the role of re-trapping in IR stimulated luminescence.

We use the terminology time-resolved IRSL (TR-IRSL) while referring to the ns – μs time scales and IR stimulated phosphorescence (IRSP) while referring to the ms – s time scales. If these measurements are made immediately following an IRSL measurement we use the terminology post-IR TR-IRSL or post-IR IRSP, respectively. The 'post-IR' measurements are always made at elevated temperatures.

8.2 Experimental details

Sample measurements were carried out on two different Risø readers to cover the three different time scales. IR (830 nm) stimulation was achieved using IR LED's and the detection of the blue emission (350-415 nm) was achieved using a combination of the Schott BG-39 and Corning 5-79 filters. The measurement details are described as follows:

Nanoseconds – microseconds: A Risø TL/OSL-20 reader was used with an integrated pulsing option to control the IR LED array, delivering ~ 130 mW/cm^2 at the sample position for 90% power. Furthermore a Photon Timer was attached to record the TR-IRSL (Lapp et al., 2009, Chapter 2 of this thesis). Measurements on this timescale were undertaken using an on-time of 50 μs and an off-time of 500 μs producing $\sim 40{,}000$ stimulation pulses during 22 s of pulsed stimulation with an energy of 6.5 μJ/cm^2 per pulse.

Microseconds – milliseconds: The same Risø TL/OSL-20 reader as above was used but with an on-time of 1 ms and an off-time of 5 ms. Approximately 9,000 pulses with an average energy of 0.13 mJ/cm^2 per pulse were delivered during 54 s of pulsed stimulation in this time range.

Milliseconds – seconds: A standard Risø TL/OSL-15 reader was used with IR stimulation from an LED array delivering $\sim$130 mW/cm^2 at the sample position (Bøtter-Jensen et al., 2003) for 90% power. A single light pulse of 1.2 s duration with a total energy of 0.16 J/cm^2 was used to stimulate the sample. The phosphorescence was detected during the following 6.8 s.

The on- and off-times mentioned above were adhered to unless otherwise specified in the text.

The work reported here has been undertaken using an orthoclase feldspar sample, which has prior been used in Ankjærgaard et al. (2009, Chapter 7 of this thesis) under the name orthoclase 3. This sample was obtained from the Geological Museum in Copenhagen, Denmark, and was crushed and dry-sieved to obtain a grain size fraction of 90–125 μm with no further chemical treatment. All aliquots used consisted of grains mounted in steel cups using silicon oil.

8.3 Extended decay form of optically stimulated phosphorescence from feldspar

The optically stimulated phosphorescence from orthoclase feldspar measured over eight orders of magnitude is shown in Fig. 8.1, where the TR-IRSL and IRSP curves on the left (a-d) have been obtained using IR stimulation at 50°C, while the curves on the right (e-h) are post-IR TR-IRSL and post-IR IRSP curves measured at 240°C following an IR stimulation at 50°C for 100 s. If the curves for the TR-IRSL and post-IR TR-IRSL are compared on the microsecond time scale (Fig. 8.1b, f), they seem very similar in shape but the post-IR TR-IRSL curve has a slightly faster decay in the first 100 μs. Moreover, the post-IR TR-IRSL signal has a relatively more intense slow component, almost by a factor of 10. On the millisecond time scale the faster decay of these curves previously observed in Figs. 8.1b and f is now seen as a very fast drop in the first 0.3 ms, while the previously observed slower decays are now seen to extend to beyond 5 ms (Figs. 8.1c and g).

A closer look at the IR and post-IR data on the microsecond and millisecond time scales in Figs. 8.1a and e shows that the red and the black curves are not completely overlapping. The slowly decaying component has a relatively higher intensity in the red curve than in the black curve, and this deviation is even more prominent in the post-IR TR-IRSL signals (Fig. 8.1e). A similar deviation was also observed in quartz OSP (Ankjærgaard and Jain, 2010, Chapter 6 of this thesis). This effect probably arises due to build-up of the slowly decaying signal. During a stimulating light pulse electrons are excited into a higher energy state (here band tail states or conduction band), and from there they decay at a rate governed by the lifetime of that state. Thus, there is an initial build up in the electron population until the rate of excitation balances the rate of decay (an equilibrium level or steady state is reached). As expected, a signal with a short lifetime (fast signal) builds up or reaches an equilibrium level much more rapidly than a signal with a long lifetime (slow signal). In the black curve the on-time is 50 μs which is sufficient to cause a steady state level for the fast signal while the slow signal only begins to build up. As the pulse width increases further from 50 μs to 1 ms there is a relative increase in the intensity of the slow signal with respect to the fast signal because the latter has
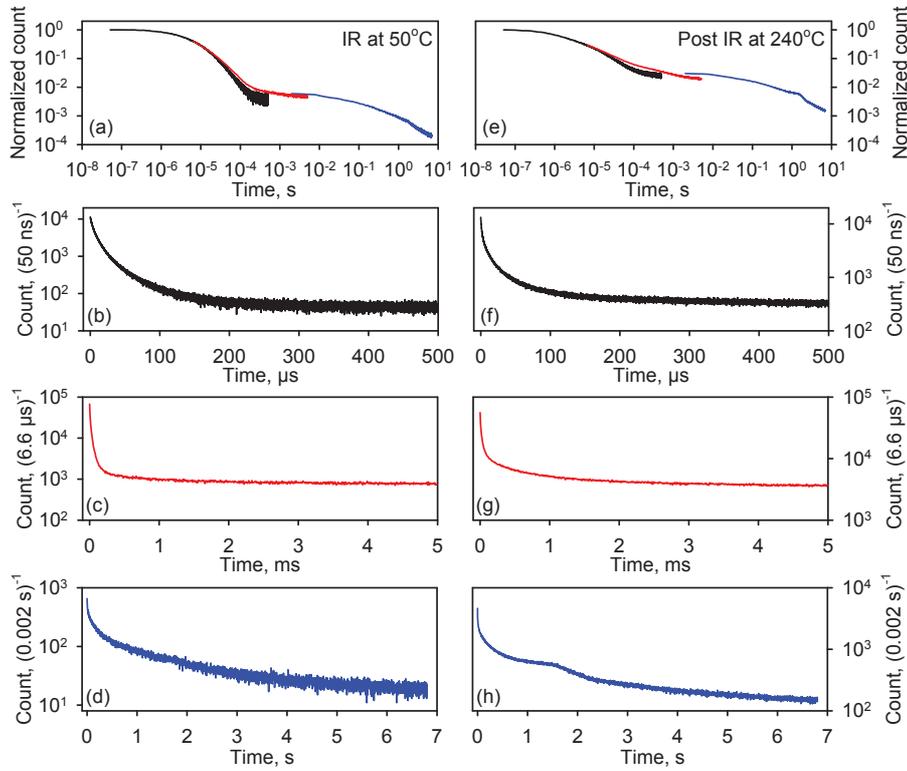
Figure 8.1: TR-IRSL together with IRSP (a-d) and post-IR TR-IRSL together with post-IR IRSP (e-h) decay curves from a single aliquot of orthoclase feldspar measured on different timescales. (a) TR-IRSL measured at 50°C: the first (black) curve is measured using an on-time of 50 μs, an off-time of 500 μs and has a resolution of 50 ns. The second (red) curve is measured using an on-time of 1 ms, an off-time of 5 ms and has a resolution of 6.6 μs. The third (blue) curve is IRSP measured using an on-time of 1.2 s, an off-time of 6.8 s and has a resolution of 0.002 s. In the first two measurements the aliquot was dosed with 45 Gy and in the third with 500 Gy followed by a preheat to 300°C for 60 s. The curves have been normalized to the initial intensity, and for comparison the red curve has been reduced by a factor 0.04 and the blue curve by a factor of 0.006. Note that the scale is double-log. The curves in (b), (c), and (d) are the black, red, and blue curves from (a) shown without normalization and on a log y axis. (e) Post-IR TR-IRSL and Post-IR IRSP curves measured at 230°C using the same on- and off-times and doses as in (a). The aliquot was dosed, preheated to 300°C for 60 s and bleached with IR at 50°C for 100 s prior to IR measurement at 230°C. All three curves have been normalized, and the red curve reduced by a factor of 0.3 and the blue curve by a factor of 0.03 for illustration of continuity. The curves in (f), (g), and (h) are the black, red, and blue curves from (e) shown without normalization and on a log y axis.

already reached an equilibrium level. This relative increase in the slow signal compared to the fast signal for longer pulse stimulation duration gives rise to the offset difference seen between the black and red curves in Figs. 8.1a and 8.1e.

The curves showing decay on the seconds time scale in Fig. 8.1d and h for the IRSP and post-IR IRSP signals both have an interesting shape around 1.5 − 2 s into the decay; a hint of a 'kink' is observed in the IRSP curve, and a very distinct 'kink' is observed in the post-IR IRSP curve. This phenomenon, which is especially visible in the post-IR IRSP signal, is investigated further in section 8.5. A similar kink has also been observed and discussed in the quartz OSP data (Ankjærgaard and Jain, 2010, Chapter 6 of this thesis).

8.4   The microsecond − millisecond time range

This section investigates the preheat and stimulation temperature dependence of the TR-IRSL and high temperature post-IR TR-IRSL signals shown as the second (red) curves in Fig. 8.1c and g respectively.

8.4.1   Preheat temperature dependence

The normalized TR-IRSL curves measured at 50°C using preheat temperatures between 270°C and 410°C are shown in Fig. 8.2a for a single aliquot of orthoclase. Fig. 8.2b shows the post-IR TR-IRSL signal measured at 240°C following the IR measurement at 50°C. The insets to Fig. 8.2a and 8.2b compares the initial fast decaying (filled circles), and the later slow decaying (open circles) signals. These curves are derived by integrating the signal between 1002.6–1009.2 μs and 2005.2–1011.8 μs, after average background subtraction (found from the average over the last 26.2 μs of the curves), with respect to the beginning of the light pulse.

Both the TR-IRSL and the post-IR TR-IRSL signals show an overall decrease with preheat temperature. The decay curve shapes are identical for the TR-IRSL signal between 270-380°C (Fig. 8.2a). For the post-IR TR-IRSL, although the shape of the slow signals is very similar, it shows a relatively faster drop compared to the fast signal (Fig. 8.2b). This apparent decrease occurs as there is a relatively thermally unstable background under these curves. This is discussed later in section 8.5.1. If a background subtraction is carried out (subtraction of data in the last 26.2 μs from the entire curve) then it can be clearly seen that the integral fast and slow signals show a very similar decrease with the preheat temperature (insets to Figs. 8.2a and 8.2b). This lack of change in decay shape, caused by a similar decrease of the fast and slow signals with preheat temperature, suggests that the same recombination centre(s) is used irrespective of the preheat temperature; thus the recombination centre must be stable up to 410°C. This is assuming that the lifetime is governed by the recombination transition.

The comparison of the insets to Figs. 8.2a and b suggests that the post-IR TR-IRSL signal is thermally more stable than the TR-IRSL signal. Since, as deduced above, the holes are stable up to 410°C, one can further deduce that the differences in signal stability must arise because of differences in the thermal stability of the trapped electrons that give rise to these signals.
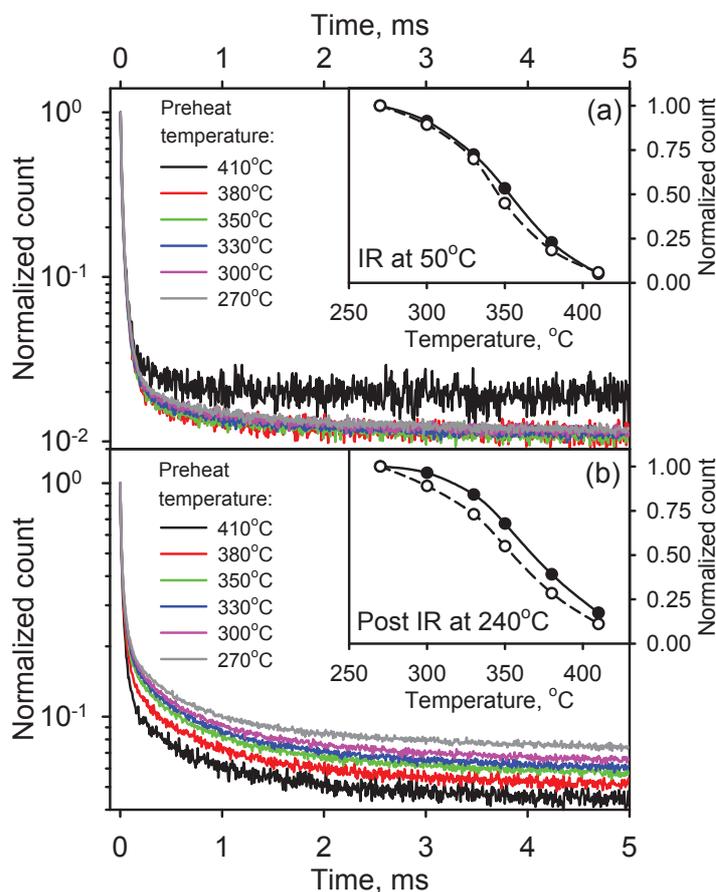
Figure 8.2: (a) Time-resolved IRSL off-time curves from a single aliquot of orthoclase for different preheats in the range: 270°C - 410°C. Note that the data is plotted in descending order for ease of display. The aliquot was dosed with 45 Gy, preheated for 60 s and stimulated at 50°C using an on-time of 1 ms and an off-time of 5 ms. The curves have been normalized to the first point in the off-time. Inset: The normalized initial off-time decay counts (integrated interval: 1002.6–1009.2 µs) as a function of preheat temperature (filled circles), and the off-time counts at 1 ms (open circles; integrated interval: 2005.2–1011.8 µs) into the off-time with respect to the beginning of the light pulse. These integrated intervals have been subtracted with a background value found as the average over the last 26.2 µs of the curve. (b) Post-IR TR-IRSL off-time curves for the same preheats, dose, and on- and off-time settings as in (a). The aliquot was dosed, preheated for 60 s, IR bleached at 50°C for 100 s and then measured at 230°C. Inset: The normalized initial off-time decay counts as a function of preheat temperature (filled circles), and the off-time count at 1 ms into the off-time (open circles) using the same integrating intervals and background subtraction as in the inset to (a).
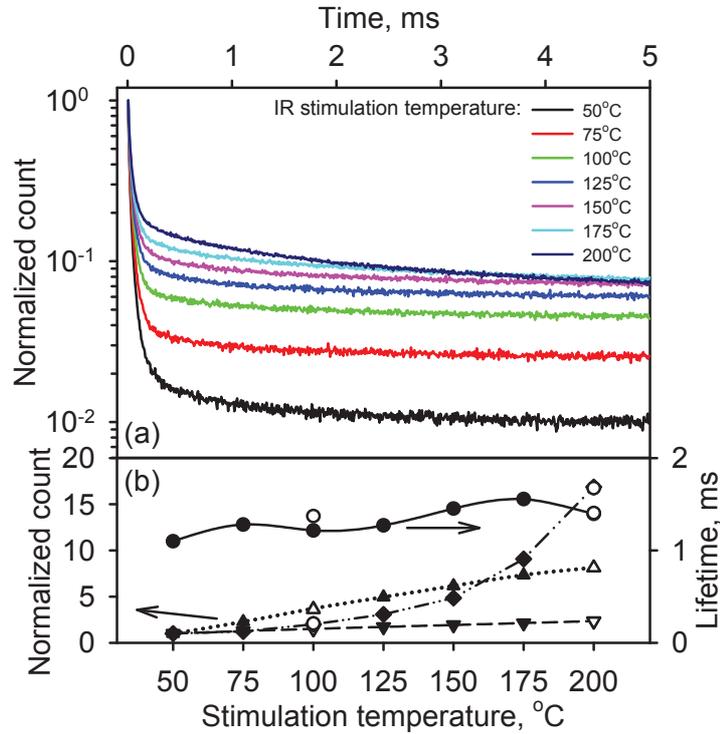
Figure 8.3: (a) Time-resolved IRSL off-time curves from a single aliquot of orthoclase measured for stimulation temperatures in the range 50°C-200°C. The aliquot was dosed with 45 Gy and heated to 300°C for 60 s prior to each measurement using an on-time of 1 ms and an off-time of 5 ms. The curves have been normalized to the first point in the off-time. (b) A summary of intensities for the three main components of these curves (as defined in the text) and the lifetime of the slow component. Right axis: Lifetime in ms found from fitting the curves after subtraction of an average background over the last 20 points and ignoring the signal in the initial 1000 μs of the off-time to isolate the slow component (filled circles). Left axis: Integration over the on-time (downward pointing triangles), the background (an average over the last 20 points, upward pointing triangles), and over the entire off-time but with the initial 200 μs removed and the constant level (background) at 5 ms subtracted (diamonds). The three plots on this axis have been normalized to their respective initial 50°C value. Note that the open symbols represent recycling points.

8.4.2 Stimulation temperature dependence

Figure 8.3 shows the dependence of the TR-IRSL signal on stimulation temperature for the same aliquot as in Fig. 8.2 using a dose of 45 Gy and a preheat to 300°C. The temperatures were varied between 50°C and 200°C, and these resulted in remarkable changes in the shapes of the TR-IRSL curves. As observed previously for the TR-OSL data on the millisecond timescale for quartz (Ankjærgaard and Jain, 2010, Chapter 6 of this thesis), it was found difficult to satisfactorily fit these curves with a multi-exponential model. Therefore, we used more intuitive approach; based on visual inspection of Fig. 8.3a, it

is clear that the slowly decaying part of the curves increase in relative importance with respect to the fast decaying part with stimulation temperature. As described earlier in section 8.3, the fast part of the off-time TR-IRSL signal quickly reaches a saturation (or equilibrium) level during the on-time, whereas the slow part of the off-time signal never reaches saturation during the on-time. Therefore, the integral over the entire on-time signal can be used as a proxy for the behaviour of the fast decaying signal. Moreover, we also know from Fig. 8.1 that there is a large background (the component decaying on a seconds time scale can be approximated as background here) underlying these data. Thus, these curves can be split into three main parts: the fast component, the slow component, and the background. To estimate the relative changes in these components with temperature, the following sections are defined: the integration over the whole on-time are used as a proxy for the initial fast decay (Fig. 8.3b, down pointing triangles), the constant background level reached after 5 ms off-time was estimated using an average over the last 20 points (Fig. 8.3b, upward pointing triangles), and the slow part is represented by the sum of the off-time but with the initial 200 μs removed and the constant background level subtracted (Fig. 8.3b, diamonds). We note that our approximation of the background may be in error as the slow component continues well beyond the 5 ms data measured here (see Fig. 8.1); unfortunately our instrument does not allow longer measurements on the ms time scale. Nonetheless, using this crude characterization of the time-resolved curves, it becomes evident that the slow component shows the strongest temperature dependence followed by the background, and the fast component shows the least stimulation temperature dependence. The slow component data (from 1–5 ms) were furthermore successfully fitted with a single exponential decay to estimate the decay rate; the calculated lifetimes are also shown in Fig. 8.3b on the right axis. These values ranging from ∼1 to 1.5 ms perhaps show a minor overall increase with the stimulation temperature.

Figure 8.4a shows the post-IR TR-IRSL signals measured for stimulation temperatures between 100°C and 240°C using the same aliquot of orthoclase. The first IR stimulation was carried out at 50°C for 100 s before the post-IR TR-IRSL curves were recorded. The data was analysed in the same manner as for the TR-IRSL signals above. The relative importance of the three different components in these curves is presented in Fig. 8.4b, and as in the TR-IRSL curves the slow component shows the strongest dependence on temperature. The fast component and the background of the post-IR TR-IRSL curves show a lesser dependence on temperature, and unlike for the TR-IRSL signal in Fig. 8.3, the changes are identical for these two parts of the signal. Furthermore, the lifetime of the slow component of the curves shows no systematic change with temperature.

These data suggest the presence of at least two dominant components (fast and slow) on the millisecond time scale and a large underlying background in both the TR-IRSL and post-IR TR-IRSL curves. Of these the slow component shows the strongest increase in intensity with stimulation temperature. However, this increase is not matched by an increase in the decay constant, (or lifetime) which shows a very weak or no temperature dependence. A similar dependence, or the lack of it, of lifetime on stimulation temperature is also observed for quartz (Ankjærgaard and Jain, 2010, Chapter 6 of this thesis) and in the blue light stimulated time-resolved exo-electron emission (TR-OSE) signal
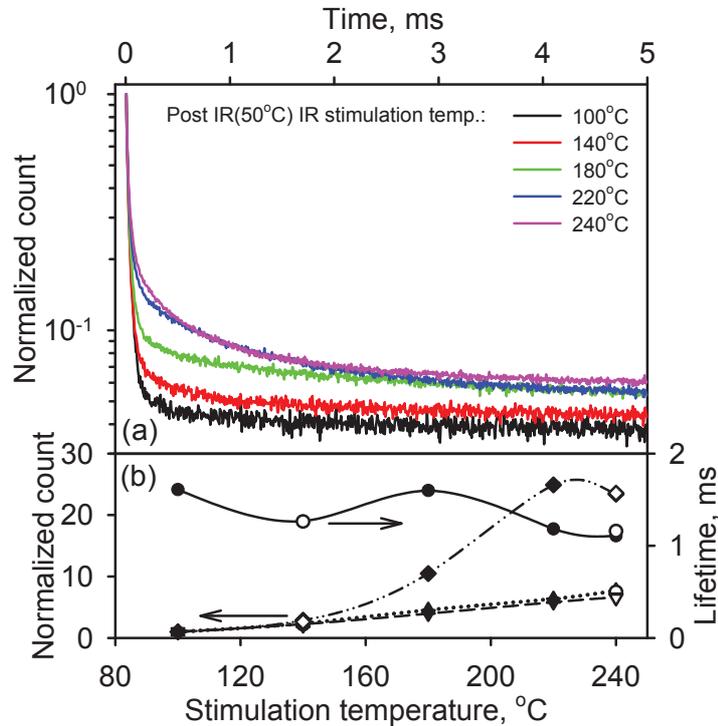
Figure 8.4: (a) Post-IR TR-IRSL off-time curves for stimulation temperatures between 100°C and 240°C for an aliquot of orthoclase. The aliquot was dosed with 45 Gy, heated to 300°C for 60 s, and bleached with IR at 50°C for 100 s prior to each post-IR TR-IRSL measurement using an on-time of 1 ms and an off-time of 5 ms. The curves have been normalized to the intensity of the first point in their off-time signal. (b) Same notation as in Fig. 8.3b, note that the filled circles belong to the right axis and the remaining data belong to the left axis.

from feldspar (Tsukamoto et al., 2010, Chapter 5 of this thesis). Interestingly, the slow part of the TR-OSE signal showed a strong systematic increase in intensity with stimulation temperature, but without an accompanying increase in the decay rate. The TR-OSE data suggests that the conduction band does not empty completely. However, these results cannot be directly applied to IR stimulation as it is well established that IR stimulation does not give an OSE signal and, therefore, it is not a conduction band phenomenon (Ankjærgaard et al., 2006). However, as we discuss later, the results may be applicable to the band tail states in feldspar (Poolton et al., 2002).

8.5 The millisecond – second time range

To measure the off-time phosphorescence decay on the time scale of seconds, it is necessary to use the approach described in Section 8.2, where the decay is measured after a single pulse of stimulation of 1.2 s using a standard TL/OSL reader. A long on-pulse is used to allow build-up of any slow components.

We now describe the preheat and stimulation temperature dependence of this signal.

8.5.1 Preheat temperature dependence

Fig. 8.5 shows how the preheat temperature affects the off-time phosphorescence signal from both the IRSP signal measured at 50°C (Fig. 8.5a) and the post-IR IRSP stimulated signal measured at 240°C (Fig. 8.5b). The preheat temperatures were varied between 270°C and 410°C. The curves in Fig. 8.5a are very similar in shape, but the intensity is reduced as the preheat temperature is increased; the 380°C and the 410°C curves have their initial intensities reduced to 5% and 0.8% of that for the 270°C curve and the latter are almost completely erased. The scattered points from the curve at 410°C curve fall on horizontal lines as the counts are down to dark counts, which when normalized, show this behaviour on a log-scale. The IRSP signal measured at 50°C are, therefore, almost erased for these two highest preheat temperatures. The post-IR IRSP signals measured at 240°C shown in Fig. 8.5b are brighter than the curves in Fig. 8.5a and very similar in shape with two exceptions: The initial fast drop is smaller in all the post-IR IRSP curves than in the IRSP curves, and, furthermore, for preheats between 270°C and 350°C, the post-IR IRSP curves have a sudden increase in decay rate (or a 'kink') at about 1.5 s. However, the last two curves for preheats of 380°C and 410°C (where the prior IRSP signal at 50°C was reduced to <5%) do not show this kink. If looking at the ISRP curves again (Fig. 8.5a), a hint of a kink is also present in these data at about 2 s although it not as pronounced as in the post-IR IRSP data.

In Fig. 8.5c the normalized initial off-time intensities together with the normalized intensities in the slowly decaying part of the curves (found by taking an average over the last 20 points) for both the IRSP and post-IR IRSP signals are summarized. The dependence on preheat temperature is almost identical for the initial and later signals, however, as observed for the millisecond time scale (see insets to Fig. 8.2), the post-IR IRSP signal is slightly more thermally stable compared to the ISRP signal. The lack of significant change in decay shapes with preheat suggests that the process involved in the luminescence generation for the IR and post-IR signals is independent of preheat temperature in the range 270°C − 410°C. If charge trapping in refuge traps following optical stimulation is an important process here, then the traps participating must have TL peaks below 270°C so they are always emptied at these preheat temperatures. The main difference between the two signals is in the conspicuousness of the kink.

8.5.2 Stimulation temperature dependence of the IRSP and post-IR IRSP signals

The IRSP signal dependence on stimulation temperature is shown in Fig. 8.6a, where the temperature during the IR stimulation was varied between 50°C and 230°C following a preheat to 300°C for 10 s. The kink observed in the preheat curves (Fig. 8.5) are present in all these curves and situated between 1 and 2 s into the off-time, although the kink itself is more or less pronounced at the different temperatures. The decay rates of the curves before the kink show significant changes with stimulation temperature, however, there is neither
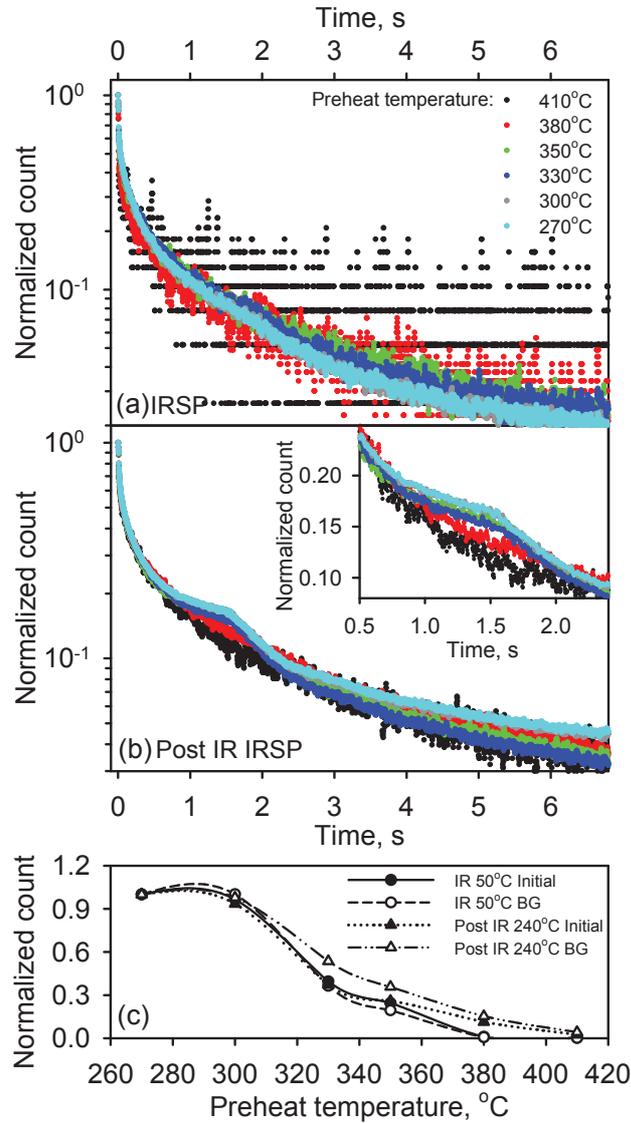
Figure 8.5: IR stimulated phosphorescence (IRSP) and post-IR IRSP curves from a single aliquot of orthoclase for different preheats between 270°C and 410°C. The aliquot was dosed with 500 Gy, preheated for 60 s and IR stimulated at 50°C with a single pulse of 1.2 s followed by detection for 6.8 s. This was followed by an IR bleach at 50°C for 100 s to empty the IR signal, and then a further IR stimulation at 240°C using the same pulse length. (a) Shows the data from first IR measurement, (b) shows the data from the final IR measurement. The curves have been normalized to the first point in the off-time. Note that the temperatures are listed in descending order. Inset: A closer look at the 'kink' in the post-IR IRSP curves at 240°C; note that both axes are linear. (c) Normalized initial off-time counts for the IRSP curves (filled circles) and post-IR IRSP curves (filled triangles) together with the normalized average over the last 20 points in the curves (given as BG in the figure) for IR (open circles) and post-IR (open triangles) signals.
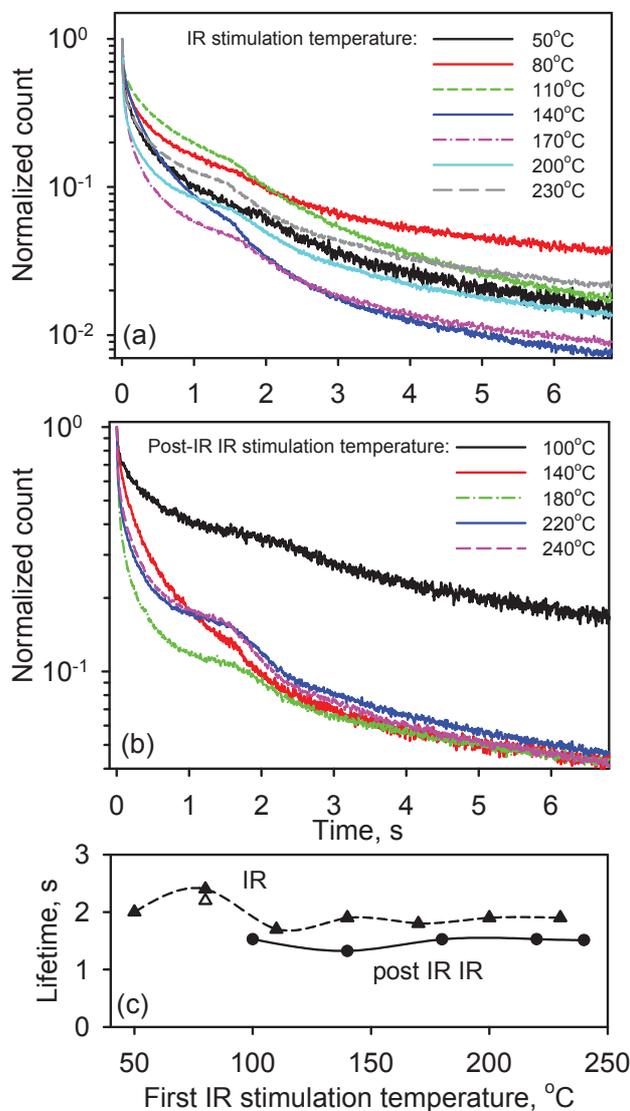
Figure 8.6: (a) IR stimulated phosphorescence (IRSP) curves from a single aliquot of orthoclase for stimulation temperatures between 50°C and 230°C in steps of 30°C. The aliquot was dosed with 500 Gy, preheated to 300°C for 60 s and stimulated with a single pulse of 1.2 s. (b) Post-IR IRSP curves measured for stimulation temperatures in the range 100°C-240°C. The same aliquot as above was dosed with 500 Gy, preheated to 300°C for 60 s, IR bleached at 50°C for 100 s and then IR stimulated at various temperatures. All curves have been normalized to the initial point in the off-time. (c) Lifetimes in seconds found from fitting the last 3 s of the IRSP curves (triangles) and post-IR IRSP curves (circles), after subtraction of an average background using the last 20 points.

a systematic increase nor a decrease. A similar non-systematic behaviour is observed for the post-IR IRSP curves measured at 240 °C (Fig. 8.6b).

The curves after the kink show a very similar decay rate, except for the 110°C IRSP curve. The tail of the curves from 3 s and onwards in both Figs. 8.6a and b was fitted with a single exponential to characterize the shape, and the lifetimes are summarized in Fig. 8.6c. The lifetimes do not show any significant variation with temperature above 100°C. This behaviour was also observed in quartz, although the kink in quartz was not visible at all the stimulation temperatures (Ankjærgaard and Jain, 2010, Chapter 6 of this thesis).

8.5.3 The effect of change in prior IR stimulation temperature on the decay form of the post-IR IRSP signal

The measurements here were made following those presented in Fig. 8.6a. After each IRSP measurement at different temperatures there was a post-IR IRSP measurement at a constant temperature of 240°C. Each prior IR measurement was carried out for 100 s after irradiation and a preheat of 300°C for 10 s. In order to compare the shapes of the different signals, each curve is normalised to its initial intensity and shown in Fig. 8.7a. The temperatures indicated in the legend refer to the prior IR stimulations before the Post-IR IRSP measurements.

The data show a steep relative increase in the signal intensity of the slowly decaying signal with respect to the fast decaying signal with an increase in the temperature (except for the last curve at 230°C). The kink is conspicuous at all temperatures, although to different degrees, and it occurs approximately at the same time. The prominence in the kink does not show a systematic decreasing or increasing trend with temperature: it is clearly visible in the curves for 50°C and 80°C, less prominent in the 110°C curve and 170°C curve and almost invisible in the 140°C curve. Interestingly, in the 200°C curve, it is not only a kink, but a small peak superimposed on an overall decaying curve. In the 230°C curve the kink is still very visible although the peak structure is less obvious.

The initial intensity (filled circles) and the average value over the last 10 points (empty circles), normalised to the 50°C data, for each curve are shown in Fig. 8.7b. These data show that (i) an increase in the prior IR temperature causes an overall decrease in the intensity of the post-IR IRSP signal, and (ii) the initial signal (proxy for the curve before the kink) (filled circles, Fig. 8.7b) decreases relatively much more rapidly with temperature than the slowly decaying signal after the kink (open circles, Fig. 8.7b). It is likely that the reduction in the initial intensity with high prior IR temperatures (200°C and 230°C) causes the kink in the curve to be much more visible and therefore it appears as a peak. We note that such a peak was also predicted from on a numerical model based on four energy states for quartz by Ankjærgaard and Jain (2010, Chapter 6 of this thesis).

As in quartz it is highly likely that these IRSP signals originate due to charge storage and release from the shallow traps [see Ankjærgaard and Jain (2010, Chapter 6 of this thesis)]. We discuss this again later with the photo-
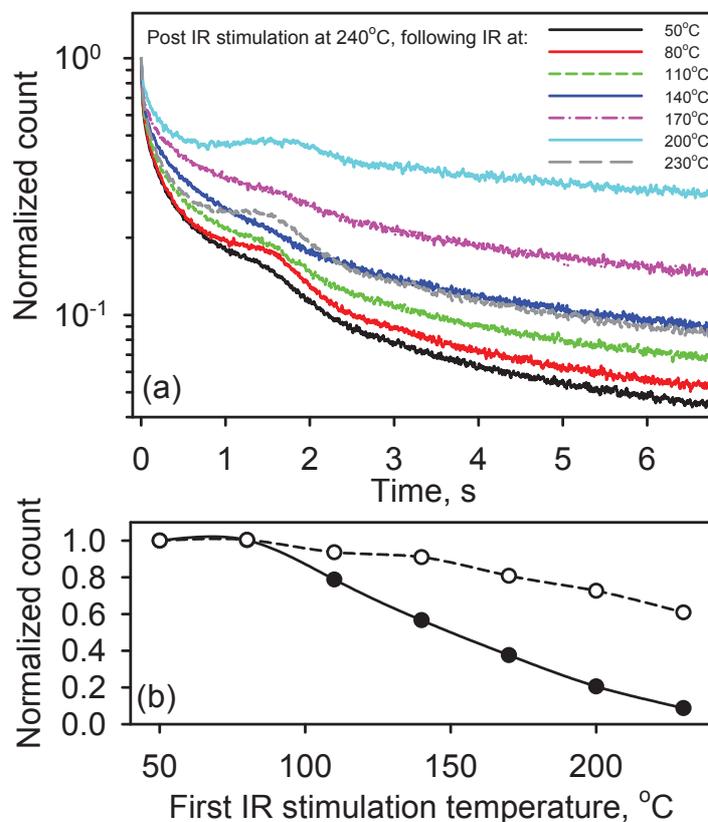
Figure 8.7: Changes in the Post-IR IRSP curves measured at constant temperature due to a prior IR bleach at variable temperatures. The aliquot was dosed with 500 Gy, preheated to 300°C for 60 s and IR bleached at the different temperatures, given in the legends, for 100 s prior to the post-IR IRSP measurements at 240°C. All curves have been normalized with the intensity of the initial off-time point. (b) Variation in the initial intensity (filled circles) and the background (average over the last 20 points) (open circles) of the post-IR IRSP signal as a function of prior IR stimulation temperature. The data are normalised to their value for 50°C.

transferred TL (PTTL) data in section 8.5.5. One possible reason for a rapid decrease in the intensity of the initial signal with prior IR temperature could be a reduction in re-trapping in the shallower traps with an increase in the IR stimulation temperature. This suggests that the post-IR IRSP signal has a likely contribution from at least two sets of shallow traps, one that are highly thermally unstable (earlier part), and the other (later part) that are relatively thermally stable within our temperature range.

8.5.4 'Kink' position for different stimulation pulse durations

In all the phosphorescence curves with a kink presented so far, the kink has always been situated between 1 and 2 s into the off-time. But by changing the duration of the on-time, it is possible to shift the position of the kink, this is
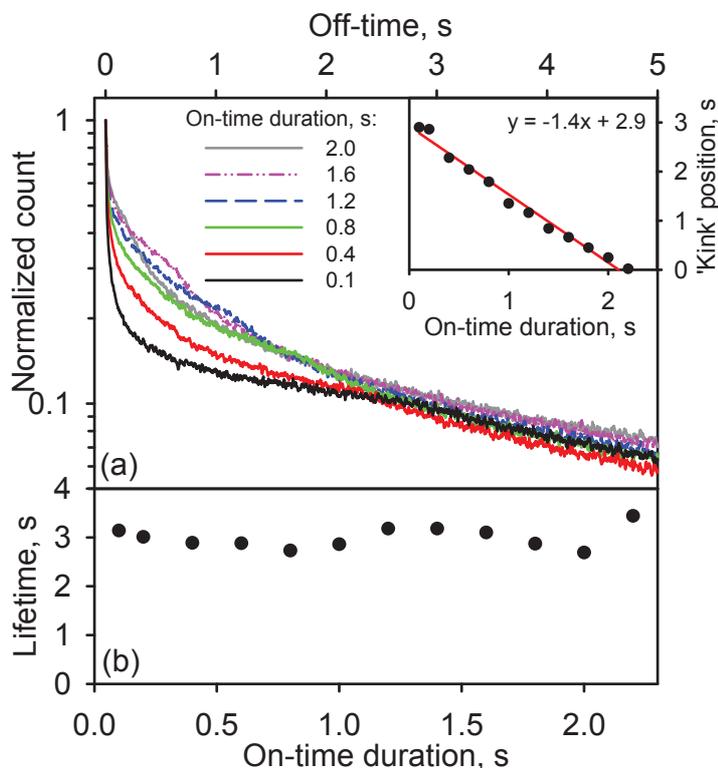
Figure 8.8: (a) Post-IR IRSP curves for different stimulation pulse durations. An aliquot of orthoclase was dosed with 200 Gy, preheated to 300°C for 60 s, IR bleached at 50°C for 100 s and then IR stimulated again at 240°C with a single pulse of length varying between 0.1 s and 2.2 s. The curves have been normalized to the intensity of the initial off-time data, and only the first 5 s of the off-time data is shown. Inset: changes in the position of the kink (sudden change in the decay rate) as a function of stimulation pulse duration. The data have been fitted to a straight line. (b) Lifetimes found from exponential fitting of the portion of the off-time curve after the 'kink' after subtraction of the average constant background estimated using the last 20 points in the off-time.

shown in Fig. 8.8a for on-times between 0.1 and 2.0 s. There exists a linear relationship between the on-time duration and the position of the kink in the off-time which is shown in the inset to Fig. 8.8a.

Figure 8.8b shows the lifetime of the latter part of the curves from 3 to 5 s, and these are broadly constant for different on-times. The effect causing the movement of the kink, therefore, does not affect the decay rate of the slow part of the curves.

8.5.5   Traps giving rise to IR stimulated phosphorescence

To get an insight into which traps play a role in causing long lived phosphorescence signals, a series of TL curves were measured to examine the possible charge recuperation due to short IR stimulations; this is called phototransferred TL (PTTL). An aliquot of orthoclase feldspar was dosed with 200 Gy,
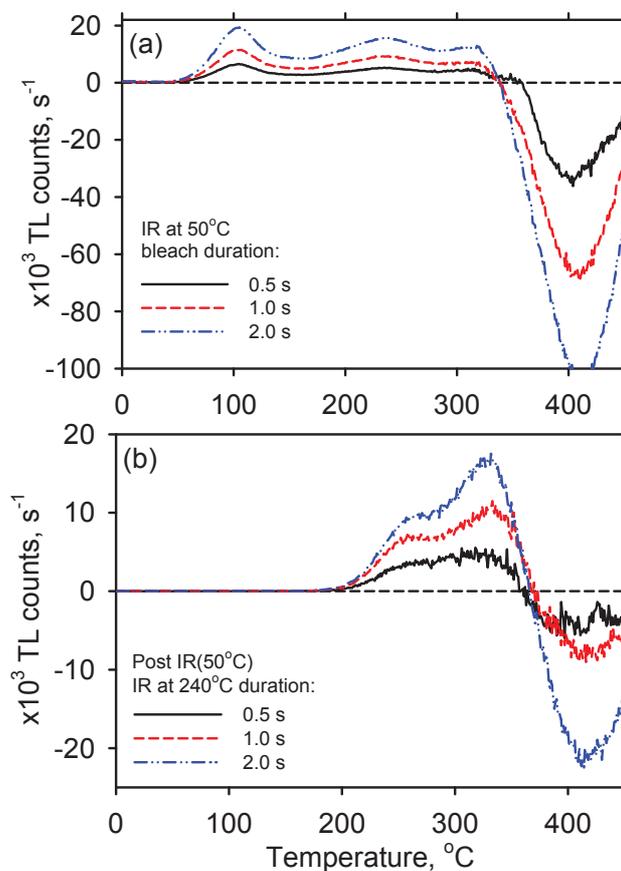
Figure 8.9: TL difference curves showing the effect of photo-transfer in ortho-clase feldspar due to short IR and elevated temperature post-IR IR stimulations of different durations (0.5 s, 1 s, and 2 s). An aliquot of orthoclase was dosed with 200 Gy and heated to 300°C for 60 s prior to these measurements: (a) TL curves measured (to 450°C at 5°C/s) after bleaching the sample with IR at 50°C for different durations. A TL curve with 0 s prior light stimulation has been subtracted from these curves. (b) TL curves measured (450°C at 5°C/s) after two consecutive bleaches with IR: the first IR bleach at 50°C for 100 s, and a second IR bleach at 240°C for times 0.5, 1 and 2 s. TL curves measured in the same way but with 0 s IR stimulation (only heating to 240°C for 0.5, 1 and 2 s) has been subtracted from these curves. Note that all curves shown in the figure have been obtained by subtraction of TL before illumination from that after illumination.

preheated to 300°C for 60 s, and IR stimulated at 50°C for different durations (0, 0.5, 1 and 2 s) before measuring the TL to 450°C. To study the effect of charge transfer due to the IR, Fig. 8.9a shows the series of 'difference' TL curves (found from subtracting the TL measurements with no (0 s) IR stimulation from those with prior IR stimulation). These curves show that charge is transferred optically during the IR bleach from a main peak at ∼410°C into two broad peaks centred at ∼107°C, ∼242°C (and possibly another peak at

~320°C); this is observed as negative counts in the figure. The charge in the refuge traps builds up continuously for IR stimulations between 0.5 and 2 s; these positive counts are PTTL due to photo-transfer. These peaks might consist of multiple peaks as they are rather broad. The phosphorescence observed following IR stimulations at 50°C possibly arises by charge leaking from these traps.

In a similar manner TL signals were obtained with the same dose and preheat as in Fig. 8.9b, but the short IR stimulations were replaced by a long IR bleach at 50°C for 100 s and this was followed by post-IR IR stimulations at 240°C for different durations (0.5, 1 and 2 s) before TL measurements. Figure 8.9b shows the 'difference' TL signals after subtraction of the TL signal without the second IR stimulation, but with preheating to 240°C for 0.5, 1 and 2 s respectively. The main peak at ~410°C was reduced by about 50% due to the IR bleach at 50°C for 100 s seen as negative counts. Figure 8.9b shows that holding the sample at 240°C during the second IR stimulation removes all trapped charge below 200°C, and transfers charge into a main peak at ~330°C and a smaller peak at ~265°C. These peaks build up with increasing post-IR IR stimulation time. The peaks are very close in temperature to peaks observed due to transfer from the first IR seen in Fig. 8.9a, (note that there was also a hint of a peak at 330°C in Fig. 8.9a). The phosphorescence observed following the post-IR IR stimulation at 240°C are very likely to reflect charge leakage from the two traps at ~265°C and ~330°C. Interestingly, the source trap in the post-IR IR stimulation is still the same as in the IR stimulation.

From the curves in Fig. 8.9a it may be suggested that several traps play a role in the IR stimulated phosphorescence signals from this feldspar sample. In Ankjærgaard and Jain (2010, Chapter 6 of this thesis) a simple model consisting of three traps and a luminescence recombination centre was developed to describe the behaviour of quartz phosphorescence. A key feature of the model is that it can predict a kink observed in the quartz phosphorescence curves (much like that observed for feldspar in Figs. 8.5 through 8.8) by a large transfer and subsequent build-up from one of the traps to another. By using this model it would be possible to simulate the occurrence of the kink in the feldspar phosphorescence curves (see Figs. 8.5, 8.6, and 8.7) and possibly to some extent the change in the kink position (Fig. 8.8), but the temperature dependence in Figs. 8.6 and 8.7 are complex and could not be produced with the simple model. Further studies on the temperature dependence of the phosphorescence signals and the PTTL peaks must be undertaken before developing a more complete model to explain the phosphorescence from feldspar.

8.6   Summary and discussion

The decay form of time-resolved luminescence and optically induced phosphorescence in orthoclase feldspar have been observed to cover time scales of over 8 orders of magnitude from 50 ns to ~8 s (Fig. 8.1). The TR-IRSL and post-IR TR-IRSL signals on these different time scales are very similar in shape, although there is a tendency for the post-IR TR-IRSL signal to show a larger effect from build-up during the on-time compared to the TR-IRSL signal. It is interesting that the overall decay form of the TR-IRSL and IRSP signals observed here for feldspar is broadly comparable to the decay form of the blue light

stimulated time-resolved and phosphorescence signals in quartz, even though feldspar and quartz are fundamentally different systems. This implies that the processes giving rise to these forms are of more universal nature.

The decay shapes of the TR-IRSL (Fig. 8.2) and IRSP (Fig. 8.5) signals are only weakly dependent on the preheat temperature in the range 270–410°C. For all preheat curves, the post-IR IR induced signals are more stable than the first IR induced signals. The data suggests that in the microsecond to millisecond regime where recombination lifetimes may be important, the holes are not significantly depleted by the preheat. On the seconds time scale, where the role of shallow traps becomes more important (as demonstrated from the photo-transfer TL curves), the traps that give rise to the phosphorescence signals must always fill to the same relative extent during optical stimulation, irrespective of the preheat temperature.

Unlike for the preheat data, both the TR-IRSL, the post-IR TR-IRSL signals, and their phosphorescence counterparts show major changes in the decay form with stimulation temperature. For both the TR-IRSL and post-IR TR-IRSL data it is observed that these changes arise because of a strong temperature dependent increase in the slowly decaying signal, relative to the initial decay and the underlying background. However, interestingly, this increase is not accompanied by a strong, matching increase in the decay rate of the slow component (Figs. 8.3b and 8.4b). A similar weak dependence of the slow ms to s scale components lifetimes with stimulation temperature was also observed in quartz (Ankjærgaard and Jain, 2010, Chapter 6 of this thesis). There the presence of a second centre that does not show thermal quenching as a possible explanation was suggested. Although this explanation can also be extended to feldspars, there exists an alternative explanation which is discussed below.

Independent results obtained using blue light stimulation from the time-resolved OSE data [Fig. 5f of Tsukamoto et al. (2010) or Fig. 5.5f in Chapter 5] also show a significant increase in the signal intensity with stimulation temperature without a change in the decay rate; it was inferred that this slow component represents the conduction band electron population. The IR energy used here does not allow a direct transition to the conduction band. IR excitation causes electrons to be lifted from the ground state to the first excited state of the trap, and from there it is likely that a proportion of the excited state electron population reaches the band tail states (Poolton et al., 2002). The band tail electron population will increase with temperature due to greater and greater influx from the IR excited state of the trap to the band tail states. If the electrons from the band tail states then recombine using an athermal mechanism [e.g. (Poolton et al., 2002)] then one would observe an increase in the intensity without a matching increase in the decay rates (lifetimes). Thus, one may conclude that one possible explanation for the slow component observed on the ms scale represents the emptying of the conduction band tail states.

The dependence of IRSP and post-IR IRSP decay curves on stimulation temperatures is much more complex than for the TR-IRSL and post-IR TR-IRSL signals. A kink is observed in the curves between 1 and 2 s into the off-time, and the decay rates of the curves before the kinks do not show a systematic change with stimulation temperature. On the other hand, the decay rates of the curves after the kinks do not show any significant change with stimulation temperatures (Fig. 8.6c). The data with variable prior stimulation

temperature suggests that there could be at least two sets of traps with widely different thermal stability that take part in the phosphorescence process on the seconds scale.

Our PTTL data confirms the presence of at least three shallow traps with different thermal stabilities that recuperate during IR and post-IR stimulations. The role of these traps in producing the 'kink' is not clear. We considered the simple three-trap, one centre model of Ankjærgaard and Jain (2010, Chapter 6 of this thesis); although it was possible to simulate the kink, it was not possible to simulate the temperature dependence of the signal before the kink. Future studies into the lifetimes of these TL peaks and the dependence of their intensities on stimulation temperature are required to get further insight into the exact role of these traps in phosphorescence.

In summary, based on these data it can be argued that during optical stimulation there is temperature dependent filling of the band tail states and shallow traps in feldspar. The slow ms component reflects the occupancy and the emptying of the band tail states as a result of electrons originating from the excited state of the dosimetric trap during IR stimulation. During the IR stimulation there is some charge transfer to the shallow traps (recuperation effect). These shallow traps then release charge due to thermal decay thus giving rise to the phosphorescence decays on the seconds time scale (almost approximated as a background on the millisecond timescale). It is possible that this charge release occurs both to the conduction band and possibly to the band tail states; the latter hold charge for longer duration, thus causing a delay in recombination, and thereby gives rise to a kink structure.

8.7 Conclusions

1. It is shown here that the time-resolved IRSL and IR stimulated phosphorescence signals measured at 50°C using the blue emission in our orthoclase feldspar exist over at least 8 orders of magnitude in time (from 50 ns to >8 s). The decay form of elevated temperature post-IR signals at 230°C is broadly similar to those obtained from the prior IR.

2. The holes that participate in the recombination process are thermally stable in the range 270°C–400°C. The decreasing trends seen in the intensity of these signals with preheat temperature (pulse anneal curves), therefore, reflect the thermal stability of the electron population.

3. It is suggested that the slowly decaying component on the ms time scales (the two TR-IRSL signals) represents the electron population in the band tail states.

4. On the seconds time scale (phosphorescence signals) a conspicuous kink is observed at about 1.5 s. This phosphorescence has contribution from at least two sets of refuge traps with very different thermal stabilities. The decay form of the signal before the kink shows a complex dependence on stimulation temperature, while that for the signal after the kink does not show significant changes with temperature. The complex temperature dependence of the curve before the kink requires further investigation. The latter part of the curve might possibly represent input to the band tail states from only the more stable set of traps.

5. TL data obtained with and without prior IR stimulation confirms that several shallow traps show recuperation during IR and post-IR IR stimulations. This implies that a significant proportion of charge from the band tail states undergoes re-trapping during IR stimulation. These traps most likely generate the phosphorescence signals observed here.

In summary, based on these data it can be argued that the slow millisecond decay reflects the occupancy of the band tail states during and shortly after the IR stimulation, while the phosphorescence decay on the second timescale is caused by charge release from refuge (shallow) traps to the conduction band and possibly to the band tail states.

References

Ankjærgaard, C. and Jain, M. (2010). Optically stimulated phosphorescence in quartz over the millisecond to second time scale: insights into the role of shallow traps in delaying luminescent recombination. *Journal of Physics D: Applied Physics*, 43:255502 (12pp).

Ankjærgaard, C., Jain, M., Kalchgruber, R., Lapp, T., Klein, D., McKeever, S. W. S., Murray, A. S., and Morthekai, P. (2009). Further investigations into pulsed optically stimulated luminescence from feldspars using blue and green light. *Radiation Measurements*, 44:576–581.

Ankjærgaard, C., Murray, A. S., Denby, P. M., and Bøtter-Jensen, L. (2006). Measurement of optically and thermally stimulated electron emission from natural minerals. *Radiation Measurements*, 41:780–786.

Bøtter-Jensen, L., McKeever, S. W. S., and Wintle, A. G. (2003). *Optically Stimulated Luminescence Dosimetry*. Elsevier, Amsterdam, The Netherlands. ISBN: 0–444–50684–5.

Buylaert, J. P., Murray, A. S., Thomsen, K. J., and Jain, M. (2009). Testing the potential of an elevated temperatures IRSL signal from K-feldspar. *Radiation Measurements*, 44:560–565.

Chithambo, M. L. (2007). The analysis of time-resolved optically stimulated luminescence: II. Computer simulations and experimental results. *J. Phys. D: Appl. Phys.*, 40:1880–1889.

Clark, R. J. and Bailiff, I. K. (1998). Fast time-resolved luminescence emission spectroscopy in some feldspars. *Radiation Measurements*, 29:553–560.

Clark, R. J., Bailiff, I. K., and Tooley, M. J. (1997). A preliminary study of time-resolved luminescence in some feldspars. *Radiation Measurements*, 27:211–220.

Lapp, T., Jain, M., Ankjærgaard, C., and Pirzel, L. (2009). Development of pulsed stimulation and photon timer attachments to the Risø TL/OSL reader. *Radiation Measurements*, 44:571–575.

Pagonis, V., Ankjærgaard, C., Murray, A. S., Jain, M., Chen, R., Lawless, J., and Greilich, S. (2010). Modelling the thermal quenching mechanism in quartz based on time-resolved optically stimulated luminescence. *Journal of Luminescence*, 130:902–909.

Poolton, N. R. J., Kars, R. H., Wallinga, J., and Bos, A. J. J. (2009). Direct evidence for the participation of band-tails and excited-state tunnelling in the luminescence of irradiated feldspars. *Journal of Physics: Condensed Matter*, 21:485505 (10pp).

Poolton, N. R. J., Ozanyan, K. B., and Wallinga, J. (2002). Electrons in feldspar II: a consideration of the influence of conduction band-tail states on luminescence process. *Phys. Chem. Minerals*, 29:217–225.

Sanderson, D. C. W. and Clark, R. J. (1994). Pulsed photostimulated luminescence of alkali feldspars. *Radiation Measurements*, 23:633–639.

Thomsen, K. J., Murray, A. S., Jain, M., and Bøtter-Jensen, L. (2008). Laboratory fading rates of various luminescence signals from feldspar-rich sediment extracts. *Radiation Measurements*, 43:1474–1486.

Tsukamoto, S., Denby, P. M., Murray, A. S., and Bøtter-Jensen, L. (2006). Time-resolved luminescence from feldspars: New insight into fading. *Radiation Measurements*, 41:790–795.

Tsukamoto, S., Murray, A. S., Ankjærgaard, C., Jain, M., and Lapp, T. (2010). Charge movement in minerals studied by optically stimulated luminescence and time-resolved exo-electron emission. *Journal of Physics D: Applied Physics*, 43:325502 (9pp).

Chapter 9

Towards a non-fading signal in feldspar: insight into charge transport and tunnelling from time-resolved optically stimulated luminescence

M. Jain and C. Ankjærgaard

Radiation Research Division, Risø National Laboratory for Sustainable Energy, Danish Technical University, DK-4000 Roskilde, Denmark

Abstract

Feldspars are an attractive alternative to quartz for extending the dose range, and for dating volcanic terrains such as on Mars and Iceland. Unfortunately, charge stored in the feldspar lattice undergoes anomalous fading leading to an underestimation in the dose estimates. In this paper we use the time-resolved optically stimulated luminescence (TR-OSL) technique to investigate the processes that give rise to the signal following infrared (IR), green and blue stimulation, with an objective to understand tunnelling and charge transport during thermo-optical excitations. We show that the TR-OSL shape is governed by the energy of excitation and the subsequent charge recombination route through the excited state of the trap, the band tail states or the conduction band. The role of band tail states in charge recombination is specifically examined using the signal shown to decay over several ms; we identify two dominant recombination routes, viz., phonon (0.05-0.06 eV) assisted diffusion, and quantum mechanical tunnelling, depending on the energy state of the detrapped electron. As would be expected, diffusion in the band tails is identical for both resonant and non-resonant excitations, where in the latter case the band tail state occupancy likely arises from thermalisation of conduction band electrons. The important outcome of this study is a comprehensive physical model based on a single dosimetric trap that successfully explains wide-ranging luminescence phenomena in feldspars, in particu-

lar, the luminescence efficiency and thermal partitioning of charge in different energy states and the subsequent recombination routes. The model predicts three different systematic approaches to preferentially sampling the most stable signal. We finally present evidence for a non-fading signal using one of these methods based on pulsed IR stimulation.

9.1   Introduction

Feldspars are an attractive alternative to quartz for extending the dose range as they show a higher luminescence saturation dose. The main obstacle in the routine application of feldspars, however, is athermal or 'anomalous' fading (Wintle, 1973; Visocekas, 1985). Different models have been proposed to describe the mechanism giving rise to fading in feldspars (Templer, 1986; Visocekas, 1985; Aitken, 1985), but it is now generally accepted that that the fading is caused by quantum mechanical tunnelling from the ground state of the trap (Poolton et al., 2002a,b; Li and Li, 2008; Kars et al., 2008) and that this process can be described by a power-law decay (Tachiya and Mozumder, 1974; Delbecq et al., 1974; Huntley, 2006). A correction for the dose under-estimation arising from this fading effect can be attempted using a simple analytical solution to the t^{-1} dependence of the luminescence decay (Huntley and Lamothe, 2001). The solution has several assumptions, the most critical being the form of the fading curve during extended irradiation (Morthekai et al., 2008). Unfortunately, the age range where correction might be valid is rather limited and does not allow full utilisation of the extended luminescence dose-response characteristic of feldspar for extending the measurable dose range. The biggest challenge in developing a more realistic correction model is exact knowledge of charge distribution and luminescence generation in feldspars (Larsen et al., 2009). Ideally, one would like to identify components in the luminescence signal that undergo a less severe or no fading. But this objective requires a better understanding of the charge transport in the feldspar crystal.

The knowledge of the structure of the trap and the band gap is the key issue. It has been suggested that the IRSL signal used in dosimetry arises from a single trap (Baril and Huntley, 2003), corresponding to the thermoluminescence peak at ∼400°C (at 5°C/s) (Murray et al., 2009). Based on optical bleaching experiments it has been proposed that the majority of the trapped charge stimulated by blue-green light is also accessible by the infra-red (Duller and Bøtter-Jensen, 1993; Jain and Singhvi, 2001). This interpretation is also supported by similarity of the dose response curves measured by blue and IR light (Blair et al., 2005). Previous work led by Poolton has made significant contributions to understanding the band structure. Poolton et al. (2002a,b) suggest that the IRSL from feldspar is a product of two very different processes; (i) localised recombination by tunnelling from the excited state of the trap to the recombination centre, and (ii) electronic transfer through the conduction band tail states to the recombination centre. The band tail model proposed by Poolton et al. (2002a,b) is particularly successful in predicting the rising continuum observed in the excitation spectra (Poolton et al., 2002b). During

the writing of this manuscript a new article by Poolton et al. (2009) presents several low temperature measurements (10 K to room temperature) that give experimental evidence of the existence of band tails in feldspars. They conclude that the band tails occupy $\sim$0.4 eV below the conduction band. Although these experimental data explain the characteristic resonant and non-resonant excitation spectrum in feldspars (Bøtter-Jensen et al., 2003), the recombinant transport and charge partitioning between the conduction band and band tail states during OSL dosimetry measurements, which are typically made above room temperature, is not well understood.

One method of directly studying the recombination process is by time-resolved optically stimulated luminescence (TR-OSL), which has the potential to distinguish the different recombination routes on the basis of the time scales involved. An understanding of the role of the excited state and band tail states during a room temperature (or higher) optical stimulation can be achieved by examination of the charge transport following a stimulation pulse. It is hoped that this understanding will throw light on the role of electron-hole separation in luminescence generation, and thus help develop methods based on preferential selection of the most distant electron hole pairs in feldspars. The objective of this work, thus, is to contribute to the understanding of the processes that govern OSL generation in feldspars, and thereby isolate the process that is the least affected by ground state tunnelling. To achieve this objective we compare the response of feldspar to resonant (IR) and non-resonant (green), excitation, while detecting the blue emission, using both sedimentary and rock feldspar samples. Our IR excitation includes elevated-temperature IRSL as this signal shows different dosimetric characteristics compared to the room temperature IRSL signal (Jain and Singhvi, 2001; Thomsen et al., 2008).

9.1.1 Previous studies on TR-OSL of feldspars

Previous work on TR-OSL from feldspar has mainly focussed on multi-exponential analysis to understand the relative roles of the recombination centres that participate in the process (Sanderson and Clark, 1994; Clark et al., 1997; Clark and Bailiff, 1998; Chithambo and Galloway, 2000; Denby et al., 2006; Tsukamoto et al., 2006). Up to five decaying exponentials have been identified with lifetimes within: 30-50 ns, 300-500 ns, 1-2 µs, $\sim$5 µs, and >10 µs (Clark et al., 1997; Clark and Bailiff, 1998; Chithambo and Galloway, 2000; Tsukamoto et al., 2006). Clark et al. (1997) studied the TR-IRSL signals in three different emission windows (280-380 nm, 350-575 nm, and 460-625 nm) and Clark and Bailiff (1998) extended this study by using a set of bandpass filters to measure the TR-IRSL at 300, 350, 400, 450, 500, and 550 nm. Both studies found that lifetimes within these detections windows lie within the above given lifetime groups. Some of the lifetimes were attributed to the internal transitions within the recombination centres (Clark and Bailiff, 1998). The 30-50 ns timescales for the very fast decay show that the relaxation lifetime at the recombination centre, if any, must be of the order of few ns or less.

In addition to the analysis of the form of the TR-OSL decay curves, there have been two important applications of this technique to understand anomalous fading. Sanderson and Clark (1994) using pulsed blue light stimulation tried to identify a non-fading TR-OSL component in a volcanic lava sample, which showed a 50% loss of signal following 4 days of storage. They con-

cluded that components occurring on the 40 ns - 8 µs timescale show major signal loss due to fading, but that both the faster and slower components did not appear to show signs of fading. This suggestion was pursued a decade later by Tsukamoto et al. (2006) using pulsed IR LED stimulation on Na- and K-feldspars. They concluded that the longest (∼20 µs) component found in their samples seemed more stable over a storage period of 30 days compared to the short lived components, and furthermore, that the relative contribution from this long component was greater in K-feldspars than in Na-feldspars. Tsukamoto et al. (2006) also compared equivalent dose (D_e) estimates using pulsed IR-OSL (data collected in the off-time) with those using CW IR-OSL. However, given the scatter in their data it is not possible to derive a unique conclusion. This work was also continued by Huot (2007) but he concluded that it was unclear whether pulsed stimulation helped to isolate a less fading signal.

These authors made the implicit assumption that the TR-OSL decay can be approximated by a sum of decaying exponentials. Ankjærgaard et al. (2009, Chapter 7 of this thesis) discuss that this assumption is most likely not true. In this study we further explore this assumption by trying to pin down the underlying transport mechanisms during resonant and non-resonant excitations. We also re-examine possible associations between a component in the TR-IRSL signal and anomalous fading. More specifically, we study the changes in the TR-OSL decay shape as a function of photon energy, thermal energy, storage after irradiation, and thermo-optical pre-treatments, towards developing a comprehensive model for recombination in feldspars. The results are described and discussed in the different sections below.

9.2 Experimental details

9.2.1 Instrumentation

Measurements were carried out on a Risø TL/OSL-20 reader using blue, green and IR LED stimulation. The reader was equipped with an integrated pulsing option to control the LEDs, and a Photon Timer attachment to record the TR-OSL (Lapp et al., 2009, Chapter 2 of this thesis). Green light stimulation was performed with a 525 nm (FWHM = 45 nm) LED array with a Schott GG455 filter in front of each LED cluster delivering a total of ∼37 mW/cm^2 CW stimulation at the sample position. Blue stimulation was carried out using 470 nm LED arrays with a Schott GG420 filter in front of each LED cluster delivering a total of ∼50 mW/cm^2 at the sample position. The IR stimulation was performed with an 870 nm (FWHM = 40 nm) LED array delivering ∼100 mW/cm^2 CW stimulation at the maximum operating current. All time-resolved curves presented here were measured using an on-time (pulse width) of 50 µs and an off-time (time elapsed between two consecutive pulse) of 500 µs, unless otherwise mentioned.

9.2.2 Samples

Five samples have been used for this study, three feldspar end member mineral specimens (orthoclase, albite and anorthite) and two potassium-rich feldspar sediment extracts. Two of the rock samples, an orthoclase and an albite were

obtained from the Geological Museum in Copenhagen and were gently crushed and dry-sieved to obtain a grain size fraction of 90-125 μs with no further chemical treatment. The third rock sample, an anorthite, was supplied by Dr. John Bridges, University of Leicester in crushed (grain sizes 90-250 μs) form. These three minerals were chosen to represent the extreme varieties rich in K, Na, and Ca in the ternary composition-diagram of feldspars. All three samples have previously been used in Ankjærgaard et al. (2009, Chapter 7 of this thesis), but there this orthoclase was named orthoclase 3. The two K-rich sediment extracts (previously used in Thomsen et al. (2008), laboratory codes 963806 and 951020) were obtained by first wet-sieving and treatment with HCl and H_2O_2 of the bulk sample to remove carbonates and organic material. The K-feldspar enriched fraction was then separated using a heavy liquid solution ($<\rho < 2.58$ g/cm^3) and etched for 40 min. with diluted HF (10%) to clean the grains and to remove the outer alpha-irradiated layer. After etching, any contaminating fluorides were dissolved using HCl before final rinsing and drying.

All the data presented here were measured on aliquots consisting of about 500 grains mounted on stainless steel cups using silicon spray

9.2.3 Luminescence detection

We chose to restrict our measurements to the blue emission as this is the most widely used in dating. The conventional, most commonly used filter combination for detection of blue emission in feldspars (4 mm Corning 7-59 and 2 mm Schott BG-39: 350-415 nm) resulted in enormous breakthrough with the green LED stimulation. An alternative filter combination consisting of a 6 mm thick Chroma D410 and 5 Comar 435 IK filters (25 mm dia., 1 mm thickness: 400-430 nm) was, therefore, used during green stimulation. This alternative filter combination has a lower as well as a narrower transmission than the conventional filters (7-59 + BG-39), which results in reduced sensitivity. By comparison using IR stimulation, the net luminescence transmission is found to be 8.6 times larger for the conventional blue filter pack compared to the alternative filter pack. Therefore, we decided to keep the conventional filter pack for IR stimulation and the alternative filter pack for green stimulation.

To test the effect of the two filter combinations TR-OSL curves were measured at 50° for the same aliquot of the orthoclase sample. The results normalised to peak counts (last point in the on-time) are shown in Fig. 9.1a, and the same data (filled circles and lines) are also shown on a double-log plot in the inset. It is clear that the two signals have exactly the same shape during both the on- and the off-time; we can, therefore, directly compare the IR and green stimulated signals even though they have been detected using two different filter combinations.

In the following sections all IR stimulation data are measured using the BG-39 and 7-59 filter combination, while all green light stimulation data are measured using the D410 and 435 IK filter combination.

9.2.4 Terminology and signal analysis

The terminology and abbreviations used throughout this article are defined in the Appendix.
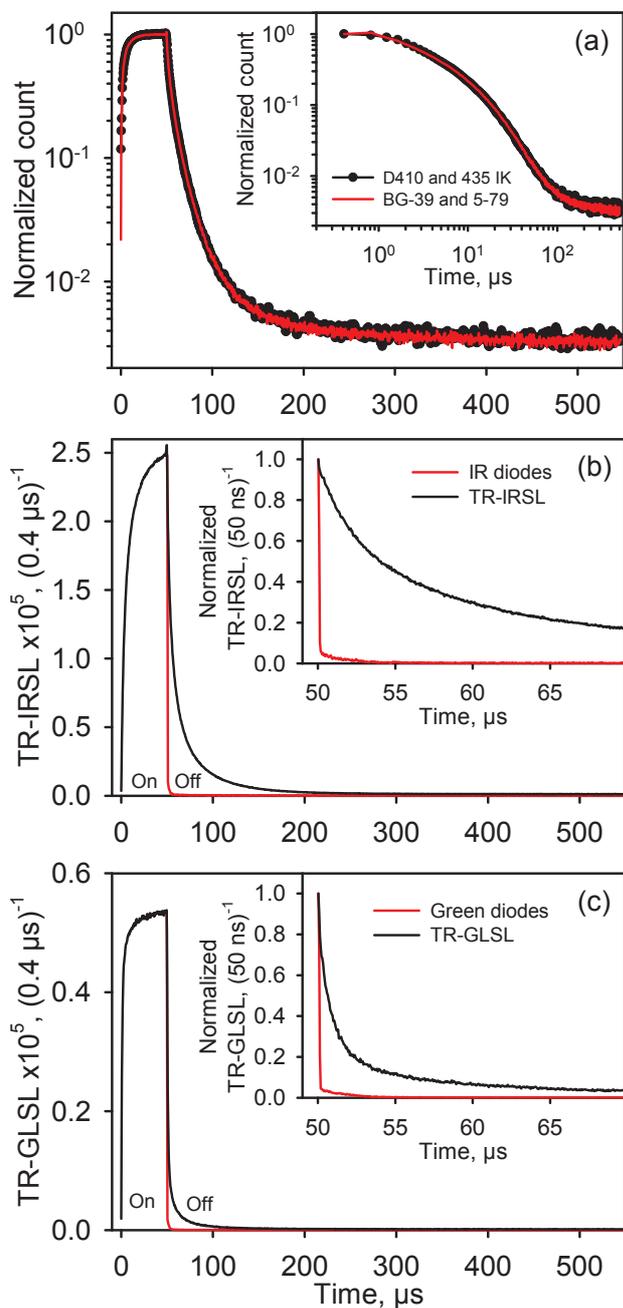
Figure 9.1: (a) TR-IRSL shape for orthoclase detected using the D410 and 435 IK filters (filled circles) compared to the TR-IRSL shape detected using the BG-39 and 5-79 filters (red line). The sample was given a dose of 20 Gy, preheated to 250°C for 60 s and stimulated at 50°C. The inset shows the off-time decay data on a log-log scale. (b) TR-IRSL curve (BG-39 and 5-79 filters) from the orthoclase feldspar measured at 50°C following irradiation with 25 Gy and a preheat to 260°C. (c) TR-GLSL (BG-39 and 5-79 filters) from the same sample measured at 50°C following irradiation with 90 Gy and a preheat to 260°C (a higher dose was given as the sensitivity of the green system was poorer than for the IR system). The fall time of the IR and green LED's are plotted in (b) and (c) respectively. The insets show the initial 20 ţs data, with a much higher resolution (50 ns)$^{-1}$.

Signal analysis of the TR-OSL curves is challenging mainly due to two factors: Firstly, the LED switch-off time is typically <150 ns, therefore, the form of the fast decay could be somewhat affected by the LED switch-off time. Secondly, the lack of knowledge of the exact mathematical form of the feldspar TR-OSL curve complicates the signal analysis. The TR-OSL data for IR (Fig. 9.1b) and green stimulations (Fig. 9.1c) shows that the signals drop rapidly following the LED pulses. The insets show a closer view of the initial signal. The IR signal is slower than the pulse fall time, whereas the green signal follows the LED's initially and then gets somewhat slower. After this rapid initial drop, the later part of the TR-IRSL curve is seen to decay on the µs to ms time scales (Fig. 9.1b, c). As is discussed in detail below, the TR-OSL decay form is not simply a linear sum of exponential decays. To analyse our data we, therefore, resort to a somewhat semi-quantitative analysis based on visual examination of the TR-OSL curves and isolation of the fast and slower parts of the signals. We define two integral regions termed as the 'Fast signal' and the 'Slow signal' which are used throughout the article (see the Appendix for details).

9.3 TR-OSL shape vs. stimulation photon energy

By using the two filter combinations described in Section 9.2.3, the orthoclase sample was dosed, preheated and measured using both IR and green stimulations to compare the signal shapes. Fig. 9.2a shows a comparison of normalized off-time decay shapes for TR-IRSL at 50°C, post-IR TR-IRSL at 230°C and TR-GLSL at 50°C. The fall-time of the stimulation light from the IR LED's is shown for reference; the green LED fall time is not plotted but it overlies the IR LED curve. Of the three signals observed here, the green signal has the fastest initial decay compared to the two IR signals. The post-IR IR signal measured at 50°C is initially slightly faster than the IR signal, but after a few tens of µs the two signals cross over, and thereafter the IR signal decays faster than the post-IR IR signal. At about 300 µs into the off-time the IR signal reaches a similar constant level as the green signal; the post-IR IR signal reaches a constant level about 10 times higher (relative to the initial decay) compared to the two signals measured at 50°C because of the thermal effect discussed later. Interestingly, towards the later part of the curves (400-500 µs), all three signals decay at the same rate.

The TR-IRSL and TR-GLSL data show that the decay forms are related to the stimulation photon energy; therefore, it would be interesting to explore the trend further with blue light stimulation. However, the use of the blue detection filters precludes this possibility. As the closest alternative, we attempted a comparison of the IR, green, and blue stimulations in the UV detection (note that the earlier work summarized in the introduction has shown that the TR-OSL decay forms are broadly similar in the blue and UV detection windows). The normalized TR-BLSL, TR-GLSL, and TR-IRSL off-time curves detected in the UV emission are compared in Fig. 9.2b. All three signals were measured at 50°C following irradiation (90 Gy) and a preheat to 250°C for 60 s using the orthoclase sample. These data show the trend that the TR-OSL from blue stimulation decays faster than green, which decays faster than IR. On closer inspection, the decay rate of the TR-BLSL and TR-GLSL are in fact very similar; the main difference is the relative proportion of the Fast and the Slow
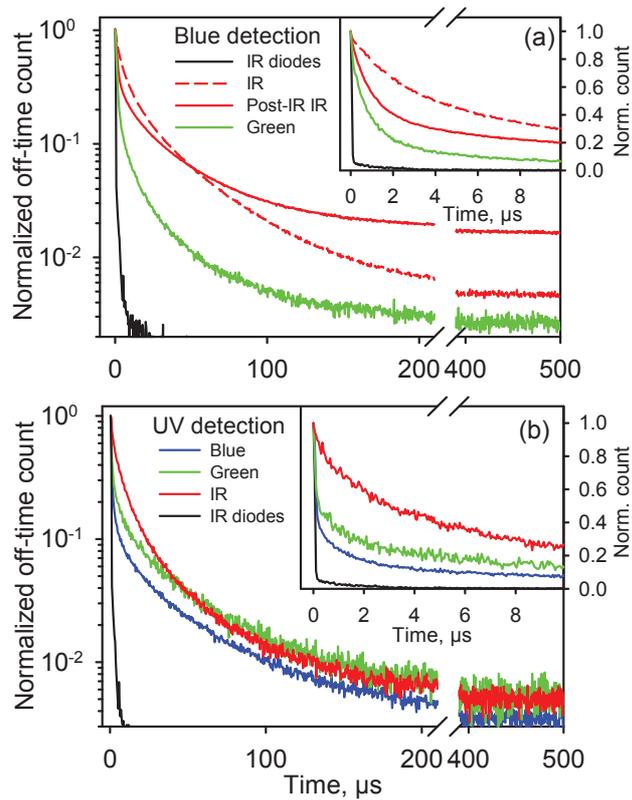
Figure 9.2: (a) Normalized off-time decay shapes for TR-GLSL and TR-IRSL at 50°C, and post-IR (50°C for 100 s) TR-IRSL at 230°C using the orthoclase sample. Prior to each measurement, the sample was dosed with either 100 Gy (green) or 25 Gy (IR stimulations), and preheated to 300°C for 60 s. The fall-time of the IR LED's measured using an attenuation filter inserted beneath the PM-tube is shown for reference. All curves are normalized to the last point in the on-time. The inset shows the initial 10 μs of the off-time decay shapes using a higher resolution of 50 ns. (b) Blue light stimulated TR-BLSL, TR-GLSL and TR-IRSL off-time signals measured at 50°C in the UV emission (U340 filters) using the same orthoclase sample. The measurements used a dose of 90 Gy and a preheat to 300°C for 60 s, and the curves have been normalized to the last point in the on-time. The inset shows the initial 10 μs of the off-time decay shapes for a higher resolution of 50 ns.

decaying signals (inset to Fig. 9.2b). A relative difference in the initial fast drop of ~60% and ~50% in the TR-BLSL and TR-GLSL signals, respectively, accounts entirely for the differences in the two TR-OSL decay shapes. The TR-IRSL decay curve on the other hand is much slower than both the TR-BLSL and the TR-GLSL signals and is similar to that observed in the blue detection window.

The strong dependence of the TR-OSL decay form on the stimulation energy likely arises from different electronic pathways, a function of the energy level occupied by the evicted electron. According to Baril and Huntley (2003), the IRSL trap is believed to lie at >2.5 eV below the conduction band, while Poolton et al. (2002a) based on theoretical considerations suggest that the trap depth is ~2 eV. Stimulating this trap with blue light (2.63 eV) would most likely cause a direct transition of the trapped electron to the conduction band. Even, if green light (2.36 eV) causes sub-band excitation, it is likely that there will be some transitions to the conduction band because of phonon assistance (See Figure 1 of Poolton et al. (1995). However, for IR light (~1.4 eV) the excitation is sub conduction-band; the trapped electrons are transferred to the excited state of the trap (Poolton et al., 2002a, 2009) and from there they either recombine with holes directly by tunnelling and/or via band tail transport. Supporting evidence come from exo-electron studies where it has been shown that an optically stimulated exo-electron signal arises from blue light stimulation but not from the IR stimulation (Ankjærgaard et al., 2005); this observation has been taken to indicate that while blue stimulation places charge in the conduction band, the IR stimulation does not. Our recent study on time-resolved optically stimulated exo-electron (TR-OSE) emission of feldspars shows that at the end of the blue light stimulation pulse the OSE signal drops about as fast as the OSL signal reflecting a quick emptying (or thermalisation) of the conduction band Tsukamoto et al. (2010, Chapter 5 of this thesis).

The similarity between the TR-OSE and TR-OSL observations suggest that the very fast initial decay (Fast signal) in our blue data must reflect the emptying of the conduction band; this implies that relaxation within the recombination centre from an excited state, if any, must be in ns or shorter time scales, which supports results from the fast pulsing OSL studies (e.g. Clark et al. (1997)). Since the initial drop in the green data is identical to that in the blue, we by analogy suggest that a significant population evicted by green light also recombines via the conduction band; the only difference between green and blue stimulations is in the relative intensities of the Fast and the Slow decaying signals. The IR stimulated signal shows a slower rate of decay than both blue and green (Fig. 9.2b); we propose that this is because the initial TR-IRSL originates due to a relatively slower nearest-neighbor recombination from the excited state of the trap and the proximal band tail states.

Unlike the Fast signal, the Slow signal (from about 70 μs in the off-time) has an almost identical shape irrespective of the stimulation photon energy at 50°C (Fig. 9.2b). We propose that all these Slow signals (IR, blue and green) originate from a distant- recombination through a slower transport within the band tail states.

The different IR, green and blue transitions are depicted in Fig. 9.3 (transition b). The recombination from around the excited state of the trap is shown as e_2 (the dashed line for tunnelling and the blue band for proximal recombination from the band tail states), and the band tail transport are shown as d_1
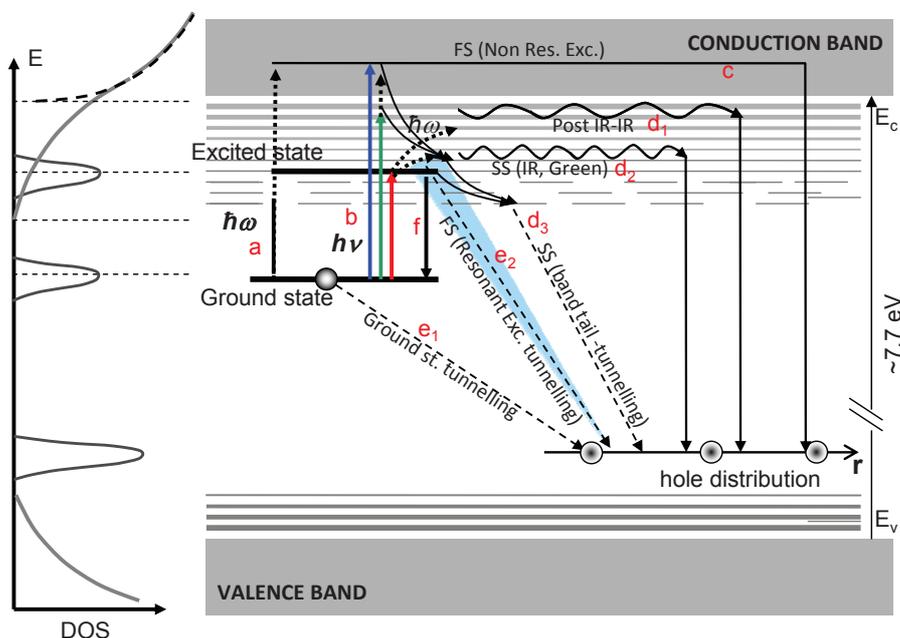
Figure 9.3: A schematic model for feldspar luminescence. The left side of the diagram shows the distribution of the density of states (Poolton et al., 2002b). The right side shows the band model with the different transitions inferred from the TR-OSL measurements: (a) Thermal excitations. The dashed region of the arrow denotes a continuum of allowed transitions from the bottom of the conduction band tails states to the conduction band. (b) Optical excitations IR, green and blue. IR excitation causes transition to the excited state. Green stimulation causes a sub-conduction band transition, whereas the blue causes a conduction band transition. The different curved arrows indicate transitions involving phonon absorption or phonon emission (thermalisation). (c) Recombination through the conduction band. (d) Transitions from the band tail states: d_1 - the high energy, high mobility states, d_2 - the low energy, low mobility states, d_3 - the lowest disconnected states. The transitions $d_1 \ldots d_2$ occurs by phonon assisted diffusion (PAD) whereas d_3 leads to a tunnelling recombination. There exists a continuum of transitions between d_1 and d_2 ($d_1 \ldots d_2$); we have shown only two of these to demonstrate the recombination volume dependence on the occupied energy state. In the text we generally use d_1 to represent low energy transitions and d_2 to represent high energy transitions. (e) tunnelling from the ground state (e_1) and the excited state (e_2) of the dosimetric trap; the dashed line indicates the tunnelling recombination from the excited state, and the blue shaded area shows proximal, nearest-neighbour recombination from the band tail states around the excited state. (f) Retrapping. FS denotes 'Fast signal' and SS denotes 'Slow signal' as discussed in the text. The thickness of the horizontal lines in the band diagram indicates the density of states (see the corresponding left diagram). The distance to the recombination site within a distribution of surrounding holes is denoted by the radius vector r (we clarify that this is only a schematic representation to aid visualisation - this band diagram as such does not contain any distance information). Thus, r defines the maximum probable donor-acceptor separation for a transition. The accessible crystal volume in the different transitions scales with r^3. The proximity of the recombination arrow to the trap signifies how localised the recombination is; as shown in the model, r gradually varies from highly localised transitions (e.g. e_1 and e_2) to delocalised transitions (e.g. c). Thus, the probable volume in which an electron can find an acceptor will vary with the extent of electron mobility in the order $e_1 \ll e_2 < d_3 < d_2 < d_1 < c$. Since the number of acceptor sites is proportional to volume, the bigger the volume the higher the probability of recombination.

and d_2. This model is discussed and tested in detail in the following sections.

9.4   TR-OSL shape vs. thermal energy

Feldspars show a characteristic increase in IRSL signal with an increase in the stimulation temperature (e.g. Duller and Bøtter-Jensen (1993); Rieser et al. (1997); Bailiff and Barnett (1994). Unlike quartz, however, the increase in the intensity of IRSL is not matched by a simultaneous increase in the decay rate (e.g. see Poolton et al. (2002b)). This observation perhaps suggests that the IRSL decay rate does not reflect the detrapping rate but instead the recombination probability; the higher the stimulation temperature the greater the recombination probability. We hypothesised in the above section that the Slow TR-OSL signals originate from transport in the band tails, while the Fast signals originate either from around the excited state of the trap (IR), or from the conduction band (green and blue). If this hypothesis is correct then we should see different thermal dependencies of these signals; for example the band tail transport or conduction band transitions may require very different thermal assistance.

To test the hypothesis, the stimulation temperature dependence of TR-IRSL, post-IR TR-IRSL and TR-GLSL curves were investigated on the same aliquot. The data are shown in Figs. 9.4a, 9.4c, and 9.4e, respectively. The TR-OSL decay rate and the signal intensity are discussed separately in the following sub sections:

9.4.1   Dependence of the decay rate on stimulation temperature

The insets to Fig. 9.4 show a closer view of the Fast signal decay. In the TR-IRSL data there is a large increase in the decay rate from 50 to 100°C, and thereafter the change in the decay rate is very small and gradual. At the higher temperatures the initial fast drop almost accounts for 80% of the signal intensity (see Fig. 9.4a, inset). The post-IR TR-IRSL signal also shows a similar trend for the Fast signal. In contrast, the TR-GLSL signal does not show a detectable change in the initial decay rate with stimulation temperature (Fig. 9.4e inset). Note that the fast decay for all the green measurements is still significantly slower than the LED fall time (see Figs. 9.1c and 9.2a); therefore, the apparent constancy is not an instrumental artefact.

The decay rate is an indicator of the lifetime in a particular state. An increase in the decay rate of the Fast TR-IRSL signal with an increase in the temperature from 50-100°C is important. We suggested in section 9.3 the possibility that the Fast IR signal arises by tunnelling from the excited state of the trap (Fig. 9.3, transition e_2). With an increase in temperature, an increasing proportion of electrons escape from the excited state of the trap into higher energy band tail states (Fig. 9.3, transitions $d_1 \ldots d_2$). This additional thermally induced loss decreases the life time of the excited state, observed as a faster decay of the Fast TR-IRSL signal, while the increased transfer to the band tails states increases the relative intensity of the Slow TR-IRSL signal (Fig 9.4a). For the post-IR TR-IRSL signal, the recombination mechanism is likely to be similar. Since the first temperature of the post IRSL signal is
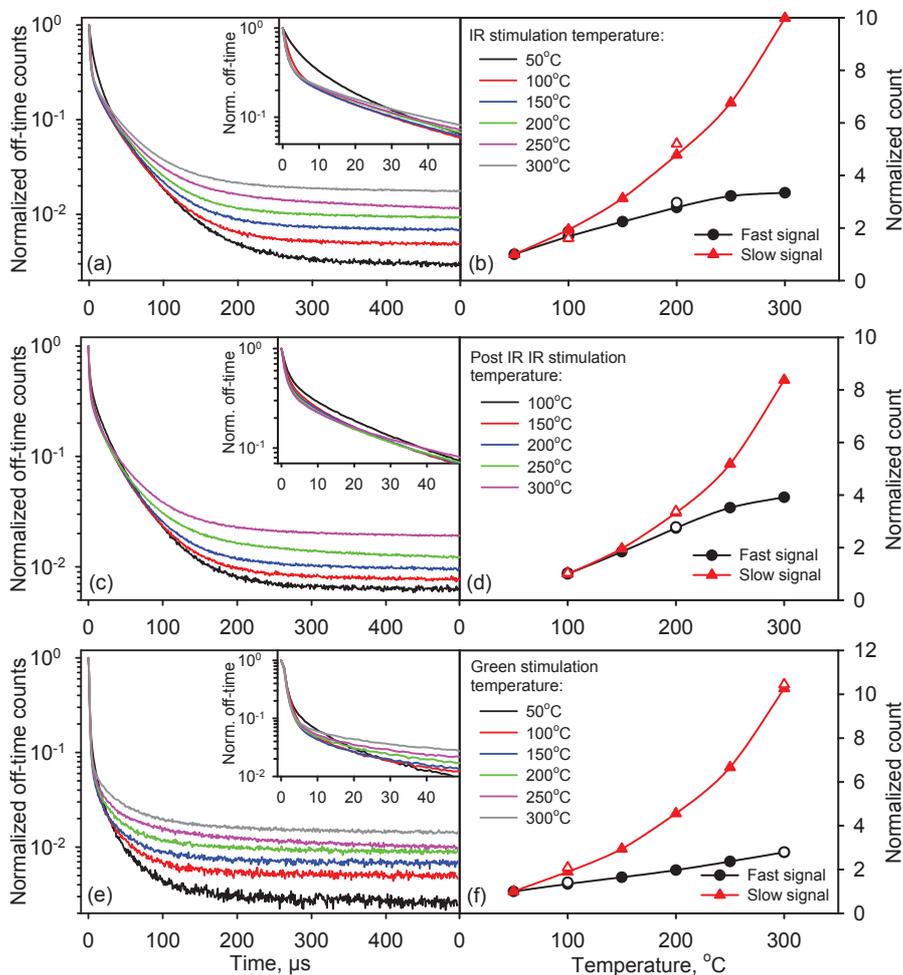
Figure 9.4: Stimulation temperature dependence of the TR-IRSL, post-IR TR-IRSL, and TR-GLSL off-time signals for an aliquot of orthoclase feldspar using temperatures between 50°C and 300°C following a preheat to 300°C for 60 s (the legends are shown in the right hand side diagrams). The IR measurements used a dose of 25 Gy and the green measurements a dose of 100 Gy. All curves have been normalized to the last point in the on-time, and insets show the initial 50 µs of the off-time curves. The summary curves (on the right hand side) show the normalized behaviour of the Fast (circles) and Slow (triangles) signals of the time-resolved curves. All open symbols denote recycling points. (a) TR-IRSL off-time curves. (b) Summary of the TR-IRSL curves from (a). (c) Post-IR TR-IRSL off-time curves following IR stimulation at 50°C for 100 s. Note that the lowest stimulation temperature is 100°C and not 50°C as this is a post-IR signal. (d) Summary of the post-IR TR-IRSL curves from (c). (e) TR-GLSL off-time curves. (d) Summary of the TR-GLSL curves in (e).

already quite high (100°C), we do not see any large differences in the decay rate; thus, these data are consistent with the changes observed for the TR-IRSL signal.

The TR-GLSL data are quite different from the IRSL data. Firstly, there is no apparent dependence of the Fast TR-GLSL decay rate on stimulation temperature. Secondly, the Fast TR-GLSL decay rate is greater than the TR-IRSL decay rate at 50°C (insets to Figs. 9.4a, e). Both these observations are consistent with our earlier interpretation that the Fast TR-GLSL signal originates from conduction band recombination (Fig. 9.3, transition c). Since the thermal assistance mechanism is not required in the conduction band route, the rate of recombination should not depend upon the stimulation temperature. Moreover, since the wavefunction is most delocalised for the conduction band, transition c is expected to be faster than transitions e_2 (Fig. 9.3; the degree of localisation in Fig. 9.3 is denoted as the distance r of the recombination site from the trap, i.e. the maximum probable donor-acceptor separation for recombination).

In contrast to the Fast TR-IRSL signal, the rate of depletion of the Slow signal seems to decrease with an increase in the stimulation temperature (for e.g. data between 50-300 µs in Figs. 9.4a, c, e); this decrease was also confirmed by subtracting the average background signal from the data (not shown). The slow signal arises from sub conduction band (E_c) transport via the band tail states. An increase in the electron energy with temperature leads to a more extended wave-function, which together with an exponential increase in the density of states (Poolton et al., 2009) can lead to an increased probability of hopping, or in other words relatively high electron mobility. But an increase in mobility should allow a quicker recombination because of greater availability of accessible accepters, and, therefore, a faster emptying of the band tail states. However, retrapping can be an equally important effect in the band tail emptying because of the spatial association of an evicted electron to parent trap. It is possible that at low temperatures the parent trap exerts a high probability for retrapping since the electron is less mobile and therefore in the proximity, and this effect is not quite balanced by the advantage offered by higher mobility in the band tail states at the higher temperatures.

9.4.2 Dependence of signal intensity on stimulation temperature

The temperature dependencies of the Fast and Slow signals for IR and green stimulations are shown in Fig. 9.4b, 9.4d, and 9.4f, respectively, and they all show the same relative behaviour: The Fast signal increases by a factor of 3-4, whereas the Slow signal increases by a factor of $\sim$ 8-10 with stimulation temperature for all the TR-OSL curves. The most important feature of these data is the large difference between the Slow and Fast signal increase.

The same data are shown on an Arrhenius plot (log intensity vs. the inverse of thermal energy; the slope of the plot gives the activation energy) in Figs. 9.5a, b. The Fast signal for the green stimulation shows a clear exponential dependence with an activation energy of 0.06 eV (Fig. 9.5a). If the green photon energy is sufficient to cause direct ionisation (i.e. transition above the conduction band edge) then thermal assistance is not expected. But if the excitation is sub-conduction band then an additional amount of thermal en-
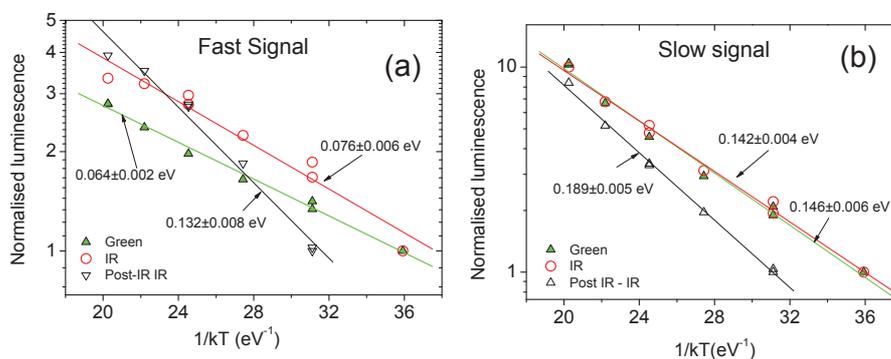
Figure 9.5: Arrhenius plots of (a) Fast and (b) Slow signals obtained using IR, post-IR IR and green light stimulation. The data were obtained from Figs. 9.4b, 9.4d and 9.4f for this analysis.

ergy is required for ionisation; however, this effect requires the existence of band tail states (or the Urbach tails). A finite activation energy for our Fast TR-GLSL signal therefore suggests that the green photons likely cause a sub Ec excitation; in other words the trap depth should be >2.4 eV (2.36 eV + 0.06 eV). The lack of thermal dependence of the initial (Fast signal) TR-GLSL decay rate (Fig. 9.4e) suggests that the recombination probability is the same once an electron enters the conduction band, irrespective of the occupied energy level in the band. An increase in temperature will simply place a greater fraction of electrons in the conduction band and this consequently increases the Fast signal intensity (Fig. 9.4f) but all these electrons will have the same lifetime (Fig. 9.4e, inset) because they are equally delocalised.

An alternative explanation for a finite activation energy for the Fast TR-GLSL signal could be that the green photons cause direct transition to the conduction band (i.e. trap depth < 2.36 eV) but an additional energy is required to avoid a quick thermalisation of the electron to the band tail states. However, this explanation implies that thermalisation plays a dominant role in conduction band emptying. In this scenario, the residence time of electrons in the conduction band should vary significantly with stimulation temperature; the higher the temperature the longer the lifetime. As discussed in the previous section the Fast TR-GLSL does not show any change in the decay rate with temperature, which suggests that this alternative explanation is unsupported by our data. The lack of detectable change is conduction band emptying rate is also supported by the TR-OSE data at different temperatures for blue light (Fig. 4f of Tsukamoto et al. (2010)).

Although both the IR and the post-IR IR Fast signals, show significant temperature dependence, they do not follow an exponential trend as observed for the green data (Fig. 9.5a). The temperature dependent increase likely occurs because of possibility of direct detrapping to proximal available states in the band tails above the excited state, from where follows the transition e_2. However, some excited-state electrons will further thermally excite to higher energy band tail states by phonon assistance (upward arrows around transition a in Fig. 9.3) from where they undergo transitions $d_1 \ldots d_2$. This effect causes an increased leakage from the Fast route (e_2) to the Slow route ($d_1 \ldots d_2$) with

temperature, resulting in a deviation from an exponential trend. Note that the high temperatures data are lower than that expected from the exponential trend based on the low temperature data (Fig. 9.5a) which supports this interpretation.

The temperature dependence of the Slow signals give some important insights into the role of the band tail states in the recombination process. Most importantly, the Slow signals show exactly the same dependence for the IR and the green stimulations giving an activation energy of ∼0.14 eV (Fig. 9.5b). This result strongly supports our hypothesis at the end of section 9.3 that the Slow signal in both resonant (IR) and non-resonant (green and blue) excitations has the same origin shown as d_2 in Fig. 9.3. A consideration of thermal diffusion within the lattice and the potential recombination volume shows that the activation energy corresponds to three times the active phonon energy mode (Poolton et al., 2002b). Thus our activation energy corresponds to the phonon mode of ∼0.05 eV which is in excellent agreement with measured phonon energies for strong lattice vibrations in feldspars (See Poolton et al. (2002b) for discussion). The Slow signal from the post-IR IR is also well described by an exponential increase corresponding to an activation energy of ∼0.19 eV, i.e. lattice phonons of ∼0.06 eV. As we discuss later, the post-IR IR excitation requires a larger crystal volume for luminescence generation as all the nearest neighbour acceptors are already depleted during the prior IR stimulation. Thus, a larger phonon mode may be necessary for transport; these transitions are shown as the dashed curved, upwards pointing arrows from the IR trap, and 'd_1' in Fig. 9.3. The temperature dependence data suggests that there exists a continuum of transitions between d_1 and d_2 ($d_1 \ldots d_2$). We have shown only two of these to demonstrate the recombination volume dependence on the occupied energy level in the band tail states.

In summary, since the IR energy matches the excited state energy of the trap, and the green approximates its ionisation energy, the Fast signal arising from these processes shows a rather small thermal dependence. A relatively greater thermal dependence should be seen in signals arising from transport through the band tail states due to the Phonon Assisted Diffusion (PAD) mechanism described in Poolton et al. (2002b); this behaviour is observed for the Slow signals which show much larger activation energy of 0.14 eV compared to the Fast signal for both the IR and the green stimulations (Fig. 9.3, transition d_2). PAD will apply both to green and IR stimulation, as it is not really important how the electrons were placed in the band tails in the first place; therefore an identical behaviour of the Slow signals for both green and IR stimulations strongly supports a band tail recombination mechanism. For the green stimulation, the electrons enter the band tails directly because the excitation is sub E_c, or a minor amount can additionally enter the band tails because of thermalisation from the conduction band; these transitions are shown as curved downward pointing arrows from the conduction band in Fig. 9.3. For IR stimulation, a proportion of electrons make a thermal escape from the excited state of the trap into the band tail states - the curved upward pointing arrows in the Fig. 9.3. From here they either take the same routes $d_1 \ldots d_2$ depending on the stimulation temperature.

An interesting feature of these data is that for both IR and post-IR IR excitations the Fast signals show a non-exponential trend, whereas the Slow signals show an exponential trend. This is probably because after a finite du-

ration (approx. few tens of microseconds) all detrapped electrons follow an equilibrium energy distribution in the band tail states depending on the ambient temperature. Recombination from each equilibrium level corresponds to a finite recombination probability that gives rise to our Slow signal. Following Boltzmann's distribution, the mean energy increases linearly with temperature. At the same time the density of available states increases exponentially with energy (Fig 9.3, left). Thus an increase in temperature corresponds to an exponential increase in occupancy of the equilibrium energy states, reflected as an exponential increase in luminescence in Fig. 9.5b.

Its worth noting that previously published data (e.g. Poolton et al. (2009); Rieser et al. (1997) derived from continuous wave stimulation will be dominated by Fast signals and, therefore, will not directly reflect the activation energies involved in band tail transport. The density of states as well as the distribution of centres is likely to vary from sample to sample, and, therefore, CW stimulation is likely to give a distribution of activation energies resulting from an averaging of the two processes. Our data based on pulsing is able to selectively observe the band tail states and confirm the proposal of Poolton et al. (2002a,b) that the 0.05-0.06 eV phonon mode is responsible for hopping (i.e. PAD) in these states.

These data support our earlier findings on long lived TR-IRSL signals in feldspars (Ankjærgaard and Jain, 2010, Chapter 8 of this thesis). In this earlier work we observed a phosphorescence component decaying on ms time scales showing a conspicuous, strong temperature dependent increase compared to the adjacent components, but no accompanying change in the decay rate. We suggested there independently of the present data that the slowly decaying signal on the ms time scales probably reflects an instantaneous population in the band tails following the IR stimulation. Comparison with this earlier work suggests that we are observing the same ms component in the present article, although at a much shorter time scale.

9.5 The effect of ground state tunnelling

The photon energy and the thermal dependence data suggest that the Fast IR signal originates from around the excited state of the trap, while the Slow signal mainly originates from a longer transport within the band tails. In this section we study the effect of storage after irradiation (ground state tunnelling) on the shape of the TR-IRSL and the post-IR TR-IRSL signals. If our hypothesis on the origins of the Fast and Slow signals is valid then we should see a change in the relative amounts of the Fast and Slow signals following delay after irradiation. Specifically, if the Fast signal has a more localised origin than the Slow signal (Fig. 9.3; transition e_2 compared to transitions d_1 and d_2), then it should be preferentially affected because of depletion in the proximal hole population after the ground state tunnelling (transition e_1) (note that the extent of localisation of these different transitions is denoted by the length of the vector 'r' in Fig. 9.3. This length denotes the maximum probable donor-acceptor separation for recombination via a certain route).

To study the effect of storage, five samples with different fading rates were chosen. The anomalous fading is usually quantified by the g-value, given as the signal loss per decade of normalised storage time (Aitken, 1985). The samples
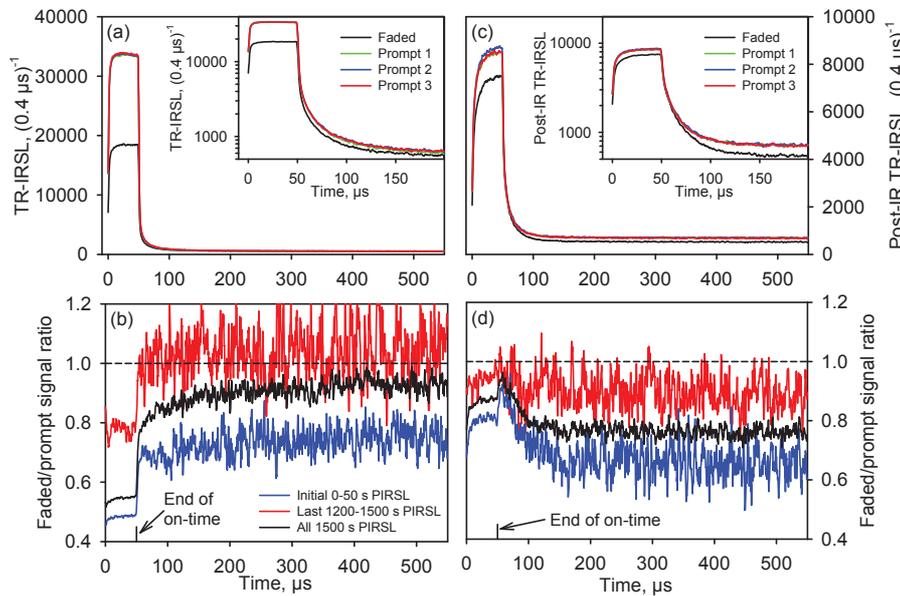
Figure 9.6: (a) TR-IRSL curves from three prompt and a delayed measurement following 48 days of storage of the albite feldspar. The first prompt (Prompt 1) was measured prior to the delay (faded) and the last two (Prompt 2 and 3) were measured after the delay. The albite sub sample was dosed with 45 Gy, preheated to 250°C for 60 s and first measured (with or without storage) for 1500 s using IR at 50°C and then with post-IR IR at 225°C also for 1500 s. The insets show the graphs on a semi-log scale. (b) TR-IRSL ratio curves derived by dividing the delayed (faded) signal by the average over the three prompt curves from (a). Furthermore, the ratio curves are calculated for three different time integration intervals: The total PIRSL signal integrating over all pulses emitted during all the 1500 s, the initial PIRSL signal integrating over pulses emitted in the 0-50 s, and the last part of the PIRSL signal, integrating over pulses emitted in the last 1200-1500 s. The dashed line at 1 indicates the value for a non-faded ratio signal. (c) Same data as (a) but for the post-IR TR-IRSL signals (d) same data as (b) but for the post-IR TR-IRSL signals.

examined here are: three minerals specimens, orthoclase (g ∼ 3 %/decade), albite and anorthite (g ∼ 20 %/decade), and two feldspar KF rich sediment extracts also used in Thomsen et al. (2008), 963806 (g ∼ 3.1 %/decade), and 951020 (g ∼ 3.3 %/decade) (all g-values are stated for the initial CW-IRSL measured at 50°C in the blue emission after a preheat of 250°C for 60 s; a 2 days normalisation period was used for the calculations).

The samples were dosed, preheated to 250°C for 60 s, followed by prompt TR-IRSL and post-IR TR-IRSL measurements. The irradiation and preheat were then repeated followed by a storage for 48 days prior to re-measurement. Subsequently two more prompt measurements were made to ensure that the sensitivity of the sample or the setup has not changed during the 48 days. The prompt and delayed TR-IRSL and post-IR TR-IRSL curves are shown for the albite feldspar in Figs. 9.6a and 9.6c, respectively. Both the pulsed IRSL (PIRSL) and the post-IR PIRSL curves were measured for 1500 s using an

on-time of 50 μs and an off-time of 500 μs; the curves result from the sum of all the pulses produced during the 1500 s of stimulation. Fig. 9.6a shows that the intensity of the on-time signal in the delayed IR measurement has been reduced by about 50% compared to the three prompt measurements while the intensity of on-time signal in the delayed post-IR signal has only been reduced by about 10%. The insets to these figures show the same data on a log-log scale for the initial 200 μs. The IR data strongly confirm the earlier suggestions of Sanderson and Clark (1994) and Tsukamoto et al. (2006) that the off-time signal has a lower fading than the on-time signal.

For closer examination, the ratio curve of the delayed signal and the average of the three prompt signals is plotted for TR-IRSL (Fig. 9.6b) and post-IR TR-IRSL (Fig. 9.6d). Here the curves have been produced by adding up pulses obtained during three different time intervals during the entire measurement period: the initial 0-50 s, the last 1200-1500 s, and the total 0-1500 s. Fig. 9.6b shows that in all three cases the TR-IRSL on-time signal fades much more than the off-time signal. Most importantly, the off-time IR signal at 50°C obtained from integration of the last part of the measurement (1200-1500 s) does not fade at all; it has an average ratio of 1.02 ± 0.02 for the off-time data between 350 and 550 μs. This can be compared to the average ratio of 0.77 ± 0.01 for the data in the on-time.

For the post-IR TR-IRSL measurement, the off-time signal fades more rapidly than the on-time signal (Fig. 9.6d). As in the case of TR-IRSL, it is observed that the post-IR TR-IRSL derived from the later part of the measurement (1200-1500 s) fades less compared to that derived from the initial part of the measurement (0-50 s). Moreover, the difference in fading between the on-time and the off-time signals is less pronounced in the 1200-1500 s ratio curve (on-time: 0.93 ± 0.01, off-time: 0.88 ± 0.01) compared to the initial 0-50 s ratio curve (on-time: 0.80 ± 0.01, off-time: 0.71 ± 0.01). A remarkable change in fading is observed at the transition between on-time and off-time; at the end of the on-time the ratio is increased significantly during a few μs, after which it decreases to a lower value over approximately 50 μs. It is most visible in the ratio curves for the initial signal and the total signal and almost not visible in the last PIRSL signal. Similar behaviour is observed for the other four samples in the post-IR IR curves.

For the five samples, the on- and off-time ratios as described above have been calculated for the IR and post-IR IR signals during the initial and latter part of the PIRSL curves, and these are all given in Table 9.1. Similar behaviour is observed in all five samples, although it is more pronounced in the samples with large fading rates. The general behaviour can be summarized in three points:

(i) During a pulsed IR measurement at 50°C, the off-time signal is much more stable compared to the on-time.

(ii) During a pulsed post-IR IR measurement at 225°C, the on-time signal is more stable compared to the off-time. The on-time signal in the post-IR TR-IRSL data has a similar or lower stability as the off-time signal in the TR-IRSL data.

(iii) The off-time signals obtained by integrating pulses during the later part of the pulsed IR and post-IR IR measurements are more stable than those

Table 9.1: Average faded/prompt ratios and corresponding standard errors ($\pm$) calculated for the on-time (0-50 μs) and the latter part of the off-time (350-550 μs) for the TR-IRSL and post-IR TR-IRSL curves from five different feldspar samples. These are listed for both the initial (0-50 s) part of the PIRSL signal (columns 2-5) and the latter (1200-1500 s) part of the PIRSL signal (columns 6-9). These two time intervals (if adding up the light sum during the stimulation pulses) correspond to 4.5 s and 27 s of CW stimulation time respectively. The measurement details are as given in Fig. 9.6 and the doses used were: Orthoclase (45 Gy), albite (45 Gy), anorthite (1200 Gy), K-feldspar, sample code: 963806 (180 Gy), and K-feldspar, sample code: 951020 (18 Gy).

	Initial 0-50 s PIRSL time (~4.5 s CW time)				Latter 1200-1500 s PIRSL time (~27 s CW time)			
	IR on	IR off	Post-IR on	Post-IR off	IR on	IR off	Post-IR on	Post-IR off
Orthoclase	0.86 ± 0.00	0.90 ± 0.00	0.87 ± 0.00	0.86 ± 0.00	0.94 ± 0.00	$\mathbf{0.98 \pm 0.02}$	0.95 ± 0.00	0.79 ± 0.00
Albite	0.48 ± 0.00	0.75 ± 0.01	0.80 ± 0.00	0.71 ± 0.01	0.77 ± 0.01	$\mathbf{1.02 \pm 0.02}$	0.93 ± 0.01	0.88 ± 0.01
Anorthite	0.46 ± 0.00	0.92 ± 0.02	0.73 ± 0.00	0.46 ± 0.00	0.71 ± 0.00	$\mathbf{1.04 \pm 0.02}$	0.84 ± 0.01	0.65 ± 0.00
963806	0.96 ± 0.00	1.04 ± 0.01	0.93 ± 0.00	0.96 ± 0.00	0.98 ± 0.00	1.05 ± 0.01	$\mathbf{1.01 \pm 0.00}$	0.96 ± 0.00
951020	0.79 ± 0.00	$\mathbf{1.02 \pm 0.02}$	0.96 ± 0.00	0.84 ± 0.01	0.92 ± 0.06	$\mathbf{0.98 \pm 0.01}$	0.94 ± 0.01	0.89 ± 0.01

obtained from integrating the initial part.

Our fading data suggest that in the conventional continuous wave measurements used for dosimetry, the IRSL signal will be less stable than the post-IR IRSL signal since both these measurements will be dominated by their respective on-time signals (compare the on-time signals in Figs. 9.4b and 9.6d); this inference is consistent with results reported in earlier work reported from our laboratory (Thomsen et al., 2008; Buylaert et al., 2009). The most important observation is that 4 out of 5 samples do not show detectable fading in the off-time TR-IRSL signal for the latter part of the measurement (Table 9.1, column 7). The 5th sample shows a $5 \pm 1\%$ increase because of storage; this requires further investigations. These values are in sharp contrast to the $\sim 5\text{-}50\%$ decrease in the on-time signal observed in these samples. Thus, we conclude that this signal does not fade under our experimental conditions.

The fading data strongly supports our interpretation of the origins of the Fast and the Slow signals as shown in Fig. 9.3. The ground-state tunnelling consumes the nearest electron-hole pairs (Fig. 9.3, transition e_1). During IR stimulation the electrons are lifted to the excited state from where they can undergo retrapping (transition f), tunnelling or proximal band tail recombination (transition e_2), or distant recombinations following thermal transitions into the band tails (transitions d_1 and d_2). Since the wavefunction from the excited state is more extended than in the ground state, recombinations which were not probable from the ground state become possible within the laboratory time scales. Thus, the on-time signal (Fast signal) is dominated by the quickest recombinations arising from the relatively closer remaining donor-acceptor pairs after the fading delay (transition e_2, dashed line). In the off-time, the signal dominated by the nearest neighbour recombination from the excited state drops rapidly because of the combination of excited to ground state transition in the trap (transition f) and quick nearest neighbour recombination from around the excited state of the trap (i.e. the occupied band tails states closest to the excited state; transition e_2 - blue shaded area). The slower off-time signal (Slow signal) is then dominated by distant pairs which had very low probability of recombining from the ground state within the laboratory time scales. As the electrons in these distant pairs cannot recombine easily by tunnelling from the excited state, they have a relatively higher probability for retrapping or for lateral migration into the band tails (PAD; the tunnelling probability decreases exponentially with distance, therefore, there will be an exponential increase in the probability of retrapping/band tail transport for electrons with farther holes). Since the electrons giving rise to the Slow signal did not have close nearest neighbours (i.e. low probability for ground state tunnelling) to begin with, it is not surprising that the Slow signal shows a high stability.

These effects will be more pronounced in the initial part of the pulsed IRSL measurement than in the latter part, since the prior IR illumination causes a reduction in the nearest neighbours thereby increasing the probability that any visible recombination arises from 'distant pair' contribution through the band tail transport (confirmed by data in Figs. 9.6b, d). Thus, the slow signal after prior IR illumination has the maximum likelihood of selecting the most stable configuration of electron and hole trapping centers. This combined selection gives rise to a stable signal in our otherwise rapidly fading samples.

The post-IR IR signal during the subsequent on-time must also be a combination of tunnelling from the excited state and band tail routed recombination assisted by the elevated temperature (Fig. 9.3, transition d_1), if it arises from the same trap. The latter route is, however, expected to be more important compared to TR-IRSL because of increased partitioning into the band tail states due to the temperature effect. Moreover the tunnelling from the excited state will be less important as a large proportion of the nearest neighbours are used up by the prior IR measurement (50°C for 100 s). A combination of these two effects causes a much larger Slow-to-Fast signal intensity ratio in post-IR TR-IRSL compared to the TR-IRSL (Fig 9.2a). Since the dominant mechanism is relatively distant recombination in the post-IR IRSL signal, the difference in the stabilities of on- and off-signals is much smaller in comparison to the TR-IRSL signal. It is, however, intriguing that there appears to be a trend in the post-IR IRSL signal (Fig. 9.6d, Table 9.1) which suggests that the off-time signal is less stable then the on-time signal in the three out of five samples (Table 9.1); this could suggest that the high temperature IR might excite trapped electrons in some deeper, unstable (tunnelling wise) traps to low energy band tails and from where they undergo a slow recombination. These traps are otherwise not accessible by room temperature IR excitation. This speculation requires further investigations.

9.6   Effect of thermal and optical history on the recombination process

The results discussed above suggest that the key feature in feldspar OSL generation is the proximity between the electron and the hole trap. This implies that any prior thermal (e.g. preheat) or optical treatment (bleaching) will strongly affect the recombination process, depending on how it changes the donor-acceptor distribution (i.e. the mean separation). In the following subsections we investigate the effect of prior thermal and optical annealing on the signal shapes. These investigations also serve as a test of the feldspar model described in Fig. 9.3 and have practical implications for understanding the effect of prior conditioning in dosimetry.

9.6.1   Prior thermal anneal (preheat)

The effect of preheat in the range 260°C and 460°C is shown in Fig. 9.7 for the TR-IRSL (9.7a), post-IR TR-IRSL (9.7c) and TR-GLSL (9.7e) off-time curves. The TR-GLSL decay becomes gradually faster with the preheat temperature, while the TR-IRSL decay rate becomes significantly slower for the highest two temperatures. The respective Fast and Slow signals are shown in Figs. 9.7b, 9.7d, and 9.7f, and these show that in case of TR-IRSL, the Fast signal depletes more rapidly than the Slow signal above 340°C, whereas for the TR-GLSL the Slow signal depletes more rapidly than the Fast signal. We note that the constant instrumental background is far smaller than the signal even at highest temperatures; therefore, the effects observed are not an instrumental artefact. The post-IR TR-IRSL shows behaviour in between these two cases, i.e. the Fast and Slow signals deplete approximately at the same rate.
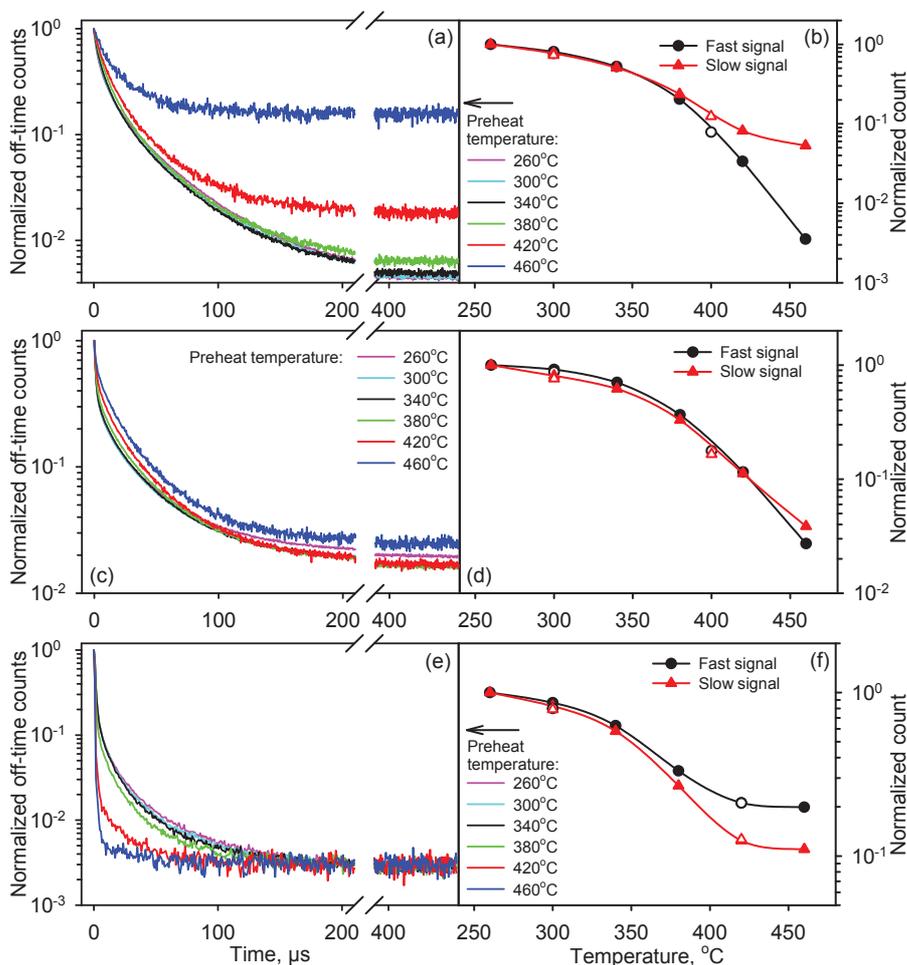
Figure 9.7: Preheat temperature dependence of the TR-IRSL, post-IR TR-IRSL, and TR-GLSL off-time signals for an aliquot of orthoclase feldspar. The aliquot was given a dose of 25 Gy (IR stimulations) or 100 Gy (green stimulation) followed by a preheat between 260°C - 460°C for 60 s in different cycles. All curves have been normalized to the last point in the on-time. The summary curves (on the right hand side) show the normalized behaviour of the fast (circles) and slow (triangles) signals of the time-resolved curves. All open symbols denote recycling points. (a) The TR-IRSL off-time curves measured at 50°C. (b) Summary of the TR-IRSL curves. (c) The post-IR TR-IRSL off-time curves measured at 230°C following IR stimulation at 50°C for 100 s. (d) Summary of the post-IR TR-IRSL curves. (e) The TR-GLSL off-time curves measured at 50°C. (d) Summary of the TR-OSL curves. Note that the legends for (a) and (e) are shown in (b) and (f) respectively.

These data suggest that for the same preheat temperature the relative partitioning between the Fast and Slow recombinations is dependent on the stimulation energy, IR or green. To understand these data it is important to include purely thermal excitations in the feldspar model; these are depicted as transitions 'a' (dashed arrows) in Fig. 9.3. According to the band structure shown in Fig. 9.3, there should exist a continuum of thermal excitations from the bottom edge of the band tail states to the excited state of the trap and eventually to the conduction band. Once the electrons occupy these different energy states, they will behave exactly in the same manner as they do during thermo-optical excitations discussed in section 9.4. In particular, thermally evicted electrons in the band tail states undergo localised recombination, the extent of which depends upon electron mobility (PAD) which in turn depends on the occupied energy level. The higher the temperature, the higher the occupied energy level, the more delocalised the recombination.

With this perspective, we look at the preheat dependence of the TR-OSL data again. Because there exists a continuum of transitions in the band tails, there is a corresponding continuum of recombination volumes accessible during the preheat. The preheat causes a recombination front which gradually sweeps increasing volumes with temperature, thereby, resulting in an increase in the mean nearest neighbour (donor-acceptor) distance. Since the Fast IRSL signal arises from a more localised recombination compared to Slow signal, i.e. transitions e_2 compared to $d_1 \ldots d_2$, respectively (Fig. 9.3), it gets preferentially more affected (depleted) by preheat than the Slow signal (Fig. 9.7b). Based on this reasoning the depletion trend is expected to be reversed for green stimulation since the Fast signal TR-GLSL represents the delocalised conduction band route (Fig. 9.3, transition c), while the Slow signal represents, a relatively more localised band-tail route (transitions d_2); this is exactly what is observed in our data (Fig. 9.7f). These changes in the relative importance of the localised and delocalised recombination routes govern the TR-IRSL and TR-GLSL decay shapes observed in Figs. 9.7 and 9.7e, respectively. For example, in the TR-GLSL data, the conduction band route (Fast signal) becomes increasingly clearer due to rapid dampening of the band tail signal (i.e. the Slow signal) by localised recombinations during the preheat (Fig. 9.7e).

In summary, the observation of the reversal in the depletion of the Fast and Slow signals for IR and green excitations lends further supports to our proposed model on the origins of TR-OSL for resonant and non-resonant excitation. For dosimetry, these results imply that a preheat of at least 350°C, where one begins to observe differences in the relative depletion of the Fast and Slow signals, should be used to preferentially isolate a stable signal. In general, the higher the preheat temperature the more stable the signal because of an increase in the mean donor-acceptor distance; these distant pairs are more likely to survive ground state tunnelling. Note that this dependence on preheat should not to confused with the widely understood thermal stability of the electron trap based on the trap depth.

9.6.2   Prior optical annealing (bleaching)

In order to investigate the relative changes in the Fast and Slow signals as a function of optical exposure a long pulsed measurements of 1500 s duration (IR signals) and 500 s duration (green signal) were undertaken using an on-time of
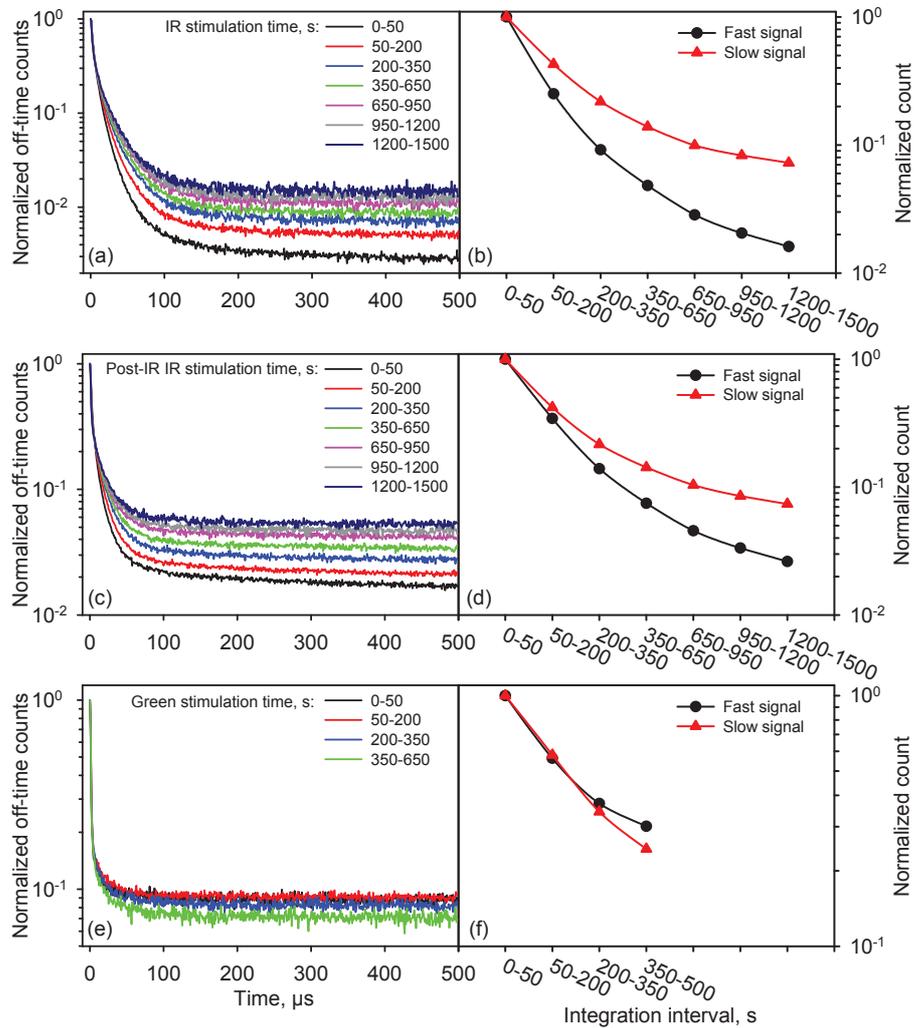
Figure 9.8: Stimulation time dependence of the TR-IRSL, post-IR TR-IRSL, and TR-GLSL off-time decay curves from orthoclase feldspar normalized to the last point in the on-time. The sample was preheated to 250°C for 60 s following a dose of 45 Gy (IR signals) or 100 Gy (green signal). The TR-IRSL signal was measured at 50°C for 1500 s, the post IR (at 50°C for 100 s) TR-IRSL signal was measured at 225°C for 1500 s, and the TR-GLSL was measured at 50°C for 500 s. The stimulation pulses produced during the stimulation time intervals given in the figures were added up to produce the normalized off-time curves shown on the left had side; the legends show the stimulation time intervals during which the TR-OSL signals were added to produced these curves. The summary curves on the right hand side show the normalized behaviour of the fast (circles) and slow (triangles) signals of the time-resolved curves. Each point in the summary was normalized to the duration of the stimulation time interval, as these are of unequal length, so as to be able to compare the data. The data were then further normalised to the first point on the plots. All open symbols denote recycling points. (a) TR-IRSL off-time curves, (b) summary of the TR-IRSL curves, (c) post-IR TR-IRSL off-time curves, (d) summary of the post-IR TR-IRSL curves, (e) TR-GLSL off-time curves, and (f) summary of the TR-GLSL curves. Note that the integration intervals for the green stimulation are not identical to those of the IR stimulations.

50 μs and an off-time of 500 μs. The post-IR TR-IRSL signal was measured at 225°C. By summing up the signals from stimulation pulses emitted during different intervals of the pulsed measurements, the progressive change in the off-time decay shape with pulsed stimulation time (this time can be considered as the duration of prior bleaching with the same wavelength as the measurement) can be observed. The data are shown in Fig. 9.8a for the TR-IRSL and in Fig. 9.8c for the post-IR TR-IRSL for the pulse integration intervals 0-50 s, 50-200 s, 200-350 s, 350-650 s, 650-950 s, 950-1200 s, and 1200-1500 s. The TR-GLSL signals are shown in Fig. 9.8e using integration intervals of 0-50 s, 50-200 s, 200-350 s, and 350-500 s.

The summaries of the Fast and Slow signals derived from these data are shown in Figs. 9.8b, d, f. Both the IR and the post-IR IR signals show that the Fast signal decreases much more rapidly in contrast to the Slow signal with the prior IR or post-IR IR bleach duration. In the limited data we have for green light, there is a tendency for this trend to be reversed. Here the Fast signal depletes less rapidly than the Slow signal with the prior bleach duration. We note that the observed behaviour of the Fast and Slow signals in the two TR-IRSL signals is representative as it was also observed in the other two feldspar specimens of completely different composition (the albite and the anorthite).

The interpretation of the bleaching data is similar to the preheat data. For IR stimulation the nearest holes are preferentially used up by excited state tunnelling as the stimulation proceeds (Fig. 9.3, transition e_2). Essentially, the recombination front progresses as IR stimulation sweeps out increasingly distant pairs. Since the Fast signal arises from a more localised recombination (the tunnelling from around the excited state), than the Slow signal (distant recombinations through the band tails), the former is affected much more by prior bleaching than the latter. The green data on the other hand, should show a reverse trend since its Fast signal arises from a delocalised recombination (Fig. 9.3, transition c), i.e. from the conduction band and is, therefore, not limited by hole concentration, whereas, its Slow signal arises through a more localised recombination through the band tails (Fig. 9.3, transition d_1), and, therefore, suffers because of prior reduction in hole concentration by recombination of thermalised electrons during bleaching.

These data again confirm our model for recombinations in feldspar. The practical implications of these data for dosimetry are that the longer the IR bleach before an IRSL measurement, the more stable the IRSL signal. This was exactly observed in the g-value comparison of early and late CW-IRSL signals by Thomsen et al. (2008). Note that this approach does not apply to the green stimulation because of delocalised recombination.

9.7 Mechanisms for band tail emptying

The discussion in the previous sections suggests that electrons in the band tail states recombine via phonon (0.05-0.06 eV) assisted diffusion, irrespective of whether they arrive from the excited state of the trap (1.42 eV excitation) or from the conduction band (2.63 eV excitation). The change in the initial TR-IRSL decay rate with IR stimulation temperature (Figs. 9.4a and 9.4c), further suggests an increased partitioning from the excited state to the higher energy band tail states. It is expected from the Boltzmann's distribution that
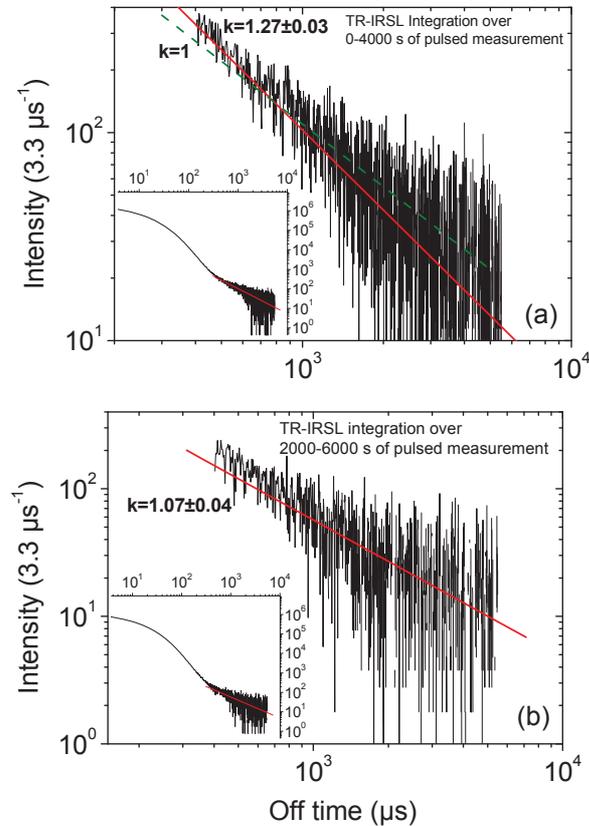
Figure 9.9: Off-time TR-IRSL signals from an aliquot of orthoclase feldspar after a dose of 45 Gy and a preheat to 250°C for 60 prior to the TR-IRSL measurement at 20°C for 6000 s. The TR-OSL measurement were made using an on-time of 10 µs and an off-time of 5.5 ms. (a) Data obtained from integrating pulses from 0-4000 s, (b) data obtained from integrating pulses from 2000-6000 s. The insets to the two figures show the entire off-time data, whereas the main figures show data only >400 µs fitted to the power law: $I = t^{-k}$ after Huntley (2006) shown as red lines. The dashed green line indicates a slope of $k = 1$.

a proportion of these electrons will eventually completely thermalise and come to occupy the deep, disconnected, band tail states. The eventual fate of these thermalised electrons is investigated below.

An aliquot of orthoclase feldspar was given a dose of 45 Gy and was preheated to 250°C for 60 s prior to the TR-IRSL measurement lasting 6000 s. We chose an IR on-time of 10 µs, and a longer off-time of 5.5 ms and the minimum temperature of 20°C possible in our measurements.

The data are shown in Figs. 9.9a and 9.9b where the pulses between 0-4000 s and between 2000-6000 s have been integrated, respectively. These data are plotted on the log-log scale and show two straight line components: 50-300 µs and >300 µs (See the figure insets). A straight line fitted to the latter part of the data (after removing the initial 400 µs of the off-time), shows that the TR-IRSL decay follows the $t^{-1.27}$ (Fig. 9.9a) and $t^{-1.07}$ (Fig. 9.9b) relationship.

Note that data collected 100 μs after the light pulse (an order of magnitude higher than the on-time) could be considered to arise from instantaneous illumination, see Visocekas (1985). Huntley (2006) shows that tunnelling induced fading for a random distribution of holes around a trapped electron follows a power law where the exponent of 't' is expected to vary between 1-1.5. Our slowly decaying data on the time scale of the >400 μs agrees very well with this prediction. We can, therefore, conclude that a significant proportion of the Slow signal arises from emptying of the deep, disconnected band tail states by tunnelling. This mechanism is shown as transition d_3 in the Fig. 9.3.

The exponent for the decaying signal between the fast initial decay (represented by our Fast signal) and the Slow signal (i.e. the signal between 50 and 300 μs) is ~2.5 (see the two insets; the fitting is not shown). This slope is too high to be attributed to tunnelling. As discussed earlier, this relatively rapidly decaying signal arises from a sub E_C phonon (0.05 eV) assisted transport; note that all the earlier characterizations of the Slow signal in this article pertain to this component as the measurements only extended to 500 μs. The overall decay form of this signal likely consists of several exponentials (or possibly a stretched exponential), because of different electron energy states in the band tails.

Based on a crude estimate from our data measured at 20°C, ~80% of the charge carried to the band tails (Slow signal) recombines by phonon assisted diffusion, and ~the remaining 20% by tunnelling. These numbers will change with the stimulation temperature and the density of states in the sample.

9.8 Discussion: The feldspar model

9.8.1 Processes

Based on the different investigations above we conclude that the fast decay in the TR-OSL (Fast signal) represents tunnelling from the excited state for IR stimulation, and a conduction band routed recombination for green and blue stimulations. On the other hand, the slower decay (Slow signal), which extends up to milliseconds arises from a relatively sluggish recombination from the band tails caused by a combination of phonon assisted diffusion and tunnelling. This model predicts that for IR stimulation the Slow signal preferentially selects electrons that lack proximal donor-acceptors, and, therefore, is more stable. This prediction is confirmed from the fading experiments in all the samples examined. The model is discussed in detail below.

The Slow TR-GLSL and TR-IRSL signals show an exponential dependence on stimulation temperature. Using these signals, the activation energy for thermally assisted diffusion in the band tails is calculated to be 0.14 eV, corresponding to a lattice phonon mode of 0.05 eV, see Poolton et al. (2002b) for details. This energy is indistinguishable for IR and green stimulation and, therefore, truly characterises the lattice phonons involved in band tail transport, irrespective of whether the excitation was resonant or non-resonant. This similarity in the Slow signal behaviour for IR and green stimulations is an important direct evidence for band tail transport in feldspars.

Unlike the Slow signal, the Fast signal shows an exponential dependence on temperature only for the green stimulation (activation energy 0.06 eV). This behaviour suggests that the trap depth for the dosimetric trap should be

slightly greater than 2.4 eV since Fast TR-GLSL signal is a conduction band routed phenomenon. The Fast TR-IRSL and post IR TR-IRSL signals do not show clear exponential dependence on thermal energy as charge loss occurs via both the excited state and the band tail states.

The rate of decay of the fast signal is independent of stimulation temperature for the green stimulation, which suggests that the recombination rate does not depend upon the energy level in the conduction band (transition c, Fig. 9.3). On the other hand, for the IR stimulation we see a strong increase in the decay rate of the Fast signal with stimulation temperature (up to 100°C) possibly because of thermally enhanced transitions from the excited state to the band tail states which result in an overall decrease in the residence time of the excited state. Note that the energy transitions in the recombination centers are faster than ns time scales, therefore the change in the decay rate cannot be attributed to thermal quenching (Ankjærgaard et al., 2009, Chapter 7 of this thesis).

Different mechanisms that lead to the occupancy of the band tail states are shown as upward and downward facing curved arrows around the photoionisation transitions b in Fig. 9.3. The IR light places the electrons in the excited state; some of these electrons enter the band tail states by phonon assistance. The green stimulation causes sub-conduction-band excitation; a fraction of these enter the conduction band by phonon assistance, while the remaining electrons diffuse into the band tail states. The efficiency of transport (electron mobility) is variable within the band tail states because of wider wavefunction and greater density of states with energy. Therefore, the fact that the Slow signal for both IR and green excitation is characterised by the same activation energy (0.14 eV) suggests that a significant proportion of the excited electrons thermally decay/excite to occupy an equilibrium energy distribution, irrespective of the excitation energy (downward facing curved arrows in Fig. 9.3). Following Boltzmann's distribution, the mean energy increases linearly with temperature. At the same time the density of available states increases exponentially with energy (Fig. 9.3, left). Thus an increase in temperature corresponds to an exponential increase in occupancy of the equilibrium energy states, reflected as an exponential increase in luminescence in Fig. 9.5b.

Although we have not measured thermal dependence of the blue stimulated signal because of instrumental limitations (blue detection), the similarity of TR-OSL shapes for the blue and green excitations suggests that the blue excitation behaves like the green; however, because of its higher energy it transports a significantly greater proportion of electrons ($> 20\%$ at the room temperature) to the conduction band (See discussion in section 9.3).

A majority of the electrons then leave the band tails via thermal hopping mechanisms, $d_1 \ldots d_2$ (Fig. 9.3) in the band tails, depending on the equilibrium thermal energy level. However, importantly, at room temperature we show that recombination can also occur via tunnelling from the deeper band tail states within the band gap (Fig. 9.9; Fig. 9.3 - transition e_2). Thus, the residence time within the band tails is determined by the energy level occupied; the former process dominates the first 300 μs of the TR-IRSL off-time data, while the latter recombination is obvious from ~300 μs to up to several milliseconds. At higher energies there is both an exponential increase in the density of states (See Fig. 9.3, left diagram) as well as a more widespread electron wavefunction; a combination of the two causes an efficient sub E_C transport

(i.e. a faster signal which decays in the first 300 μs). While in the deep band tails, the thermalised electrons are permanently, for our time scales so to speak, embedded in deep, disconnected potential wells, and from here they undergo a slow (tens of ms) tunnelling transition to holes, or to shallow electron traps (Ankjærgaard and Jain, 2010, Chapter 8 of this thesis) elsewhere in the lattice. For these latter electrons a power-law decay is expected, a behaviour arising for a random distribution of acceptors around a trapped electron (e.g. see Tachiya and Mozumder (1974); Huntley (2006)). This model of different recombination routes depending on the electron energy assumes that band tail states are characterised by a variety of well depths, widths and separations (Poolton et al., 2002a,b). The model implies that there will always be a predictable temperature dependent partitioning between the two band tail emptying mechanisms ($d_1 \ldots d_2$ vs. d_3). At 20°C we find that ~80% of the electrons in the band tails follow the PAD route, while ~20% follow the tunnelling recombination route.

We further propose, based on our preheat data, that thermal excitations have the same effect as the optical excitations, except that there exists a continuum of excited levels, from the bottom of the band tail states. This is shown as the dashed arrow region in transition a (Fig. 9.3). Once in these different energy levels in the band tail states, the electrons behave in the same manner as those after optical excitations.

Most of our post-IR IR data can be explained in terms of the above model; it can originate in the same manner as the IR signal, although the thermally assisted process is more important here. However, there is one intriguing observation that does not fit the model, i.e. the on-time signal of elevated temperature post-IR TR-IRSL is somewhat more stable than the off-time signal (see Fig. 9.6b and d). This observation perhaps suggests that there may be another deeper trap that contributes to the slow signal in the post IR-IRSL signal; this requires further investigation. Nonetheless, the on-time signal, which dominates CW post IR-IRSL signal is well explained by single trap model shown in Fig. 9.3.

9.8.2 Luminescence efficiency

We define luminescence efficiency as the luminescence photons produced per excited electron. According to the model (Fig. 9.3), luminescence can be produced following different routes: conduction band (c), thermally assisted hopping through the band tail states ($d_1 \ldots d_2$), tunnelling from the basal, disconnected band tail states (d_3), and tunnelling from the excited state of the trap (e_2). As discussed in the model above, there is a strong competition and thermal partitioning between these different routes, especially in the band tail states. At the same time these recombination processes compete with retrapping (f), an effect that can be especially important for electrons with distant recombination centres.

We discussed in the previous section that the electron mobility strongly varies within these different energy states. In general, the higher the energy the greater the electron mobility. Thus, the probable volume in which an electron can find an acceptor will vary with the extent of electron mobility in the order $e_1 \ll e_2 < d_3 < d_2 < d_1 < c$; ground state tunnelling is the most localised recombination, while conduction band recombination accesses, in principle, the entire crystal. This effect is schematically shown as vector r in the Fig. 9.3

which illustrates the maximum separation between the electron and the hole that can be overcome to produce luminescence from a particular energy level (note that this is only a schematic representation to aid visualization - the band representation in Fig. 9.3 as such does not contain any distance information). The accessible volume scales with r^3. Since the number of recombination sites is proportional to volume, the larger the accessible volume the higher the probability of recombination.

According to this model the luminescence production in feldspars is strongly limited by the availability of luminescence centres in the volume accessible by the excited electron. Particularly, there will be a strong competition between recombination and retrapping both during thermal and optical measurements. Thus, a decrease in the luminescence intensity of the IRSL or TL signals, is in most cases a reflection of decrease in the local hole population, and not the electron population; this interpretation is consistent with the observations based on radiofluorescence (Trautmann et al., 1999). The electrons that do not recombine are re-trapped either in the same dosimetric trap, or in some shallow refuge traps (Ankjærgaard and Jain, 2010, Chapter 8 of this thesis). The competition between recombination and retrapping can be varied by changing the stimulation energy, either thermally or optically, and thereby having a different partitioning between the more localised vs. less localised route. An important evidence for this interpretation is the existence of strong post-IR BSL or IRSL signals in feldspars (Jain and Singhvi, 2001; Thomsen et al., 2008). Thermal assistance increases the chances of finding an acceptor in different ways discussed in the previous section, therefore, an increase in the IRSL signal occurs with an increase in the stimulation temperature; since this is only a partitioning effect it does not really affect the shape of the signal. One important implication of the above interpretation is that the post-IR IRSL signal may just be a more efficient way of sampling the same dosimetric IRSL trap, while preferentially selecting an electron population with distant hole pairs. This interpretation is opposed to that made by Jain and Singhvi (2001) who proposed two different trap types to explain high temperature IR behaviour of K-feldspar.

9.8.3   Thermal dependence of IRSL signal (pulse anneal curves)

The efficiency effect explained above can also explain the effect of preheat on IRSL intensity, i.e. the shape of the pulse anneal curves. It is common knowledge that, unlike quartz, the IRSL signal following laboratory irradiation decreases continuously with preheat temperature (e.g. Duller (1994); Li and Tso (1994)). One commonly accepted explanation for such data is that the IRSL signal arises from a distribution of traps with different energies. As we conclude in section 9.6.1, the main effect of preheat is to remove holes by recombination through the band tail states (Fig. 9.3 - transition a). The higher the preheat, the greater the volume swept by electrons and, therefore, the lower the recombination probability for the subsequent optically excited electrons. This effect is expected to be much more severe for the laboratory irradiated samples then for the natural samples, as in the natural samples a majority of the very localised transitions would already have occurred by ground state tunnelling (transition e_1 in Fig. 9.3; note that e_1 is the most localised transition). Moreover, this effect will be more severe for IR stimulation than for green or blue

stimulation. *Based on the model we conclude that the pulse-anneal measurements (variation in IRSL intensity as a function of preheat temperature) do not measure the trap's thermal stability (thermal trap depth) but rather IRSL sensitivity arising from tunnelling stability.* A pulse anneal curve should, therefore, be interpreted to reflect the stability of the existing electron-hole pairs, a function of the mean electron-hole separation, rather than the potential energy of the trapped electron.

Since higher temperature stimulations access a greater volume of the crystal (higher luminescence sensitivity), the model predicts that the shape of the pulse anneal curve will depend on the stimulation temperature. The curves measured at higher temperature will apparently appear to be more stable since the distant holes are more stable than the proximal holes. Thus it is possible to produce different pulse anneal curve shapes from a single electron trap. Since these data do not reflect depletion of the electron trap, using them for estimation of trap depth will be erroneous.

The above interpretation of the luminescence efficiency may raise questions on the utility of test dose correction in feldspar dosimetry. It is conceivable that the correction signal largely arises from a new electron-hole distribution arising from the test dose that does not reflect the state of the sample after thermal erosion. Whether or not this effect is important depends upon the spatial distribution of e-h pairs arising from the test dose. Nonetheless, it is conceivable that, if a test dose has to be used for better dose response reproducibility, then exactly the same preheat treatment should be used for the regeneration and test dose to ensure that there are similar mean electron separations in the two cases. This interpretation explains earlier results that an identical treatment helps in getting a better dose recovery in feldspars (Blair et al., 2005).

9.8.4 Origin of the post-IR IRSL signal

The first IR bleaching consumes the proximal pairs by recombination from around the excited state of the trap (Fig. 9.3, e_2). The luminescence efficiency decreases because of reduction in the accessible hole population from the excited state of the trap; this is seen as a rapid decrease in the signal. The later high background level in the room temperature IRSL curves indicates a quasi-equilibrium between the rate of excitation and the rate of retrapping. A subsequent IR measurement at elevated temperature is able to access a greater volume of the crystal through the high energy band tail states (d_1 in Fig. 9.3) and thus able to access distant holes; therefore there is a rejuvenation of the IRSL signal. Since this post-IR IRSL signal is borne out of preferentially isolated distant electron-hole recombinations (the most proximal pairs are removed by the first IRSL), it is much less affected by ground state tunnelling, and hence is more stable. This is shown in the data of Thomsen et al. (2008); Buylaert et al. (2009).

The model predicts that the higher the post- IR IR stimulation temperature, the greater is the volume swept by excited electrons. Since an increase in the potential recombination volume increases the probability of distant electron-hole recombinations, it is predicted that the stability of the post IR-IRSL signal will increase with the stimulation temperature. This electron-hole pair stability will also be reflected in the pulse-anneal curves discussed in the previous section.

9.8.5   Thermoluminescence in feldspars

One important inference from the preheat data is that during thermal stimulation, significant localised recombinations occur through the excited state of the trap and through the band tail states (transition a, Fig. 9.3). This interpretation can explain broad TL peaks even though the dosimetric trap lies at >2.4 eV, and suggests that we may need to revisit our earlier estimates of E and s analysis in feldspars (e.g. Trautmann et al. (1997); Li and Tso (1994); Murray et al. (2009)) in the light of alternative recombination pathways during thermal excitation.

Based on a consideration of the density of states (Fig. 9.3, left diagram), we predict two coexistent TL peaks in feldspars: (a) a relatively narrow, lower temperature peak with a sharp rise and a sharp fall, arising from the excited sate (1.5 eV optical depth) of the trap and (b) a broad higher temperature peak with a gradual rise and sharp fall, arising from the high-energy band tails states and the conduction band (>2.4 eV optical depth). The net luminescence curve will be a convolution of the availability of net electron occupancy in each state and the probable recombination volume associated with that state (see discussion in the previous section). This prediction is consistent with a broad TL peak observed in feldspars, sometimes with two humps at around 100 and 300°C. If one assumes an optical to thermal depth ratio of 1.7 for silicates then the predicted E values for the two peaks based on TL analysis will be 0.9 and >1.5 eV. However, feldspar TL data is in general difficult to analyse because of the very broad shape of the feldspar TL peak. Numerical simulations of our model to include both the energy states as well as the localised-volume dependent recombination sensitivity can test these predictions. Also, thermally stimulated exo-electron measurements can throw further light on this subject.

9.9   A look forward

Based on the model (Fig. 9.3), the best method to isolate a stable signal in feldspars is to selectively look at the distant pairs. Our model shows several possible ways of selecting the non-fading or least fading signal from feldspars for routine dating applications:

(a) Thermal preconditioning of the sample: Based on the model as well as our preheat dependence data (section 9.6.1), a higher preheat sweeps out a greater volumes of nearest neighbours (donor-acceptors); the preheat recombination front expands radially with both temperature and time. The larger the volume, the lower the probability that the remaining distant pairs would fade in nature. Thus one can selectively look at the most stable traps. The best results will be obtained by restricting thermal energies such that the equilibrium population is below the conduction band; this can only be determined from an exact measurement of the trap depth. From our measurements we think that a preheat of 350°C would greatly help in isolating a less fading signal.

(b) Low energy optical or thermo-optical pre-conditioning of the sample: Based on our prior bleach data (section 9.6.2), an elevated temperature IR bleach can be used to obtain the same result as that with thermal
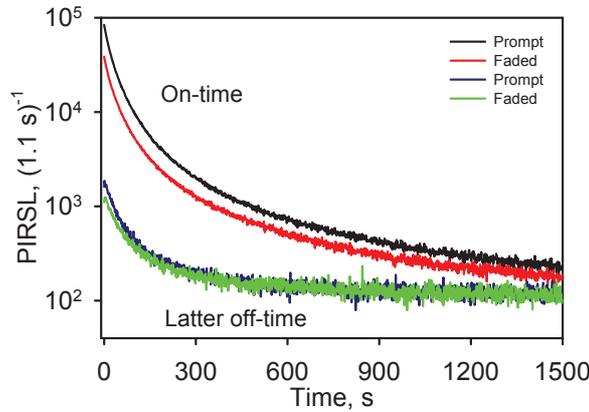
Figure 9.10: PIRSL curves for the Prompt 1 and delayed (faded) measurements. These curves are calculated by integrating different sections of the TR-IRSL curves from Fig. 9.6b down the pulsed measurement time. The different integration intervals are: the on-time: 0-50 µs, and the latter off-time: 300-500 µs.

pre-conditioning. However, an optical bleach is likely to be much more efficient at eliminating nearest neighbours since it causes a direct transition to the excited state which corresponds to a peak in the density of states (Fig. 9.3); from here a large number of electrons can efficiently tunnel out to the nearest centres (the Fast TR-IRSL signal). Thermal effects on the other hand will be more diffuse because of significant transport (thermal hopping) in the band tail states. In principle a broad band IR illumination covering the energy of the band tail states above the ground state would be an ideal pre-treatment of the sample to isolate the least fading signal; in practice this can be easily achieved by stepwise illumination with different energies. Similarly a stepwise increase in temperature could be used for a fixed photon energy; in such an approach both an increase in the prior IR temperature and the post IR temperature will give more stable signals. Promising results have been obtained in this class of measurements using a prior-IR (50°C)-bleached, elevated-temperature IRSL signal (230°C) at our laboratory (Thomsen et al., 2008; Buylaert et al., 2009). The limiting case for this class of measurements will be a high temperature IR bleach (to annihilate all the pairs that can tunnel out in the geological time scales), followed by a resonant excitation that uses the conduction band route to access the most distant acceptors.

(c) Direct examination of the distant pair recombination: we have concluded earlier that the Fast TR-IRSL signal arises by tunnelling from the excited state, whereas the Slow signal arises from the band tail states. Thus, according to our model, the Slow signal selectively arises from distant pair recombinations. A combination of methods (b) and (c) would allow us to isolate a non-fading signal in our otherwise highly fading samples. This amounts to examination of the Slow signal after a prior IR illumination, which can be equivalent to analyzing the data collected during the later part of the TR-IRSL measurement. The pulsed IRSL (PIRSL) curves de-

rived from different sections of our TR-IRSL data are shown in Fig. 9.10 for albite feldspar. It is clear that the delayed signal from the 350-550 μs integration in the off-time is faded in comparison to the prompt signal in the first 200 s of the measurement. Thereafter, the prompt and the delayed signals are almost identical throughout the remaining of the 1500 s measurement. On the other hand the two signals obtained from integrating the on-time differ significantly throughout the 1500 s (note that this on-time signal would govern the fading characteristics of the CW-IRSL signal). The data suggests that a non-fading signal can be measured with pulsed IRSL by gating the counting interval to the off-time and only using the data obtained in the later part of the PIRSL measurement (i.e. by ignoring the initial data equivalent to the first 9 s of the CW-IRSL measurement with our stimulation intensity). Based on our fading measurements we think that this pulsed signal should be more stable than the CW post-IR IR measurements ((Thomsen et al., 2008; Buylaert et al., 2009) (See Table 9.1); nonetheless, the post-IR IR measurement has a high sensitivity and, therefore, is attractive for routine applications.

All these different methods of isolating a stable signal rely on the fact that there exist isolated traps with distant centers (acceptor sites), such that it is not possible to trap any holes in the vicinity during burial irradiation. Such a scenario is not possible for a random distribution model (Huntley, 2006) where every electron trap has a similar surrounding distribution of hole trapping centers. At a given time during burial there exist a continuum of distant (stable) and proximal (unstable) pairs. However, this association is dynamic in time - for example, at a given instance a stable electron can potentially become unstable because of trapping of a hole in a nearby empty center. Because of this dynamic nature of electron hole trapping, one cannot conclude whether there exist geologically stable electrons in feldspars or not unless the exact distribution of traps and holes is known. A useful understanding in this direction can be obtained by specific examination of the scales of luminescent heterogeneities (Larsen et al., 2009), and quantitative estimation of donor - acceptor distances in feldspars, and by generation of large body of empirical data that can test the geological stabilities of the proposed stable signals. If the proposed signals do not fade over geological time scales then it is likely that feldspar consists of associated donor-acceptor pairs rather than random distribution of acceptors.

9.10   Conclusions

A comprehensive model of feldspar luminescence is proposed for the first time. The model is based on a single dosimetric trap and it highlights the important role of band tail states in explaining a range of observed thermal (TL) and thermo-optical (OSL) phenomena in feldspars.

It is demonstrated through TR-OSL measurements that electron transport route following an optical excitation pulse strongly depends on the energy of the incident photon. Following excitation there occurs (a) a fast recombination either from the excited state of the trap (for resonant IR excitation at ∼1.4 eV; <100 μs) or from the conduction band (for non-resonant excitations at

2.63 and 2.36 eV; <1 μs), and (b) a slow recombination (up to several milliseconds) from the band tail states irrespective of the excitation photon energy. For non-resonant excitations, the band-tail states are populated by direct sub conduction band transition (green photons, $\sim$2.36 eV) and/or by thermalisation of conduction band electrons. The band-tail transport includes two main thermally competing pathways: a relatively efficient sub E_c transport assisted by strong lattice vibrations corresponding to 0.05-0.06 eV phonons ($d_1 \dots d_2$), and a slow tunnelling recombination from localised, deep lying, disconnected band tails (d_3). The tunnelling recombination can be observed for several ms and follows a power law.

Pure thermal excitation uses a continuum of band tail states; the evicted charge undergoes the same localised recombination routes as after optical excitation. In particular, the prior thermal anneal (preheat) results in an expanding recombination (fading) front that increases the mean donor-acceptor distance; this helps in isolating a more stable signal. According to this model an estimation of trap depth based on thermal anneal data is erroneous.

The model predicts three different possible ways of isolating the most stable signal in feldspars (a) intense thermal pre-treatment ($>350°C$), (b) sub E_c optical pre-shine (e.g. IR bleach at different energies and/or temperatures) followed by observation of distant e-h recombinations (high temperature post-IR IRSL), and (c) selective observation of the band tail transport using pulsed stimulation. These methods can be used in combination. Of special importance to the sediment dating application is the discovery of a non-fading signal (on our laboratory time scale) in samples that otherwise show a very high fading rate in the CW-IRSL measurements ($g_{2d} \sim 20\%$/decade). This non-fading signal is generated using pulsed stimulation and is observed to be more stable than the post-IR TR-IRSL signal. Future effort should focus on a thorough testing and inter-comparison of these methods to solve the long standing problem of anomalous fading.

Acknowledgements

Appendix

We define the duration of each stimulation LED pulse as the on-time, and the duration between two pulses as the off-time [see also Lapp et al. (2009, Chapter 2 of this thesis)]. During a pulsed measurement, the Photon Timer records the time of arrival of photons detected relative to the beginning of the preceding LED pulse. The total number of these stimulation pulses depends on the measurement time. We use the following abbreviations to describe the TR-OSL signals on the basis of stimulation wavelength:

TR-OSL: Time-resolved optically stimulated luminescence (for all photon energies).

TR-IRSL: Time-resolved optically stimulated luminescence measured using IR stimulation. This signal is measured at 50°C unless stated otherwise.

Post-IR TR-IRSL: Time-resolved optically stimulated luminescence measured using an elevated temperature (230°C unless otherwise stated) IR stimulation after a prior IR bleach (at 50°C for 100 s unless otherwise stated).

TR-GLSL: Time-resolved optically stimulated luminescence measured using green light stimulation. This signal is measured at 50°C unless stated otherwise.

TR-BLSL: Time-resolved optically stimulated luminescence measured using blue light stimulation.

E_c: Conduction band edge

During the off-time decay, the very initial part will be dominated by the fast decay followed by a more slowly decaying signal (Figs. 9.1b, c). To be able to make quantitative distinctions between behaviour of the different parts of the TR-IRSL, post-IR TR-IRSL, and TR-GLSL signals, it is imperative to define some signal integration intervals. This is a challenge since the exact decay form of components in the TR-OSL curves is not known. In the absence of a mathematical model to resolve our components, we followed a simpler approach of defining integration intervals by visual examination so as to identify the major changes in the curve shapes. Based on several examinations of our data we finally found that the very initial and the late parts of the TR-OSL decay curves behave very differently under different measurement conditions. The challenge then was to optimise the integration intervals to obtain a good separation of the physical processes giving rise to these different parts of the curves. The criteria chosen to estimate these initial and late signals, hereafter the 'Fast signal' and the 'Slow signal', are described below.

The Fast signal: The simplest extraction of the Fast signal is the integration of the first few channels of the time resolved decay curve. However, since the signal drops very rapidly (Figs. 9.1b, c), there is a risk of significant contamination from the slowly decaying part of the signal. To minimise this problem we chose to integrate over the total signal obtained during the on-time (0-50 μs) as a proxy for the fastest decaying signal in the off-time decay curve. In the on-time the Fast signal undergoes a quick build-up to an equilibrium level where the rate of stimulation equals the rate of luminescence production (note that the latter includes recombination and a quick ns relaxation), whereas the slower signal, which is orders of magnitude slower, is only beginning to build up (Ankjærgaard and Jain, 2010, Chapter 8 of this thesis). By integrating the curve only in the off-time one obtains the worst ratio of the Fast to slow signals, since the slow component has built up to its maxima at the end of the on-time. On the other hand, integration of the entire on-time area reduces this contamination by including additional channels where the Fast to slow ratio is relatively higher, and at the same time gives good counting statistics. We estimate that contamination of slow signal in the on-time integral is less than 5%. This estimation method is a useful compromise

as we are only interested in the relative changes in the intensity of the Fast signal under different conditions and not the absolute Fast signal intensity.

The Slow signal: Ankjærgaard and Jain (2010, Chapter 8 of this thesis) show that in the IR and post-IR signals from a K-feldspar sample there exists a distinct, strongly stimulation-temperature dependent component, which is evident from a few tens of microseconds to over several milliseconds. In the present study the slowly decaying component clearly evident from about 100-550 μs (Fig. 9.2b) shows the same behaviour as the above mentioned slow component of Ankjærgaard and Jain (2010, Chapter 8 of this thesis). To quantify this signal, termed the 'Slow signal' we use an integration over 100-550 μs of the IR off-time signal (50 μs is the end of on-time) to allow for the decay of the Fast signal. For the TR-GLSL signals, the initial decay is much faster than in the IR signals; see Fig. 9.2c, so here the 'Slow signal' is instead defined to be the integration over the 60-550 μs in the off-time signal.

References

Aitken, M. J. (1985). *Thermoluminescence Dating.* Academic Press, INC., London, UK. ISBN: 0–12–046380–6.

Ankjærgaard, C. and Jain, M. (2010). Optically stimulated phosphorescence in orthoclase feldspar over the millisecond to second time scale. *Journal of Luminescence*, 130:2346–2355.

Ankjærgaard, C., Jain, M., Kalchgruber, R., Lapp, T., Klein, D., McKeever, S. W. S., Murray, A. S., and Morthekai, P. (2009). Further investigations into pulsed optically stimulated luminescence from feldspars using blue and green light. *Radiation Measurements*, 44:576–581.

Ankjærgaard, C., Murray, A. S., and Denby, P. M. (2005). Thermal pretreatment in the OSL dating of quartz: Is it necessary? *Radiation Protection Dosimetry*, 119:470–473.

Bailiff, I. K. and Barnett, S. M. (1994). Characteristics of infrared-stimulated luminescence from a feldspar at low temperature. *Radiation Measurements*, 23:541–545.

Baril, M. R. and Huntley, D. J. (2003). Optical excitation spectra of trapped electrons in irradiated feldspars. *Journal of Physics: Condensed Matter*, 15:8011–8027.

Blair, M. W., Yukihara, E. G., and McKeever, S. W. S. (2005). Experiences with single-aliquot osl procedures using coarse-grain feldspars. *Radiation Measurements*, 39:361–374.

Bøtter-Jensen, L., McKeever, S. W. S., and Wintle, A. G. (2003). *Optically Stimulated Luminescence Dosimetry.* Elsevier, Amsterdam, The Netherlands. ISBN: 0–444–50684–5.

Buylaert, J. P., Murray, A. S., Thomsen, K. J., and Jain, M. (2009). Testing the potential of an elevated temperatures IRSL signal from K-feldspar. *Radiation Measurements*, 44:560–565.

Chithambo, M. L. and Galloway, R. B. (2000). A pulsed light-emitting-diode system for stimulation of luminescence. *Meas. Sci. Technol.*, 11:418–424.

Clark, R. J. and Bailiff, I. K. (1998). Fast time-resolved luminescence emission spectroscopy in some feldspars. *Radiation Measurements*, 29:553–560.

Clark, R. J., Bailiff, I. K., and Tooley, M. J. (1997). A preliminary study of time-resolved luminescence in some feldspars. *Radiation Measurements*, 27:211–220.

Delbecq, C., Toyozawa, and Y. Yuster, P. H. (1974). Tunneling recombination of trapped electrons and holes in KCl:AgCl and KCl:TlCl. *Physical Reviews B*, 9:4497–4505.

Denby, P. M., Bøtter-Jensen, L., Murray, A. S., Thomsen, K. J., and Moska, P. (2006). Application of pulsed osl to the separation of the luminescence components from a mixed quartz/feldspar sample. *Radiation Measurements*, 41:774–779.

Duller, G. A. T. (1994). A new method for the analysis of infrared stimulated luminescence data from potassium feldspars. *Radiation Measurements*, 23:281–285.

Duller, G. A. T. and Bøtter-Jensen, L. (1993). Luminescence from potassium feldspar stimulated by infrared and green light. *Radiation Protection Dosimetry*, 47:683–688.

Huntley, D. J. (2006). An explanation of the power-law decay of luminescence. *J. Phys.: Condens. Matter*, 18:1359–1365.

Huntley, D. J. and Lamothe, M. (2001). Ubiquity of anomalous fading in K-feldspar and the measurement and correction for it in optical dating. *Canadian Journal of Earth Science*, 38:1093–1106.

Huot, S. (2007). *Investigations of alternative and innovative ways of performing luminescence dating in an attempt to extend the age range*. Unpublished Ph.D. thesis, Aarhus University, Denmark.

Jain, M. and Singhvi, A. K. (2001). Limits to depletion of blue-green light stimulated luminescence in feldspars: implications for quartz dating. *Radiation. Measurements*, 33:883–892.

Kars, R. H., Wallinga, J., and Cohen, K. M. (2008). A new approach towards anomalous fading correction for feldspar irsl dating-tests on samples in field saturation. *Radiation Measurements*, 43:786–790.

Lapp, T., Jain, M., Ankjærgaard, C., and Pirzel, L. (2009). Development of pulsed stimulation and photon timer attachments to the Risø TL/OSL reader. *Radiation Measurements*, 44:571–575.

Larsen, A., Greilich, S., Jain, M., and Murray, A. S. (2009). Developing a numerical simulation for fading in feldspar. *Radiation Measurements*, 44:467–471.

Li, B. and Li, S.-H. (2008). Investigations of the dose-dependent anomalous fading rate of feldspar from sediments. *Journal of Physics D: Applied Physics*, 41:225502–225516.

Li, S.-H. and Tso, M.-Y. W. (1994). Lifetime determination of osl signals from potassium feldspar. *Radiation Measurements*, 27:119–121.

Morthekai, P., Jain, M., Murray, A. S., Thomsen, K. J., and Bøtter-Jensen, L. (2008). Fading characteristics of martian analogue materials and the applicability of a correction procedure. *Radiation Measurements*, 43:672–678.

Murray, A. S., Buylaert, J. P., Thomsen, K. J., and Jain, M. (2009). The effect of preheating on the IRSL signal from feldspar. *Radiation Measurements*, 44:554–559.

Poolton, N. R. J., Bøtter-Jensen, L., and Duller, G. A. T. (1995). Thermal quenching of luminescence processes in feldspars. *Radiation Measurements*, 24:57–66.

Poolton, N. R. J., Kars, R. H., Wallinga, J., and Bos, A. J. J. (2009). Direct evidence for the participation of band-tails and excited-state tunnelling in the luminescence of irradiated feldspars. *Journal of Physics: Condensed Matter*, 21:485505 (10pp).

Poolton, N. R. J., Wallinga, J., and Murray, A. S. (2002a). Electrons in feldspar I: on the wavefunction of electrons trapped at simple lattice defects. *Phys. Chem. Minerals*, 29:210–216.

Poolton, N. R. J., Ozanyan, K. B., and Wallinga, J. (2002b). Electrons in feldspar II: a consideration of the influence of conduction band-tail states on luminescence process. *Phys. Chem. Minerals*, 29:217–225.

Rieser, U., Hutt, G., R., K. M., and W., S. (1997). Feldspar irsl emission spectra .at high and low temperatures. *Radiation Measurements*, 27:273–278.

Sanderson, D. C. W. and Clark, R. J. (1994). Pulsed photostimulated luminescence of alkali feldspars. *Radiation Measurements*, 23:633–639.

Tachiya, M. and Mozumder, A. (1974). Decay of trapped electrons by tunnelling to scavenger molecules in low temperature glasses. *Chemical Physics Letters*, 28:87–89.

Templer, R. H. (1986). The localized transition model of anomalous fading. *Radiation Protection Dosimetry*, 17:493–497.

Thomsen, K. J., Murray, A. S., Jain, M., and Bøtter-Jensen, L. (2008). Laboratory fading rates of various luminescence signals from feldspar-rich sediment extracts. *Radiation Measurements*, 43:1474–1486.

Trautmann, T., Krbetschek, M. R., Dietrich, A., and Stolz, W. (1999). Feldspar radioluminescence: a new dating method and its physical background. *Journal of Luminescence*, 85:45–58.

Trautmann, T., Rieser, U., and Stolz, W. (1997). Activation energies of irsl traps in feldspars. *Radiation Measurements*, 27:193–197.

Tsukamoto, S., Denby, P. M., Murray, A. S., and Bøtter-Jensen, L. (2006). Time-resolved luminescence from feldspars: New insight into fading. *Radiation Measurements*, 41:790–795.

Tsukamoto, S., Murray, A. S., Ankjærgaard, C., Jain, M., and Lapp, T. (2010). Charge movement in minerals studied by optically stimulated luminescence and time-resolved exo-electron emission. *Journal of Physics D: Applied Physics*, 43:325502 (9pp).

Visocekas, R. (1985). Tunneling radiative recombination in labradorite: its association with anomalous fading of thermoluminescence. *Nucl. Tracks Radiat. Meas.*, 10:521–529.

Wintle, A. G. (1973). Anomalous fading of thermoluminescence in mineral samples. *Nature*, 245:143–144.

Chapter 10

Optimising the separation of quartz and feldspar optically stimulated luminescence using pulsed excitation

C. Ankjærgaard[1], M. Jain[1], K. J. Thomsen[1], and A. S. Murray[2]

[1] *Radiation Research Department, Risø National Laboratory for Sustainable Energy, Danish Technical University, DK-4000 Roskilde, Denmark*
[2] *Nordic Laboratory for Luminescence Dating, Department of Earth Science, Aarhus University, Risø DTU, DK-4000 Roskilde, Denmark.*

Abstract
In luminescence dating, the two most commonly used natural minerals, quartz and feldspar, are exposed to different dose rates in the natural environment, and so record different doses. The luminescence signals also have different stabilities. For accurate dosimetry, the signals from these two minerals must be separated, either by physical separation of the mineral grains, or by instrumental separation of the luminescence signals. The luminescence signals from quartz and feldspar have different luminescence lifetimes under pulsed optical stimulation. This difference in lifetime can be used to discriminate between the two signals from a mixed quartz-feldspar sample. The purpose of this study is to identify optimum measurement conditions for the best separation of quartz OSL from that of feldspar in a mixed sample using pulsed stimulation and time-resolved OSL. We integrate the signal from 5 μs after the LEDs are switched off until just before the LEDs are switched on again, with the pulse *on*-time equal to the pulse *off*-time of 50 μs. By using only the initial interval of the pulsed OSL decay curve (equivalent to 0.2 s of CW-OSL using blue light at 50 mW/cm^2) we find that the quartz to feldspar pulsed OSL intensity ratio is at a maximum. By using these parameters with an additional infrared (IR) stimulation at 175°C before measurement (to further reduce the feldspar signal intensity), we obtain a factor of 25 enhancement in signal separation compared to that from a conventional prior-IR

CW measurement. This ratio can be further improved if the counting window in the pulse *off*-time is restricted to detect between 20 and 50 μs instead of the entire *off*-period.

10.1   Introduction

In the luminescence dating of geological and archaeological material, it is important to separate the signals from the two ubiquitous natural luminescent dosimeters, quartz and feldspar, because they record different doses. This difference in dose can arise from differences in (i) the internal dose rate and/or (ii) the residual dose due to incomplete zeroing of the luminescence signal prior to deposition. Moreover, the dose measured using luminescence is usually underestimated in feldspars because of the well known anomalous (athermal) fading problem (Wintle, 1973; Aitken, 1998; Huntley and Lamothe, 2001). Quartz is usually considered to be a more reliable dosimeter than feldspar because quartz does not show anomalous fading and because the dosimetric signal in quartz is more rapidly emptied during daylight exposure (Godfrey-Smith et al., 1988; Thomsen et al., 2008). The two minerals quartz and feldspar are usually separated by physical and chemical treatment prior to measurement (Wintle, 1997).

However, physical separation of the minerals is not always possible, for example, because of feldspar micro-inclusions in quartz or because the measurements are to be made in the field (where only bulk samples are available and chemical separation impractical). One approach to reduce feldspar contamination is by using elevated temperature infrared (IR) stimulation prior to continuous wave (CW) OSL measurement (Jain and Singhvi, 2001; Wallinga et al., 2003). This is referred to as an IR bleach. This approach may present difficulties because at high temperatures both the fast and the medium components in quartz OSL are depleted significantly by IR exposure (Jain et al., 2003). Another possible instrumental method for isolating a quartz signal from a mixed quartz-feldspar sample is pulsed optical stimulation (POSL). This approach relies on the fact that the shapes of the time-resolved OSL (TR-OSL) of quartz and feldspar are very different [e.g. Chithambo and Galloway (2000); Denby et al. (2006)]. This approach was tested in a previous laboratory experiment in which dosed quartz (23 Gy) and un-dosed feldspar (0 Gy) were mixed together (Denby et al., 2006; Thomsen et al., 2006). It was shown that by using pulsed blue stimulation (with a prior IR stimulation) the measured dose was indistinguishable from the known quartz dose of 23 Gy even in the presence of a feldspar contamination of 40% (by mass). These authors used a pulse *on*-time equal to the pulse *off*-time of 50 μs and a delay of 5 μs prior to measuring the light emitted during the pulse *off*-time. (The pulse *on*-time is the length of time the light source is turned on during a single pulse period; the *off*-time is the corresponding period without illumination). This work (using the same *on*- and *off*-time settings of 50 μs and 50 μs) was continued in Thomsen et al. (2008) where post-IR pulsed blue light stimulation of eleven natural

samples show that the quartz dose can be measured accurately without any prior chemical separation.

In this paper, we investigate the LED pulse *on-* and *off*-time settings required to maximise the proportion of quartz signal from a mixed quartz and feldspar sample. To be able to quantify the individual contributions from the two components, we work with a synthetic signal obtained by summing up quartz and feldspar signals measured separately. The analysis and results presented here are based on time-resolved OSL (TR-OSL) measurements for *on*-times varying from 8 to 1000 µs, with measurements based on data recorded using a photon timer attachment (Lapp et al., 2009, Chapter 2 of this thesis). Pulsed optically stimulated luminescence (POSL) measurements obtained without the use of the photon timer, such as those described by Thomsen et al. (2008), are discussed in Sections 10.5.3 and 10.6.

10.2 Experimental details

10.2.1 Instrumentation

Sample measurements were carried out on a Risø TL/OSL-20 reader with an integrated pulsing option to control the stimulation LEDs, and with a photon timer attachment with a detection resolution (bin-width) of 100 ps to record the TR-OSL (Lapp et al., 2009, Chapter 2 of this thesis). Because each photon detected is individually time-stamped and the event stored in memory, the bin-width (specified as $2^n \cdot 100$ ps) can be changed after data collection. Blue light stimulation was performed with a 470 ± 30 nm (FWHM) LED array delivering 50 mW/cm^2 CW stimulation at the sample position. IR stimulation was performed with an 870 ± 20 nm (FWHM) LED array delivering 100 mW/cm^2 CW stimulation, and a 7.5 mm thick Hoya U340 filter was inserted between the sample and the PM-tube.

We define the duration of each stimulation LED pulse as the *on*-time, and the duration of the pause before the next stimulation pulse as the *off*-time, see also Lapp et al. (2009) or Chapter 2 of this thesis. The lengths of both the *on-* and *off*-times can be set independently to lie between 0.2 µs and 9.9 s (*on*-time) and between 0.6 µs and 9.9 s (*off*-time), although the pulse shape deteriorates for pulse widths <6 µs. Furthermore, the pulsed stimulation attachment has an option to gate the signal such that only photons detected in the *off*-time are counted. The starting point of this gating period can be shifted up to a maximum of 5 µs after the end of the *on*-pulse; this feature can be useful for rejection of the very fast decaying signals in gated pulsed OSL. During a pulsed measurement, the photon timer records the time of arrival of photons detected relative to the beginning of the LED pulse. The total number of these stimulation pulses depends on the pulsed stimulation time: $\sim$pulsed stimulation time [s]/(*on*+*off*-time [µs]).

10.2.2 Samples

All the work reported here has been undertaken using 90–125 µm sedimentary quartz grains (sample: WIDG8) and 180–250 µm potassium-rich feldspar grains (sample: 951020FK). The quartz grains were extracted by sieving, heavy liquid separation and HF treatment, as described in Wintle (1997) and the absence of
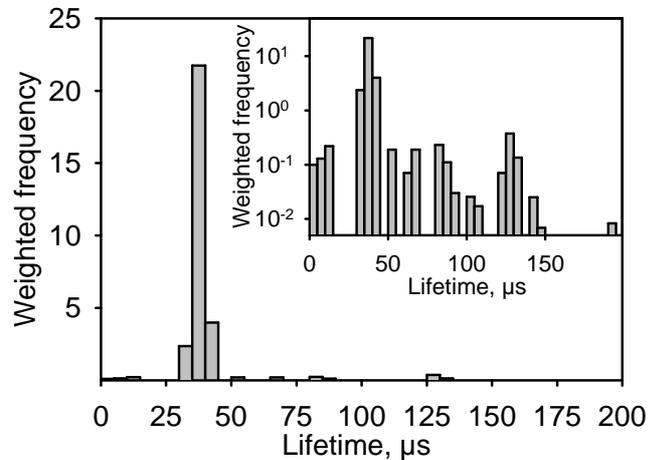
Figure 10.1: Weighted histogram of lifetimes present in the 30 quartz samples listed in Table 10.1. Each lifetime is given a weight corresponding to the fractional amplitude for that component. Therefore, in a sample with lifetimes λ_1 and λ_2 and corresponding amplitudes A_1 and A_2, then λ_1 will have a weight of $A_1/(A_1 + A_2)$ and λ_2 will have a weight of $A_2/(A_1 + A_2)$. The weights within each lifetime interval on the x-axis of the distribution are then added up to give the height of the column. In a weighted histogram both the distribution of lifetimes are shown as well as the relative importance of these lifetimes. The log of the histogram is shown inset.

significant feldspar contamination was confirmed by tests using IR stimulation. The feldspar fractions were obtained by sieving, density separation using heavy liquid, first with $\rho = 2.62$ g/cm^3 and then with $\rho = 2.58$ g/cm^3, and finally an HF treatment (10%, 40 min). In all measurements presented here the feldspar sample was given a dose 10 times that of quartz (80 Gy and 8 Gy, respectively) in order to make the signal intensities of comparable size. This was done deliberately to gain as much signal as possible. All measurements were carried out using only one aliquot of quartz and one of feldspar such that the results are directly comparable; both aliquots consisted of grains mounted in steel cups using silicon oil. Both aliquots were preheated to 260°C for 10 s prior to OSL measurements at 125°C.

10.3   Luminescence lifetimes in quartz - how universal are they?

The separation of quartz OSL from a mixed quartz-feldspar sample relies on the fact that the TR-OSL shapes (and thereby the luminescence lifetimes) of quartz and feldspar are different. To examine whether the lifetime(s) in quartz are sample specific or whether they are universal, the TR-OSL curves from 30 quartz samples of various geological origin, of which some were heated material, were used to extract lifetimes. Three of the quartz samples (BR1, 4, and 7) were extracted from bricks that was heated to more than 500°C during manufacture.

Sample code	Location	Initial cts [0.8 μs⁻¹]	A_1 [0.8 μs⁻¹]	λ_1 [μs]	A_2 [0.8 μs⁻¹]	λ_2 [μs]	A_3 [0.8 μs⁻¹]	λ_3 [μs]
990222	Denmark	1,073	-	-	1,062	36.3	77	63.5
981001	Denmark	2,149	-	-	1,746	32.5	396	67.9
000902	Taiwan	1,032	-	-	968	34.2	86	81.5
000905	Taiwan	318	-	-	288	38.1	-	-
010804	Scotland	258	-	-	155	30.7	94	126.2
963601	Tanzania	36,111	-	-	34,682	37.7	1,319	85.3
963602	Tanzania	79,791	-	-	78,279	39.2	1,370	105.6
963603	Tanzania	48,001	-	-	46,508	38.3	1,224	104.5
973604	Tanzania	85,822	-	-	85,600	40.4	715	194
973605	Tanzania	73,870	-	-	71,501	38.4	2,027	92.3
973606	Tanzania	33,570	-	-	32,986	38.0	557	120.4
90SL33	Zambia	42,484			34,319	35.2	7,979	54.7
90SL63	Zambia	117,572	-	-	118,051	40.7	-	-
SLP0	Zambia	105,482	-	-	104,281	39.6	723	147.8
SLP7	Zambia	111,742	-	-	110,792	40.2	-	-
FP1	North India	2,558	2,379	36.7	139	84.8	-	-
FP2	North India	91	-	-	83	37.2	13	132.3
KPY2	North India	219	-	-	185	39.5	10	122.2
KPY3	North India	12,695	-	-	12,552	37.6	-	-
TR-55	West India	6,317	-	-	6,189	36.9	-	-
IG-Plains-2	North India	29,327	-	-	28,894	37.5	-	-
000301	Russia	9,134	2,014	10.2	7,023	39.4	-	-
GSF-1-34	Germany	198	-	-	171	43.7	-	-
GSF-2-34	Germany	2,760	-	-	2,511	36.1	189	86.5
WIDG8*	North Australia	49,803	-	-	49,978	38.6	-	-
010301	Norway (Burnt flint)	4,552	482	6.7	4,015	38.0	-	-
994901	Norway (Brick)	5,764	566	5.0	5,093	37.9	-	-
BR1	Denmark (Brick)	2,144	-	-	2,146	36.4	-	-
BR4	Denmark (Brick)	9,499	-	-	8,583	36.2	846	82.2
BR7	Denmark (Brick)	6,693	-	-	6,653	39.0	170	142.7

Table 10.1: Results from fitting the *off*-time TR-OSL decay from 30 sedimentary quartz samples after a dose of 50 Gy (*except WIDG8, which received 8 Gy). Note that the quartz grains extracted from the bricks have been heated to more than 500°C, and that the flint sample has been heated to an unknown temperature. A preheat to 260°C for 10 s was applied prior to stimulation at 125°C. The initial TR-OSL decay intensity is given in column 3, and amplitudes and lifetimes from the exponential components in columns 4-5, 6-7 and 8-9.

All samples were initially bleached using blue light, and given a dose of 50 Gy (WIDG8 was given 8 Gy), preheated to 260°C for 10 s and stimulated at 125°C (this preheat and stimulation temperature are commonly used in quartz dose measurements). All *off*-time curves were fitted with decaying exponentials and they consisted of either one or two components. For each sample the fractional amplitude for each lifetime was calculated. The results are summarises in Table 10.1.

In Fig. 10.1, a weighted histogram of the measured lifetimes is shown for the 30 quartz samples. The weightage is given by the fractional amplitude to determine the dominant lifetime component in quartz TR-OSL. The inset to Fig. 10.1 shows the histogram on log-scale for a better visualization of those lifetimes which have relatively low contribution to the measured signal (see Table 10.1 for individual values). From this figure it is clear that using the measurement conditions given above on these samples, the dominant component in quartz TR-OSL has a lifetime within the range 35–40 μs and in some cases, much less important secondary components with lifetimes <15 μs and/or from 50–200 μs.

The quartz sample, WIDG8, used in the synthetic mixed quartz-feldspar sample under investigation in this paper has a lifetime of 38.6 μs and is therefore a good representative of the bulk behaviour of quartz samples as presented in Fig. 10.1. Feldspar, on the contrary, is a much more complex dosimeter and it has been suggested that the TR-OSL signal may not be a linear sum of independent exponential processes (Ankjærgaard et al., 2009, Chapter 7 of this thesis) although it can be adequately described by four exponential components in the *off*-time range discussed here (Clark et al., 1997; Ankjærgaard et al., 2009, Chapter 7 of this thesis). Both the latter papers present components analysed as exponentials from several feldspar specimens and it is evident that these different types, irrespectively of mineral composition, have similar components falling within narrow bands.

The two minerals comprising the synthetic quartz-feldspar mixed sample have therefore been chosen as representatives of a general behaviour of their mineral class and as a result our results are expected to be applicable to other mixed quartz-feldspar sediments.

10.4   The effect of feldspar contamination

In a mixed quartz and feldspar sample, the measured luminescence signal can, to first order, be approximated as the sum of two components. Because the proportions and the OSL sensitivities of the two components are usually unknown, it is difficult to quantify their individual contributions to the net OSL signal. In this paper we have therefore chosen to measure quartz and feldspar signals separately and subsequently add the two signals to generate a synthetic mixed sample signal. In Fig. 10.2a, normalised CW-OSL decay curves for blue light stimulation of quartz (Q) and feldspar (F) are shown. The post-IR blue stimulation curves (Q_{IR} and F_{IR}) are also shown, where an IR bleach at 175°C is carried out prior to the blue light stimulation. All signals have been normalized to the initial blue light stimulated quartz intensity. Wallinga et al. (2003) showed that IR stimulation at elevated temperatures preferentially reduces the feldspar luminescence in a mixed quartz-feldspar sample. This observation is
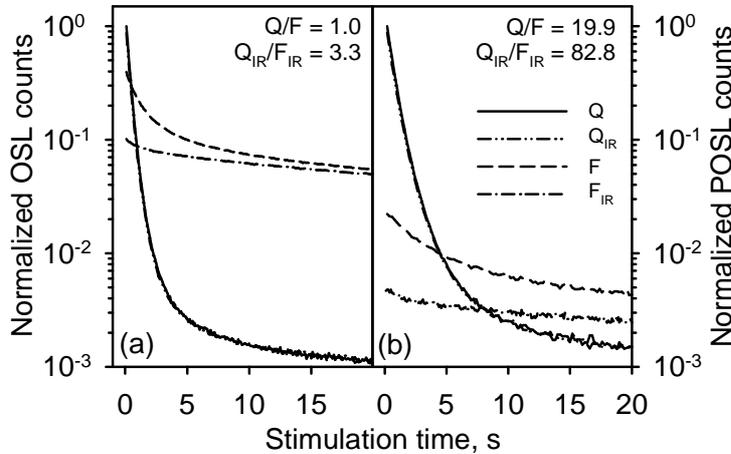
Figure 10.2: (a) CW-OSL decay curves for blue light stimulation of quartz (Q, full line), feldspar (F, dashed line), post-IR stimulated quartz (Q_{IR}, dash dot dot line) and post-IR stimulated feldspar (F_{IR}, dash dot line). Note that the two quartz curves are overlying. The quartz sample was given a dose of 8 Gy and feldspar, 80 Gy. Both samples were pre-heated to 260°C and stimulated with blue light at 125°C for 50 s ($\sim$6·10^{18} photons/cm^2) giving a bin resolution of 0.1 s/bin using 500 bins. The IR stimulation was at 175°C for 100 s. All the signals are normalised with the initial 0.1 s quartz CW-OSL. (b) The same structure as in (a), but using pulsed-OSL stimulation for an *on*-time of 50 μs and an *off*-time of 50 μs and pulsing for 100 s to obtain the amount of stimulating photons as in (a). The signals were counted only during the *off*-time and gated so that the initial 5 μs in the *off*-time was not counted, the number of bins is the same as that of (a), such that the resolution is now 0.2 s/bin. All the signals are normalised with the initial 0.2 s quartz POSL.

supported by the data presented in Fig. 10.2a, where the initial feldspar intensity has decreased by 75% compared to that without prior IR stimulation while the quartz intensity has only decreased by 14%. Thus by applying an IR bleach at 175°C prior to blue light stimulation an increase in signal separation is obtained. This increase can be quantified by defining a quartz to feldspar ratio (Q/F) using the intensities of the initial (0.2 s) blue light stimulated signals. If only blue light stimulation is employed this ratio is defined as unity; if a prior IR bleach is used the ratio increases to 3.3. Thus, using an elevated temperature post-IR blue light stimulation protocol increases the quartz to feldspar luminescence separation by a factor of 3.3 in case of CW-OSL. In the following sections we investigate on different configurations of pulsed optical stimulation to further increase the Q/F ratio.

In Fig. 10.3, the time-resolved luminescence signals from quartz and feldspar are shown for an *on*-time of 50 μs and an *off*-time of 500 μs using the blue LEDs. Note that the curves are shown on different log y axes. The data were derived by summing all the photons resulting from 40,000 pulses in the 22 s of total stimulation time. The feldspar luminescence signal has a very fast initial rise which is followed by a much slower rise after a few hundreds of ns of stimulation during the *on*-pulse (Chithambo and Galloway, 2000; Ankjærgaard
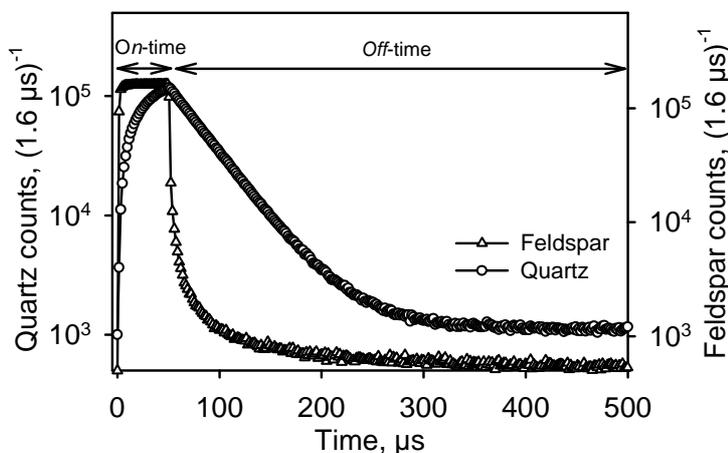
Figure 10.3: Quartz and feldspar time-resolved OSL curves produced by adding up signals from all pulses produced in 22 s, for an *on*-time of 50 μs and an *off*-time of 500 μs. Note that the curves are each referred to their own log y axis and that the full *off*-time has not been shown. The quartz was given a dose of 8 Gy and feldspar a dose of 80 Gy; both were then preheated to 260°C for 10 s and stimulated at 125°C.

et al., 2009, Chapter 7 of this thesis) while the quartz signal increases more slowly and does not reach a constant equilibrium level within the 50 μs *on*-period. A similar trend is present in the signal decay observed in the *off*-time i.e., the TR-OSL decay of quartz is much slower than that of feldspar. The fast decay in feldspar TR-OSL (the major part of the signal) disappears in only a few tens of μs, although there are relatively weak slow decays which take several hundreds of μs to decay. The quartz signal decays more slowly and reaches a near constant level towards the end of the 500 μs *off*-time. Note that this apparent constant level is made up of PM-tube 'dark counts' and very slowly decaying luminescence signal(s) (Chithambo, 2007a). In the following sections we make use of this difference in the TR-OSL decay rates of the two minerals to maximise the ratio of quartz to feldspar OSL signals.

10.5   Selection of *on*- and *off* periods for best signal discrimination

Figure 10.4 shows the quartz and feldspar *off*-time decay shapes for the sum of the initial 20,000 consecutive pulses (corresponding to a total of $\sim 2 \cdot 10^{16}$ photons delivered per cm^2, or about 0.2 s of continuous wave OSL) for a 10 μs *on*-time and a 500 μs *off*-time. The area under the normalised feldspar curve during the 50 μs *on*-pulse is close to twice that of the quartz curve (e.g. see Fig. 10.3) and this dominant feldspar contribution is rejected by quite simply ignoring the signal observed during the *on*-time. Furthermore, the initial 5 μs *off*-time where the feldspar signal decrease by a factor of ~ 20 has also been omitted (i.e. the fast decay in the feldspar has reduced to a negligible level). In Fig. 10.4, these parts of the signal have been removed. In contrast, the quartz
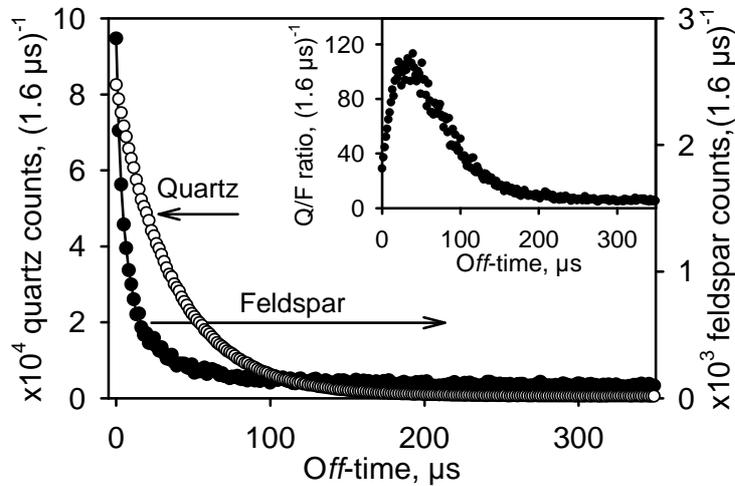
Figure 10.4: Quartz and feldspar *off*-time decay shapes for an *on*-time of 10 μs and an *off*-time of 500 μs, using the sum of the pulses produced in 10.2 s, equal to a total equivalent CW-OSL measurement time of 0.2 s. The pre-treatment and doses are identical to that of Fig. 10.3. Note that the curves are each referred to their own y axis and that the full *off*-time has not been shown. The initial 5 μs of both the quartz and feldspar *off*-time has been removed. Inset: Ratio of the quartz to feldspar *off*-time decay curves. The difference in the decay rates of the two curves gives rise to an asymmetric peak with a maximum at about 40 μs.

signal has a longer lifetime and as a result the ratio of the quartz to feldspar signals increases with time during the *off*-period until about ∼40 μs (Fig. 10.4 inset), where an enhancement in the quartz and feldspar separation of ∼115 is obtained. For *off*-times >40 μs the ratio starts to decrease, because of the relatively slower decay of a weak feldspar component compared to that from quartz in this time regime. Clearly, the best separation of quartz and feldspar OSL signals for an *on*-time of 10 μs is obtained if the pulsed OSL signal is detected only in a small window centred on 40 μs. In the following section we will investigate how the optimum separation depends on the length of the *on*-time.

10.5.1 Quartz to feldspar TR-OSL (*off*-time) ratio

To find the optimum *on-*and *off*-times, we first investigated which part of the POSL signal gave the best ratio of the quartz to feldspar signals during the *off*-time. TR-OSL curves were measured for both quartz and feldspar for four *on*-times: 10, 50, 100 and 500 μs, while the *off*-time was kept constant at 500 μs. This *off*-time of 500 μs was chosen to ensure that the time-resolved data for both minerals approached a constant level before commencement of the next pulse (see Fig. 10.3). This means there is effectively no memory of the previous pulse in the data of the subsequent pulse. We confirmed that the background was negligible by measuring blank samples consisting of heated (one hour at 700°C) quartz and feldspar samples. In order to compare TR-OSL curves with

Table 10.2: Pulsed stimulation time, number of produced pulses and summed pulse equivalent CW-OSL time as a function of the *on*-time (*off*-time kept constant at 500 μs). The LED stimulation power intensity is 50 mW/cm^2, corresponding to ∼1·10^{17} stimulation photons per unit time per cm^2 or 8.5·10^{-17} mJ. No. of pulses produced during stimulation = pulsed stimulation time [s]/(*on*+*off*-time [μs]). Total equivalent CW-OSL measurement time = *on*-time [μs]·Number of pulses produced during stimulation.

On-time, [μs], (pulse off-time kept constant at 500 μs)	10	50	100	500
Pulsed stimulation time, t_{pulsed}, [s]	102	22	12	4
No. of pulses produced during stimulation, (divided by 10^3)	200	40	20	4
Total equivalent CW-OSL measurement time, t_{CW}, [s]	2	2	2	2
No. of pulses added in each curve in Fig. 10.5(a-d), (divided by 10^3)	20	4	2	0.4
Equivalent CW-OSL measurement time in Fig. 10.5a-d, t_{CW}, [s]	0.2	0.2	0.2	0.2

different *on*-times, it is important to ensure that the number of stimulation photons reaching the sample is constant despite the change in *on*-time. This can be achieved by adjusting the number of stimulation pulses and hence the total stimulation time employed in each experiment, t_{pulsed}:

$$t_{\text{CW}} = t_{\text{pulsed}} \cdot \left(\frac{on\text{-time}}{on+off\text{-time}} \right), \qquad (10.1)$$

In this experiment, TR-OSL curves for both quartz and feldspar were measured using the four *on*-times stated above. The pulsed stimulation time, t_{pulsed} is chosen in each measurement such that the number of stimulation photons reaching the sample is equivalent to 2 s of CW stimulation (∼2·10^{17} stimulation photons/cm^2). Table 10.2 lists the *on*-times used and the corresponding pulsed stimulation time, t_{pulsed} when t_{CW} is kept constant at 2 s. We have chosen only to look at this initial signal since this is most commonly used in dose estimation of natural quartz samples. The measurement conditions are as given in Section 10.2.2; note that the two aliquots were bleached using CW blue light at 260°C for 100 s (for quartz) or 2000 s (for feldspar) between each experiment. The results are shown in Fig. 10.5. For each of the four different *on*-times, five different curves are displayed. The five curves each represent a summation interval equivalent to 0.2 s of CW stimulation, but they all have a different starting point for summation. In Fig. 10.5a, the initial black dotted curve represent the data measured during the initial 20,000 pulses (or t_{CW} = 0.2 s), whereas the red curves represent the data measured during the consecutive 20,000 pulses (next 0.2 s) and likewise for the remaining three curves. Thus the five curves show the effect of placing the summation interval at different starting points on the POSL decay curve. Note also, that the black curve is identical to the curve shown inset in Fig. 10.4. The number of pulses summed in each curve for the other three *on*-times are given in Table 10.2, row 5.
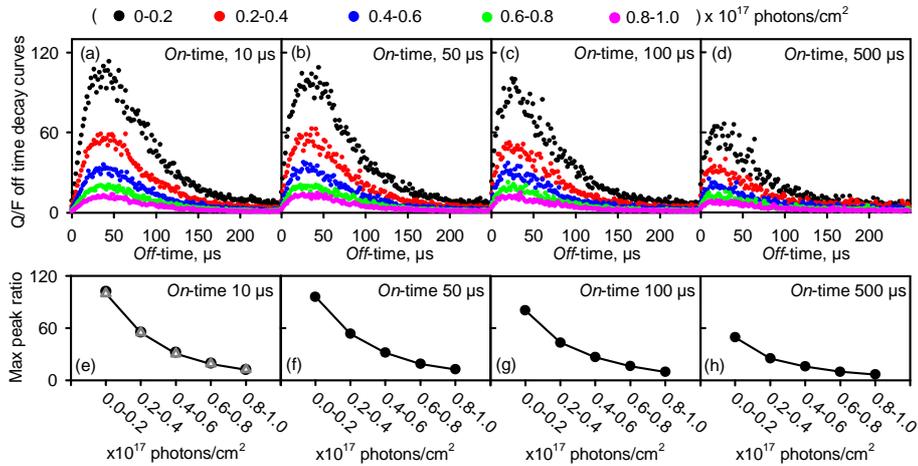
Figure 10.5: Upper: Ratio of quartz to feldspar *off*-time decay signals for different *on*-times (a-d). The number of pulses added in each *off*-time decay signal depends on the *on*-time (given in Table 10.2, last two rows). The number of pulses is added such that each of the five curves has received 0.2 s of equivalent CW-OSL time (or $\sim 2 \cdot 10^{16}$ photons/cm^2). Lower: Summary of the curves in the upper figures, showing the maximum ratio of quartz to feldspar *off*-time decay signal for each of the five curves for varying *on*-time (e-h). The grey triangles shown in (e) are are repeat points of (a) to show the excellent reproducibility. It is seen that the initial pulse summation for each *on*-time gives the best signal separation. The pre-treatment and doses are identical to that of Fig. 10.3.

A summary of the peak maxima (optimum quartz/feldspar separation) of the 20 data sets displayed in Figs. 10.5a-d is given in Figs. 10.5e-h. The data were measured in the same order as presented in the figures. In Fig. 10.5e, the grey triangles represent the maxima from the recycling measurement of the data for 10 μs *on*-time, collected after the 500 μs *on*-time measurement. The excellent reproducibility in Fig. 10.5e confirms that the observed trends are not artifacts of any sensitivity changes. There are three key observations to be made from Fig. 10.5:

(i) The maximum quartz/feldspar ratio decreases as a function of increasing summation (i.e. the best separation is obtained using the very initial POSL signal. This decrease is caused by the fact that the rate of depletion of trapped charge during optical stimulation is much greater for quartz than for feldspar, i.e. the quartz CW decay is much faster than that of feldspar (see Fig. 10.2a).

(ii) The maximum quartz/feldspar ratio is obtained 30–40 μs into the *off*-time regardless of the length of the *on*-time. Thus the optimum signal separation is obtained if the counting window is restricted to encompass this time interval. However, it is worth nothing that such a restricted counting window would result in a significant decrease in the intensity of the measured signal and thus may not be practical.
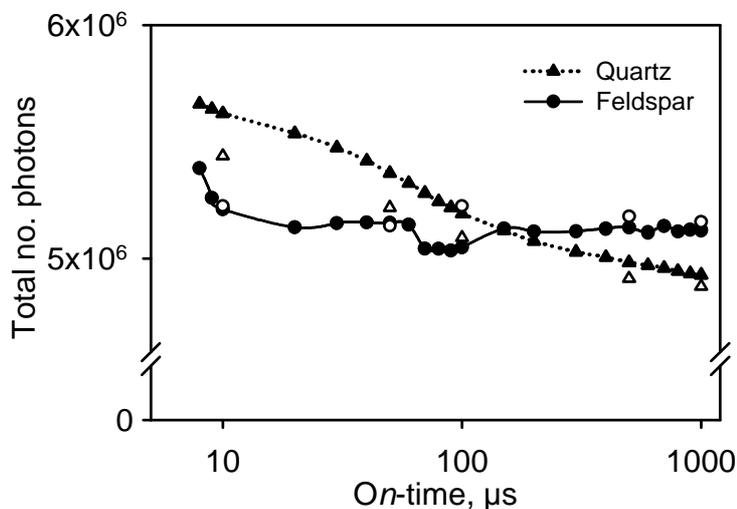
Figure 10.6: The total number of photons from quartz (triangles) and feldspar (circles) detected during stimulation by a fixed $\sim 2 \cdot 10^{17}$ photons/cm^2 (equal to 2 s of CW stimulation) as a function of *on*-time. The average total count over all *on*-times and corresponding standard deviations are for quartz: 5,313,588 $\pm$ 315,171 and feldspar: 5,318,937 $\pm$ 524,830.

(iii) The maximum quartz/feldspar ratio decreases as a function of *on*-time for the same summation interval. If it is assumed that the total emitted luminescence (e.g. the photons measured in both the *on*- and *off*-time) for a given number of stimulation photons is constant irrespective of the duration of the *on*-time, a decrease in the *off*-time signal will occur to compensate for an increase in the *on*-time signal (Bøtter-Jensen et al., 2003; Chithambo, 2007b). Both quartz and feldspar *off*-time signals will therefore undergo a decrease with an increase in the *on*-time. However, since the rate of depletion of trapped charge is faster in quartz than in feldspar, the quartz/feldspar ratio is expected to decrease as a function of *on*-time.

In the following section the assumption of constant luminescence efficiency is tested, and in Section 10.5.3 the optimum length of this *on*-time is investigated.

10.5.2   Luminescence efficiency as a function of *on*-time

To determine if the observed decrease in the optimum quartz/feldspar ratio as a function of *on*-time is caused by relative differences in rate of depletion of trapped charge for quartz and feldspar, it is necessary to establish if the luminescence efficiency is constant regardless of the duration of the *on*-time.

To test this, a series of 22 experiments in which the *on*-time varied between 8 and 1000 μs were undertaken for both quartz and feldspar. In each measurement the *off*-time was kept constant at 500 μs and the pulsed stimulation time, t_{pulsed}, adjusted such that the number of stimulation photons reaching the sample was equivalent to those in $t_{\mathrm{CW}} = 2$ s, see Eqn. (10.1). All photons

detected in both the *on-* and *off*-time were summed to produce the net lumi-
nescence signal. The results for both quartz and feldspar are shown in Fig. 10.6
(filled symbols). The luminescence detected from feldspar is as expected close
to constant for all *on*-times (8 to 1,000 μs). The excellent recycling (open sym-
bols) confirms that any sensitivity change is negligible. The luminescence from
quartz has decreased by <10 % for an *on*-time of 1,000 μs compared to that
of 8 μs. However, the recycling values indicate that at least part of this 10%
decrease is caused by sensitivity change. This is an unexpected observation
and requires further investigations (we have confirmed by direct comparison
with conventional counting that there is no loss of counts in TR-OSL data col-
lection process). Nevertheless, the observed decrease in luminescence efficiency
for quartz of about 10% is not sufficient to account for the much larger (∼50%)
decrease in the quartz/feldspar ratio observed between an *on*-time of 10 μs
compared to that of 500 μs (see Fig. 10.5a and Fig. 10.5d). This additional
decrease can only be due to the increased depletion of the signal as the *on*-time
is increased.

10.5.3   Optimizing the length of the *on*-time

It was concluded from Fig. 10.5 (Section 10.5.1) that the best Q/F signal
peak ratio is obtained by using only the signal obtained during the very initial
period equivalent to 0.2 s of continuous stimulation for the shortest *on*-time
of 10 μs. We now discuss more detailed measurements of how the Q/F signal
ratio depends on the *on*-time to separate feldspar and quartz signals, if one
were to integrate the area under the *off*-time signal. The purpose of these
investigations is to optimise the duration of the *on*-time for the best signal
separation in POSL measurements.

TR-OSL curves were measured for *on*-times varying between 8 and 1000
μs while the *off*-time was kept constant at 500 μs, to ensure that both signals
(quartz and feldspar) had time to reach a constant level before the next stim-
ulation light pulse arrived at the sample. The pulsed stimulation times were
calculated using Eqn. (10.1). Photons emitted from the sample were counted
only during the *off*-time, with the counting system gated to ignore any photons
observed during the first 5 μs of *off*-time, thereby ignoring the initial intense
but rapidly decaying signal from feldspar. In Fig. 10.7a, these *off*-time lumi-
nescence light sums from quartz and feldspar are shown as a function of the
on-time, with integrals normalised to the response of the shortest *on*-time of
8 μs; the two signals decay approximately at the same rate up to an *on*-time
of 80 μs, hereafter the quartz signal decays more rapidly. The ratio of these
two curves is shown as an inset to Fig. 10.7a. It is difficult to evaluate the
magnitude of the signal separation from this ratio plot without comparing it
to the Q/F intensity ratio observed for conventional CW-OSL measurements.
Because of hardware limitations a true CW-OSL measurement was not possi-
ble with our prototype experimental configuration, and so an average of the
total light detected in the stimulation period (i.e. both *on-* and *off*-times,
see Fig. 10.6) was used as an approximation for light output during CW-OSL.
This average is used to normalize the curve in the inset to Fig. 10.7a; this ratio
represents how much better the separation is relative to the CW-OSL mea-
surement mode. From these data, the best quartz feldspar signal separation
seems to be obtained from an *on*-time between 10 and 50 μs; we obtain a >40
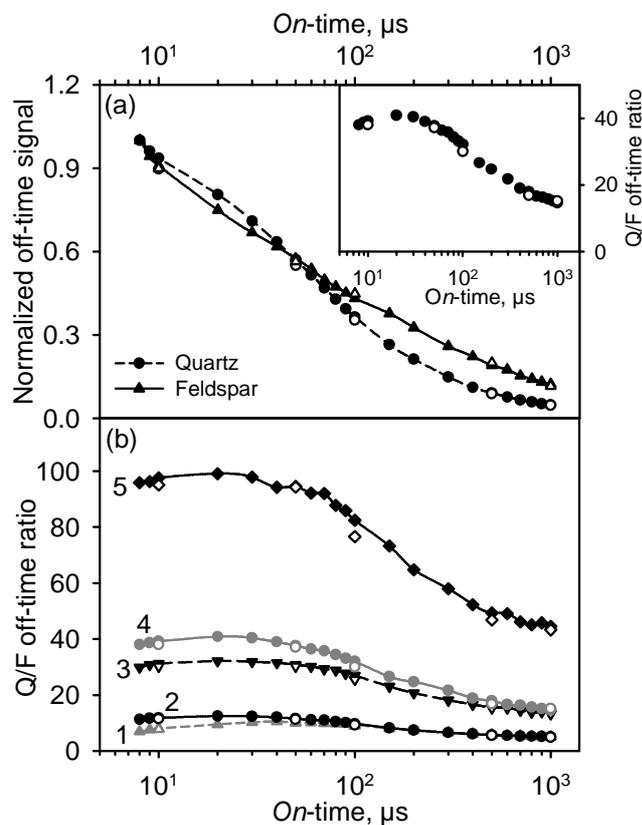
Figure 10.7: The total number of photons counted in the *off*-time from quartz (circles) and feldspar (triangles) and gated to reject the initial 5 µs as a function of *on*-time. The *off*-time was kept constant at 500 µs, and the stimulating photons were kept constant to a fixed ∼2·10^{16} photons/cm^2 (equal to 0.2 s of CW stimulation) independent of the *on*-time. Inset: Quartz to feldspar *off*-time ratio calculated from the curves in (a), the open symbols are recycling points. (b) Quartz to feldspar *off*-time ratio curves calculated for different measurement conditions as a function of *on*-time, and with a fixed *off*-time of 500 µs. The curves are listed in increasing order: **1** (grey triangles): Total stimulation time equal to 2 s of CW time, everything counted during the *off*-time. **2** (black circles): Total stimulation time equal to 2 s of CW time, everything counted in the *off*-time but gated to reject the initial 5 µs. **3** (black triangles): Total stimulation time equal to 2 s of CW time, the *off*-time signal gated to be counted between 20 and 60 µs (centred around the peak from Fig. 10.5a–d). **4** (grey circles): Total stimulation time equal to 0.2 CW time, everything counted in the *off*-time but gated to reject the initial 5 µs. **5** (black squares): Total stimulation time equal to 0.2 s CW time, the *off*-time signal gated to be counted between 20 and 60 µs. Pre-treatment and doses as in Fig. 10.3.

times increase in signal separation when using an *on*-time between 10 and 50 μs compared to using CW stimulation. For *on*-times longer than 50 μs, the signal separation steadily worsens since the rate of depletion of trapped charge is faster in quartz than in feldspar, as previously described in Section 10.5.1.

In Fig. 10.7b, the curve shown in the inset to Fig. 10.7a has been reproduced as curve 4. A significant improvement in the separation of quartz and feldspar signals (Q/F ~40) can be obtained if (i) the equivalent of only the first 0.2 s of CW light is used to stimulate the POSL curve, (ii) an *on*-time in the range of 10–50 μs is employed, (iii) counting is only during the *off*-time, and is gated to ignore photons from the initial 5 μs of the *off*-time.

Examination of the TR-OSL curves for these different *on*-times shows that the separation can be further improved by restricting the counting window to lie between 20 and 60 μs in the *off*-time (see Fig. 10.4, inset and Fig. 10.5a–e) rather than counting during the entire *off*-time. Curve 5 in Fig. 10.7b gives the quartz to feldspar ratio for pulse *off*-time signals measured between 20 and 60 μs during the *off*-time period, again using the equivalent of only the initial 0.2 s of CW light. The maximum in the quartz/feldspar ratio now increases from ~40 (curve 4) to ~100 (curve 5), compared to a conventional CW-OSL measurement of unity. Less light is now detected, so narrowing the gating interval to obtain a better separation is done at the cost of loss in signal intensity.

Unfortunately, some samples are so dim that such signal losses are unacceptable. In such cases one could increase the stimulation interval chosen for dose determination; e.g. one could include light detected from 2 s of equivalent CW stimulation instead of the optimal 0.2 s of equivalent CW stimulation. The effect on the Q/F ratio of this is shown in Fig. 10.7b (curve 1, 2, and 3). In curve 1 all photons are detected in the *off*-period. This gives a relatively flat curve with a maximum separation of ~10 occurring for *on*-times between 30 and 60 μs. In curve 2, gating is employed to remove the initial 5 μs of the *off*-periods (e.g. the same as in curve 4, but with a longer integration time of 2 s instead of 0.2 s). This improves the separation slightly compared to curve 1 and a maximum separation of ~12 is obtained for *on*-times between 20 and 40 μs. In curve 3 the counting window is set from 20-60 μs (e.g. the same as curve 5, but again with a longer integration time of 2 s). This improves the separation further and a maximum of ~32 is obtained in the region 20–40 μs.

10.5.4   Optimizing the length of the *off*-time

In the previous section, we showed that the best *on*-time settings were in the range 10 to 50 μs (Fig. 10.7), but those measurements were all done with an *off*-time of 500 μs to make sure that both the feldspar and quartz signals had time to decay to a constant level before stimulation with a new pulse. For a practical application, one would like to know the shortest possible *off*-time that gives a satisfactory quartz to feldspar signal ratio; this would minimize the total measurement time.

Fig. 10.8 shows the quartz to feldspar signal ratio for a constant *on*-time of 20 μs and an *off*-time varying from 6 to 1000 μs. The pulsed stimulation time, t_{pulsed}, was adjusted such that $\sim 2{\cdot}10^{16}$ photons/cm^2 (equal to 0.2 s of CW stimulation) reached the sample. Gating is employed to remove the initial 5 μs of the *off*-periods. The individual quartz and feldspar curves used to construct
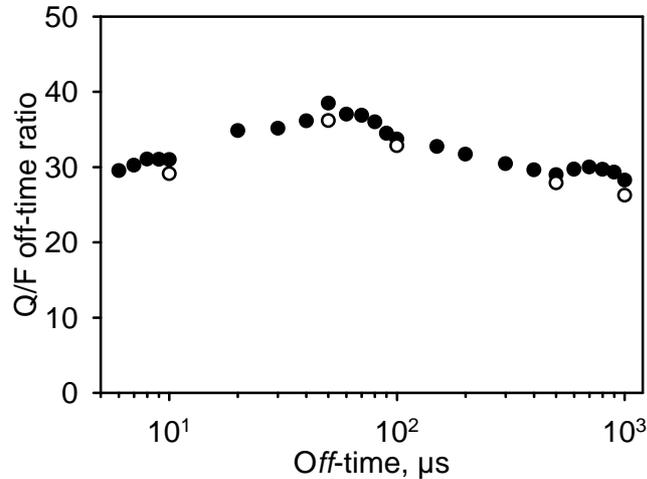
Figure 10.8: Quartz to feldspar *off*-time ratios for a constant *on*-time of 20 μs (filled circles). The measurement was gated to omit the initial 5 μs of the *off*-time signal and to count in the remaining *off*-time. The amount of stimulating photons were kept constant to a fixed ~2·10^{16} photons/cm^2 (equal to 0.2 s of CW stimulation) independent of the change in *off*-time. Recycling points are shown as open circles. Pre-treatment and doses identical to that of Fig. 10.3.

this graph have been normalized to the corresponding CW curves in the same manner as explained in Section 10.5.3 for Fig. 10.7. The Q/F ratio steadily increases up to an *off*-time of ~40 μs where it becomes almost constant at a maximum Q/F ratio of ~38; it then slowly starts to decrease from ~80 μs. The initial increase is presumably caused by the residual signal from the previous pulse, with a lifetime of ~38 μs (i.e. the quartz signal has not had time to decay significantly before the onset of the subsequent pulse). Therefore most of the signal contribution occurs in the *on*-time interval for shorter *off*-times, and vice versa. Similarly, the slow decay in the feldspar signal has not had time to build up significantly during the *on*-pulse and therefore does not affect the ratio markedly. From Fig. 10.8, the shortest *off*-time giving the best quartz/feldspar signal ratio is ~50 μs, and from Fig. 10.7b the best *on*-time would also be ~50 μs. This is the same *on*- and *off*-times used in Denby et al. (2006), Thomsen et al. (2006), and Thomsen et al. (2008). Such a choice of pulse times doubles the total stimulation time required to deliver the same power as that from CW stimulation.

10.6   Performance of separation techniques: CW-OSL vs. POSL

We now test the practical application of the optimum *on*- and *off*-periods derived above using gated pulsed OSL to stimulate the synthetic mixed sample. Unlike in the photon timer TR-OSL data, it is presently not possible to choose a specific counting interval (e.g. 20 to 50 μs) in the *off*-time. Therefore, the best separation obtainable with gated pulsed OSL corresponds to curve 4 in

Fig. 10.6. The optimum pulsed stimulation conditions (*on*-time 50 μs, *off*-time 50 μs) were tested using the same quartz and feldspar samples as in Fig. 10.2a and the results are shown in Fig. 10.2b; for reference, normalised standard CW measurements (Fig. 10.2a) gave a quartz to feldspar initial (0.2 s) OSL ratio of 1, this increased to 3.3 when an IR bleaching step was included prior to OSL measurement. The *off*-time signal integral was counted by gating the photon counter to detect the entire *off*-time, except for the initial 5 μs. The samples were measured for 100 s in total, and data collected in 500 channels, each with a width of 0.2 s; the CW-OSL measurements used in Fig. 10.2a were measured for 50 s and the data were also collected in 500 channels. The resulting quartz and feldspar POSL curves are shown in Fig. 10.2b. The feldspar signal (relative to quartz) has decreased by a factor of $\sim$20 (Q/F = 1.0 in CW mode (Fig. 10.2a); Q/F = 20 in pulsed mode); after an IR bleach (100 s at 175°C) prior to the measurement, the feldspar signal decreases by a factor of $\sim$25 compared to CW mode (Q_{IR}/F_{IR} = 3.3 in CW mode (Fig. 10.2a); Q_{IR}/F_{IR} = 83 in pulsed mode,). Thus we can obtain an improvement in rejection of the feldspar signal of $\sim$25 by using a 50 μs pulse stimulation rather than CW, at the cost of (i) doubling the pulsed stimulation time and (ii) sensitivity (rejection of the signal emitted during the *on*-time and the first 5 μs of the *off*-time).

Although the suggested protocol increases the signal separation by a factor 25 compared to CW (by prior IR bleaching in both cases), a dim sample might not have the required sensitivity to be measured using these settings. By changing the on and *off* settings from 50/50 μs to 20/80 μs, the shorter *on*-pulse will give double the intensity at the beginning of the *off*-period compared to the other *on*-time setting, but now the measurement time will not have been doubled, but increased by a factor of 5. This will give a pulsed Q/F ratio of 18.6 and a pulsed prior IR stimulated Q_{IR}/F_{IR} ratio of 76.9 - thereby giving an improvement in rejecting the feldspar signal of $\sim$23. Therefore, one way to overcome the problem of dim samples is lowering the *on*-time slightly to obtain relatively more signal intensity in the *off*-time, but this will be at the cost of longer pulsing stimulation times.

10.7   Conclusions

Based on TR-OSL data from a quartz and a feldspar sample we demonstrate that it is possible to optimise the ratio for the signal intensities from the two minerals. This is possible because of the distinct, characteristic decay shapes of the TR-OSL signals in quartz and feldspar, and because of the faster depletion of trapped charge in quartz compared to feldspar during an optical stimulation.

For a synthetic aliquot made up of a notional mixture of our quartz and feldspar samples (derived by summing the two signals), we conclude that the best separation of quartz and feldspar luminescence using gated pulsed OSL can be achieved using *on*- and *off*-time settings each of 50 μs (i.e. a pulse period of 100 μs). Under such stimulation the photons are detected only following the first 5 μs in the *off*-time period and the signal is integrated during the first 0.4 s (equivalent to 0.2 s of CW-OSL) of the measurement. If a prior IR bleaching is used, then this configuration results in a Q/F seperation ratio $\sim$25 times larger than what is possible using CW-OSL (also with a prior IR bleaching). For higher sensitivity, however at the expense of longer measurement time,

an *on-off* combination of 20–80 μs can be used to achieve a similar signal separation.

A further increase in relative intensity can be obtained if the counting window in the *off*-time is restricted to lie between 20 and 50 μs; however this is at the cost of loss of signal sensitivity and is currently only possible if a photon timer attachment is used in combination with the pulsing unit.

Acknowledgements

References

Aitken, M. J. (1998). *An Introduction to Optical Dating - The Dating of Quaternary Sediments by the Use of Photon-stimulated Luminescence.* Oxford University Press, Great Clarendon Street, Oxford, UK. ISBN: 0–1–854092–2.

Ankjærgaard, C., Jain, M., Kalchgruber, R., Lapp, T., Klein, D., McKeever, S. W. S., Murray, A. S., and Morthekai, P. (2009). Further investigations into pulsed optically stimulated luminescence from feldspars using blue and green light. *Radiation Measurements*, 44:576–581.

Bøtter-Jensen, L., McKeever, S. W. S., and Wintle, A. G. (2003). *Optically Stimulated Luminescence Dosimetry.* Elsevier, Amsterdam, The Netherlands. ISBN: 0–444–50684–5.

Chithambo, M. L. (2007a). The analysis of time-resolved optically stimulated luminescence: I. Theoretical considerations. *J. Phys. D: Appl. Phys.*, 40:1874–1879.

Chithambo, M. L. (2007b). The analysis of time-resolved optically stimulated luminescence: II. Computer simulations and experimental results. *J. Phys. D: Appl. Phys.*, 40:1880–1889.

Chithambo, M. L. and Galloway, R. B. (2000). A pulsed light-emitting-diode system for stimulation of luminescence. *Meas. Sci. Technol.*, 11:418–424.

Clark, R. J., Bailiff, I. K., and Tooley, M. J. (1997). A preliminary study of time-resolved luminescence in some feldspars. *Radiation Measurements*, 27:211–220.

Denby, P. M., Bøtter-Jensen, L., Murray, A. S., Thomsen, K. J., and Moska, P. (2006). Application of pulsed osl to the separation of the luminescence components from a mixed quartz/feldspar sample. *Radiation Measurements*, 41:774–779.

Godfrey-Smith, D. I., Huntley, D. J., and Chen, W. H. (1988). Optical dating studies of quartz and feldspar sediment extracts. *Quaternary Science Reviews*, 7:373–380.

Huntley, D. J. and Lamothe, M. (2001). Ubiquity of anomalous fading in K-feldspar and the measurement and correction for it in optical dating. *Canadian Journal of Earth Science*, 38:1093–1106.

Jain, M., Murray, A. S., and Bøtter-Jensen, L. (2003). Characterisation of blue-light stimulated luminescence components in different quartz samples: implications for dose measurement. *Radiation Measurements*, 37:441–449.

Jain, M. and Singhvi, A. K. (2001). Limits to depletion of blue-green light stimulated luminescence in feldspars: implications for quartz dating. *Radiation. Measurements*, 33:883–892.

Lapp, T., Jain, M., Ankjærgaard, C., and Pirzel, L. (2009). Development of pulsed stimulation and photon timer attachments to the Risø TL/OSL reader. *Radiation Measurements*, 44:571–575.

Thomsen, K. J., Bøtter-Jensen, L., Denby, P. M., Moska, P., and Murray, A. S. (2006). Developments in luminescence measurement techniques. *Radiation Measurements*, 41:768–773.

Thomsen, K. J., Jain, M., Murray, A. S., Denby, P. M., Roy, N., and Bøtter-Jensen, L. (2008). Minimizing feldspar OSL contamination in quartz UV-OSL using pulsed blue stimulation. *Radiation Measurements*, 43:752–757.

Wallinga, J., Murray, A. S., and Bøtter-Jensen, L. (2003). Measurement of the dose in quartz in the prescence of feldspar contamination. *Radiation Protection Dosimetry*, 101:367–370.

Wintle, A. G. (1973). Anomalous fading of thermoluminescence in mineral samples. *Nature*, 245:143–144.

Wintle, A. G. (1997). Luminescence dating: laboratory procedures and protocols. *Radiation Measurements*, 27:769–817.

Chapter 11

Summary

Methodology

An important part of this Ph.D. project was thorough testing of the software and instrumentation developed for measurement of TR-OSL to ensure the reliability of TR-OSL measurements. The second methodological aspect was to investigate on the best method for mathematical analysis (multi-exponential) of the TR-OSL data to obtain robust physical parameters. Fitting data with a sum of exponentials is an ill posed problem, and, therefore, two fundamentally different analytical methods, the Fredholm integral equation (FIE) and the non-linear least squares (NLS) method were used to fit simulated data. By comparing two fitting methods, and by using both decay data and transformed peak data it was found that marginally better parameter estimates was obtained using the NLS method to fit decay shaped data; these results are equally applicable to the CW-OSL measurements for a three component problem.

Quartz

From previous studies it is unclear whether the main component with a lifetime between 30–40 µs at room temperature (depending on the sample) represents the recombination lifetime or the excited state lifetime as both the mechanisms have been argued for in the different articles.

In this work the fitting method developed above was used on quartz TR-OSL to derive the lifetime of the main component as a function of stimulation temperature. The study of the thermal dependence of the lifetime and intensity of the main TR-OSL component (30–40 µs lifetime) together with the development and application of a kinetic model using Mott-Seitz mechanism suggested that the main component must arise as a result of decay from the excited state of the recombination centre. Thus, the conduction band must empty on a relatively much shorter time scale. It was noted that such fast emptying of the conduction band cannot be obtained by using the parameters in the currently well established kinetic model for quartz OSL, and therefore, this model can not reproduce a realistic TR-OSL decay shape for quartz.

To make a direct measurement of the charge population of the conduction band to confirm our model, the instrumentation developed to measure TR-OSL was extended to the measurement of time-resolved pulsed optically stimulated

exo-electron (TR-OSE) emission. Measurements on both quartz and feldspar using blue light stimulation show that the major part of the charge population in the conduction band empties in less than 1 μs. These results imply that that the relevant parameters in the currently established model for quartz need to be updated by at least three orders of magnitude so as to allow a fast enough recombination.

The work in this thesis then focussed on the hitherto unstudied slowly decaying TR-OSL components in quartz. To investigate the origin of these components, measurements combining different techniques were undertaken to observe the off-time decay from 50 ns to ∼8 s, covering over 8 orders of the time scale. The main conclusion from the components observed on the second times scale is that these components arise from the decay of charge re-trapped into the shallow traps (e.g. the 110°C TL trap) during and after optical stimulation. Interestingly, a component is observed that does not show an obvious dependence of lifetime on stimulation temperature. It is discussed through a model that this effect could be explained by an internal transition within a second recombination centre. However, from analogy with feldspars (discussed below), this component could also possibly allude to the presence of some band tails in quartz (strain effects are well known in quartz and these may possibly give rise to band tails); this requires further investigations. The main message of this work is that there are complex interactions amongst trap/and or recombination centres that give rise to feedback effects; of special interest is the kink observed in the phosphorescence curve. Finally a kinetic model consisting of four energy levels has been proposed to explain the observed complexity in the phosphorescence decay. The key feature of this model is localised transition from one energy state to another, either between two trap centres or internally within a luminescence recombination centre. This feature successfully reproduces the kink observed in the phosphorescence data.

For dosimetric measurements these results suggest that even during a CW-OSL measurement at 125°C, a small fraction of the measured light will originate from charge recycling through the 110°C trap (at 125°C, the lifetime of this component is ∼0.2 s and the contribution < 5%). This contribution could be made even smaller by raising the stimulation temperature, but this would be at the cost of increased thermal quenching.

Feldspar

Previous applications of TR-OSL in feldspars have been largely restricted to identification of exponential components in the signal(s). The previous work has shown that TR-IRSL off-time decay from various feldspars can be adequately fitted with a sum of up to five exponentially decaying components with lifetimes falling into well-defined groups: 30–50 ns, 300–500 ns, 1–2 μs, ∼5 μs, and > 10 μs, irrespective of the detection in either the 280–380 nm, the 350–575 nm, or the 460–625 nm band.

In this thesis different feldspar measurements have been carried out in the UV (290–360 nm) and blue (350–415 nm) emission windows so as to identify the underlying charge transport mechanisms.

In the UV emission window, green and blue light stimulation of 14 feldspar mineral specimens gave average lifetimes of 42 ± 0.1 ns, 1.10 ± 0.02 μs, 6.9 ± 0.1 μs and 43 ± 1 μs, which are broadly consistent with those found earlier by other

groups. In the slower components, no sign of thermal quenching was observed with elevated stimulation temperatures suggesting that these components possibly reflect the recombination lifetime and not the excited state lifetime. It was furthermore suggested that in fact the TR-OSL off-time decay cannot simply be described by a sum of decaying exponentials; the decay form is more complex and therefore, underlying mechanisms involved in luminescence production require a better understanding.

In the blue emission window which is more commonly used in IRSL dating, the question of processes that control the shape of the TR-OSL signal in feldspars was investigated further. The IR, elevated temperature post-IR IR, and green stimulated signals were studied. As in the case of quartz, the IR and post-IR IR signals were observed to decay from 50 ns to > 7 s. On the shorter time scales ($\sim$50 ns $-$ 500 μs) a comparison of the TR-OSL shapes and their dependence on stimulation energy, thermal energy and anomalous fading helps to understand the charge transport mechanisms during optical stimulation. It is shown that during IR stimulation the main transport processes are tunnelling through the excited state of the trap, and recombination through the band tails. The latter is further shown to have two components, a thermally assisted component and a tunnelling component, each arising from different energy states in the band tails. The data for the first time shows and explains the existence of a non-fading signal in feldspar samples (mineral and specimens) that otherwise show fading rates between 3–20 %/decade with CW-IRSL measurements.

We also investigated on the origin of the slower decaying components in TR-IRSL observed on the ms to s time scales. These data also suggest a presence of a component arising from the slow emptying of the band tails. This component is superimposed on a long-term phosphorescence decay (over several seconds) originating from complex feedbacks in shallow trap, and possibly band tail interactions.

Dating applications

The two main outcomes of this thesis which have relevance to the dating application are:

a) The observations of fading in the TR-IRSL and post-IR TR-IRSL signals. This work conclusively demonstrates from both mineral specimens of different K, Na and Ca compositions and from K-feldspar grains derived from sediments that the IR signal during the on-time has a significantly higher fading rate compared to that during the off-time. Moreover, the off-time signal obtained towards the end of pulsed IRSL measurement (between 200 and 1500 s of illumination) shows no fading; this is identified to be the most stable signal in feldspars. Contrary to the current ongoing and published research on feldspars, we suggest that the first IR measurement contains a signal that is even more stable (tunneling wise) than the post-IR IR signal. However, one needs to develop a method to sample this signal usefully for dating.

b) Another important application is regarding the separation of the quartz OSL signal from that of feldspar's in a mixed sediment sample. This has particular use for in-situ dosimetry where a physical separation of

minerals may not be possible. It is shown that by choosing an on-time equal to the off-time of 50 μs with a prior IR bleaching, the pulsed blue light stimulation will enhance the quartz signal by a factor of 25 compared to that of a conventional measurement of a mixed sample. Moreover, it is shown that an enhancement in the separated signal by factor of ∼100 can be obtained by restricting the counting window to between 20 and 60 μs in the off-time. However, this requires an instrumental modification for routine applications.

Outlook

Although the works presented in this thesis have given significant insights into charge movement in quartz and feldspar, there is much more to be done in this field using time-resolved luminescence. Here are a few suggestions:

Until now, quartz TR-OSL has been measured using the broad UV emission and it would be interesting to use narrow detection filters to find out if several centres are involved in this emission. Another area of interest could be use of time-resolved photoluminescence in both quartz and feldspar to help decouple the processes in the recombination centre from those in the band tails and the conduction band.

In feldspars, a further investigation of the transport in the band tails using TR-OSL at low stimulation temperatures would be interesting as the thermal effect would be minimal. Moreover, using a light source with a faster fall-time would give better insight into the first microsecond of the off-time.

Another area to follow up is development of a method for measuring the most stable IR signal observed in feldspar during the off-time.

Finally, a unified kinetic model of the processes participating in the luminescence emission from feldspar would be a step forward towards a routine analysis of feldspar time-resolved signal and its potential use in dosimetry.

Christina Ankjærgaard was born in Växjö, Sweden in 1980. In 1999 she began her studies in Physics at the Niels Bohr Institute at the University of Copenhagen, and in the summer of 2003 she also started as a part time research assistant at the Nordic Laboratory for Luminescence Dating (Aarhus University). This work inspired her to undertake her Masters project in this laboratory, and in September 2006 she graduated from the Niels Bohr Institute with the M.Sc. Thesis 'Electron Emission from Natural Minerals: Implications for Charge Movement and Dosimetry'. A month later she started her Ph.D. studies at the Radiation Research Division of Risø DTU and in May 2010 she successfully defended her Ph.D. thesis at the Niels Bohr Institute.

In July 2010 Christina started as a post doc at the Netherlands Centre for Luminescence Dating at the Technical University of Delft, where she is currently working on extending the dating age range using quartz and feldspar.